



HAL
open science

Contribution to the study of elastic and plastic deformation mechanisms of polyethylene and polypropylene as a function of microstructure and temperature

Bijin Xiong

► **To cite this version:**

Bijin Xiong. Contribution to the study of elastic and plastic deformation mechanisms of polyethylene and polypropylene as a function of microstructure and temperature. Materials. INSA de Lyon, 2014. English. NNT : 2014ISAL0120 . tel-01278480

HAL Id: tel-01278480

<https://theses.hal.science/tel-01278480>

Submitted on 24 Feb 2016

HAL is a multi-disciplinary open access archive for the deposit and dissemination of scientific research documents, whether they are published or not. The documents may come from teaching and research institutions in France or abroad, or from public or private research centers.

L'archive ouverte pluridisciplinaire **HAL**, est destinée au dépôt et à la diffusion de documents scientifiques de niveau recherche, publiés ou non, émanant des établissements d'enseignement et de recherche français ou étrangers, des laboratoires publics ou privés.

Thèse

Contribution to the study of elastic and plastic deformation mechanisms of polyethylene and polypropylene as a function of microstructure and temperature

Présentée devant
L'institut national des sciences appliquées de Lyon

Pour obtenir
Le grade de docteur

Formation doctorale : Microstructure et comportement mécanique
et macroscopique des matériaux-Génie des matériaux
École doctorale : École doctorale matériaux de Lyon

Par
Bijin XIONG
(Ingénieur)

Soutenue le 09 Décembre 2014 devant la Commission d'examen

Jury MM.

Rapporteur	Sylvie CASTAGNET	Directeur de recherche (CNRS) (ENSMA)
Rapporteur	Lucien LAIARINANDRASANA	Professeur (MINES Paristech)
	Jean-Marc LEFEBVRE	Directeur de recherche (CNRS) (Université Lille1)
	Gilles REGNIER	Professeur (ENSAM Paris)
	Olivier LAME	Professeur (INSA de Lyon)
	Roland SEGUOLA	Directeur de recherche (CNRS) (INSA de Lyon)

Laboratoire de recherche : MATEIS, INSA de Lyon

INSA Direction de la Recherche - Ecoles Doctorales – Quinquennal 2011-2015

SIGLE	ECOLE DOCTORALE	NOM ET COORDONNEES DU RESPONSABLE
CHIMIE	CHIMIE DE LYON http://www.edchimie-lyon.fr Sec : Renée EL MELHEM Bat Blaise Pascal 3 ^e étage 04 72 43 80 46 Insa : R. GOURDON secretariat@edchimie-lyon.fr	M. Jean Marc LANCELIN Université de Lyon – Collège Doctoral Bât ESCPE 43 bd du 11 novembre 1918 69622 VILLEURBANNE Cedex Tél : 04.72.43 13 95 directeur@edchimie-lyon.fr
E.E.A.	ELECTRONIQUE, ELECTROTECHNIQUE, AUTOMATIQUE http://edeea.ec-lyon.fr Sec : M.C. HAVGOUDOUKIAN eea@ec-lyon.fr	M. Gérard SCORLETTI Ecole Centrale de Lyon 36 avenue Guy de Collongue 69134 ECULLY Tél : 04.72.18 60.97 Fax : 04 78 43 37 17 Gerard.scorletti@ec-lyon.fr
E2M2	EVOLUTION, ECOSYSTEME, MICROBIOLOGIE, MODELISATION http://e2m2.universite-lyon.fr Sec : Safia AIT CHALAL Bat Atrium- UCB Lyon 1 04.72.44.83.62 Insa : S. REVERCHON Safia.ait-chalal@univ-lyon1.fr	Mme Gudrun BORNETTE CNRS UMR 5023 LEHNA Université Claude Bernard Lyon 1 Bât Forel 43 bd du 11 novembre 1918 69622 VILLEURBANNE Cédex Tél : 06.07.53.89.13 e2m2@univ-lyon1.fr
EDISS	INTERDISCIPLINAIRE SCIENCES-SANTE http://www.ediss-lyon.fr Sec : Safia AIT CHALAL Bat Atrium – UCB Lyon 1 04 72 44 83 62 Insa : Safia.ait-chalal@univ-lyon1.fr	Mme Emmanuelle CANET-SOULAS INSERM U1060, CarMeN lab, Univ. Lyon 1 Bâtiment IMBL 11 avenue Jean Capelle INSA de Lyon 696621 Villeurbanne Tél : 04.72.68.49.09 Fax :04 72 68 49 16 Emmanuelle.canet@univ-lyon1.fr
INFOMATHS	INFORMATIQUE ET MATHÉMATIQUES http://infomaths.univ-lyon1.fr Sec :Renée EL MELHEM Bat Blaise Pascal 3 ^e étage infomaths@univ-lyon1.fr	Mme Sylvie CALABRETTO LIRIS – INSA de Lyon Bat Blaise Pascal 7 avenue Jean Capelle 69622 VILLEURBANNE Cedex Tél : 04.72. 43. 80. 46 Fax 04 72 43 16 87 Sylvie.calabretto@insa-lyon.fr
Matériaux	MATERIAUX DE LYON http://ed34.universite-lyon.fr Sec : M. LABOUNE PM : 71.70 –Fax : 87.12 Bat. Saint Exupéry Ed.materiaux@insa-lyon.fr	M. Jean-Yves BUFFIERE INSA de Lyon MATEIS Bâtiment Saint Exupéry 7 avenue Jean Capelle 69621 VILLEURBANNE Cedex Tél : 04.72.43 71.70 Fax 04 72 43 85 28 Ed.materiaux@insa-lyon.fr
MEGA	MECANIQUE, ENERGETIQUE, GENIE CIVIL, ACOUSTIQUE http://edmega.universite-lyon.fr/ Sec : M. LABOUNE PM : 71.70 –Fax : 87.12 Bat. Saint Exupéry mega@insa-lyon.fr	M. Philippe BOISSE INSA de Lyon Laboratoire LAMCOS Bâtiment Jacquard 25 bis avenue Jean Capelle 69621 VILLEURBANNE Cedex Tél : 04.72 .43.71.70 Fax : 04 72 43 72 37 Philippe.boisse@insa-lyon.fr
ScSo	ScSo* http://recherche.univ-lyon2.fr/scso/ Sec : Viviane POLSINELLI Brigitte DUBOIS Insa : J.Y. TOUSSAINT viviane.polsinelli@univ-lyon2.fr	Mme Isabelle VON BUELTZINGLOEWEN Université Lyon 2 86 rue Pasteur 69365 LYON Cedex 07 Tél : 04.78.77.23.86 Fax : 04.37.28.04.48 isavonb@gmail.com

*ScSo : Histoire, Géographie, Aménagement, Urbanisme, Archéologie, Science politique, Sociologie, Anthropologie

Contribution à l'étude des mécanismes de déformation élastique et plastique du polyéthylène et polypropylène en fonction de la microstructure et de la température

Résumé

Les propriétés mécaniques des polymères semi-cristallins en relation avec leur microstructure ont fait l'objet d'un grand nombre d'études. Cependant, il reste encore des questions non résolues, concernant les mécanismes de la déformation plastique à température élevée, les propriétés intrinsèques de la phase amorphe interlamellaire ou encore la distribution des contraintes locales dans les sphérolites... L'objectif de cette thèse est d'adresser ces questions dans les cas du PE et du PP en fonction de la température. Pour atteindre cet objectif, une série d'échantillons de PE et PP des différents microstructures ont été préparées et caractérisés par DSC, SAXS, WAXS et spectroscopie Raman. Dans le domaine élastique, la déformation locale (ϵ_{local}) dans les régions équatoriales et polaires des sphérolites ont été mesurés par SAXS in situ. Le ratio $\epsilon_{\text{local}} / \epsilon_{\text{macro}}$ a été utilisé dans un modèle mécanique permettant le changement d'échelle de mésoscopique macroscopique. En outre, le module apparent de la phase amorphe interlamellaire M_a a été estimé par la contrainte et la déformation locale. Les M_a valeurs du PE sont dans la gamme 250 - 500 MPa, ce qui est très élevé par rapport au module du PE amorphe caoutchoutique. Dans le domaine plastique, la cavitation, la transformation martensitique et le cisaillement du cristal ont été observées par SAXS et WAXS in situ. Une concurrence entre ces mécanismes plastiques a été mise en évidence. L'augmentation de la température entraîne une disparition progressive de la cavitation et un retard de la transformation martensitique vers de plus haute déformation. La structure fibrillaire, induite par étirage à différentes températures a été étudiée par SAXS in-situ. Il a été observé que la longue période et le diamètre des micro-fibrilles dépendent de la température d'étirage de la structure initiale, via les mécanismes de « fusion-recristallisation » et « fragmentation-réarrangement ». Une étude similaire a été effectuée pour le PP.

Mots-Clés: polyéthylène; polypropylène; microstructure; propriétés mécaniques; température

Contribution to the study of elastic and plastic deformation mechanisms of polyethylene and polypropylene as a function of microstructure and temperature

Abstract

The mechanical properties of semicrystalline polymers in relation to microstructure have been the subject of a large number of studies. However, there are still some unresolved issues, for instance, plastic deformation mechanisms in elevating temperature, intrinsic properties of interlamellar amorphous phase, local stress distribution in spherulites etc. The aim of this thesis is to address these issues in the case of PE and PP in different temperatures. A series of PE and PP samples with wide range of microstructures thanks to various thermal treatments were characterized by DSC, SAXS, WAXS and Raman spectroscopy. In elastic domain, the local strain ϵ_{local} in equator and polar regions of spherulites were measured by in situ SAXS. The ratio $\epsilon_{\text{local}}/\epsilon_{\text{macro}}$ is a constant which only depends on drawing temperature. This ratio was used in a mechanical modelling as a transition factor from mesoscopic to macroscopic scale. Furthermore, the apparent modulus of the interlamellar amorphous phase M_a was estimated by the measured local stress and strain. The M_a of PE was found to be in the range 250 - 500 MPa which is surprisingly high comparing with the modulus of bulk rubbery PE. In the plastic domain, cavitation, martensitic transformation and crystal shear were observed by in situ SAXS and WAXS and their respective strain onsets were shown to be strongly dependent on crystallite thickness and temperature. It was found that competition exists between these plastic mechanisms. With increasing temperature, cavitation gradually disappears and martensitic transformation is delayed. A map for the onset of these plastic mechanisms was produced. In addition, the fibrillar structure induced by drawing at different temperature was studied by in situ SAXS. The long period and diameter of micro-fibrils proved to be dependent on the drawing temperature and also the initial structure via the melting-recrystallization and fragmentation-rearrangement mechanism. Similar investigations were performed with PP.

Key words: polyethylene; polypropylene; microstructure; mechanical properties; temperature

Table of content

General introduction.....	1
Chapter I Introduction	3
I.1 Preamble	5
I.2 Structure of PE and iPP molecules	5
2.1 Molecule structure of PE	5
2.2 Molecular structure of iPP	6
I.3 Morphology of the semi-crystalline PE and iPP	6
3.1 Crystalline structure of polyethylene [6]	7
3.2 Crystalline structure of iPP	8
3.3 Lamellar morphology	8
3.3.1 Influence of comonomer	9
3.3.2 Influence of the thermal treatment	10
3.4 Interlamellar amorphous phase.....	12
3.5 Crystal-amorphous coupling.....	12
3.5.1 Tie molecules	13
3.5.2 Stress transmitters.....	15
3.5.3 Interphase	16
3.6 Crystal aggregates and spherulite	16
I.4 Intrinsic properties of crystalline and amorphous phase.....	17
4.1 Modulus of crystal lattice	17
4.2 Modulus of interlamellar amorphous phase	17
I.5 Influence of temperature – relaxation behavior	18
5.1 γ relaxation	18
5.2 β relaxation	19
5.3 α relaxation	20
I.6 Stress strain behavior of semi-crystalline polymer	20
6.1 Stress strain curve	20
6.2 Elastic deformation.....	21
6.2.1 Microstructure evolution	21
6.2.2 Elastic Modulus	22
6.2.3 Models for elastic modulus	23
6.3 Plastic deformation.....	24
6.3.1 Crystal shear in lamella.....	25

6.3.2 Martensitic transformation in polyethylene.....	27
6.3.3 Cavitation.....	28
6.3.4 Fibrillar transformation.....	31
6.3.5 Melting and recrystallization.....	32
I.7 Conclusion of the introduction.....	33
I.8 Strategy.....	33
Chapter II Experiment method and technique.....	34
Context.....	35
II.1 structural characterization.....	35
1.1 Differential scanning calorimetry (DSC).....	35
1.2 Small angle X-ray scattering (SAXS).....	36
1.3 Wide angle X-ray scattering (WAXS).....	40
II.2 mechanical property characterization.....	41
2.1 Tensile tests.....	41
2.2 Dynamic mechanical analysis (DMA).....	42
Chapter III Materials and microstructure characterization.....	45
Context.....	46
III.1 Materials.....	46
III.2 Thermal treatment.....	46
III.3 Microstructure characterization.....	48
3.1 microstructure of polyethylene.....	49
3.1.1 Influence of comonomer concentration.....	49
3.1.2 Influence of thermal treatment.....	50
3.1.3 Stress transmitters density.....	50
3.2 microstructure of polypropylene.....	51
III.4 Conclusion.....	53
Chapter IV Elastic deformation.....	54
Context.....	55
IV.1 Article I: “In-situ SAXS study of the mesoscale deformation of polyethylene in the pre-yield strain domain: Influence of microstructure and temperature”.....	56
IV.2 Article II: “Micro-macro mechanical relationship and amorphous phase modulus in polyethylene via in situ SAXS and WAXS”.....	62
IV.3 Summary of the article.....	84
IV.4 Small strain deformation behaviour of polypropylene.....	85
4.1. Local deformation in equatorial region.....	85
4.2. Comparison between deformation behavior of PE and PP.....	87
IV.5 Conclusion of the chapter.....	87
Chapter V Plastic deformation.....	88

Context	89
V.1 Article III: “In-situ SAXS study and modeling of the cavitation crystal-shear competition in semi-crystalline polymers Influence of temperature and microstructure in polyethylene” .	90
V.2 Summary of the article	102
V.3 Martensitic transformation of polyethylene	103
3.1 Martensitic transformation onset	104
3.2 Evolution of scattering intensity of monoclinic crystal	106
3.3 Conclusion on martensitic transformation	108
V.4 Shearing at the scale of crystallite in PE	108
V.5 Competitions of plastic mechanisms onsets	111
V.6 Conclusion	114
General conclusion and perspective	116
General conclusion	116
Perspective	117
Annex	119
Context	120
1 Yield behavior	121
1.1 Influence of morphology	121
1.2 Influence of temperature	123
1.3 Conclusion for yield behavior	124
2 Fibrillar transformation behavior of polyethylene	124
Article IV ‘Impact of molecular topology and initial microstructure on the fibrillar transformation of polyethylene during uniaxial stretch at elevating temperature: in situ SAXS experiment.’	124
2.2 Fibrillar transformation of polypropylene	135
2.3 Influence of temperature	136
2.4 Conclusion	137
3 Orientation of crystalline lamella	139
3.1 Orientation of PE lamellae	139
3.2 Deformation of PP lamellae	142
3.3 Comparison of lamella deformation between PP and PE	143
Reference	144

General introduction

During the past century, synthetic polymers have taken an increasing place in the domain of transport, sports, electronics and domestic appliances due to their low density as well as good insulating properties compared to metals. During the last decades, thermoplastic polymers emerged as commodity plastics owing to their easier and less expensive processing ability compared to thermosets, and better recyclability as well. The larger part of thermoplastics consists of semi-crystalline polymers such as polyethylene, polypropylene, polyamides, polyesters, etc ... Presently, due to the forecast exhaustion of fossil energy resources, bio-sourced polymers gained an increasing attraction as sustainable alternatives to oil-based polymers. However, bio-sourced materials generally have lower mechanical performances compared to synthetic polymers, as well as higher economical cost. So that conventional synthetic polymers are still preferred in many technological domains, with an increasing commitment of recycling capability.

Researches have thus been oriented towards optimization of the mechanical and physical properties of well-known synthesis polymers via new synthesis routes, chemical modifications and /or compounding. The mechanical and physical properties of semicrystalline polymers are still the subject of numerous studies. Indeed, their increasingly use in specific conditions demands a thorough knowledge of the physical mechanisms during thermal or mechanical stress. In particular, the influence of their microstructural and molecular parameters on their properties must be well known. However, this is not easy because of the complex multi-scale microstructure of semicrystalline polymers. Polyethylene is known to be one of the simplest polymers on chemical and crystallographic structures which make it a model material for the study of the mechanical behavior of semicrystalline polymers. The study of the influence of the microstructure on the mechanical properties of the polyethylene must necessarily be a multi-scale analysis because its microstructure is organized at different scales. This complex microstructure is also dependent on the molecular parameters and the crystallization conditions.

The mechanical properties in small deformations (elastic domain) are generally influenced by crystallinity, and the thickness of the crystallite lamellae, as for example the elastic modulus. Essentially, the modulus is not only determined by the intrinsic properties of crystal and amorphous phase, but also the connection between these two phases such as interphase or tie molecule. The knowledge of the intrinsic properties of these components is quite important to the micromechanical models which help to predict the macroscopic mechanical properties in relation to the microstructural characteristics of the polymer that are well known to have a great impact on the mechanical properties. There is thus a need of appropriate experiments allowing to get access to these intrinsic properties.

Regarding plastic deformations, a lot of works have been published. The predominant deformation mechanisms include crystallites shear, cavitation, and crystal phase transformation. Many investigations revealed that the occurrence of these mechanisms is function of molecular parameters, microstructure and temperature. However, the relation between these mechanisms and the exact effect of microstructures are still not clear.

Temperature is also an important factor for the mechanical properties since it governs the occurrence of molecular mobility below the melting point and thus may strongly modify the various plastic deformation processes. It is known that the polymers go from the glass-like brittle behavior at low temperatures to a rubber-like behavior at high temperature. Semicrystalline polymers undergo various different relaxations (γ , β and α relaxations in PE) with increasing temperatures. These relaxation processes have been widely discussed but the origins are still controversial.

The aim of current work is to understand the influence of the each molecular and microstructural parameters and temperature on the mechanical properties of semicrystalline polymers. More precisely, we expect to establish correlations between microstructure, temperature and deformation behavior.

To reach these objectives, the strategy was to collect a series of PE samples with different molecular topology (comonomer concentration) and different thermal treatments to obtain a wide distribution of microstructure parameters (crystallinity, crystalline thickness, tie molecules density et al.). On the other hand, the similar microstructure could be obtained from polymers with different topology. This will allow understanding the influence of molecular parameters on the mechanical properties.

Isotactic polypropylene was also used to compare the mechanical properties between semicrystalline polymers of different natures but with similar microstructures.

Considering that the basic structure of semicrystalline polymers is at the nanoscale of the crystalline lamellae and their regular stacking with amorphous layers, in situ WAXS and SAXS experiments at different temperatures clearly appear to us as preferred experimental means for investigating the micro-mechanisms of deformation and the influence of temperature. With these techniques the microstructure parameters could be well associated to the mechanical properties.

The present thesis is divided into seven chapters. In details, the thesis is organized as follows:

Chapter 1 introduces a literature review of the chemical-physical structure of semicrystalline polyethylene and polypropylene. The chapter provides a brief summary of deformation behavior of these semicrystalline polymers during the tensile test.

Chapter 2 introduces the experimental techniques for microstructure characterization and mechanical properties analysis.

Chapter 3 describes the various materials of the study. Their microstructures are characterized by the different techniques described in the previous chapter. The influence of the molecular topology and the thermal treatment on the microstructure is also discussed in this chapter.

Chapter 4 concerns the local deformation behavior in the visco-elastic deformation domain. Mesoscopic and macroscopic deformation behavior has been connected with the ratio of local strain to macroscopic strain. Local deformation in different regions of spherulites is discussed. In addition, the intrinsic properties of interlamellar amorphous phase have been studied by combining in-situ SAXS and WAXS at different test temperatures.

Chapter 5 deals with the relationship between microstructure variation and the plasticity of the polyethylene and polypropylene. It is divided in two parts: The first part presents formation of the cavitation in the relation with microstructure and temperature. The mechanism of the cavitation formation in polyethylene semicrystalline is discussed via a modeling. The second part describes the shearing and the martensitic transition of the crystallite. The influence of the microstructure and temperature is discussed as well. Relations of these mechanisms are discussed in this part.

Chapter 6 presents the general conclusions of the present research work, discusses the main contributions, and suggests some recommendations for future research.

Annex is about the fibrillar transformation behavior of semi-crystalline PE and PP during tensile test. The influence of the initial structures will be studied in this work. The mechanisms (melt-recrystallization and fragment-rearrangement) of the fibrillar transformation are discussed as well.

Chapter I Introduction

Table of content

Chapter I Introduction	3
I.1 Preamble	5
I.2 Structure of PE and iPP molecules	5
2.1 Molecule structure of PE	5
2.2 Molecular structure of iPP	6
I.3 Morphology of the semi-crystalline PE and iPP	6
3.1 Crystalline structure of polyethylene [6]	7
3.2 Crystalline structure of iPP	8
3.3 Lamellar morphology	8
3.3.1 <i>Influence of comonomer</i>	9
3.3.2 <i>Influence of the thermal treatment</i>	10
3.4 Interlamellar amorphous phase	12
3.5 Crystal-amorphous coupling	12
3.5.1 <i>Tie molecules</i>	13
3.5.2 <i>Stress transmitters</i>	15
3.5.3 <i>Interphase</i>	16
3.6 Crystal aggregates and spherulite	16
I.4 Intrinsic properties of crystalline and amorphous phase	17
4.1 Modulus of crystal lattice	17
4.2 Modulus of interlamellar amorphous phase	17
I.5 Influence of temperature – relaxation behavior	18
5.1 γ relaxation	18
5.2 β relaxation	19
5.3 α relaxation	20
I.6 Stress strain behavior of semi-crystalline polymer	20
6.1 Stress strain curve	20
6.2 Elastic deformation	21
6.2.1 <i>Microstructure evolution</i>	21
6.2.2 <i>Elastic Modulus</i>	22
6.2.3 <i>Models for elastic modulus</i>	23
6.3 Plastic deformation	24
6.3.1 <i>Crystal shear in lamella</i>	25
6.3.2 <i>Martensitic transformation in polyethylene</i>	27

6.3.3 Cavitation.....	28
6.3.4 Fibrillar transformation.....	31
6.3.5 Melting and recrystallization.....	32
I.7 Conclusion of the introduction.....	33
I.8 Strategy	33

I.1 Preamble

Polyethylene (PE) and isotactic polypropylene (iPP) are two of the most significant semi-crystalline polymers among the most prominent commodity plastics. These representatives of the family of polyolefin make up nearly 50% of the world's plastics market. The rapid development of new catalysts has allowed the tailored design of macromolecules with defined semi-crystalline morphologies and thus defined properties, such as toughness, stiffness, wear resistance, transparency, etc. Very often, this semi-crystalline morphology provides and controls the physical properties polymers. Therefore, the analysis and control of the morphologies of semi-crystalline polymers as well as an understanding of the micromechanical processes of deformation and fracture are crucial to material development, modification, and failure analysis.[1]

The search for a relationship between molecular structure and mechanical properties of semi-crystalline polymers has been a motive for extensive studies in the past [2]. The mechanical properties of semi-crystalline polymers depend on various factors (see **Figure 1.1**). Firstly, they are decided by the nature of the materials such as a chemical structure, molecular weight and its distribution. Secondly, the properties can be changed by the formation of morphology through processing. This relationship between materials, morphologies and properties is complicated and is not fully understood [3]. This thesis aims to develop further understanding of that relationship.

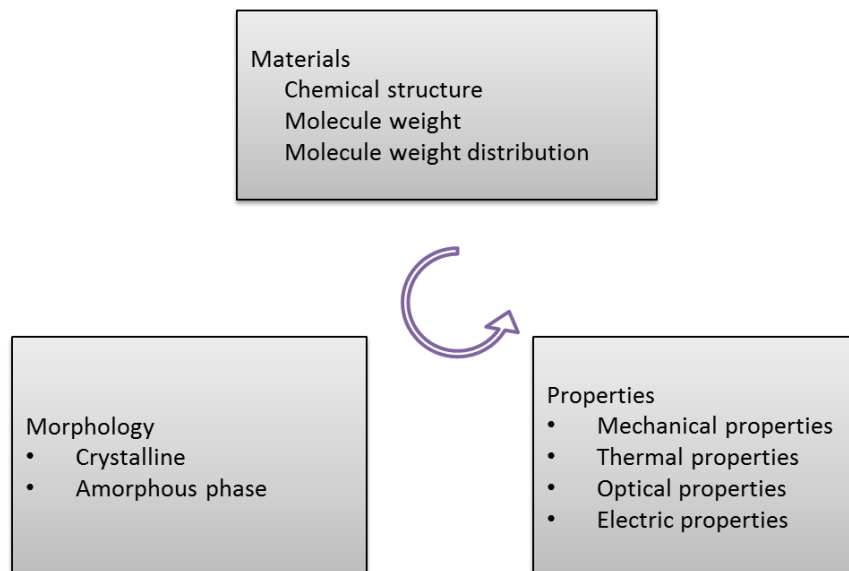


Figure 1.1. Relations between the materials, morphology and properties of semi-crystalline polymers.

I.2 Structure of PE and iPP molecules

2.1 Molecule structure of PE

PE is the simplest polyolefin and made by the polymerization of ethylene monomer. The polyethylene has a very simple structure with a long chain of carbon atoms where two hydrogen atoms are attached to each carbon atom (see figure 2.1). Polyethylene macromolecules adopt a stable conformation planar zigzag (see Figure 2.1).[4]

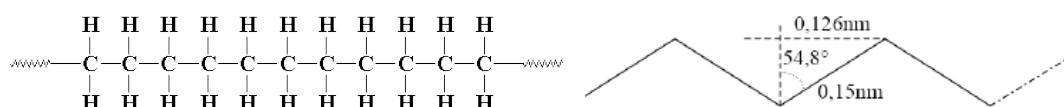


Figure 2.1. Schematic of polyethylene with a planar zigzag conformation.

It is classified into several different categories based on its density and chain branching. The most important polyethylene grades are High-density polyethylene (HDPE), Linear low-density polyethylene (LLDPE) and Low-density polyethylene (LDPE) (see Figure 2.2).

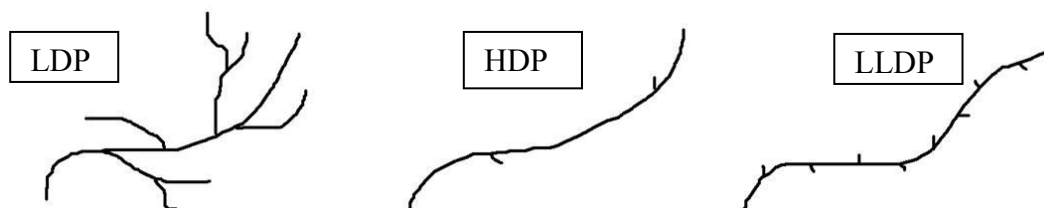


Figure 2.2. The different categories of polyethylenes

HDPE has a low degree of branching and thus high crystallinity. The lack of branching is ensured by an appropriate choice of catalyst (for example, chromium catalysts or Ziegler-Natta catalysts) and reaction conditions. LLDPE is defined by a density range of 0.915–0.925 g/cm³. LLDPE is a substantially linear polymer with significant numbers of short branches, commonly made by copolymerization of ethylene with short-chain alpha-olefins (for example, 1-butene, 1-hexene and 1-octene). LDPE has a high degree of short and long chain branching. It was produced by bulk polymerization in high pressure conditions. The low density and low crystallinity of LDPE are the result of its highly branched structure.

2.2 Molecular structure of iPP

Isotactic polypropylene (iPP) can be made from the monomer propylene by Ziegler-Natta polymerization and by metallocene catalysis polymerization. iPP is the most stereo-regular structures of PP which means all the methyl groups are on the same side of the chain (see Figure 2.3).

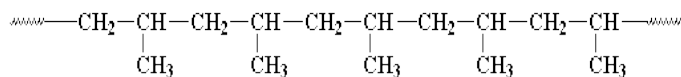


Figure 2.3. Schematic of isotactic polypropylene.

To reduce the steric hindrance effect of methyl group, the chain of iPP is in a left or right handed (or both) 2*31- helix conformation with either an ‘up’ or ‘down’ position of the methyl groups (see Figure 2.4 for a helix with ‘down’ position of the methyl groups). Figure 2.4 shows the contours of the helix as a triangular bar. This representation is used in the description of the crystal phases of polypropylene.[5]

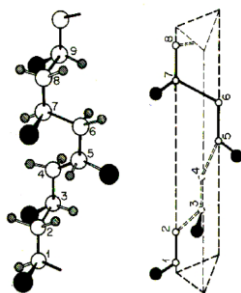


Figure 2.4. Helical structure of isotactic polypropylene with ‘down’ positions of the methyl groups (black spheres).

I.3 Morphology of the semi-crystalline PE and iPP

Semi-crystalline polymers are those that consist of two or more solid phases, in at least one of which molecular chain segments are organized into crystal, and in other phases chains are

disordered. The non-crystalline phases form a continuous matrix in which the crystalline regions are embedded. Most polyolefin are semi-crystalline. Their specific morphology is governed by molecular characteristics and preparation conditions.

3.1 Crystalline structure of polyethylene [6]

In crystallographic terms the *unit cell* is the smallest entity that contains all the information required to construct a complete crystal. The lengths of the sides can be identical or different. The lengths of axes are designated a , b , and c , and the angles between faces, α , β , and γ , as illustrated in Figure 3.1. A complete crystal can be constructed from a unit cell by translating it repeatedly along each of its axes.

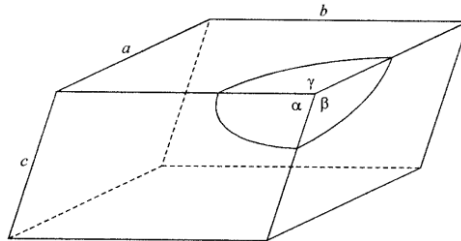


Figure 3.1. Schematic of a unit cell.[6]

Polyethylene exhibits three types of unit cells: orthorhombic, monoclinic, and hexagonal. The orthorhombic unit cell is the most common; for all practical purposes it may be considered to be the only one present in samples.

Orthorhombic Unit Cell

The orthorhombic unit cell is a cuboid, each of its axes having a different length while the angles made by adjoining faces are all 90° . The orthorhombic unit cell is variously illustrated in Figure 3.2. These values were measured for high density polyethylene at room temperature. The density of a unit cell with these dimensions is 1.00 g/cm^3 . This value is widely accepted and is commonly used in the calculation of the degree of crystallinity from sample density.

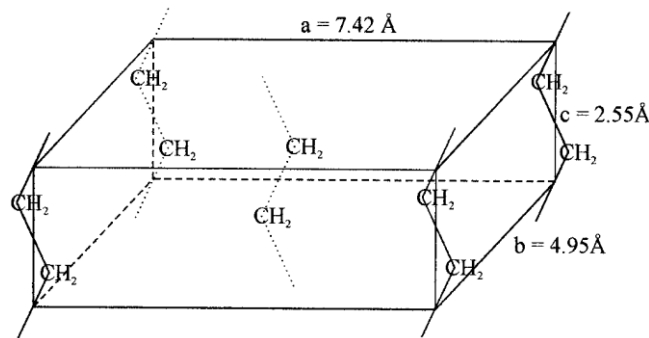


Figure 3.2. Schematic of PE orthorhombic crystal cell.[6]

Monoclinic Unit Cell

The monoclinic crystal form of polyethylene is a metastable phase formed under conditions of elongation. It may be present to a small extent in commercial samples that have undergone cold working after initial molding. The orthorhombic phase could transform to the monoclinic phase. This phenomenon will discuss in the section 4. The configuration and dimensions of the monoclinic unit cell are shown in Figure 3.3.

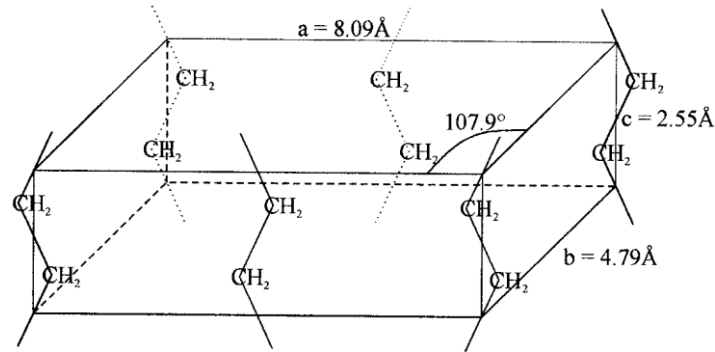


Figure 3.3. Schematic of PE monoclinic crystal cell.[6]

3.2 Crystalline structure of iPP

Isotactic polypropylene is a polymer with a number of crystal modifications. In all of the crystal structures the chain is packed in the lattice as a helix conformation with either an ‘up’ or ‘down’ position of the methyl groups. A triangular is used in the description of the crystal phases of polypropylene (see Figure 2.4). Among those structures, α form is the most common. Here we just discuss the structure of α phase

The α -phase of iPP is described by an alternation, in the b -axis direction, of layers parallel to the ac -plane and composed of only left handed (L) or right-handed (R) helices, indicated in Figure 3.4 by white and gray triangles, respectively. The position of the methyl groups in both the left or right-handed helix can be positioned ‘up’ or ‘down’ (up or dw). Due to the possibility of the chains to be situated ‘up’ or ‘down’, two limiting α -phases (α_1 : disordered, α_2 : ordered) can be recognized (see Figure 2.4). The monoclinic unit cell has the following parameters $a = 6.65 \text{ \AA}$, $b = 20.96 \text{ \AA}$, $c = 6.5 \text{ \AA}$, and $\beta = 99.62^\circ$. The overall density is 0.946 g/mol (room temperature).[5]

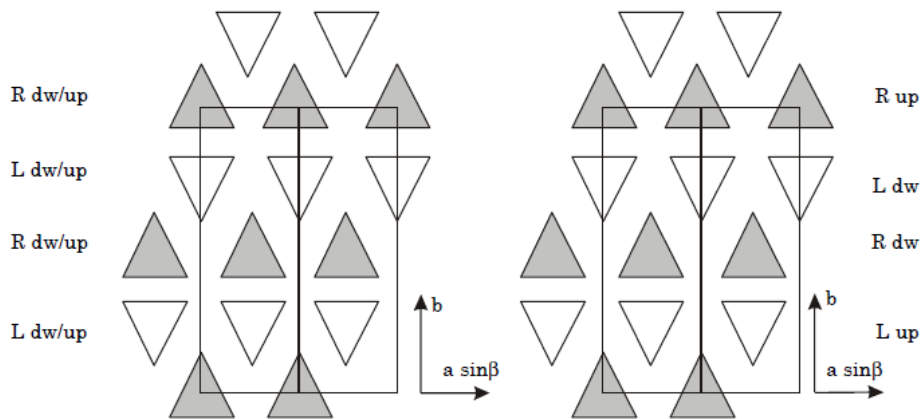


Figure 3.4. Schematic of iPP crystal cell.[5]

3.3 Lamellar morphology

The main features of crystalline lamellae can be illustrated by a PE single crystal lamella grown from dilute solutions, as shown in Figure 3.5. The polymer crystal is slightly pyramidal with an overall tent-like structure in a lozenge shape. From the electron diffraction pattern, the polymer chains are found to be parallel to the thickness direction of the lamella. The polymer chains are believed to be folded back and forth on the upper and lower lamellar surfaces.[7]

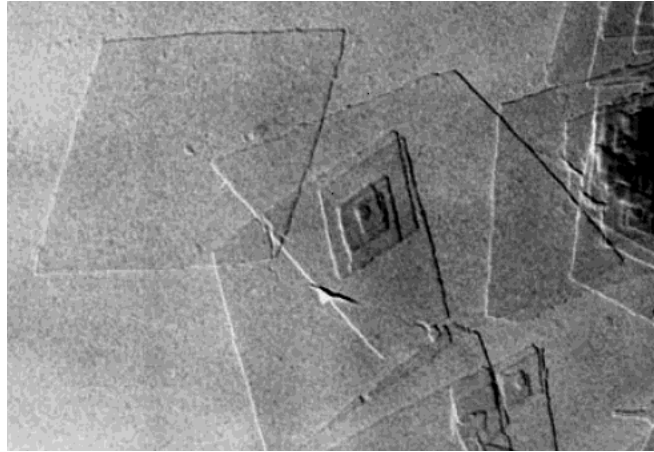


Figure 3.5. TEM image of single polyethylene crystal [8].

When crystallized from the melt, the crystal organized as a lamella with a twist in b axial as shown in Figure 3.6. The growth direction of polyethylene lamella is toward the b -axis [6]. The chains fold normal to the lamella surface and the lamellae grow in the radial direction from the center of spherulite. The organization of lamellae in spherulite will be discussed in section 3.6. Studies using electron and atomic force microscopy [9,10,11] and x-ray diffraction [12] provided the evidence for the twisted structures. Two models have been proposed to explain the lamellar twist. One is believed to be the surface stress of the lamellar crystals [13,14] and the other is attributed the consecutive formation of screw dislocations [15,16]. Twisted lamellae are also reported to have an S-shaped cross section when they are cut perpendicularly to the growth direction [16,17]. This structure is explained based on the reorientation of polymer chains and the stress on the lamellar surfaces, and self-induced fields during crystallization [17].

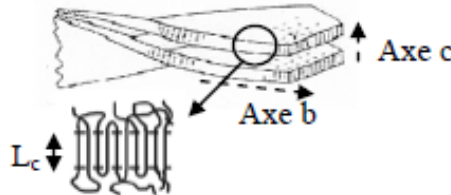


Figure 3.6. Schematic of lamellae stacks [18].

The thickness of the crystallites can be obtained by techniques of X-ray scattering and differential scanning calorimetry. However, their length and width can not be measured with the regular method. Although the thickness of the lamellae seems to be the most influential parameter on the mechanical properties, it would be interesting to know the other two dimensions in order to calculate the form factor which is the ratio between the thickness and the length (or width). For composite materials, it is known that the shape factor significantly influence the mechanical properties.[19] Thus, it can be assumed that it plays the same role in the semi-crystalline polymers.[20]

3.3.1 Influence of comonomer

The topology of the molecule is the major factor determining the thickness of the crystallites, especially the defects of the chains. The comonomer is excluded from the crystal during crystallization. Thus the critical thickness of the crystal depends on the length between two comonomers or defects. Furthermore, the intramolecular sequence distribution is considered significant to determine the average lamella thickness and distribution for short chain-branched polyethylenes [21]. On the other hand, it is evidenced that the some of the comonomer units are included in the lattice as point defects instead of being excluded and forming a separate amorphous phase.[22] However, whatever the defect is in or out the crystal lamella, the lamella thickness decreases with increasing comonomer content.

3.3.2 Influence of the thermal treatment

The thermal history of a polymer, in particular between *glass transformation temperature* T_g and melting temperature T_m , greatly influences the thickness of the lamellae. With different thermal history, the lamellae process different thicknesses as they are not formed under the same conditions (time, temperature). Even if the influence of crystallization conditions on the lamellae has been widely studied, some points still remain controversial, especially with regard to the mechanisms of crystallization during annealing. Among those thermal treatment, annealing, quenching, isothermal crystallization are most studied methods.

Quenching

During quenching, the temperature decrease so fast that the time for the lamellae thickening is not enough. The thickness of the crystallites is determined during the creation. It depends on the cooling rate and comonomer concentration. The faster quenching, the thinner crystallites are. However, quenching of a polyethylene sample in water or in liquid nitrogen leads to materials with the same crystallinity [23]. This value of the crystallinity is a characteristic parameter of the solid phase depending on the nature of the polymer [24]. In this case, L_c is in the order of magnitude with distance between two consecutive entanglement points along one chain. It is only a function of the rigidity of the chain, and independent of the molecular weight [23].

Isothermal crystallization

During an isothermal crystallization from the melt, large crystallites with more perfect crystal structure are formed by growing very slowly. The crystallinity is dependent on time and temperature of crystallization. Indeed, the crystal growth temperature-dependence is controlled by the competition between kinetic and thermodynamic phenomena. It is determined by the nucleation and growth of the crystal [25]. High temperature favors a large crystal growth rate but also enhanced crystal solubility. Regarding the nucleation, it occurs when the temperature drops far below the melting temperature T_m . By enhancing the equilibrium solubility, increasing temperature decreases supersaturation, interfacial energy and thus nucleation vanish at T_m . Decreasing temperature to the glass temperature T_g , however, also causes nucleation to vanish or become infinitesimal because of the drastic increase of fluid viscosity. Therefore, nucleation for polymer melt is limited to the temperature range between T_g and T_m , and a maximum nucleation rate is expected between these two temperatures. [25]

The lamella thickness is a function temperature. L_c is determined in the first place by the temperature T at which the crystals have formed, or more precisely by the supercooling ΔT , where $\Delta T = T_f^\infty - T$, where T_f^∞ represent the melting temperature of the infinitely extended crystal. [26]

Annealing

Semicrystalline polymers generally change their physical properties when they are heated to elevated temperatures below the melting point. These changes are related to alterations of the morphology [27]. It is known that polymer chains in the solid state are reorganized from the initial structure to thermally more stable ones by annealing at various temperatures below the melting point. The heat treatment results in a reorganization of the structure leading to a state of order with a lower free energy.

One of the most important annealing effects is the increase of the thickness of the crystals in the chain direction when semi-crystalline polymers are heated above a certain temperature. [28] The general features of lamellar thickening measured by the large increase in long spacing are well established. However, the mechanism underling the lamella thickening is not properly understood. The three most often cited molecular mechanisms to account for the lamellar thickness increase in annealing are: (1) refolding by 'solid state' diffusion; (2) 'selective melting of thinner lamellae and recrystallization to thicker lamellae' and (3) the fold surface 'premelting', which has been reviewed by Fischer. [27]

According to the ‘solid state’ diffusion mechanism, the chain diffuses along the c-axis with a snaking like refolding. The change of the overall structure can be described adequately by the scheme of Figure 3.7 proposed by Statton.[29] This is based on the observation that the c-axis is thickened and remains perpendicular to the lamellar surface during the annealing process. Recently, Rastogi et al[30], found double thickness of crystal lamella during the annealing of ultra-high molecule weight polyethylene and proposed a mechanism as shown in schematic Figure 3.8. Once the film is heated above the α -relaxation temperature, the thermodynamic driving force for lamellar thickening, necessary to minimize the surface free energy, will cause the chains to slide within the lamellae. The sliding chain within one lamella will push the chain in the adjacent lamella, as shown schematically by the bold line, representing the test chain (see Figure 3.8). Indeed, some limited refolding by solid state diffusion probably does occur, e.g.in non-equilibrium systems, such as cold or hot drawn systems containing numerous highly stressed defective crystals. However, the solid state diffusion can not explain the long period increase during annealing and the time dependency of the annealing effects.

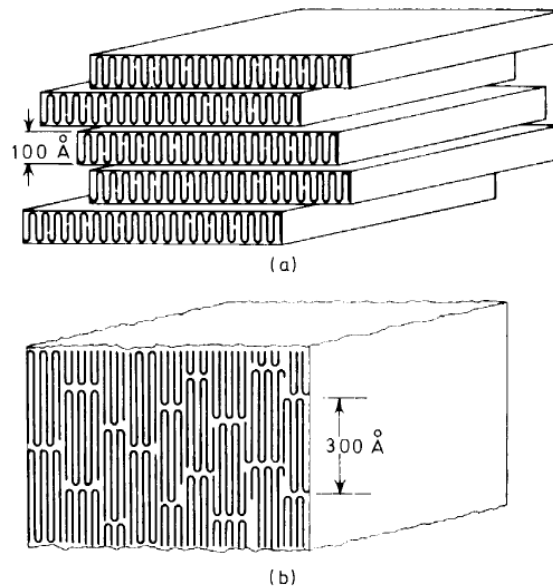


Figure 3.7. The arrangements of chains in sections of a lamellar aggregate. (a) Before annealing (b) after annealing. According to Stratton.[29]

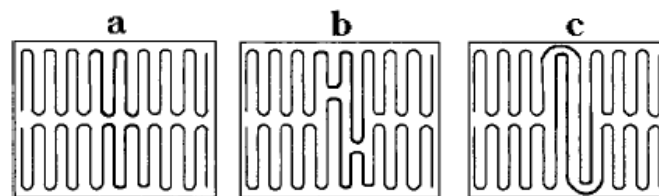


Figure 3.8. schematic model to explain the doubling phenomenon in the regularly stacked adjacent of ultra-high molecule weight polyethylene. According to Rastogi[30].

On the other hand, Hoffman and Kilian proposed that the thickening of lamella is from the partial melt and recrystallization of the crystal [31,32,33]. It is believed that the increase of the long period during the annealing process is from the reconstruction of lamella structure by the partial melt of the crystal. In annealing, a portion of the crystallites are molten, while a portion is still there. The recrystallization is complex in this situation. The presence of unmelted crystals makes the crystallization nucleation easier, although supercooling is low. However, there no direct

evidence to support this mechanism.

Jonas pointed out that the crystalline perfection increases through the removal of defects at the interface of the crystals [34,35]. However, according to McCready [36], the thickness of the amorphous lamellae remains constant when the thickness of the crystallites increases. Crystal growth in the direction of the chains is contrary to this observation since the amorphous lamellae are expected to decline to make way for crystallites. It then proposes a model of "cannibalism" small crystals where large crystals devour the small crystals (see Figure 3.9). This phenomenon was also observed by Petermann [37]. The removal of thin slices would have the effect of increasing the average thickness of the lamellae present in the polyethylene.

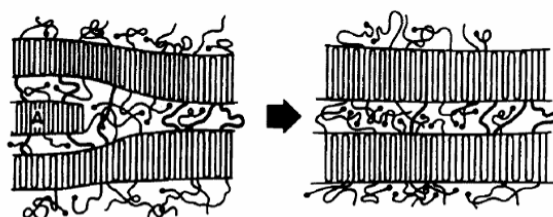


Figure 3.9. Model of cannibalism small crystallites larger crystallites during annealing

Thus, the mechanisms involved in annealing are not yet well defined. However, it can be concluded as follows:

Annealing takes place in several steps. When melting a portion of the crystal, there is a decrease in density. This is the fusion of smaller crystallites. Throughout the temperature maintenance, large crystallites can grow in the previously molten zone. Concomitantly, unmelted crystallites may also thicken thanks to the mobility of the chains in the crystal. At the end of the heat treatment, there may be non-crystallized due to low supercooling, which may nevertheless crystallize at lower temperature [36].

3.4 Interlamellar amorphous phase

The crystal lamellae are separated by an amorphous phase layer. The interlamellar thickness could be measured but the width and length are hard to be obtained. Direct microscopic measurement of the thickness of the interlamellar layer is hard to be achieved. The uncertainty between the boundaries of crystal and amorphous phase prevent the quantitative analysis of interlamellar thickness. However, the SAXS could be a good method for the measurements of the thickness of the interlamellar layer because it is sensitive to periodic changes in electron density. Fischer and Schmidt[38] were the first to detect changes in interlamellar thickness by using a SAXS procedure in quenched polyethylene after annealing and shown that the interlamellar thickness is a function of temperature. Kavesh[39] found that an equilibrium exists between lamellar and interlamellar regions below crystallization temperature. Upon increasing temperature, the lamellae become thinner while interlamellar space increases, but the changes are reversible over this temperature range.

The density of interlamellar amorphous layer of polyethylene is different to the purely amorphous phase. Mandelkern et al.[40] found that the enthalpy of fusion data yielded an amorphous density of 0.90 g/cm^3 by extrapolating linearly to zero crystallinity. It is bigger than the value obtained by extrapolation of melt densities to room temperature, which is 0.85 g/cm^3 .

Based on the density augmentation phenomenon for the interlamellar amorphous phase, many authors believed that there should be a phase with a density between amorphous phase and crystal to accommodate of interlamellar layer, such as 'interphase' or 'hard amorphous'. However, this needs more evidences to supporting. This will be discussed in next part.

3.5 Crystal-amorphous coupling

Interlamellar amorphous layer and crystalline lamellae are physically coupled by various elements. This physical coupling has a great influence on the mechanical properties. Recently it

has been one of the subjects with many studies. Despite the great interest, many questions are still remaining.

3.5.1 Tie molecules

Tie molecule (TM) is a molecule that connects at least two different crystals lamellae. It is a molecular segment which initiates in one crystalline domain, crosses the amorphous region and connects an adjacent crystalline phase. TM provides the strength to keep the crystalline and amorphous phases from separating under load. These tie molecules are believed to be responsible for high elongation, exceptional toughness and impact resistance, and good resistance to slow-crack growth, as well as environmental stress cracking [41].

Direct experimental evidence of TMs by transmission electron microscopy has never been obtained although this technique is particularly well suited for studying objects with a typical size of just a few nanometers. However, studies of the crazing of semi-crystalline polymers by transmission electron microscopy have demonstrated that molecular connections necessarily exist between the crystalline lamellar to enable their transformation into fibrils, on the scale of a few hundreds of nanometers, at the tip of a propagating crack [41].

Origin of the tie molecule

There are two reasons for the presence of the tie molecule in melt-crystallized semi-crystalline polymers [41].

First, the transient entanglements formed in the melt are preserved throughout the crystallization process. In the solid state, these entanglements constitute topological defects that are excluded from the crystalline phase and thus build up molecular connections between the crystallites if the two intervening chains belong to two adjacent crystallites.

Second, the scaling relation between the random coil dimension in the molten material and the crystallite thickness in the solidified material. Polymers crystallize from the melt in the form of chain folded lamellae whose thickness does not exceed a few tens of nanometers which is much smaller than the size of the random coil conformation in the melt. Several crystalline lamellae can grow within the sphere of gyration of chain as long as the chain molar weight is sufficiently high (see Figure 3.10).

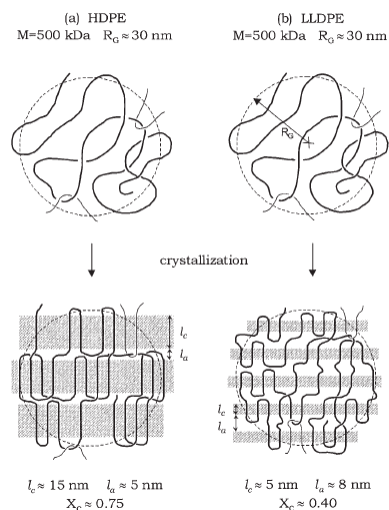


Figure 3.10. Schematic molecular topology of semi-crystalline polymers before and after crystallization: (a)HDPE; (b)LLDPE.[41]

The formation of the tie molecule is significantly influenced by the molecule topology. The probability of forming TMs and chain entanglements enhances with increasing molecular weight. This is evidenced by the reduced draw ability and the increase in the strain hardening and tensile strength.

Incorporating side chains by copolymerization is another way to increase the TM concentration [42,43]. Indeed, co-units with bulky side groups are excluded from the crystal; this process results in an increase in random chain folding accompanied by a high rate of TMs [41]. However, copolymerization involves a reduction of the crystallinity and a concomitant drop in the stiffness and yield stress.

Evaluation of TM content: Brown's Model

To our knowledge, there is no direct experimental data on tie molecule density in literature. However, theoretical approaches specifically addressing the evaluation of the chain topology in the amorphous layers of semi-crystalline polymers have been developed on the basis of the statistics of chain molecules by Huang and Brown [44,45]. The general assumptions of this model are that the crystallites are pre-existing entities and that the amorphous chains exit from the crystal surface obey random-walk or Gambler's ruin statistics in the domain between two neighboring crystallites. It is considered that the chain topology in a crystalline polymer is preserved during the crystallization stage. In this instance, the probability for a chain in the melt to build up intercrystalline TMs during crystallization is given by the probability of finding chain segments long enough to span an amorphous layer and the two adjacent crystalline lamellae. This concerns chain segments longer than $L=2L_c+L_a$, where L_c is the crystal lamellar thickness and L_a is interlamellar thickness. The TM probability is then given by the following equation based on Gaussian statistics for the chain segments at the moment of crystallization:

$$p = \frac{1}{3} \frac{\int_L^\infty r^2 \exp(-b^2 r^2) dr}{\int_0^\infty r^2 \exp(-b^2 r^2) dr} \quad (2)$$

with $b^2 = \frac{3}{2} \langle r^2 \rangle$, where $\langle r^2 \rangle$ is the mean-square value of the end-to-end distance of the entire chain in a random coil conformation. The value L for the lower limit of integration of the upper integral holds for the computation of the number of chain segments having an end-to-end distance greater than L . The $1/3$ factor represents for the fact that only chain segments with their end-to-end vector normal to the crystalline lamellar surface can actually make TMs. This probability of occurrence of TMs concerns an isolated chain.

This equation is valid for monodisperse systems. To account for the polydispersity, it should be introduced the molecular weight distribution of n (M):

$$\bar{p} = \frac{\int_0^\infty n p dM}{\int_0^\infty p dM} \quad (3)$$

where $n dM$ represents the number of molecules with a molecular weight between M and $M + dM$.

From this model, Huang and Brown calculated the fraction of tie molecules for PE with different concentration of comonomers. It is shown that the content of comonomers strongly influences the density of tie molecule (see figure 3.11).

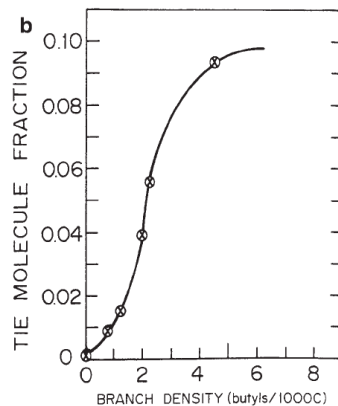


Figure 3.11. TM Fraction in function of comonomer density.[44]

However, this model can not take into account the influence of entanglements which play very important role in the stress hardening. Yeh and Runt[46] proposed to improve Huang and Brown's model by taking into consideration the chain entanglements in the amorphous layers. It turns out that the probability of chain entanglement is much greater than that of conventional TMs, and thus the latter can be neglected. However, this model is very hard to estimate the tie molecule and entanglements density for the isothermal crystallization sample which has much lower concentration of tie molecule and entanglement.

On the other hand, several indirect methods such as the natural ratio of deformation or hardening have been proposed to estimate the density of tie molecules and entanglements. Indeed, it has been shown that these parameters are correlated to the density of tie molecules and entanglements [47]. These methods will be discussed in a section following.

3.5.2 Stress transmitters

Previously, we discussed that during crystallization with folding chains, some molecules could be out the crystal, and then re-enter to the same crystal, or pervade the amorphous layer and enter an adjacent crystal. Entangled loops from adjacent lamellae can also form tie molecules. These are sketched in Figure 3.12.

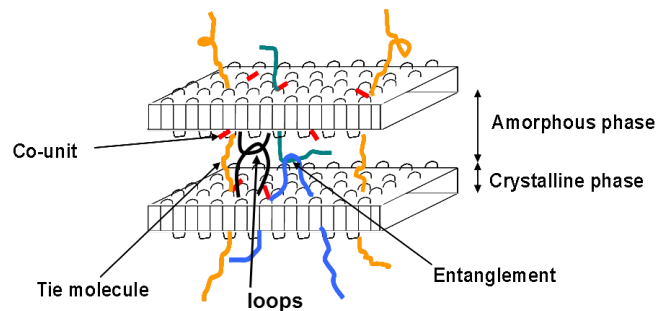


Figure 3.12. Schematic of the crystalline and amorphous lamella with different stress transmitters.

The presence of these connecting elements (tie molecules, loops) was first suggested by Keith and Padden [48] and then by Yoon Flory [49].

However, the mechanical efficiency of these links is sensitive to the temperature. Around the α relaxation temperature, the tie molecule relaxes due to the activation of the crystal stem mobility. According the description of Boyd [50], the crystal mobility permits the lengthening of a tight tie chain through shortening of two loops which permits more deformation of the amorphous fraction (see Figure 3.13).

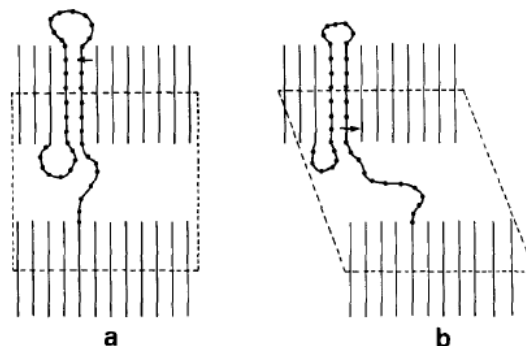


Figure 3.13. Further relaxation of the amorphous fraction resulting from mobility in crystal in α region [50].

Below the α relaxation temperature, these mechanical connections between the amorphous and crystalline phase enable the stress transform between these two phases. In our work, they are defined as "stress transmitters".

3.5.3 Interphase

In the non-crystalline regions, it is known that a third phase is present between the crystalline and amorphous phases, since the boundary between ordered crystalline regions and the disordered non-crystalline regions cannot be sharp (see Figure 3.14) [51,52,53,54].

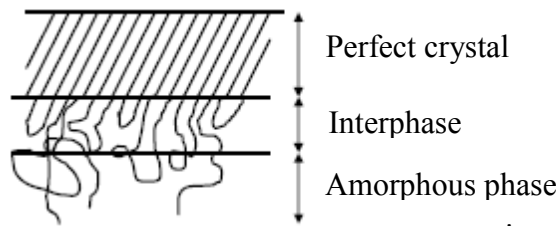


Figure 3.14. Interphase of semi-crystalline polymers

Some of the chains that emanate from the basal plane of the lamellar crystallites return to the same crystallite but not necessarily in juxtaposition. Other chains terminate in the amorphous phase or span multiple crystallites. The transition from well-ordered crystals to random amorphous chains is accompanied by a high chain flux and a highly restricted conformational environment. As a result a diffuse boundary or interphase is formed.[53]

The thickness of this interfacial region in linear polyethylene has been determined to be in the range of 10-30 Å and 7 – 13 vol%, depending largely on the molecular weight and chemical nature of the sample[52]. Increase in the molecular weight or co-unit content increases the fraction of interfacial material[51].

A variety of techniques such as ^{13}C nuclear magnetic resonance (n.m.r.), small angle neutron scattering (SANS), Raman spectroscopy and dielectric relaxation have shown that the interfacial region is a significant component in semi-crystalline polyethylene. Indeed, because of their differences in density and molecular mobility, it does not behave in the same manner as the amorphous phase or crystalline phase. Therefore, it is expected to influence the macroscopic mechanical properties of PE.

3.6 Crystal aggregates and spherulite

When polymers are crystallized from the melt, the lamellar crystals usually form more or less aggregates. The most common kind of aggregate is the spherulite, when crystallinity higher than 35% for polyethylene[55]. In spherulite, the lamellae are arranged radially (see figure 3.15) and the chains in the crystallites are lying tangentially.

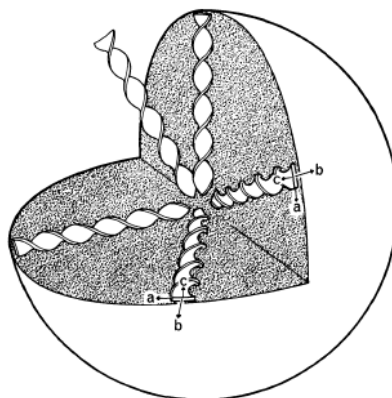


Figure 3.15. Schematic illustration of spherulites showing the crystal orientation for polyethylene.[56]

The architecture of spherulite has been studied in depth by Bassett et al. [57]. The principal observations they made is that the radiating lamellae so often exhibit a regular twist (see section

3.3). Another characteristic is lamella branching. This phenomenon enables to fill of the spherulite volume as it grows up. Crystal branches at a screw dislocation so that there is a mismatch between the mother and daughter crystals. Then the daughter lamellae tend to splay away from the motion. As more and more daughter crystals are formed, a sheaf-like structure developed [58].

Schultz [59] pointed out that the diameter of the spherulite depends essentially on the phenomenon of nucleation. For high supercooling, for example during fast cooling, the nucleation is dominating, which causes a large amount of spherulites. The size of spherulites will be small. For crystallization at low supercooling, the number of nuclei will be low so that the large spherulites will grow.

I.4 Intrinsic properties of crystalline and amorphous phase

4.1 Modulus of crystal lattice

The crystal lattice of polyethylene is anisotropic. In an orthorhombic lattice, three Young's modulus are related to the a, b, and c axes, i.e. E_a , E_b and E_c .

E_c can be measured by X-ray scattering (283GPa), Raman spectroscopy (290Gpa), and inelastic neutron scattering (329Gpa) at room temperature [60]. The molecule chains aligned along the c-axis thus the modulus is very high due to the stiffness of the chemical covalent. Comparatively, E_a and E_b are much smaller, i.e. 7.5 GPa and 6.9 GPa respectively. However, all the lattice moduli are much higher than the Young's modulus measured from macroscopic stress-strain curves.

The lattice moduli also show strong temperature dependence. This could be illustrated with calculations by Lacks and Rutledge (see Table 4.1) [61]. It should be noted that these computations were made with an assumption that the crystal is a perfect lattice. If there is a defect in the crystal, the modulus should be decreased.

Table 4.1. Young's modulus of lattice in three axils [61].

modulus	0 K	100 K	200 K	300 K	400 K
E_a (GPa)	10.5	9.5	7.9	7.5	5.7
E_b (GPa)	9.5	8.8	7.8	6.9	6.6
E_c (GPa)	318	312	301	283	259

4.2 Modulus of interlamellar amorphous phase

For polyethylene and polypropylene, the glass transition temperature of the amorphous phase is lower than room temperature; therefore the amorphous phase is in the rubbery state at room temperature. Chain entanglements are the cause of rubber-elastic properties in the liquid state. The kinetic theory of rubber elasticity, which was particularly developed by Flory, leads to the following equation for the amorphous phase of thermoplastic polymers above the glass transition temperature [62]:

$$G_N^0 = \frac{\rho RT}{M_e} \quad (5)$$

where G_N^0 is the shear modulus at plateau, ρ the amorphous phase density, R the ideal gas constant, T the temperature and M_e the molar mass between entanglements. For PE with M_e 1.4 kg/mol, G_N^0 is only 4.5 MPa at ambient [63]. This value is much smaller than the value fitted with Tsai-Halpin equation from bulk PE modulus which gets 130 MPa for polyethylene amorphous phase at room temperature [64]. This difference may be ascribed to the stress transmitter structures which could enhance the amorphous phase. On the other hand, the shape factor also strongly influences the amorphous phase modulus. The interlamellar amorphous phase is confirmed between two crystal lamellae having a high shape factor. When the interlamellar separation occurs under tensile stretch, the amorphous matters would have to flow from the surroundings into the opening gap

between the lamellae. This phenomenon is restricted by the confinement effect. It results in an increase of the amorphous modulus which is no longer a Young's modulus but a combination of Yang's and bulk moduli.

I.5 Influence of temperature – relaxation behavior

Semicrystalline polyethylene shows a strong dependence of elastic properties on the temperature. The elastic modulus curve of polyethylene against the temperature can be divided into distinct regions. These regions are directly related to the mobility of chains or groups can be studied by DMA (dynamic mechanical analysis) (see Figure 5.1). At very low temperatures, polyethylene behaves like a glass and exhibit a high modulus. As increasing the temperature, the modulus decreases. The fall in modulus through the glass transition region for semicrystalline polymer is between one and two orders of magnitude, i.e. much less than for thoroughly amorphous polymers, and the change in modulus or loss factor with temperature is much more gradual, indicating a broader relaxation time spectrum. At high temperatures, molecular mobility is severely curtailed by the crystalline phase that generates specific relaxation phenomena in comparison to amorphous phase. The semi-crystalline polyethylene undergoes three different relaxations: γ , β and α (see Figure 5.1). The origins of these three relaxations have been widely discussed but are still controversial.

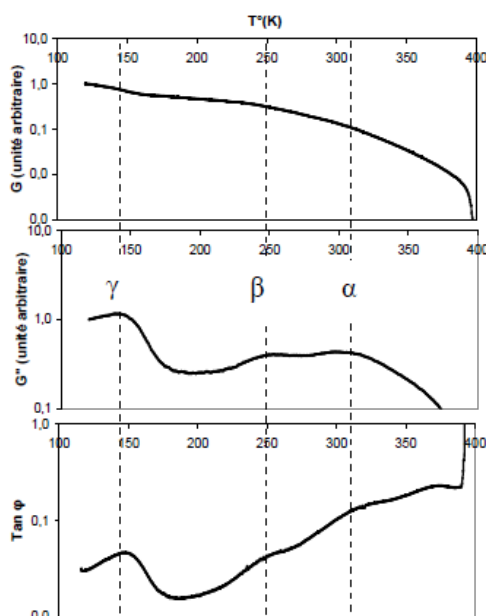


Figure 5.1. G' , G'' and $\tan\phi$ of PE in function of temperature [18].

Let's start at low T when all mobilities are locked. Then increasing temperature will result in the activation of the various relaxations.

5.1 γ relaxation

The γ relaxation of PE takes place between 120 and 180 K.

Many authors proposed that γ relaxation is due to the movement of small chain segments presented in the amorphous phase [64]. Some consider that this relaxation can be attributed to the glass transition [65].

However, Sinnott and Hoffman [66] also observed this relaxation in the study of a single crystal of PE. They concluded that the γ relaxation was related to defects in the crystalline phase and was caused by the reorientation of chains in the crystal. Nitta et al. [65] held the same opinion. Further, they noted that the temperature T_γ increases with the number of carbon atoms presented in the chains folds at the crystal surface.

Based on these assumptions, Khanna [67] explains that this relaxation is associated with movements of small segments (3 or 4 CH₂) of the amorphous and in addition to the reorientation of dangling chains present in the crystal and in amorphous.

Boyd et al claimed that γ processes can be regarded as 'sub-glass' relaxation. They further suggest that process involves molecular motions that are relatively short range in character in comparison with those associated with the glass-rubber (β) relaxation (see Figure 5.2).

The γ relaxation depends on comonomers concentration and thermal history [55]. This is quite logical in the assumption that the γ relaxation is due to the movement of crystal chains and chain folds at the interface between the crystalline and the amorphous phase since the comonomers affect the surface topology of the crystal.

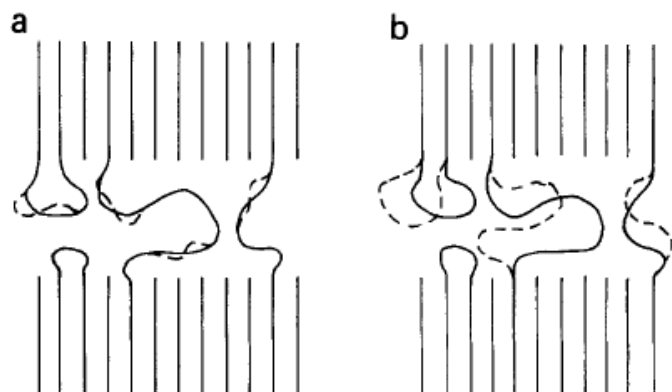


Figure 5.2. (a) Schematic representation of molecular motion localized or confined to certain portions of amorphous chains and postulated to be of the type responsible for γ relaxations. (b) More general amorphous phase segmental motion underlying the β relaxation. [50]

5.2 β relaxation

The β relaxation occurs in the temperature range 200 – 270 K. It is detected in branched PE (for comonomers density more than 0.6 mol %) or ultra high molecule weight PE [68].

Many authors considered β relaxation of PE as the glass transition [50,67]. As a matter of fact, this relaxation is not detected for a single crystal [66]. As a result, Khanna [67] deduced that β relaxation of PE is related to the amorphous phase. It would be associated to the movement of branches in the amorphous phase. This theory is supported by the correlation between the intensity of β transition and the amorphous phase content. The transition temperature T_β correlates to the molecular weight M_w and the type of branch.

Other authors considered that β relaxation of PE associates with the glass transition of the interphase [68]. More specifically, it is ascribed to the movement of chain segments present in the interphase, such as loops and molecules links. The intensity of this relaxation is indeed strong when the interphase content is high.

The comonomer density significantly affects the β relaxation: T_β depends on the nature of the branch. Furthermore, the amplitude of the relaxation is a function of comonomers concentration [55,68]. This can be explained by the fact that the higher the comonomer concentration, the higher content of interphase is.

Nitta [65] proposed that, for HDPE, the β relaxation is associated with the glass transition of the interphase while for LDPE, it is associated to molecular movements in amorphous portions of the chains which mobility is restricted by the crystalline lamellae.

It is difficult to conclude on the exact origin of this relaxation. The higher the comonomers concentration, the lower the crystallinity and the higher the amorphous phase content.

5.3 α relaxation

The α relaxation appears in the temperature range 270 – 350 K. Reneker [69] proposed a mechanism of diffusion of crystal defect. Many authors also believed that the α transition is related to molecular motion within the crystal along the chain axis [65,68].

Boyd [50] proposed another theory: the α relaxation take place in the amorphous phase via the activation of chain mobility crystal. Khanna [67] also considered that the α relaxation is attributed to the interphase movement or the chains connecting amorphous and crystalline phase. Furthermore, he explained that the temperature T_α increases with increasing thickness of the crystal is due to the increase of the chain stems in the crystal which requires more energy to be in motion. Sinnott [66] reported 2 relaxation process α_1 and α_2 assigned to chain motions within and between crystal blocks in the lamellae. To sum up, the origin of the α relaxation is most likely due to the mobility of the chains in the crystal, either directly or indirectly.

I.6 Stress strain behavior of semi-crystalline polymer

6.1 Stress strain curve

The tensile test measures the resistance of a material to a static or slowly applied force. Figure 6.1 shows a typical stress-strain curve for a semi-crystalline polymer and the evolution of the sample shape during tensile test.

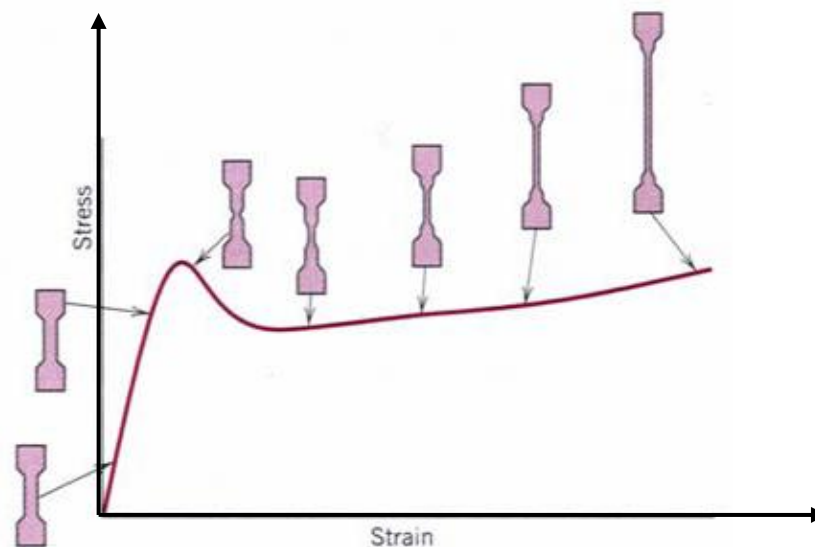


Table 6.1. A typical stress-strain curve with sample shape evolution during tensile test.

During tensile deformation, first occurs a linear elastic region; then yielding appears accompanied by a drop in stress and the formation of a neck; stress increases gradually due to straightening of polymer chain, and finally fracture (see Figure 6.1).

In the linear elastic region, the deformation is reversible. When the stress is removed, recovery is almost instantaneous. Once the yield stress is exceeded the polymer deforms plastically. This causes permanent deformation [70]. Plastic deformation involves several mechanisms that will be discussed in the following sections.

Natural draw ratio

Tensile drawing of the semi-crystalline polymers below the melting temperature is often accompanied by necking. After yield, the stress drops due to the localization of the plastic deformation i.e. a quick cross-section reduction. This plastic localization or necking proceeds to a strain value that is called the natural draw ratio, λ_n . Beyond yielding, neck propagates over the whole length of the sample at nearly constant engineering stress. At the end of the process, the

whole sample is plastically deformed with a uniform draw ratio equal to λ_n . Figure 6.2 show how the parameter λ_n is measured

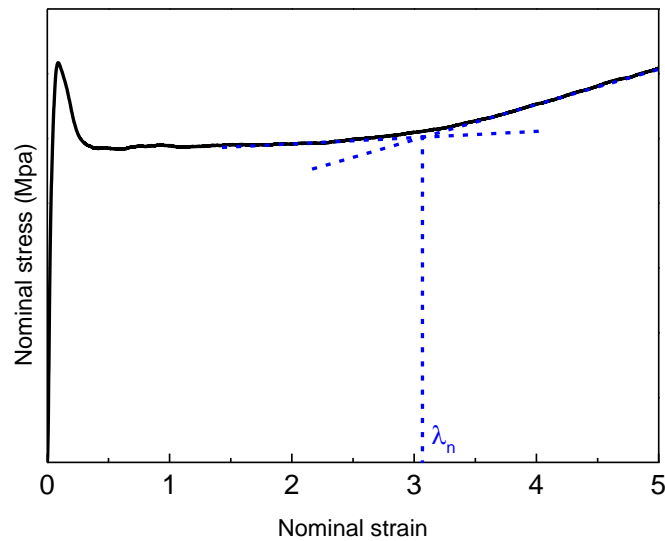


Figure 6.2. Indication of natural draw ratio λ_n from a stress strain curve.

The natural draw ratio that develops in solid polymers under tensile drawing is a direct consequence of the constitutive law of the material, but its physical origin is still not well understood from both structural and molecular aspects. However, for the semi-crystalline polymers, the natural draw ratio is an external manifestation of the intimate deformation processes of the material, which depend on its specific structural features. It is correlated with the density of tie molecules and is particularly useful for predicting long-term properties of polyethylene [47].

6.2 Elastic deformation

6.2.1 Microstructure evolution

Generally, for the semi-crystalline polymers, the elastic domain is very small. The yield strain is usually lower than 1.5%. Within a very low strain, the deformation could be mainly assigned to the amorphous phase because the crystalline is much stiffer than the amorphous phase in the case of polyethylene.

Three modes of deformation in the amorphous component have been postulated as being associated with lamellar structure [70]. They are: interlamellar separation, interlamellar shear and lamella stack rotation (see Figure 6.3). These mechanisms mainly depend on the orientation of lamellar.

The interlamellar slide mode involves simple shear of the amorphous region between lamellar crystals with the shear direction being parallel to the lamella surface. Evidence of interlamellar shear is provided by the variation of lamellar orientation detected by SAXS, in deformed PE at room temperature and above [71]. This mode is predominant for the lamellae at 45° orientation angle with respect to the tensile force. This deformation mode is a relatively easy mechanism to operate compared with other modes.[72]. It is in competition with chain slip in the crystal during a deformation [73]. However, the difference is that this interlamellar shear is almost completely reversible as observed by Young et al.[74]

Interlamellar separation mode involves changes of the distance between adjacent lamellae (Fig. 6.3b). Generally, it occurs in the lamellae whose normal is parallel to the tensile force. When the interlamellar separation occurs, the amorphous matter has to flow into the opening gaps between the lamellae from the surroundings. If this does not happen, the separation mode must involve the

large density changes or cavitations. This deformation mechanism should greatly depend on the local properties and microstructure of the interlamellar amorphous phase, i.e. taut tie molecules density and modulus of the interlamellar amorphous phase.

On the other hand, reversibility of deformation associated with interlamellar separation was found for strains as high as 0.4 [75]. The high reversibility of deformations due to interlamellar separation is said to be governed by the rubbery behavior of the tie molecules and the entropic lack stresses induced by their elongation.

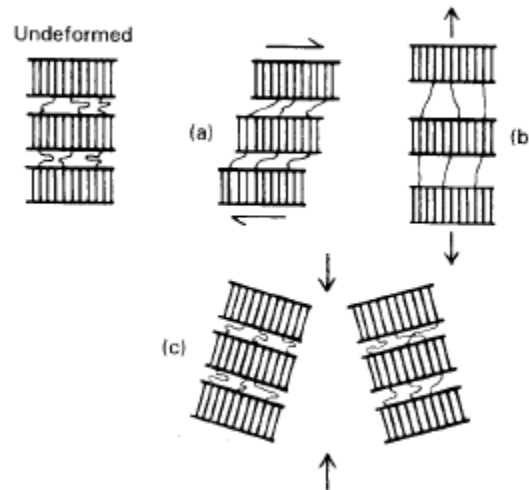


Figure 6.3. Models of deformation in amorphous region: (a) interlamellar slip, (b) interlamellar separation, (c) stack rotation.

The movement of surrounding amorphous regions and orientation of lamellae often needs rotation of the lamellae stacks (Figure. 6.3c). A direct observation of rotation of stacks of lamellae was obtained by Tagawa [76]. He reported that the lamellar units containing three to ten lamellar crystals acted as one body and did not separate into single lamellae during deformation.

6.2.2 Elastic Modulus

Linear elastic deformation is governed by Hooke's law, which writes as:

$$\sigma = E\varepsilon \quad (4)$$

where σ is the applied stress, E is a material constant called Young's modulus, and ε is the resulting strain. This relationship only applies in the linear elastic range. It should be noted that not all elastic materials undergo linear elastic deformation. Some polymers may present nonlinear deformation.

In modulus calculation it is assumed that deformation is homogeneous at low strains and that deformation occurs only in the gauge region of the sample. Ideally the strain used in the calculation of modulus is defined as the elongation of the specimen relative to its original gauge length. The standard deviation for a series of specimens cut from a single sample should not exceed 5% for a given calculation method [6].

For the majority of isotropic samples, the elastic modulus increases approximately linearly with the degree of crystallinity. Except in the case of high co-unit copolymers, the data for linear and branched polyethylenes follows the same approximate relationship (see Figure 6.4).

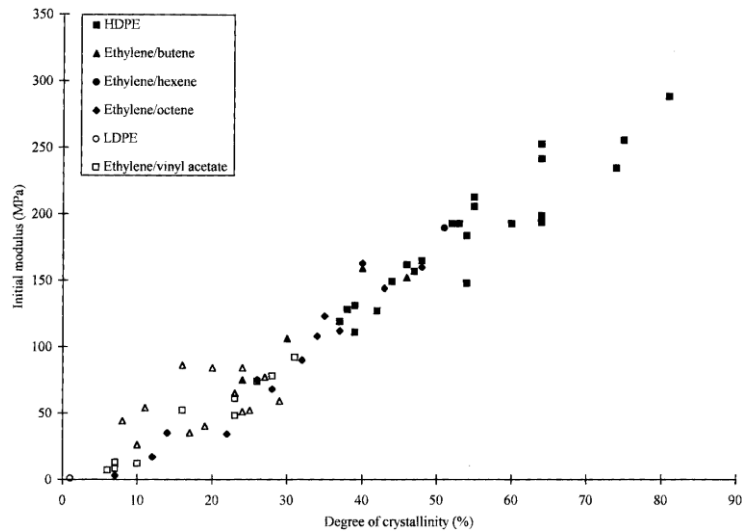


Figure 6.4. Plot of initial modulus as a function of crystallinity for various isotropic polyethylene samples.[77]

The elastic modulus of high density polyethylene strongly depends on the molecular orientation. This relationship has been illustrated by the experiments performed on high density polyethylene drawn to various ratios in Figure 6.5. At the highest degrees of orientation, the elastic modulus of the resulting fibers approaches that calculated for perfectly aligned polyethylene.

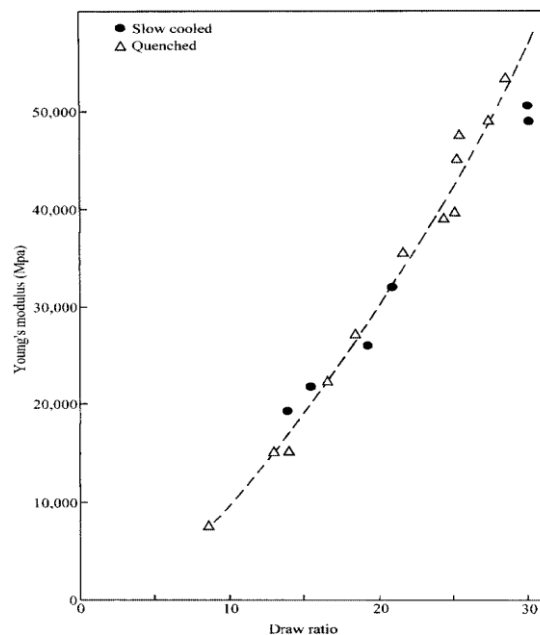


Figure 6.5 Plot of Young's modulus of high density polyethylene as a function of orientation.[78]

6.2.3 Models for elastic modulus

For the semicrystalline polymers consisting of amorphous phase and crystalline phases, the macroscopic modulus not only relates to the intrinsic properties of the amorphous and crystalline phases, but also to the coupling of these two phases. There are two classic couplings, Voigt and Reuss, series and parallel coupling respectively (see Figure 6.6).

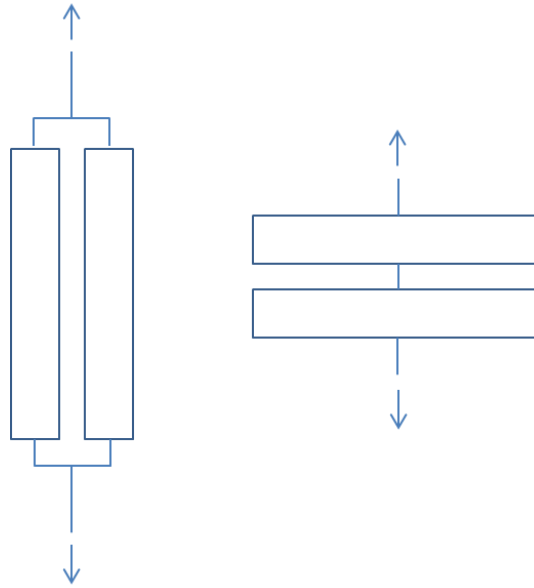


Figure 6.6.schematic of Voigt and Reuss couplings.

For the voigt coupling condition, the average modulus E could be written as:

$$E = E_c V_c + E_a V_a \quad (6)$$

Where V_c and V_a are the volume fraction of crystalline and amorphous phase, E_c and E_a are the modulus of crystal component and amorphous phase.

For the Reuss coupling condition, there is:

$$\frac{1}{E} = \frac{V_c}{E_c} + \frac{V_a}{E_a} \quad (7)$$

Halpin and Kardos[20] developed a model to predict the moduli of isotropic crystalline polymers by a simple extension of an earlier analysis for fibrous composites. The modulus can be written as:

$$E = E_m (1 + a\eta V_f) (1 - \eta V_f)^{-1} \quad (8)$$

$$\text{where } \eta = \left(\frac{E_f}{E_m} - 1 \right) \left(\frac{E_f}{E_m} + 1 \right)^{-1} \quad (9)$$

The subscripts m and f refer to the matrix and reinforcing fibers in the composites, otherwise the amorphous phase and crystalline components in the semicrystalline polymer, and V_f is the volume fraction of crystalline component, and a is an adjustable parameter.

On the other hand, some authors have tried to take into account the mechanical coupling between the amorphous and crystalline phases [55,79,80,81]. However, as there is little information about the density and stiffness of tie molecules, it is difficult to analyze their real influence on the elastic modulus.

6.3 Plastic deformation

When some semi-crystalline polymers subjected to a uniaxial load, they exhibit a distinctive cold drawing phenomenon. During cold drawing, the sample yield and then neck is induced. As neck propagating, the initial lamellar structure transforms to an oriented fibrous structure and its strength and modulus increase significantly in the tensile direction. Although neck and cold drawing are easily observed at a macroscopic level, the mechanism whereby the spherulite transform to the fibrous structure at the molecular level are very complex that it is still subject of debate. A lot of works on plastic deformation mechanisms of semi-crystalline polymers have been published. Among these deformation mechanisms, it is governed by various such as crystallites shear, cavitation, martensitic transformation et al. These mechanisms will be presented in this section.

6.3.1 Crystal shear in lamella

Under increasing shear stress, the initial reversible elastic response of a crystal eventually gives way to plastic behavior. The plastic deformation mainly involves the deformation of crystalline lamellae by various crystallographic processes. Slip is the dominant mode of plastic deformation of polymer crystals[70]. When a critical shear stress is reached on the slip plane in the slip direction, dislocation motion occurs on the slip plane and causes the two parts of the crystal separated by the plane to undergo a relative translation.

Crystallographic slip is characterized by two vectors, (hkl) and $[uvw]$, which defined as the ‘slip system’. The vectors (hkl) and $[uvw]$ represent the ‘slip plane’ unit normal vector and the ‘slip direction’ of the slip plane, respectively. Figure 6.7 shows a possible slip plane of polyethylene crystal.

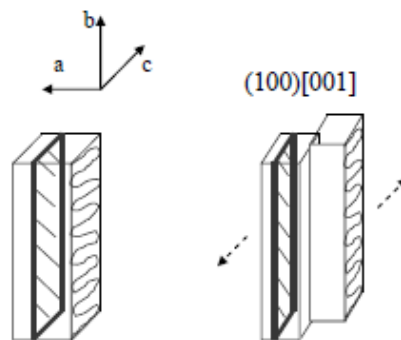


Figure 6.7. Schematic of slip plane of polyethylene crystal.

Polymers have long chain structure. This requires the preferred slip plane contains the molecule chain to avoid the break of the chain during the slip. This means the slip plane must be of the $(hk0)$ type for PE crystal. This could be confirmed from that the PE chains can remain unbroken through very large deformations observed by Peterlin[82]. Geil[83]observed similarly that the chain slip without chain unfolding or fracture occurs in PE single crystals for elongations up to at least 150%.

There exists two type of dislocation in a crystal established by its Burgers vector. When the Burgers vector is parallel to the chain axis the deformation is called ‘chain slip’, and when perpendicular it is called ‘transverse slip’. Both types of dislocations in a crystal are governed first by minimum energy considerations, based on the line energy of the dislocation. Shadrake and Guiu[84] calculated the line energy of dislocation for ten kinds of possible dislocations in a orthorhombic PE crystal. They found that $[00c]$ screw dislocations have the lowest line energy. For each slip system, it has a critical shear stress (see Table 6.1). The slip plane (100) has relatively smaller critical shear stress.

Table 6.1.The critical stress for different slip systems [70].

polymer	Slip system	critical shear stress τ_0 (MPa)
PE	$(100)[001]$	7.2
	$(010)[001]$	15.6
	$(110)[001]$	>13
	$(100)[010]$	12.2

Chain slip can occur in two different ways to achieve the same macroscopic deformation: fine slip and coarse slip [70,72]. When fine slip occurs, a small amount of slip occurs equally on a large number of parallel planes (Figure 6.8 a). This will result in a change of the angle between the molecular chain axis and the normal to the lamellar surface. Whereas, when coarse slip occurs,

only a few parallel planes slip (Figure 6.8 b). The angle between the chain axis and lamellar normal will not change. These two types of slip are observed from SAXS and WAXS according to the angle difference between chains and lamella surface.

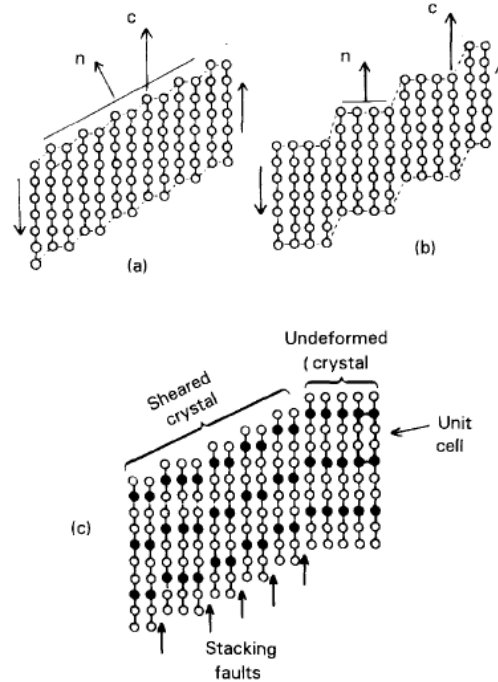


Figure 6.8. Schematic illustrations of different degrees of fineness of slip. (a) fine slip; (b) coarser slip; (c) shearing of a lattice that has a large lattice translation vector in the chain direction by fine slip of partial dislocation.[72]

At yield point, the major mechanism involves the start of the crystal slip[85]. To simplify the study and modeling of the yield stress σ_y , it is supposed that only the crystal shear induces the yield. Shearing of crystalline lamellae was the subject of numerous studies and it is now accepted that it is controlled by nucleation and motion of screw dislocations in the direction of the chain axis [001] [86]. Therefore, the dislocation model associates the critical stress with the yield stress. The yield stress could be expressed as:[86,87]

$$\sigma_y = \frac{K}{\pi} \alpha(T) \exp\left[-\left(\frac{2\pi\Delta G_c}{L_c K b^2} + 1\right)\right] \quad (10)$$

$$\text{With } \alpha(T) = \frac{b}{r_0} \exp\left(\frac{2\pi\Delta E_0}{L_c K b^2}\right) \quad (11)$$

Where K is the shear modulus of crystal, b is the burgers vector, L_c is the thickness of the lamella, r_0 is the dislocation radius, E_0 is the core energy.

This model successfully associated the yield stress with L_c , however, it does not consider other factors which could influence the yield, such as tie molecules and couplings.

Studies have shown that the molecular topology as the molecular weight, comonomer concentration, and entanglement content also had an influence on the plastic deformation [2,41,77]. In fact, prior to reaching the yield stress, the viscoelastic material undergoes deformations mainly governed by the amorphous phase. Shearing of crystallites occurs then. The mechanical coupling between the amorphous phase and the crystalline phase is crucial for the plastic deformation. It is supposed that the force applied to the lamella is the same regardless of the number of tie molecules. However, the more density of tie molecules, the lower the stresses will be concentrated at the points of anchoring of the tie molecules. In this situation, the crystal is going to slip sooner.

Nitta et al. [118, 119] had constructed a model that takes into account the influence of tie molecules. The model considered the microstructure of PE by lamellar stacks linked with tie molecules (see Figure 6.9). When loaded in tension, the lamellae are then subjected to bending due to the support of tie molecules. If there are more tie molecules which is close to each other, it is more difficult to break the lamellar. This distance between the tie molecules is a function of the number of tie molecules: the higher the density of molecules, the closer the tie molecules to each other. At the macroscopic scale, they also found that there is a linear dependence of the yield stress on the tie molecule fraction.

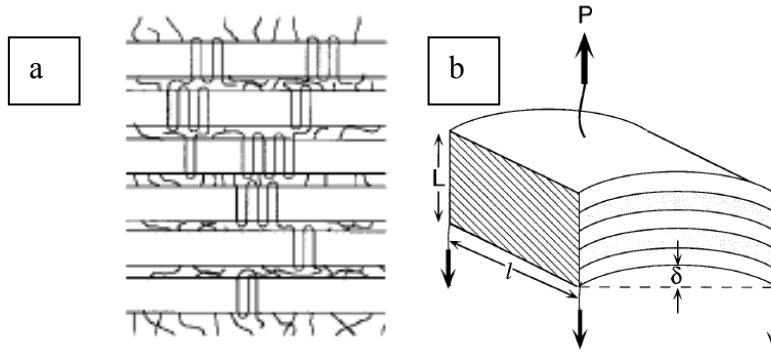


Figure 6.9. schematic of lamella stacks linked with tie molecules. (a) without deformation; (b) bending lamellar cluster after deformation.

Temperature also plays an important role on the deformation of the crystallites. Crystallite shear via dislocation mechanisms is strongly influenced by temperature [72,88,89]. As known when temperature is higher than a transition temperature, the modulus of crystalline polymers drops significantly. Indeed, the crystal can relax above this temperature, which could improve the mobility of chains promoting the nucleation of dislocations.

At macroscopic scale, the yield stress relates to the temperature and strain rate with Eyring equation. It is expressed as:[88]

$$\frac{\sigma}{T} = \frac{R}{v} \left(\frac{\Delta H}{RT} + \ln \frac{2\dot{\epsilon}}{\dot{\epsilon}_0} \right) \quad (12)$$

where R is the gas constant, v is frequency, ΔH is activation energy, $\dot{\epsilon}$ is strain rate. At a constant tensile rate, σ is linearly related to temperature.

In conclusion, the density of stress transmitters is an important parameter to induce shear of crystallites. Their role is to transmit the stresses of the amorphous to crystalline phase. The higher the density, the higher the stress concentration at the edges of the crystallite, which significantly influences the shearing of the crystallite. Therefore, it is important to take into account in modelling of the plastic deformation.

6.3.2 Martensitic transformation in polyethylene

The martensitic transformation was observed in PE which involves a mechanism transforming the orthorhombic to a monoclinic lattice. Occurrence of stress induced martensitic phase transformations in polymer crystals is indicated by x-ray reflection and electron diffraction [90,91,92,93].

The monoclinic form in PE is a metastable phase and only appears under stress. After relaxation at room temperature, the monoclinic phase is converted back into orthorhombic phase [94]. Furthermore, the monoclinic phase is unstable above 110 °C. Kikuchi and Krimm [95] found that when deformed single crystals were annealed and converted from the monoclinic phase back to the ordinary orthorhombic structure, the crystals changed the fold plane from (110) to (100). This led them to suggest that the monoclinic structure is an intermediate state in the fold-plane transformation.

This transformation is induced by a transverse slip process according to Young [96]. Like any slip system, this transverse slip is more or less depending on orientation with respect to the shear stress. As a result, not all the lamellae in the spherulite undergo the martensitic transformation. However, the lamellae which the transformation occurs are not yet clear identified.

Indeed, some authors argue that it occurs in the lamellae located at the equator.[97] But this is contradicted with Butler[92] who found that normal of transformed lamellae is inclined relative to the tensile direction which could conclude equatorial lamellae do not occur transformation. Moreover, studies have shown that the martensitic transformation can also occur on the lamellae oriented to the tensile direction, which is the case of polar lamellae.[98,99]

Recently, Butler [90,91,92,93,100] studied the martensitic transformation of bulk crystallized PE with in-situ WAXS and SAXS. Two PE are compared: HDPE (high density PE) and LLDPE (linear low density PE). In both cases, the increase of monoclinic phase is portioned to the decrease of orthorhombic phase. For both materials (HDPE and LLDPE), processing occurs near the yield stress. However, it occurs at lower macroscopic strain for HDPE than that for LLDPE. Butler explained by the fact that the amorphous phase of the LLDPE may be deformed more than HDPE, thus plastic deformation does not take place on the same macroscopic deformation. Similarly, HDPE with thicker crystallite undergoes martensitic transformation at lower deformations. Therefore, it seems that the martensitic transformation is influenced by the microstructure parameters of PE. But there are very few investigations on this.

6.3.3 Cavitation

Cavitation phenomenon is observed during deformation in many semi-crystalline polymers and generates many changes in the microstructure. Numerous voids (cavities) both nanometer and micrometer size are formed inside amorphous phase between lamellae during deformation of a polymer (see Figure 6.10). This cavitation is observed only in tension, never in compression or shearing.

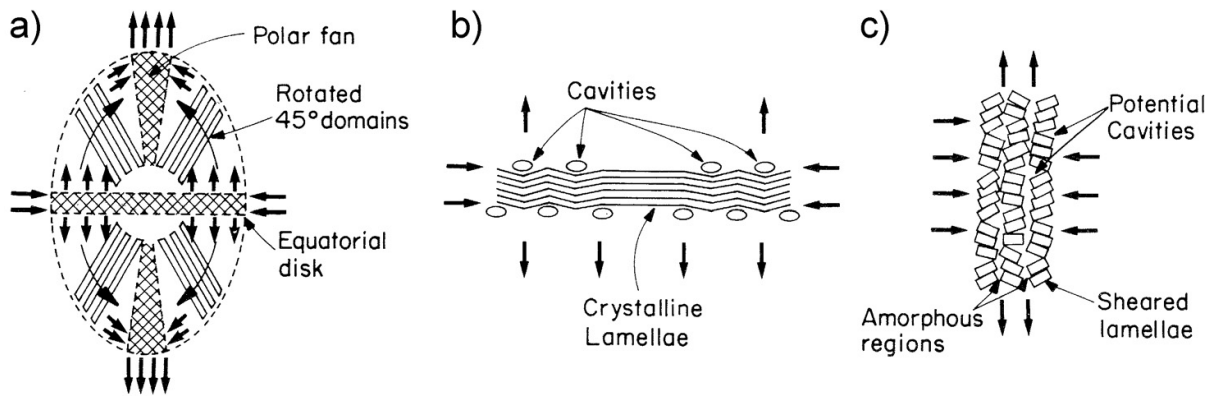


Figure 6.10. (a) Tensile deformation of a spherulite; (b) Lamellae kinking and formation of cavities in equatorial zones of a spherulite; (c) Lamellae fragmentation occurs in polar fans of spherulites, potential cavities may be also expected.[101]

The cavitation has been detected by microscopic, X-ray scattering and volume strain measurements [90,102,103]. Among these methods, the small angle X-ray scattering (SAXS) is one of the most popular methods for characterization of polymers internal cavitation [104,105,106,107]. The cavities scatter X-ray strongly due to the big electron density contrast between matter and voids. Recently, instead of the classic X-ray source the synchrotron radiation has been often applied for the studies of polymers [104,105,108]. The main advantage synchrotron X-ray radiation source is the possibility of recording of SAXS patterns in real time during the tensile deformation. The time of single pattern acquisition on synchrotron beamline is reduced to 1–30 s. The larger cavities (with a size exceeding 0.5 μm) scatter the light and this scattering is visible as a whitening of the material. Many authors observed stress-whitening of deformed polymers, but most of these observations had only qualitative nature [109,110].

Usually the cavitation process is observed in polymers present spherulite morphology. The cavitation may appear in a spherulite boundary or inside it. It has been confirmed by scanning electron microscopy that both are possible [111]. Cavitation inside a spherulite can be expected in its equatorial or polar parts. In these regions, the shear does not dominate. According to Castagnet et al, [112] the cavities appear initially in the equatorial regions of the spherulite. It is believed that the lamellae are subjected to a local tensile stress in this region, causing the lamellar separation which could favor the initiation of the cavitation. On the other hand, Nitta et al [113] observed the initiate of cavitation in both regions by in situ observation of uniaxial deformation of isolated individual large spherulite of isotactic polypropylene (see Figure 6.11). In the case of a spherulite with few tangential lamellae, arc shaped cracks appear in the polar zone of the spherulite and then the radial craze-like fracture begins in the equatorial region perpendicular to the stretching axis. In the case of a spherulite with a large number of tangential lamellae, however, the radial crazing appears in the equatorial zone and then cracks are initiated in the polar region. They explained that the crack formation depends on the anisotropy in strength of crystalline lamellae.

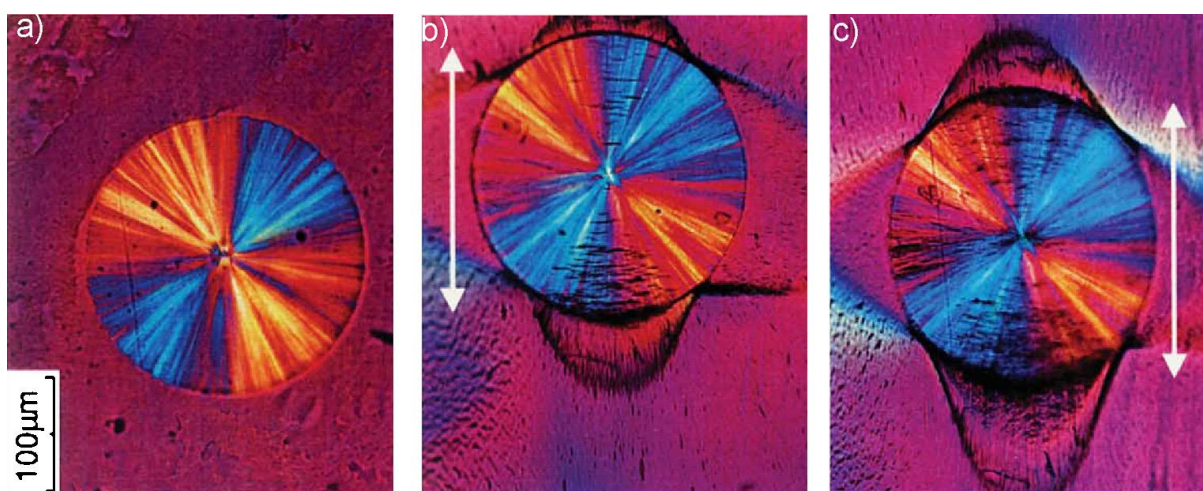


Figure 6.11. In situ observation of the deformation of a PP spherulite, crystallized at 130°C, embedded in a smectic matrix. The arrows indicate the stretching direction. The longitudinal strains were (a) $\varepsilon = 0$, (b) $\varepsilon = 0.042$, (c) $\varepsilon = 0.062$. [113]

Many polymers cavitate during deformation, however, polymer morphology and experimental conditions are crucial. Pawlak and Galeski [105] compared mechanical properties of eight polymers deformed in tension and in plane strain compression. In the compression mode of deformation cavitation was not observed in any of the polymers while in tension some polymers cavitated. The polymers cavitated with higher crystallinity and thicker crystals. Moreover, Castagnet [114] assumed that cavities nucleate and grow in the amorphous phase, located in the interface between the amorphous and crystalline lamellae. Therefore, the interface properties can influence the process of cavitation.

Cavitation changes the macroscopic yield stress σ_y . This phenomenon could be observed from the curves of tensile and compression experiments (see Figure 6.12) obtained by Galaski et al [105]. The conclusion from the experiments is that with an increase of deformation there is a kind of competition between two possible processes: cavitation of amorphous phase and plastic deformation of crystals. If the crystals are compliant, defected, then their plastic deformation is easy while the strength of amorphous phase prevents for cavitation. If the crystals are thick, with reduced number of dislocations (dominant type of defects) the breaking of amorphous phase is easier and occurs first. [101]

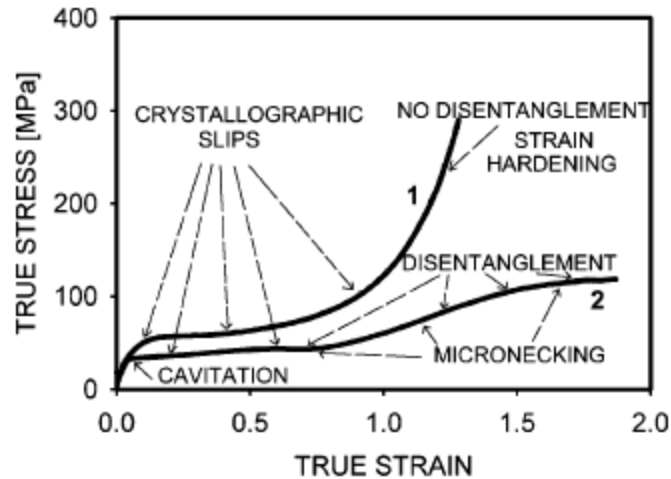


Figure 6.12. Stress strain curves of HDPE obtained from tensile and compression. Curve 1 is from die compression and curve 2 is from tensile test.[105]

Humbert et al.[108] presented similar explanation of yield stress decrease observed in tension. They compared stress for breaking of amorphous phase (σ_{cav}) and stress of plastic deformation of crystals (σ_{sh}). They calculated the dependences of those stresses as a function of crystal thickness and showed that certain critical thickness exists, above which the cavitation is more probable. For examined PE, the critical thickness was 19 nm. When crystals are thinner and $\sigma_{sh} < \sigma_{cav}$, the shear of crystal occurs. However, in this situation, if the difference between σ_{sh} and σ_{cav} is small, some limited cavitation also possible occurs after crystal shear. If $\sigma_{sh} \ll \sigma_{cav}$, the crystal shearing is initiated without cavitation. When $\sigma_{sh} \gg \sigma_{cav}$, the cavitation will occur very quickly before crystallite shear.

The onset of cavitation could be determined by in situ SAXS measurements. It was observed that cavitation could appear before yield, exactly at yield and after yield. In the study of Humbert et al.[108], all types of the cavitation had been observed in PEs with different microstructures. For the PEs with thicker crystalline lamella, the cavities initiate before yield whereas it appears after yield for the PEs with thinner crystalline lamella. They also found that thermal treatment significantly influence the onset of cavities. For example, a quenched PE does not show a scattering of cavities, but after annealing cavitation could appear before or after yield. It is explained that the thermal treatment increases the crystalline thickness and perfection of crystallite which favors the initiation of cavitation.

The influence of molecular parameters on cavitation was also examined [115]. It appears that the cavitation is more important when the molecular weight is small. The author explains this by the fact that a lower molecular weight results in less entanglement during crystallization.

Castagnet [114] also observed the influence of the amorphous phase on cavitation formation. In annealed materials, small coarse crystallites can be present in the amorphous phase. The mobility of the amorphous is diminished by the presence of small crystallites. This low mobility prevents nucleation of cavities during separation of the lamellae. On the other hand, Seguela [41] remarked that the direct consequence of the change in crystal lamellae thickness is the change of the intercrystalline tie chain density. The smaller crystal thickness should include a significantly greater tie chain density. This structural factor is favorable for preventing cavitation at the border of crystal fragments at moment of lamella fragmentation in spherulite with thin lamellae [116].

Temperature is another important parameter influencing the cavity formation. Pawlak and Galeski [111] described the properties of polypropylene deformed at temperatures of 25, 40, 70 and 100 °C (see Figure 6.13). The rapid decrease of light transmittance by polymer was observed shortly after yield, when the experiments were done at 25 or 40 °C. The whitening of specimens was the evidence of micro cavitation. Also SAXS analysis confirmed cavitation process (in nano scale) at

25–40 °C. However, in the higher temperatures the scattering of X-ray scattering on voids and whitening were not observed.

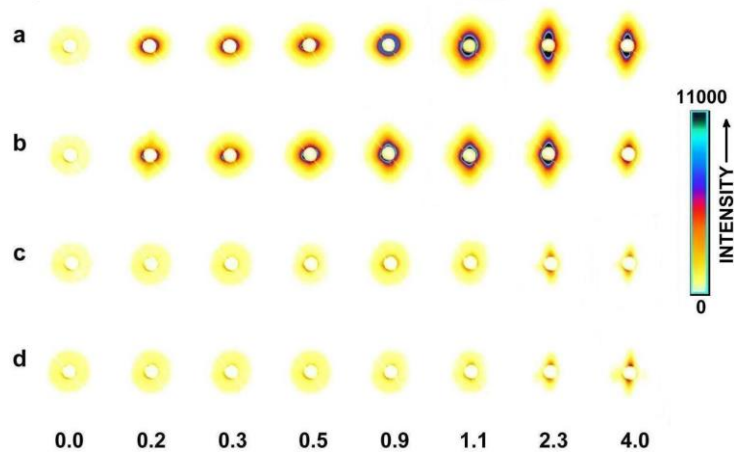


Figure 6.13. Small-angle X-ray scattering from PP samples after deformation. Numbers indicate local strains. Temperatures of deformation: (a) 25°C, (b) 40°C, (c) 70°C, (d) 100°C. Horizontal deformation.

In conclusion, the cavitation formation ability is mainly determined by the crystalline parameters such as crystallinity, lamella thickness. There are many works about the influence of crystalline structure. On the other hand, amorphous phase structure also plays an important role on preventing cavitations formation. However, there are few works on it. The more studies on the role of amorphous phase need to be done.

6.3.4 Fibrillar transformation

The deformation at large strains of semi-crystalline polymers often involves conversion of spherulite structure into an oriented fibrous structure known as fibrillar transformation [71,117,118,119,120,121]. Previous studies by Petellin et al. have been conducted on single crystal mat, using TEM and SAXS. These authors found that the dimension of the crystalline blocks of the fibrils in the stretching direction was close to the thickness of the initial single crystals before deformation [117,120,122]. The crystalline blocks in the deformed materials were believed to be fragments of the precursor PE single crystal. Based on these reports, the fibrillar transformation process were described as the fragmentation of the lamellar crystals into blocks that rearrange into the micro-fibrils via chain unfolding from the fracture surface of the crystal blocks. This model was referred to as Peterlin's model.

This model assumes that the polymer crystals, i.e. the lamellae, are constructed by adjacent re-entrancy folded chains and between the lamellae there are relatively rare tie molecules. The plastic deformation of crystalline plastics proceeds in three steps (see Figure 6.14) [71]:

1. Plastic deformation of the original lamella structure. The lamellae stacks undergo rotation, sliding and chain slip until the pre-deformed lamellae reach the position of maximum compliance for fracture by micro-necking.
2. Transformation into fibrous structure. Every single lamella transforms into micro-fibrils with one to three hundred angstroms in width, consisting of folded chain blocks from primarily lamella. The chains bridging the crack are partially unfolded during the micro-necking process. They connect in axial direction the blocks in the micro-fibril as intrafibrillar tie molecules.
3. The plastic deformation of the fibril structure. It proceeds by longitudinal sliding of the micro-fibrils past each other and it is limited by interfibrillar tie molecules.

However, regarding bulk crystallized PE samples, it turned out that the axial long period of the

drawn micro-fibrils could be 30 % larger or 50 % smaller than the original long period. The long period after deformation seemed to be independent of the value in the starting material but a function of drawing temperature. It increased with the drawing temperature, the higher the drawing temperature the greater the long period after deformation. This phenomenon cannot be explained by the fragmentation and rearrangement model only. Additional phenomena have to be taken into account.

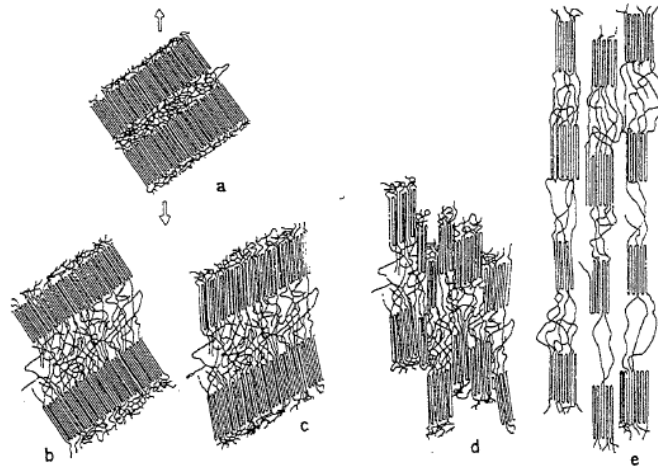


Figure 6.14 steps of deformation in semi-crystalline polymers

6.3.5 Melting and recrystallization

To explain the long period change upon drawing, the melting-recrystallization process was proposed for the first time by Yoon and Flory [49]. After, many authors in the explanation refer to mechanisms involved in the fibrillar deformation transformation [77,123,124].

Based on thermodynamics, Juska and Harrison [125] also proposed the melting and recrystallization mechanism during the formation of the fibrous structure in semi-crystalline polymers. They suggested that the applied mechanical energy would weaken the van der Waal's bonds between the chains in polymer crystals and enhance the potential energy of the system. When the total accumulated energy reached a critical value the melt phase would become stable and chain unfolding would occur at the drawing temperature. The formation of the micro-fibrils structure had to undergo a transition from crystalline to rubbery state then extension nucleation and recrystallization (Figure 6.15). However, no direct evidence has been provided to support this theory.

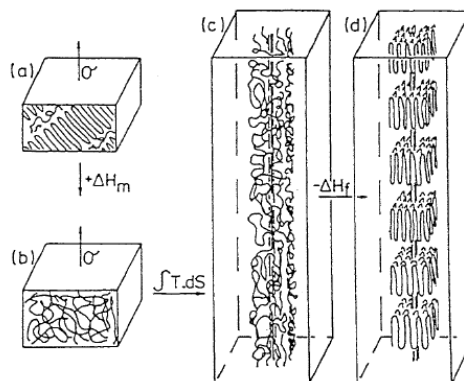


Figure 6.15. Melting and recrystallization step of crystallites during tensile deformation

It has also been proposed that melting would occur via stress induced deformation at the melting point. But this effect does not exceed a few degrees. This phenomenon of local melting may occur

only for tests carried out at high temperatures, near the melting temperature [126]. In conclusion the high degree of molecular chain unfolding may be responsible for very local fusion. However, this could not alone explain the fibrillar transformation and other mechanisms such as crystallographic slip and fragmentation of lamellae have to take into account.

I.7 Conclusion of the introduction

It could be noted that although studies on the mechanical properties of semi-crystalline polymers are numerous, there are still some unresolved issues:

1. How to estimate the density of stress transmitters and how much it is?
2. Presence or absence of a third phase (interphase)?
3. Modules of the amorphous phase? The influence of stress transmitters and interphase on this modulus?
4. What is the manner that stress and strain transform from mesoscale deformation to macroscopic deformation?
5. What is the influence of mechanical coupling on the mechanical behavior?
6. What is the influence of microstructure parameters and temperature on the competition between cavitation and crystal shear?
7. What is the influence of microstructure and temperature on the martensitic transformation of polyethylene?
8. The mechanism of fibrillar transformation: fragmentation - rearrangement or melt – recrystallization? What is the influence of interphase and stress transmitters on the fibrillar transformation?

This present work tries to answer some of the questions listed above, in order to progress in the understanding of the mechanical behavior of semi-crystalline polymers.

I.8 Strategy

The general object of this thesis is to understand the influence of the each microstructural and molecular parameters on the mechanical properties of semi-crystalline polymers. More precisely, we expect to establish correlations between microstructure and deformation behavior.

To reach these objectives, the strategy was to collect a series of PE samples with different molecular topology (comonomer concentration) and different thermal treatments to obtain a wide distribution of microstructure parameters (crystallinity, crystalline thickness, stress transmitters density et al.). On the other hand, the similar microstructure could be obtained from polymers with different topology. This will allow understanding the influence of molecular parameters on the mechanical properties.

The isotactic polypropylene also used to compare the mechanical properties between semicrystalline polymers of different natures but with similar microstructures.

In-situ SAXS and WAXS was performed to observe the evolution of microstructure. This technique allows probing the real microstructure evolution during deformation. With this technique the microstructure parameters could be well associated to the mechanical properties.

Chapter II Experiment method and technique

Table of content

Context	35
II.1 structural characterization.....	35
1.1 Differential scanning calorimetry (DSC)	35
1.2 Small angle X-ray scattering (SAXS)	36
1.3 Wide angle X-ray scattering (WAXS)	40
II.2 mechanical property characterization.....	41
2.1 Tensile tests	41
2.2 Dynamic mechanical analysis (DMA)	42

Context

In this chapter the experimental techniques are presented. It is divided into two aspects microstructure characterization and mechanical property characterization.

II.1 structural characterization

1.1 Differential scanning calorimetry (DSC)

In this work, DSC was used in two ways:

- To measure the heat flow during the heating process in order to determine crystallinity
- To measure the onset of crystallization T_c^{onset} during cooling

Principle

The basic principle underlying this technique is that when the sample undergoes a physical transformation such as phase transitions, more or less heat is needed to maintain sample and reference at the same temperature as shown in **Figure 1**. By observing the difference in heat flow between the sample and reference, one may thus measure the amount of heat absorbed or released during such transitions.

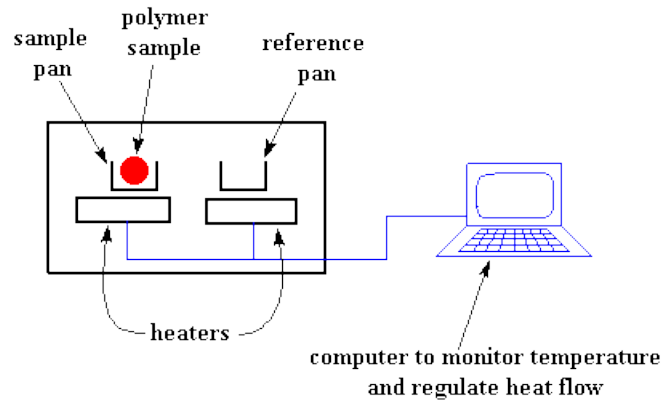


Figure 1. Schematic of DSC principle.

In DSC, the difference in heat flow to the sample and reference at the same temperature is recorded as a function of temperature. Since the DSC is at constant pressure, heat capacity C_p is equivalent to enthalpy changes [127]:

$$C_p = \left(\frac{dq}{dT}\right)_p = \left(\frac{\partial H}{\partial T}\right)_p \quad (1)$$

where dH/dT is the measured heat flow.

The area under such a curve between any two temperature limits yields an enthalpy change:

$$\Delta H = \int_{T_1}^{T_2} \left(\frac{\partial H}{\partial T}\right)_p dT = \int_{T_1}^{T_2} C_p dT \quad (2)$$

Experiment condition

The crystallinity of the polymers has been analyzed with a DSC7 apparatus from Perkin-Elmer at a heating rate of 10 °C/min under nitrum 25 ml/min. The sample of about 8 to 10 mg measured with aluminum pan. The temperature and heat flow scale were calibrated using high purity Indium at the same heating rate. The crystallization onset, T_c^{onset} , and crystalline temperature T_c were determined according the procedure described in the Perkin-Elmer manual at a cooling rate of 10°C/min.

Parameters measured from DSC curves

There are two different processes: exothermic or endothermic which depend on heating or cooling. The heating and cooling DSC curves were shown in **Figure 2**. The corresponded parameters can be obtained from these curves.

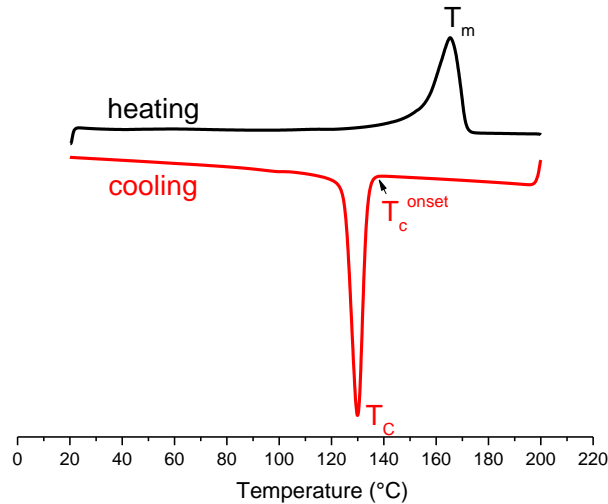


Figure 2. Scheme figure of DSC heating and cooling curves.

Crystalline temperature T_c and initial crystalline temperature T_c^{onset}

The crystalline temperature T_c is corresponded to the peak temperature of cooling curves. T_c^{onset} temperature can be measured directly in the cooling curves as shown in Figure 2

Crystallinity

In case of semicrystalline polymer, the melting enthalpy ΔH_m obtained by integration of dH/dT in the temperature range of the melting endotherm provides an access to calculating the crystallinity X_c :

$$X_c = \frac{\Delta H_m}{\Delta H_\infty} \quad (3)$$

where ΔH_m is enthalpy of melting, ΔH_∞ is enthalpy of fusion of melting of a perfect crystalline material i.e. 290 J/g and 207 J/g for polyethylene and polypropylene respectively [128,129].

1.2 Small angle X-ray scattering (SAXS)

Small angle X-ray scattering was used to study the lamella structure.

- To measure the long period of the lamella structure.
- To measure the thickness of the crystalline and interlamellar amorphous phase
- To measure the orientation of the crystal lamellae

Principle of SAXS

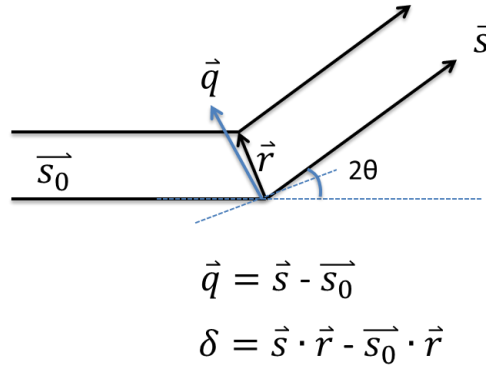


Figure 3. Schematic of scattering by two centers.

A schematic description of scattering principle is shown in Figure 3.

The angle between the incident and scattered beams is the scattering angle 2θ and \vec{r} is the vector distance between two scattering points. The phase difference between the two scattering waves is $\vec{q} \cdot \vec{r}$.

$$q = |\vec{q}| = \frac{4\pi}{\lambda} \sin \theta \quad (4)$$

where λ is the wave length; \vec{s} and \vec{s}_0 are unit vectors in the direction of the scattered and incident beams, respectively.

For a statistically isotropic scattering particle, the scattering intensity could be deduced by the equation:

$$I_0(q) = 4\pi \int_0^\infty \gamma(r) \frac{\sin(qr)}{qr} r^2 dr \quad (5)$$

where $\gamma(r)$ is the so-called correlation function. It can be obtained by the inverse Fourier transform with equation:

$$\gamma(r) = \frac{1}{2\pi^2} \int_0^\infty I_0(q) q^2 \frac{\sin(qr)}{qr} dq \quad (6)$$

At low q region, i.e., for $qr \ll 1$, Equation 6 can be expressed as:

$$I_0(q) \cong I_0(0) \exp\left(-\frac{R_g^2 q^2}{3}\right) \quad (7)$$

where R_g is the radius of gyration of the particle.

This is the so-called Guinier's law, which is a most useful relation in SAXS analysis since it allows to obtain R_g^2 and $I_0(0)$ from scattering data in the region of smallest angles without any prior assumption on the shape and internal structure of the particles under investigation.

Experimental conditions

SAXS provides global information about the morphological structure of a material in reciprocal space. Within small scattering angles ($0-2^\circ$), the resolved d spacing is in the range of 10-100 nm, corresponding to typical semicrystalline domain spacing [130].

For the deformation experiments, we used a home built stretcher and performed in situ SAXS at D2AM beam line of the European synchrotron Radiation Facility (ESRF). The monochromatic X-ray beam was directed through two sets of double slits to the sample, which was mounted on the stretcher as illustrated in Figure 4. For the in situ tensile test, the specimens with gauge length 6.5 mm (11 mm for polypropylene), width 4 mm and thickness about 0.5 mm. The width of the beamstop was 3 mm, and the diameter of the detector of the CCD Princeton camera was 6 cm. The spectrum 2D was obtained by a camera. The wave-length was chosen at 0.154 nm (8 keV) and the distance between detector and specimen was set at 1.27m for polyethylene and 0.86m for

polypropylene. These distances enable for record spectra with q space $0.002 \sim 0.95 \text{ nm}^{-1}$ and $0.01 \sim 1.6 \text{ nm}^{-1}$ respectively.

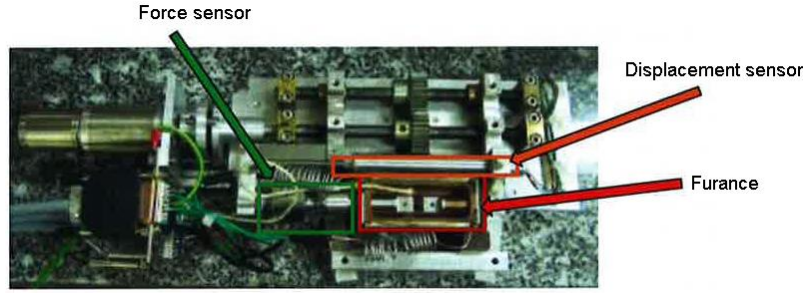


Figure 4. Mini tensile test machine for the in situ SAXS.

A symmetric stretching was used to make sure that the measured area on the sample is always in the same place. The tensile rate was 0.25 mm/min for polyethylene specimen and 0.1 mm/min for polypropylene specimen. To study the influence of temperature, the polyethylene samples were tested at 25°C , 50°C , 75°C and 100°C whereas the polypropylene samples were tested at 25°C , 70°C and 120°C respectively. The exposure time is a balance between deformation and scattering intensity. It should be carefully chosen that the deformation is as small as possible and the scattering intensity is strong enough for the recording. For the polyethylene specimen, the exposure time was chosen at 5s. The deformation was 0.4% during the exposure. For polypropylene, the exposure time was chosen at 10s which the deformation was 0.9% during the exposure. The transfer time of the spectrum was 9s for the specimen of polyethylene and 6s for polypropylene.

Data treatment

In order to obtain the absolute scattering intensity $I(q)$ as a function of scattering vector q , the experimental data have to be subtracted from the background and calibrated by the transmission coefficient. For the correction, three spectrums were saved for every measurement:

- The spectrum with specimen I_0
- A spectrum without specimen I_{db} : direct beam
- Background noise without beam and specimen I_b

The intensity scattered by samples can be defined as

$$I = (I_0 - I_b) - T \times (I_{db} - I_b) \quad (8)$$

With the absorption coefficient $T = \frac{I_0^0}{I_{db}^0}$

I_0^0 and I_{db}^0 are measured by the photomultipliers placed before and after the specimen respectively.

The scattering intensity also needs to be normalized with the thickness of the samples. It follows as

$$I = \frac{(I_0 - I_b) - T \times (I_{db} - I_b)}{ep} \quad (9)$$

with $ep = -\frac{\ln T}{\mu}$

where μ is the absorption coefficient of materials. It is calculated by the first spectrum with the initial thickness of the sample.

Long period L_p

For the calculation of the L_p , the Lorentz-corrected intensity profiles, $Iq^2(q)$, were used as shown in Figure 5.

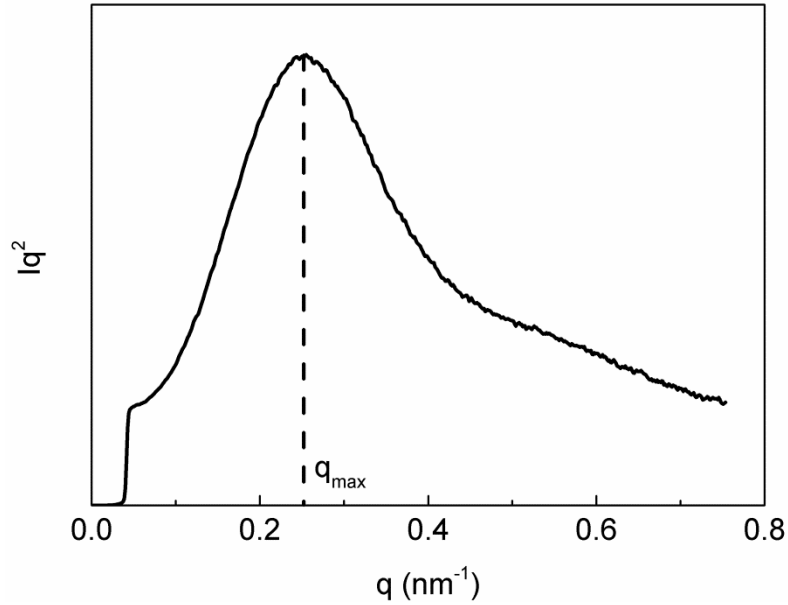


Figure 5. Schematic of Lorentz corrected SAXS intensity profile.

The long period L_p can be calculated with the Bragg's equation:

$$L_p = \frac{2\pi}{q_{max}} \quad (10)$$

with q_{max} the correspondence of the maximum peak. The standard deviation of the L_p data does not exceed 1 nm.

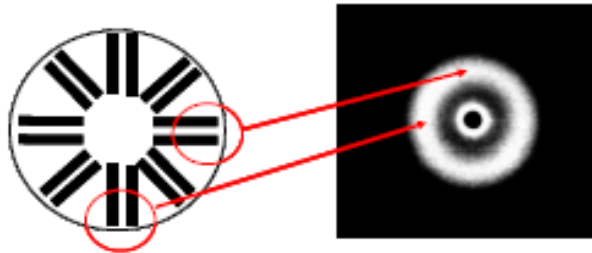


Figure 6. Schematic of spherulit scattering in different regions.

Figure 6 shows the scattering of the spherulite. The lamellae in the equatorial region scatter in 90° direction (vertical) whereas it scatters in 0° direction (horizontal) for polar lamellae. Therefore, it is possible to analysis the scattering intensity from different region separately. With the azimuthal integration, information can be determined on the orientation of the lamellae in the various regions of the spherulites as a function of strain.

Crystalline thickness L_c

The crystalline thickness can be obtained as:

$$L_c = L_p \times \frac{\rho}{\rho_c} \times X_c \quad (11)$$

$$\text{with } \frac{1}{\rho} = \frac{X_c}{\rho_c} + \frac{1-X_c}{\rho_a}$$

where L_p is long period measured from SAXS, X_c is the crystallinity from DSC, ρ is the density of the sample, ρ_c is the density of the crystal (for polyethylene is 1.002 g/cm^3 and polypropylene 0.95 g/cm^3), and ρ_a is the density of the amorphous phase (polyethylene 0.85 g/cm^3 and polypropylene 0.85 g/cm^3). Equation 11 assumes that the length and the width of the lamellae are much greater than their thickness.

Azimuthal analysis

For the sake of the orientation studies, azimuthal calculation of the SAXS intensity was computed from 2D patterns. Azimuthal intensity profiles were computed over the whole range $0\text{-}360^\circ$, using a scattering of annulus of radius spanning q range $0.1\text{-}0.5\text{ nm}^{-1}$. Azimuthal sectors used for the treatment were $\Delta\phi=5^\circ$.

1.3 Wide angle X-ray scattering (WAXS)

Wide angle x-ray scattering (WAXS) experiments can be used to qualify and quantify the crystal phases in semicrystalline polymers.

Principle

The x-ray beam (with a wavelength λ) is scattered (diffracted) by the crystal at a specific angle θ , due to the presence of crystal planes separated a distance (d). The scattering angle (2θ) is related to plane distance by the Bragg equation:

$$2d = \frac{n\lambda}{\sin\theta} \quad (12)$$

where n is an integer. The equation indicates a reciprocal relationship between the characteristic length d and $\sin\theta$.

Inter planar distances (d) in crystal are determined from unit cell dimensions. The unit cell is described by the axes a , b , c , and the angles between them: α , β , and γ . For each type of unit cell, relationships are given between the d -spacing and the indexes h , k , and l . Several crystallographic planes of the crystal lattice give rise to scattering peaks in a WAXS pattern. Figure 7 shows the WAXS intensity profiles and fitted peaks of the polyethylene and polypropylene, respectively. The reflexing indexes refer to the orthorhombic crystal form of PE and the monoclinic α crystal form of PP.

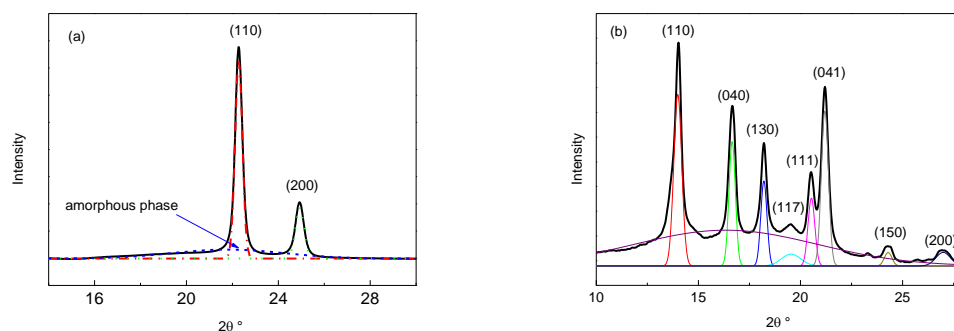


Figure 7. WAXS intensity profiles of (a) polyethylene and (b) polypropylene.

Experimental conditions

The in-situ WAXS was performed on the D2AM beam line of ESRF. The tensile test conditions are the same to the in-situ SAXS except for the exposure time is 1 s. The strain rate, transform time, the samples dimension and drawing temperature are the same to SAXS experiment.

The wavelength is 0.05133 nm (24 kV) and the distance between sample and detector is 15.85 cm . The observation q space range is 0 to 22.7 nm^{-1} , corresponding 2θ : $0\text{-}30.6^\circ$.

Fitting procedures and azimuthal treatment

A fitting procedure of the $I(2\theta)$ profiles was performed by means of gaussian equations for the crystalline reflexion and amorphous halo as well. Azimuthal analysis of the WAXS patterns were performed similar to the case of SAXS, after sectorization and extraction of the various components by the fitting procedures.

II.2 mechanical property characterization

2.1 Tensile tests

Stress and strain

When a solid object is stretched, internal forces within the material resisted any change in the dimensions of the object. These internal balancing forces are called stresses and lead to the formation of strains within the material [131]. Engineering stress is defined as the force acting upon the material (F) divided by the cross - sectional area of the sample (A_0) and is denoted by (σ_E) as shown in Equation below:

$$\sigma_E = \frac{F}{A_0} \quad (13)$$

The changes in the dimensions are called strain. The engineering strain ε is defined as the change in the length of the sample along the axis (ΔL) divided by the original length of the sample (L_0), as shown below:

$$\varepsilon = \frac{\Delta L}{L_0} \quad (14)$$

The Engineering stress and strain are applicable with assumption that the change of the length is much smaller than the original length ($\Delta L \ll L_0$) and the cross-section area (A) does not change. For the most engineering applications the above assumption is accurate. However, in case of the large deformation, even in the elastic regime it is no longer applicable and the true stress and true strain should be used.

The true stress σ_T is defined as:

$$\sigma_T = \frac{F}{A} \quad (15)$$

where A is the actual cross-section area at any time.

Now we assume that the deformation takes place at constant volume, this assumption being usual for plastic deformation. Then $AL=A_0L_0$, and if we put $L/L_0=1+\varepsilon$ where ε is the elongation per unit length. It could be obtained:

$$A = \frac{A_0L_0}{L} = \frac{A_0}{1+\varepsilon} \quad (16)$$

The true stress is given by

$$\sigma_T = \frac{F}{A} = \frac{(1+\varepsilon)F}{A_0} = (1 + \varepsilon)\sigma_E \quad (17)$$

Experiment condition

The uniaxial tensile tests were performed on a MTS machine with a load cell of 5 kN. The specimen was cutout from the compression modeled sheets with a dumb-bell type punch. The gauge length is 12 mm, with width 4.2 mm and thickness 0.5 mm. The tensile rate was chosen as $5 \cdot 10^{-3}$ which was 3.6 mm/min. For polyethylene, the test temperature was 25 °C, 50 °C, 75 °C and 100 °C respectively whereas it is 25 °C, 70 °C and 120 °C for polypropylene.

Parameters obtained from stress strain curves

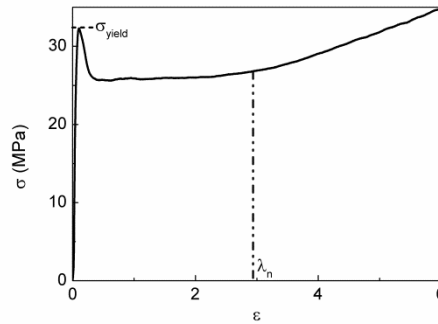


Figure 8. Stress-strain curves at room temperature of compression modeled PE.

The stress strain curves were obtained from the tensile test. The mechanical properties such as the young's modulus, yield stress and break stress etc. can be obtained from the curves as shown in the Figure 8.

1. Young's Modulus E

The Young's modulus relates to the stiffness of the material known as the elastic modulus. It is measured at the very beginning of the stress strain curves, in the elastic deformation domain where the stress linearly relates to strain. The Young's modulus is defined as the slope of the stress strain curves in the linear domain. When the linear domain is limited at high temperature, the Young's modulus is determined as the tangent to the initial point of the curve via a fitting procedure.

2. Yield stress σ_y

The yield stress is a stress at which plastic deformation of the materials starts to occur and the material can no longer return to its original dimensions when the load is released. The yield stress leads a permanent deformation of the materials. It is usually measured at the maximum of the yield peak as shown in Figure 8.

3. Natural stretch ratio λ_n

When a ductile polymer is drawn beyond the yield strain, a plastic instability generally appears accompanied with a necking phenomenon. Then a stable neck propagates all along the sample. The so-called natural draw ratio is the strain in the stable neck.

λ_n is measured with the method shown in Figure 8. It takes the intersection of two tangents: the first one is the tangent to the necking and the second one is the tangent to the stress harden.

2.2 Dynamic mechanical analysis (DMA)

Principle

DMA works by applying a sinusoidal stress or deformation to a sample of known geometry. For an applied sinusoid stress, a viscoelastic material will respond with a sinusoidal strain for low amplitudes of stress. Figure 2.8 shows the schematic of the applied stress and the response strain. The strain is out of phase with the stress applied, having a phase lag δ . This is due to the excess time necessary for molecular motions and relaxations to occur.

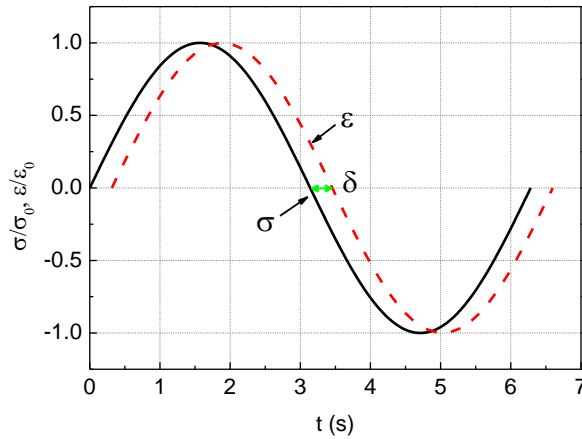


Figure 9. Schematic of the applied stress and the response strain.

The applied stress is given by:

$$\sigma = \sigma_0 e^{i\omega t} \quad (18)$$

where σ_0 is the stress amplitude and ω the circular frequency ($\omega = 2\pi f$, with f the frequency).

The strain lags behind the stress by a phase angle δ which is written as:

$$\varepsilon = \varepsilon_0 e^{i(\omega t - \delta)} \quad (19)$$

where ε_0 is the strain amplitude and δ the loss angle.

The ratio σ/ε is a complex quantity, called complex modulus $E^*(\omega)$, which is a function of ω :

$$E^* = \frac{\sigma}{\varepsilon} = \frac{\sigma_0}{\varepsilon_0} e^{i\delta} = \frac{\sigma_0}{\varepsilon_0} (\cos\delta + i\sin\delta) = E' + iE'' \quad (20)$$

The equation shows that the complex modulus obtained from a dynamic mechanical test consists of “real” and “imaginary” parts. The real (storage) part describes the ability of the material to store potential energy and release it upon deformation. The imaginary (loss) part relates to energy dissipation via viscous processes. Equation 20 can be rewritten for shear modulus as:

$$G^* = G' + iG'' \quad (21)$$

where G' is the storage modulus and G'' is the loss modulus. The phase angle is given by

$$\tan\delta = \frac{G''}{G'} \quad (22)$$

The dynamic loss modulus is often associated with “internal friction” and is sensitive to different kinds of molecular motions, relaxation processes, transitions, morphology and other structural heterogeneities. Thus, the dynamic properties provide information at the molecular level for understanding the polymer mechanical behavior.

Experimental conditions

The tests were carried out on a torsion pendulum, developed in the laboratory (see Figure 10).

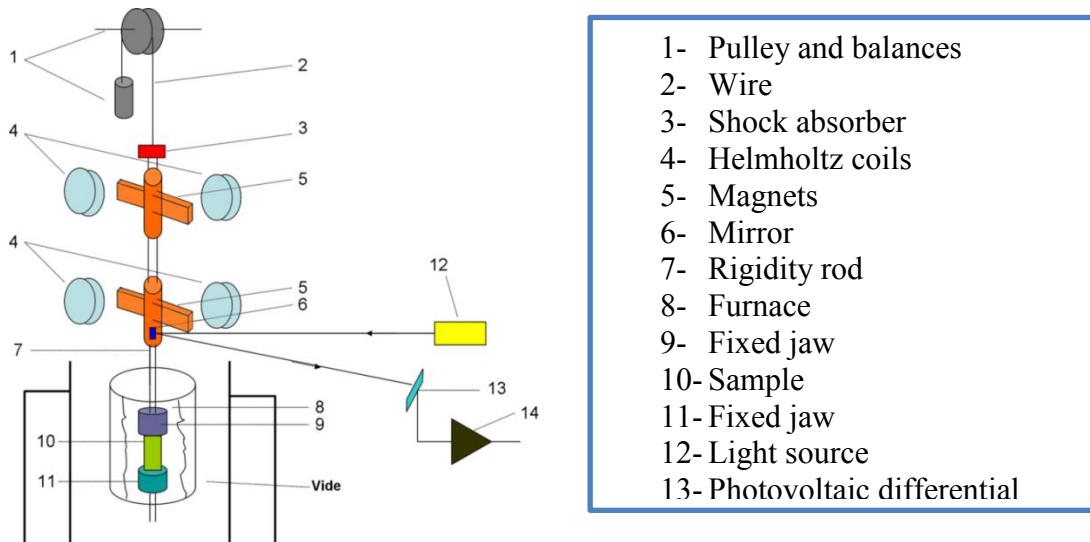


Figure 10. Schematic of torsion pendulum apparatus. [132]

The rectangular specimens were cut from the plates. The dimensions were 5mm in width, 15mm in length and 0.5 mm in thickness. The measurements were performed at a frequency of 1 Hz, in the temperature range from 100 to 400 K for polyethylene and 100 to 440 K for polypropylene specimens, at a heating rate of 1 K/min.

During a ramp temperature, the DMA can reveal the various mechanical relaxations, namely γ , β , and α . This technique allows locating the occurrence of three relaxations. It can also provide the G modulus variations as a function of temperature.

Chapter III Materials and microstructure characterization

Table of content

Chapter III Materials and microstructure characterization	45
Context	46
III.1 Materials.....	46
III.2 Thermal treatment	46
III.3 Microstructure characterization.....	48
3.1 microstructure of polyethylene	49
3.1.1 Influence of comonomer concentration	49
3.1.2 Influence of thermal treatment.....	50
3.1.3 Stress transmitters density.....	50
3.2 microstructure of polypropylene	51
III.4 Conclusion.....	53

Context

In this chapter, the materials structure and thermal treatment methods are presented.

Four polyethylenes with similar molecular weight but different hexene co-unit concentrations are used in this studies. Further, three isotactic polypropylenes with different isotacticity are used to compare the mechanical properties between different semicrystalline polymers. Then the influence of thermal treatment on the microstructure of the semi-crystalline polymer is presented.

III.1 Materials

1.1 Polyethylene

Four PE were chosen for my studies: PE A, PE B, PE C, and PE D were kindly supplied by Total chemicals. They are divided into two groups according to the molecular structure: ‘branched’ or ‘linear’. PE A and PE B were defined as ‘branched’ in relation to the high concentration of comonomer. PE C and PE D were defined as ‘linear’ due to the low comonomer concentration. Their molecular characterization are listed in Table 1.1

Table 1.1. Molecular characterization of the polyethylene

Materials	type	[C6] % mol	Mn (kDa)	Mw (kDa)	Mz (kDa)	I = Mw/Mn
PE A	branched	1.8	14.3	231	2770	16.1
PE B	branched	0.8	15.8	187	1770	11.9
PE C	linear	0.1	15.4	216	2770	14
PE D	linear	0.2	15	229	4100	15.3

[C6]: concentration of hexene co-unit;

1.2 isotactic polypropylene

Two isotactic polypropylenes (iPP) with low isotacticity are offered by Polymer Institute of Sichuan University which are referred to PP A and PP B. The iPP samples were produced with Ziegler-Natta catalysis with different catalyst density to control the isotacticity of the product.

Another iPP with high isotacticity was supplied by Ineos (Belgium), which labeled as PP C. The molecular structures of these iPPs are listed in Table 1.2.

Table 1.2 Topology parameters of the polyethylene of iPP

sample	Isotacticity (%)	Mn (kDa)	Mw (kDa)	I=Mw/Mn
PP A	96	9.3	37.1	4.4
PP B	95	7.8	39.6	5.1
PP C	98	14.0	45.8	3.3

III.2 Thermal treatment

To obtained samples with wide distribution of microstructures, different thermal treatments were employed. With different thermal history, the samples with different crystallinity, crystal thickness, and also the density of molecular couplings between crystal and amorphous phase can be obtained.

The thermal treatment methods includes: quenching, annealing, and isothermal crystallization. For PE and PP, the same treat process was employed.

Quenching

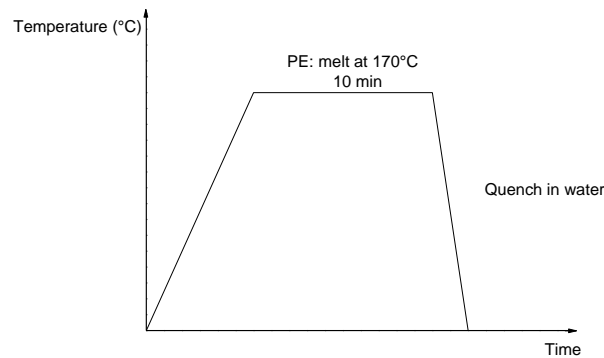


Figure 2.1. Quenching process for the polyethylene.

The quenching proceeds via melting at a temperature which is about 30 °C above the melt point and holds at this temperature for 10 min to erase the thermal history of the original materials and then cool down quickly in water. In our experiments, polyethylene is held at 170 °C for 10 min (see Figure 2.1). For the cooling in water, the cooling rate is about 35 °C/s.

For the iPP samples, the quench process is the same except melt temperature is 210 °C.

The quenching provides samples with lower crystallinity and thinner crystal lamellae. This method also promotes generation of a high density of stress transmitters.

Isothermal crystallization

The treatment consists of melting the material above melt point (170 °C for PE and 210 °C for iPP) and then quickly decreasing the temperature to a crystallization temperature T_{isotherm} close to the onset temperature of crystallization and holding at this temperature for 10 hours, then cooling the samples in the air to room temperature. (see Figure 2.2)

Many isotherm treatment temperatures were tested by increasing the temperature gradually from the crystallization temperature. In a certain temperature range, increasing T_{isotherm} was the consequence of increasing the temperature of the melting peak. But above a critical temperature, whatever the duration at that isotherm temperature, the melting peak was not increased but creating a substantial proportion of small crystallites as revealed by a second melting peak. This was due to an incomplete crystallization of the material during the isothermal treatment. The temperature of the isothermal treatment for each PE was therefore chosen to maximize the temperature of the melting peak, while ensuring that the formation of small crystallites during isotherm treatment was negligible. Isotherm treatment temperature T_{isotherm} , temperature of crystallization onset T_c (onset) and crystallization temperature T_c (peak) were listed in Table 2.1.

In isothermal process, polymer is crystallized from the melt. With this treatment, the chains have time to fold properly and to form large crystallites which makes it possible to obtain samples with high crystallinity, and low rate of stress transmitters as well.

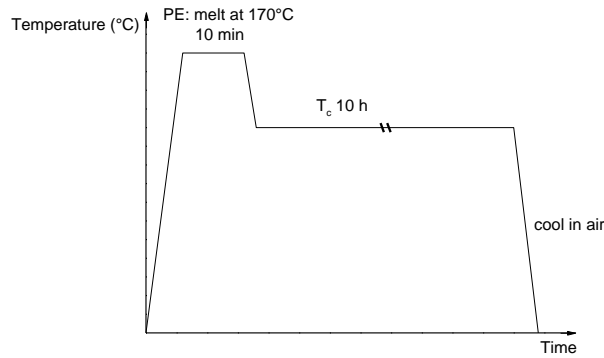


Figure 2.2. Isothermal crystallization process from melt of Polyethylene

Table 2.1. Thermal treatment temperatures for PE and iPPs (T_c and T_f from DSC)

Samples	T_c (onset) °C	T_c (peak) °C	T_f °C	T_{isotherm} °C
PE A	116.3	114.3	128	114
PE B	117.3	115.4	127.5	113
PE C	120.9	118.2	131.7	124
PE D	121.4	119.3	134	123
PP A	113.1	108.8	166.3	110
PP B	112.9	108.6	166	110
PP C	123.6	118.8	167	118

Annealing

The annealing process is carried out by heating a quenched sample at a temperature below melt temperature. In this work, the temperature was chosen as the same to the T_{isotherm} , and hold at this temperature for ten hours, and then cooled in air. (see Figure2.3).

From chapter 1, it is known that two crystallization processes could operate during annealing. During the temperature rise, smaller crystallites are melted. They form the molten zones. For holding temperature, large crystallites can be formed in the molten zones. Meanwhile, unmelted crystallites may also thicken thanks to the mobility of the chains in the crystal.

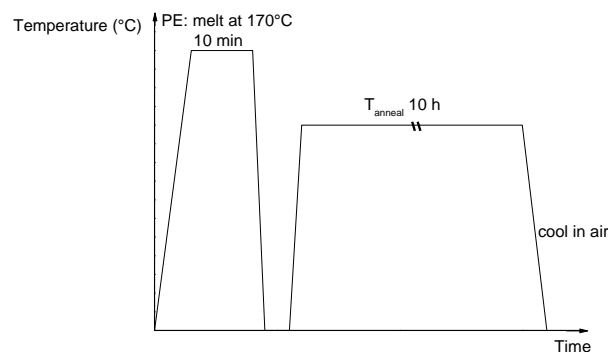


Figure 2.3. Annealing treatment process for Polyethylene

III.3 Microstructure characterization

To understand the deformation behaviour, microstructure was characterized. The thermogram parameters and crystallinity was obtained from the analysis of DSC. The crystallite and amorphous phase thicknesses were estimated by SAXS. The interphase content X_i was borrowed

from the PhD thesis of S. Humbert [133], whereas [ST] was computed from Brown's model. The natural draw ratio (λ_n) was determined by tensile tests.

3.1 microstructure of polyethylene

The microstructure parameters of the polyethylene after thermal treatment were obtained and listed in Table 3.1.

Table 3.1. Microstructure parameters of the polyethylene

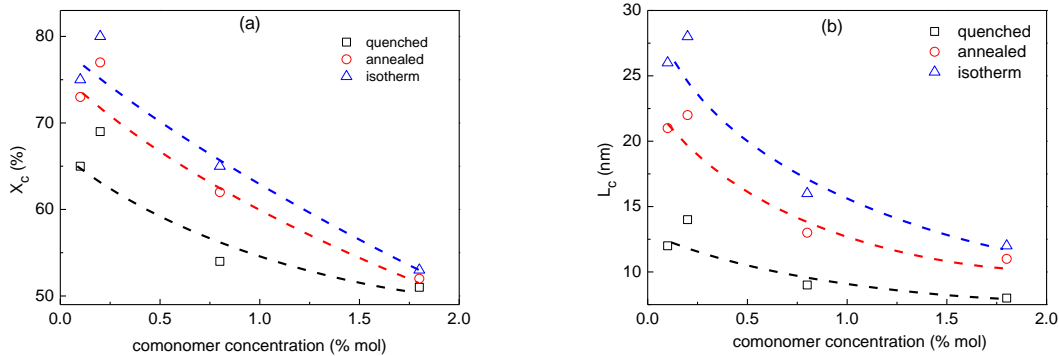
Materials	C6 %mol	Thermal treatment method	X_c (%)	L_p (nm)	L_c (nm)	X_i %	[ST] (Brown's model)	λ_n
PE A	1.8	Quench	51	17	8	13	0.244	3.5
		Anneal	52	23	11	13	0.17	4
		Isotherm	53	24	12	11	0.154	4.75
PE B	0.8	Quench	54	19	9	8	0.194	4.25
		Anneal	62	22	13	8	0.141	4.75
		Isotherm	65	26	16	4	0.094	5.5
PE C	0.1	Quench	65	20	12	5	0.194	4.5
		Anneal	73	30	21	5	0.076	6
		Isotherm	75	36	26	5	0.032	7.5
PE D	0.2	Quench	69	22	14	3	0.173	5
		Anneal	77	30	22	5	0.079	5.57
		Isotherm	80	37	28	0	0.032	7

X_i : data from Raman spectroscopy (borrowed from thesis of S. Humbert [133])

3.1.1 Influence of comonomer concentration

As mentioned in the Chapter 1, DSC permits to measure the crystallinity X_c . Because of their different molecular topology, the various PE cover a wide range of crystallinity. For the quenched polyethylenes, the more comonomer density the lower crystallinity is (see Figure 3.1a).

The thickness of crystalline lamella L_c is calculated from the long period. The calculated method was mentioned in Chapter 2. L_c is also influenced by comonomer concentration (see Figure 3.1b). For the quenched samples, L_c increases with decreasing comonomer concentration. This is because the side chains can not fold into the crystal as it is discussed in Chapter 1. Raman spectroscopy provides a way to measure the fracture of interphase X_i in polyethylene. The value of X_i is a function of comonomer concentration (see Figure 3.1c). For samples with the same thermal history, the X_i increases with increasing comonomer concentration.



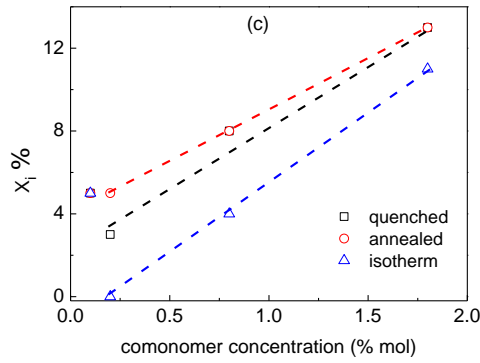


Figure 3.1.(a) X_c , (b) L_c and (c) X_i plot in function of comonomer concentration for the samples with different thermal treatments.

3.1.2 Influence of thermal treatment

The thermal treatment strongly influences the microstructure of the PE. However, their effects are different for branch and linear type.

Anneal and isotherm treatments promote X_c . The amplitude of X_c variation is 11% for PE D but only 2% for PE A (see Figure 3.1a). This means the linear PE is more sensitive to the thermal treatment than branched PE. L_c shows similar evolution with thermal treatments (see Figure 3.1b). These results prove that annealing and isothermal treatments promote higher crystallinity and thicker crystallite lamella. Furthermore, the higher crystallinity, the thicker crystalline is (see Figure 3.2). This observation can be ascribed to the crystallization-induced exclusion of the chain defects at the crystal-amorphous interface. The higher the defect content, the higher L_a and the lower L_c . Notwithstanding, it is to be noticed that the L_a variation is much weaker than that of L_c and much less sensitive to polymer composition and thermal treatment.

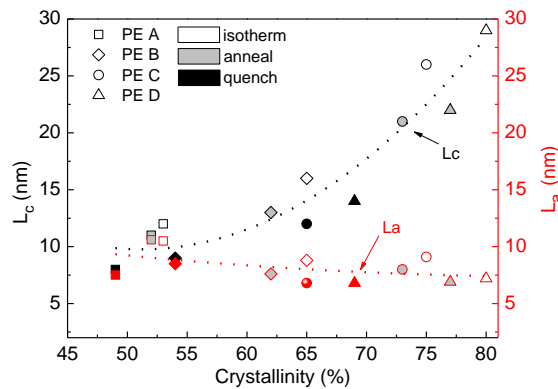


Figure 3.2. L_c and L_a in function of crystallinity

It seems that annealing slightly increases X_i (see Figure 3.1c) while isothermal treatment reduces X_i . We have seen in the literature that during annealing, due to the mobility of the chains in the crystal (α relaxation), there could be an increase in crystalline perfection through the elimination of defects at the interface of the crystals. These defects, such as comonomers or the chain ends, thus found to reject the surface of the crystallites, which may cause a greater proportion of interphase. Regarding the isothermal treatment, due to the slow crystallization process, the folding of the chain promotes a smooth crystal surface. Thus interphase content is found lower than that resulting from rapid cooling.

3.1.3 Stress transmitters density

Tie molecules and the entanglements play the role of physical coupling between amorphous phase and crystallites. The entanglement and tie molecule density of PE can not be measured directly.

However, some models permit to estimate the tie molecule density. In this work, the tie molecule density otherwise stress transmitters [ST] was evaluated by Brown's model as mentioned in Chapter I. The results were listed in Table 3.1. On the other hand, natural drawing ratio λ_n is estimated which is related to the density of stress transmitters. Figure 3.3 shows that [ST] and λ_n actually obey a very good correlation.

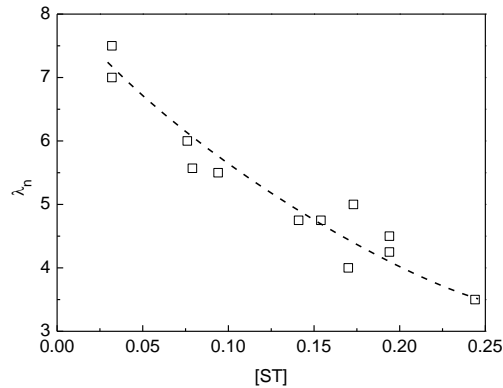


Figure 3.3. λ_n plots in function of [ST] for PE samples.

Comonomer concentration strongly affects the density of stress transmitters. [ST] increases (see Figure 3.4a) while λ_n decreases (see Figure 3.4b) with increasing comonomer concentration. This can be explained by the lower thickness of the crystallites obtained with higher co-unit concentration PE.

Regarding the influence of thermal treatments, [ST] decreases for annealing and isothermal treatment as compared to quenching which could be ascribed to formation of thicker crystallites.

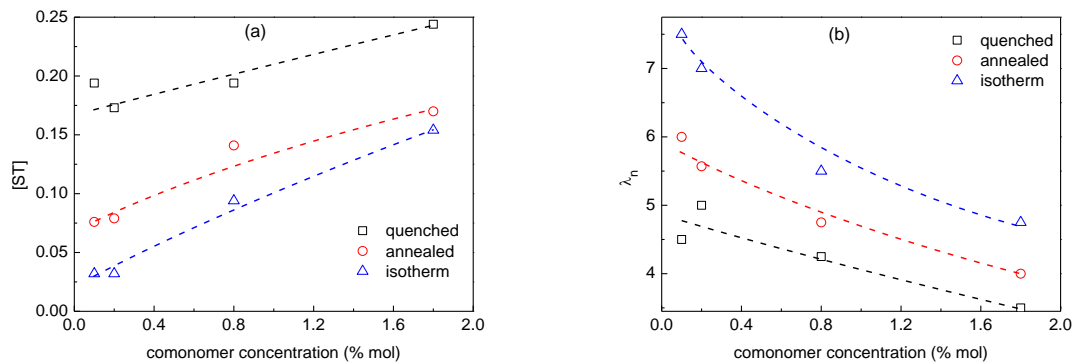


Figure 3.4. (a) [ST] and (b) λ_n plot in function of comonomer density.

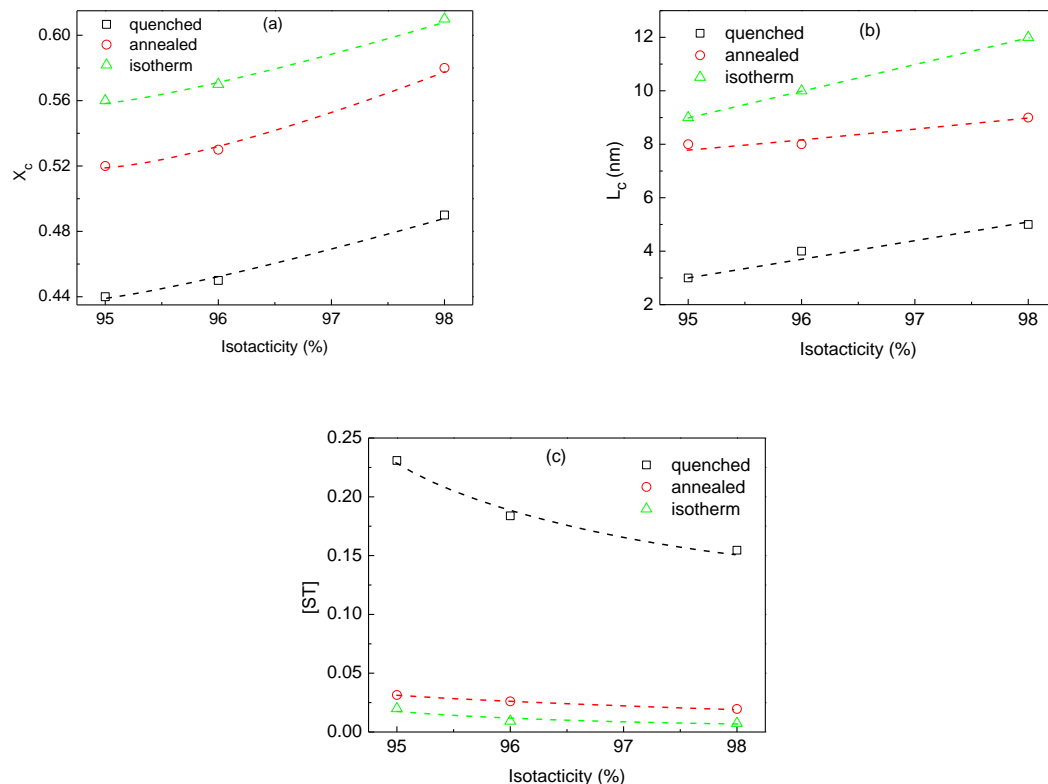
3.2 microstructure of polypropylene

The polypropylene samples were prepared with the thermal treatment methods mentioned in section 2. Similarly to PE, the microstructure was characterized with the method in Chapter 2 and the structure parameters are listed in Table 3.2.

Table 3.2. Structure parameters of iPP samples with different thermal treatment

Samples	Isotacticity %	Thermal treatment	X_c	L_p (nm)	L_c (nm)	[ST] Brown's model
PP A	96	Quenched	0.45	10	4	0,184
		Annealed	0.53	17	8	0,026
		Isotherm	0.57	19	10	0,009
PP B	95	Quenched	0.44	9	3	0,231
		Annealed	0.52	17	8	0,031
		Isotherm	0.56	18	9	0,020
PP C	98	Quenched	0.49	12	5	0,155
		Annealed	0.58	18	10	0,020
		Isotherm	0.61	21	12	0,007

Isotacticity plays an important role on the crystallization process since the microstructure is determined by molecular structure. Like the comonomer in PE, atactic sequence cannot enter the crystal or exist as a defect in the crystal. This stereoregularity defect strongly influences the crystalline structure. The increases of the crystallinity X_c (see Figure 3.5a) and crystallite thickness L_c (see Figure 3.5b) with increasing isotacticity can be observed. [ST] also decreases with increasing isotacticity (see Figure 3.5c). This could be explained by the thinner crystallite lamella from the molecules with more stereoregularity defects.

Figure 3.5. (a) X_c , (b) L_c and (c) [ST] plot in function of isotacticity for iPP.

Regarding the influence of the thermal treatments, quenched samples present the lowest X_c , L_c but highest [ST] density. After annealing, X_c and L_c increases while [ST] decreases. Similarly to PE, isothermal treatment promotes the grow of thicker crystallite and induces the highest X_c and L_c .

III.4 Conclusion

Four polyethylenes with various comonomer concentration and three isotactic polypropylenes with different isotacticity were used for our studies. The effect of molecular topology on the microstructure was investigated with these materials.

Three thermal treatments were performed on these materials to modify the microstructure. Firstly, samples with molecular parameters equivalent but microstructure different were obtained. Secondly, samples with wide range of microstructure distribution were prepared.

The molecular parameters such as comonomer concentration and molecular weight significantly influence the microstructure of polyethylene. The crystallinity X_c and crystallite thickness L_c decrease with increasing comonomer concentration. To the contrary, interphase content and tie molecule density $[ST]$ increase with increasing comonomer concentration. Furthermore, polypropylene shows similar variation with polyethylene. With the increase of isotacticity, X_c and L_c increase while $[ST]$ decreases.

The influence of thermal treatment on the microstructure was studied. Annealing and isothermal treatments enhance X_c and L_c . Annealing treatment increases slightly X_i while the isothermal treatment reduces X_i . Furthermore, $[ST]$ decreases after annealing and isothermal treatment. Thanks to thermal treatments, different microstructures were obtained for a given polymer whereas samples with similar microstructure were obtained from polymers having different molecular structures.

Chapter IV Elastic deformation

Table of content

Chapter IV Elastic deformation.....	54
Context	55
IV.1 Article I: “In-situ SAXS study of the mesoscale deformation of polyethylene in the pre-yield strain domain: Influence of microstructure and temperature”	56
IV.2 Article II: “Micro-macro mechanical relationship and amorphous phase modulus in polyethylene via in situ SAXS and WAXS”	62
IV.3 Summary of the article	84
IV.4 Small strain deformation behaviour of polypropylene	85
4.1. Local deformation in equatorial region	85
4.2. Comparison between deformation behavior of PE and PP	87
IV.5 Conclusion of the chapter	87

Context

Concerning the mechanical characterization, based on the observed mechanical behavior, several strain regimes may be distinguished for the semi-crystalline samples (Figure 1). In the early portion of the stress-strain curve (within a small strain in Figure 1), the materials obey the Hook's Law to a reasonable approximation, so that the stress is proportional to the strain. But in practice, this region is unlikely to be a perfectly straight line. As the strain increases, in the regime labeled as medium strain, the materials deviate from this linearly proportion. This non-linearly is usually associated to the "stress-induced plasticity" which is defined as the yield and necking in this regime. In regime large strain, the formed necking extended which related to the orientation of the molecule chains in axial. Finally, after the whole sample necked which occurs usually in very large strain, the stress rises until the fracture of the sample. It should be noted that mechanical properties are sensitive to the temperature, leading to the different stress-strain curves. However, the first regime has the same deformation mechanism in the different temperatures.

In this chapter, the macroscopic and the microscopic mechanical properties of polyethylene and polypropylene in the pre-yield strain domain are studied. The evolution of the microstructure in the pre-yield strain domain in the mesoscale is tracked by the in-situ small angle X-ray scattering (in-situ SAXS) and wide angle X-ray scattering (in-situ WAXS). The deformation of the lamella in different region of the spherulite and the relationship between the microscopic and macroscopic deformation are discussed. The objective is to better understand the key parameters affecting the elastic properties within a small deformation regime.

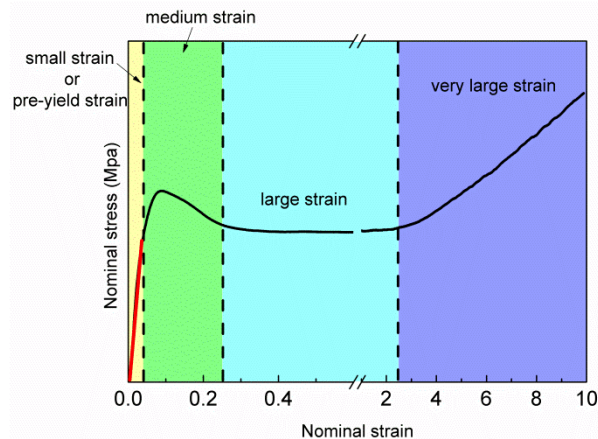


Figure 1. Schematic of the different strain regimes in terms of mechanical properties for PE and PP.

IV.1 Article I: “In-situ SAXS study of the mesoscale deformation of polyethylene in the pre-yield strain domain: Influence of microstructure and temperature”

Bijin Xionga, Olivier Lamea, Jean-Marc Chenala, Cyrille Rochasb, Roland Seguelaa, Gerard Vigiera. In-situ SAXS study of the mesoscale deformation of polyethylene in the pre-yield strain domain: Influence of microstructure and temperature. Polymer, 2014, Vol. 55, p. 1223-1227

IV.2 Article II: “Micro-macro mechanical relationship and amorphous phase modulus in polyethylene via in situ SAXS and WAXS”

Abstract

The small strain mechanical behavior of bulk polyethylene was investigated at the local scale of the lamella stacking by means of combined in-situ SAXS and WAXS at different testing temperatures. Three different thermal treatments on four materials afforded studying a wide range of crystallinities (X_c) and microstructures. The local strain in tensile direction of the amorphous phase in equatorial region of the spherulites was determined via SAXS. The amorphous to macroscopic strain ratio proved to be fairly constant in the pre-yield domain for every materials. This ratio also proved to be strongly dependant on X_c . The local tensile stress on the amorphous phase in equatorial region was assessed from the strain on the crystals as measured by WAXS, using theoretical values of the elastic constants. The apparent tensile modulus of the amorphous phase, M_a , was shown to reach a maximum value of 425 MPa at RT for $X_c = 50\%$ and exhibited a monotonic drop with increasing both X_c and temperature. Evidence was given of the major role of the molecular stress transmitters on the amorphous phase stiffness over that of structural confinement. Comparison between M_a and macroscopic elastic modulus revealed a significant modification of the mechanical coupling of the crystalline lamellae in relation to X_c that was assigned to an increasing lamella percolation throughout the spherulites with increasing X_c . This assumption was corroborated by WAXS assessment of the local stress parallel to the tensile direction in the polar lamellae that revealed an overloading of the polar regions as compared to the equator and the gradual increase of this overloading with increasing X_c .

Keywords: semi-crystalline polymers; micro-macro scale relationship; mechanical coupling; amorphous phase modulus; tie molecules.

Introduction

The microstructure of polyethylene (PE) is commonly described as a 2-phase model consisting of randomly oriented crystalline lamellae stacks intercalated with amorphous layers. During crystallization from the melt, several crystallites can grow within the sphere of gyration of a given coiled chain depending on its length.¹⁻³ This generates the so-called tie molecules (TM) or molecular stress transmitters (ST) that afford stress transfer between adjacent lamellae throughout the material. Depending on crystallinity and crystallization conditions, more or less regular chain folding can occur at the lamella surface owing to local chain rearrangements. Four types of disordered molecules can be found within the interlamellar amorphous phase : loose or tight chain loops that emerge and re-enter the same lamella, tie molecules that bridge two neighbor lamellae, chain ends or cilia and eventually unattached or free chains. It is to be noticed that chain entanglements already present in the molten polymer are rejected in the amorphous phase as topological defects during crystallization. These entanglements also contribute to transmit the stress between crystalline lamellae via the amorphous phase.^{3,4}

A 3rd phase at the crystal-amorphous interface, otherwise the interphase or transition region between the two phases, has also been identified by various techniques. This 3rd phase enables a gradient of chain segment density.⁵⁻¹¹ In the case of PE, the thickness of this interface depends on the content of structural chain defects, the chain length and the crystallization conditions.⁷ Moreover, a specific mechanical relaxation has been assigned to this 3rd phase in PE, i.e. the β relaxation extending from about room temperature to -60°C .^{12,13} This topologically constrained phase was suspected to play a specific part in the stress transfer between crystals and the amorphous phase.^{14,15} It should also have a different influence on the macroscopic behavior depending whether experiments are performed above or below the β relaxation.¹⁶ It is to be noticed that conflicting assignments have been reported in literature for the β relaxation in PE.¹⁷⁻²¹ Notwithstanding, it is generally admitted that this relaxation arises from the amorphous phase and that it is directly connected with the presence of crystallites.

The mechanical properties of semicrystalline polymers are strongly dependent on the lamellar morphology and crystallinity. This is particularly true for flexible-chain polymers having a rubbery amorphous phase at room temperature (RT), due to the modulus contrast between the two phases. But this also applies to stiff-chain polymers having a glassy amorphous phase since the crystalline state is somewhat stiffer than the glassy state.²²

Polyethylene belongs to the first class of semi-crystalline polymers. The modulus and yield stress are well known to depend on structural factors such as crystallinity and crystal thickness.²³ However, evidences have been given that macroscopic properties also depend on the intrinsic properties of the amorphous phase in relation to its chain topology. Indeed, as pointed out above, tie molecules and entangled chain loops in the amorphous phase are the very molecular elements which transmit the load between neighbor crystalline lamellae whereas unentangled loops and cilia do not. These so-called amorphous stress transmitters (ST) have been suspected by number of authors to be efficient contributors to the short-term as well as long-term mechanical properties of semi-crystalline polymers and especially PE.^{3, 24,25}

Focusing on flexible-chain polymers such as polyethylene, having a glass transition temperature far below RT, the rubbery interlamellar amorphous layer is generally considered to have a specific contribution to the macroscopic behavior in the visco-elastic regime via two kinds of deformation modes : interlamellar separation or compression and interlamellar shear.²⁶ Lamella separation is the dominant mode in equatorial regions of spherulitic PE. The resistance to the interlamellar separation depends on the microstructure of the material, more particularly on the number and distribution of the mechanically active tie molecules bridging the crystalline lamellae.^{27,28} The lateral extend of the lamellar crystals having a very high shape factor may also contribute to the apparent stiffness of the soft amorphous layer by preventing its lateral contraction, *i.e.* the Poisson's effect.^{26,29} In this case, the amorphous tensile modulus should be

closer to the bulk modulus than to Young's modulus. Consequently, the latter amorphous phase might be significantly stiffer than bulk rubbery PE in the molten state.

So far, efforts have been made for correlating long-term as well as short term mechanical properties of PE to the global chain topology. The natural draw ratio, or the strain-hardening, that both reflect the resistance of the macromolecular network to chain unfolding proved to be relevant factors for predicting such properties. Most authors argued about the major role of the amorphous phase via tie molecules as well as chain entanglements. However, the role of the chain topology of the amorphous phase on the small strain behavior of bulk PE remains under question. The debate about the amorphous phase stiffness of semi-crystalline polymers with flexible chains is an old one.³¹ It has become more acute in recent years in the context of micromechanical modelling mainly focused on PE (see for instance the discussion in ref.31) : is the amorphous modulus at RT close to the rubber-like modulus of bulk molten PE, or that of a highly crosslinked amorphous PE, or eventually that of a glassy polymer ?

In this work, the deformation behavior at the local scale of the lamellar stacking was followed up by in-situ SAXS and WAXS in order to approach the intrinsic properties of the interlamellar amorphous phase of PE in relation to crystallinity, crystal thickness and chain topology, over a wide temperature domain above RT. Endeavors have also been made to establish micro-macro scale correlations.

Experimental

Materials

Four polyethylenes with different contents of hexene counits (C6) and very close molecular weights were studied in this work. **Table 1** shows some characteristics of the materials.

Table 1. Characteristics of the polyethylenes : co-unit concentration, C6; number-average- and weight-average molecular weights, M_n and M_w ; crystallization onset, T_c^{onset} .

Materials	C6 (mol %)	M_n (kDa)	M_w (kDa)	T_c^{onset} (°C)
PE-A	1.8	14.3	49	114
PE-B	0.8	15.8	54	113
PE-C	0.1	15.4	65	124
PE-D	0.2	15	69	123

Sample preparation

The polymer pellets were compression-moulded into 500 μm thick sheets at 170°C and quenched into water at RT which were labeled “quenched”. The samples hereafter designated as “annealed” were prepared by heat-treatment of quenched sheets for 15 hours in a thermostatic oil bath at a temperature close to the crystallization onset. The samples called “isotherm” were re-melted at 170 °C and plunged for 15 hours into the same thermostatic oil bath at T_c^{onset} . During the two thermal treatments, the samples were kept into aluminium plates tightly sealed with a silicone rubber gasket to prevent oil contamination. All heat-treated materials are listed in Table 2 with their structural characteristics.

DSC analysis

The thermal behavior of the polymers was analysed with a DSC7 apparatus from Perkin-Elmer at a heating rate of 10 °C/min. The temperature and heat flow scales were calibrated using high purity indium. The crystallization onset, T_c^{onset} , upon cooling at 10°C/min was determined by using the standard Perkin-Elmer method. The crystal weight fraction, X_c , was assessed from the

ratio of the melting enthalpy of the sample to that of perfectly crystalline PE, $\Delta H_f^\circ = 290 \text{ J/g}$.³² In such computation of X_c , the interphase is excluded from the crystal content⁷ so that it should be considered as making part of the amorphous component in the framework of a two-phase model that is the case in this work. Further justification will be given below.

Tensile measurement

Dumbbell-shaped samples having 22 mm in gauge length and 5 mm in width were cut out from the 0.5 mm thick sheets. Nominal stress-strain curves were recorded on a MTS tensile testing machine at various draw temperatures in the range $25^\circ\text{C} \leq T_d \leq 100^\circ\text{C}$, using a constant crosshead speed providing an initial strain rate of $5 \times 10^{-3} \text{ s}^{-1}$. The nominal strain or macroscopic strain, ε_{macro} , was determined in the viscoelastic strain range from the displacement of the clamps owing to the homogeneous deformation of the sample prior to the yield point, after correction for the machine compliance.

The stress-strain curves were used to determine the elastic modulus of the sample using two independent recordings at each T_d value. The modulus was computed from the tangent at the origin of a 2nd order polynomial fitted on the 0-3% strain range of the experimental curves.

These tests also gave access to the natural draw ratio in the stable neck after yielding, λ_n , as described elsewhere.³³⁻³⁵ This parameter is known to be relevant of the density of stress transmitters, $[ST]$, *i.e.* intercrystalline tie molecules and chain entanglements.^{3,25} For the sake comparison λ_n data are given in **Table 2** together with $[ST]$ data computed from Brown's model.^{36,37} A 10-fold increase of $[ST]$ can be observed when λ_n drops by a factor 2. The $[ST]$ data are only given for information since Brown's model assumes no chain rearrangement during crystallization, that is only true for quenching but not for isothermal treatment.

Table 2. Physical characteristics of the heat-treated polyethylenes (see text for details).

Materials	X_c	ϕ_c	L_p (nm)	L_c (nm)	λ_n	$[ST]$	
PE-A	quenched	0.49	0.46	17	8	3.5	0.24
	annealed	0.52	0.49	23	11	4.0	0.17
	isotherm	0.53	0.50	24	12	4.7	0.15
PE-B	quenched	0.54	0.51	19	9	4.2	0.19
	annealed	0.62	0.59	22	13	4.7	0.14
	isotherm	0.65	0.62	26	16	5.5	0.09
PE-C	quenched	0.65	0.62	20	12	4.5	0.19
	annealed	0.73	0.70	30	21	6.0	0.08
	isotherm	0.75	0.72	36	26	7.5	0.03
PE-D	quenched	0.69	0.66	22	14	5.0	0.17
	annealed	0.77	0.74	30	22	5.7	0.08
	isotherm	0.80	0.78	37	29	7.0	0.03

SAXS and WAXS characterization

Small-angle X-ray scattering (SAXS) experiments were carried out on the BM02 beamline of the European Synchrotron Radiation Facility (ESRF, Grenoble, France). The 2D-patterns were recorded on a CCD camera from Ropper Scientific. Experiments were performed using an energy

of 8 keV (wavelength $\lambda = 0.154$ nm). The scale of scattering vector, q , was calibrated by means of silver behenate. Wide-angle X-ray scattering (WAXS) experiments were carried out on the same beamline at a sample-detector distance of 50 mm, using an energy of 24 keV (wavelength $\lambda = 0.051$ nm). The q -scale calibration was performed using a highly crystalline polyoxymethylene sample. Data corrections including dark current, flat field response and taper distortions were routinely performed using the *bm2img* software available on the beamline, for both SAXS and WAXS. Corrections were also carried out for the beam intensity fluctuations and for the background scattering.

Both *in-situ* SAXS and WAXS measurements during tensile drawing were performed on a stretching-stage equipped with a 5 kN load cell and a heating chamber. The dumbbell samples having 6.5 mm in gauge length and 3 mm in width were stretched at an initial strain rate of $6.4 \times 10^{-4} \text{ s}^{-1}$. The symmetric displacement of the two clamps allowed probing the same zone of the sample during the tests. Nominal strains were determined using the same procedure described in the *Tensile Measurements* subsection, including corrections for machine compliance. The recording times of the pattern were 5 s for SAXS and 2 s for WAXS in order to have the best compromise between scattering intensity and minimum strain increment during the recording.

The long period, L_p , of the lamella periodic stacking was calculated from the correlation maximum of the Lorentz-corrected intensity profile, $Iq^2(q)$, using the Bragg's relation

$$L_p = 2\pi/q_{peak} \quad (1)$$

where q_{peak} corresponds to the apex of the correlation peak.

The crystalline and amorphous lamella thicknesses, L_c and L_a respectively, were computed from the following relations

$$L_c = X_c (\rho/\rho_c) L_p \quad (\text{a}) \quad \text{and} \quad L_a = L_p - L_c \quad (\text{b}) \quad (2)$$

where $\rho_c = 1.003 \text{ g/cm}^3$ is the density of the PE orthorhombic crystal and ρ the density of the sample. Equations 2a and 2b are based on the assumption of a two-phase model with much greater lateral extend and length of the crystalline lamellae compared to thickness. This later assumption perfectly applies to the present high and medium density materials as judged from AFM observations.³⁸ Note that $X_c (\rho/\rho_c) = \alpha_c$ is the volume fraction crystallinity. The α_c , L_p and L_c data of all samples are given in **Table 2**, using the density data from a previous study.¹⁶

Results and analysis

Microstructure characterization

Figure 1 shows the crystalline and amorphous lamella thicknesses, L_c and L_a respectively, together with the natural draw ratio, λ_n , of all the samples as a function of crystallinity, X_c . The crystallinity and crystal thickness were found to be lowest ones for the *quenched* sample with the highest co-unit content and the highest ones for the *isotherm* sample with the lowest co-unit content. The annealing procedure was successfully applied to obtain intermediate levels of crystallinity and lamellar thicknesses for the four materials. A single correlation appears between L_c and X_c for the whole set of samples.

Figure 1 also shows that L_a slightly increases with decreasing X_c whereas L_c exhibits a strong increase. This observation can be ascribed to the crystallization-induced exclusion of the chain defects at the crystal-amorphous interface^{39,40} that reduces the length of the crystallizable methylene sequences. The higher is the defect content, the higher is L_a and the lower is L_c . Notwithstanding, it is to be noticed that the L_a variation is much weaker than that of L_c and much less sensitive to polymer composition and thermal treatment.

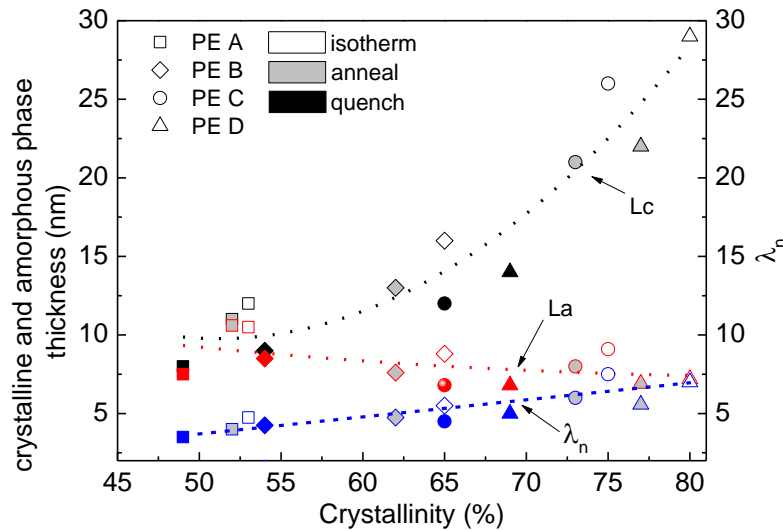


Figure 1. Crystalline lamella thickness L_c , interlamellar thickness L_a and natural draw ratio λ_n of samples as a function of crystallinity.

Figure 1 also shows the evolution with crystallinity of the natural draw ratio λ_n that has been taken into consideration in the present study as a relevant indicator of the concentration of stress transmitters $[ST]$. The draw ratio is indeed directly connected to the resistance to chain unfolding and the subsequent strain-hardening via the extensibility of the entangled macromolecular network.⁴¹ It has been reported in previous studies that λ_n exhibits a monotonic decrease with increasing $[ST]$.^{28,35} The data of **Table 2** perfectly corroborate this latter finding whereas **Figure 1** shows a roughly linear increase of λ_n with crystallinity.

In the following, special attention will be focused on the mechanical behavior of the materials in the small strain viscoelastic domain in order to probe the role of the stress transmitters of the entangled network on the mechanical coupling within the spherulites.

Local strain in the amorphous phase

The local mechanical behavior of the amorphous phase is approached in the framework of a two phase model disregarding the role of the interphase. In the present study, this assumption relies on two major points : 1) the interphase is included in the amorphous component when computing the crystal content as pointed out in the *DSC analysis* subsection; 2) all experiments were carried out above the temperature of the β relaxation that corresponds to the activation of molecular mobility in the interphase. Therefore, both the amorphous phase and interphase are in a rubbery state for draw temperatures above RT.

Hence, the high modulus contrast between the crystal and the rubbery amorphous phase is likely to have a strong impact on the macroscopic behavior of the various materials depending on their microstructure. However, due to its structural confinement at a nanometric scale between stiff crystalline lamellae, the amorphous phase may display strong modifications of its intrinsic properties with regard to bulk amorphous PE. Moreover, the chain topology modifications between the high and low crystallinity samples, due to different co-unit contents and different thermal treatments may also influence the local amorphous properties.

Upon uniaxial tensile testing, lamellae stacks in equatorial region of the spherulites separate from each other whereas they moves close together in the polar regions due to the Poisson's effect.⁴² The present study was mainly focused on the deformation of lamellae stacks in equatorial region that only undergo tensile deformation without shearing at small strains. Therefore, most properties were determined along the tensile direction. It was supposed that the deformation of the

crystal could be ignored in the viscoelastic domain compared to the deformation of the amorphous phase. Indeed, the modulus of the crystal is about 2 orders of magnitude higher than that of the amorphous phase in PE above RT, as will be discussed later.

In this hypothesis, the local change of the amorphous phase thickness is $\Delta L_a = \Delta L_p$, where ΔL_p is the long period variation as determined by *in situ* SAXS. Thus, the local strain of the interlamellar amorphous phase normal to the lamella surface in the equatorial region and parallel to the macroscopic tensile stress can be expressed as

$$\varepsilon_a = \Delta L_a / L_a \quad (3)$$

In a previous paper⁴² we focused on a scale transition factor between the macroscopic strain, ε_{macro} , and the local strain defined as $\varepsilon_{local} = \Delta L_p / L_p$. The major reason for using the local strain as defined in of Equation 3 is to get access to the intrinsic mechanical behavior of the amorphous phase.

The ε_a variations of quenched PE-D in equatorial region are plotted in **Figure 2** as a function of the macroscopic strain ε_{macro} . A fairly linear increase of ε_a versus ε_{macro} can be observed in the initial viscoelastic regime, for the various T_d values. This applies for all of the samples prepared from the four PE materials not shown on Figure 2. The $\varepsilon_a / \varepsilon_{macro}$ ratio proved to be a constant for each sample, but displays a slight sensitivity to T_d . This T_d dependence will be further discussed in the following.

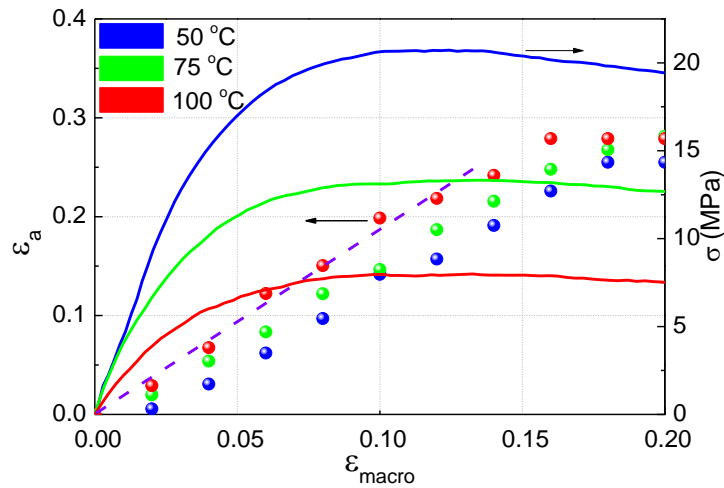


Figure 2. Local deformation behavior of interlamellar amorphous phase in equatorial region, for quenched PE-D at various T_d .

This $\varepsilon_a / \varepsilon_{macro}$ ratio is a key factor for understanding how the stress and strain are transmitted throughout the spherulites in semi-crystalline polymers in the viscoelastic regime. In the equatorial regions of the spherulites, only the parts of the twisted lamella stacks that are under grazing incidence are viewed in SAXS, i.e. those lying normal to the applied stress. Thereby, a *series* mechanical coupling can be assumed in 1st approximation in the equatorial region. In this hypothesis, the macroscopic strain should obey the following relation

$$\varepsilon_{macro} = \varepsilon_a (1 - \alpha_c) + \varepsilon_c \alpha_c \quad (4)$$

where ε_a and ε_c are the local strains in the amorphous and crystalline phase, respectively, and α_c is the volume crystallinity.

Considering that the crystal deformation is much smaller than that of the amorphous layer, Eq.4 can be reduced to

$$\varepsilon_a = \varepsilon_{macro} / (1 - \alpha_c) \quad (5)$$

Figure 3 shows the evolution of the $\varepsilon_a/\varepsilon_{macro}$ ratio as a function of $1/(1-\alpha_c)$. The fairly linear relationship for every T_d value agrees with Eq.5. Besides, this $\varepsilon_a/\varepsilon_{macro}$ ratio is greater than unity and increases with X_c . This is due to the strain amplification in the amorphous phase to compensate for the negligible deformation of the crystalline component. However, it should be noted that the experimental $\varepsilon_a/\varepsilon_{macro}$ values of Figure 3 are significantly lower than the ones predicted from Eq. 4 at RT, i.e. $2 < \varepsilon_a/\varepsilon_{macro} < 5$ for the present samples having $0.5 < \alpha_c < 0.8$. This suggests that the amorphous strain in equatorial regions is smaller than in other regions. This means that the strain distribution is highly heterogeneous over the spherulite volume.

One could be tempted to assign the above observation to the previously mentioned effect of bulk modulus that makes the amorphous phase much stiffer than a rubber under tensile testing. However, if this was the case the stiffness of the amorphous phase in equatorial region should increase with X_c , due to the slight increase of the shape factor of the amorphous layers. However, this is contradictory to observations, which means that the bulk modulus effect may be much smaller than the $[ST]$ effect.

Alternatively, the increase of the strain heterogeneity with X_c may be attributed to a modification of the mechanical coupling of the crystalline lamellae, namely an increasing percolation that would increase the loading on the polar lamellae. This would result in partial unloading of the lamella stacks in equatorial region. This point regarding the strain heterogeneity will be further addressed in the following.

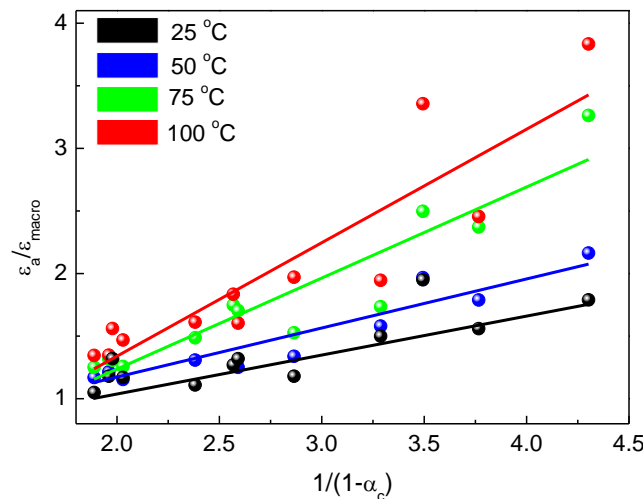


Figure 3 : Ratio $\varepsilon_a/\varepsilon_{macro}$ in equatorial regions as a function of $1/(1-\alpha_c)$ for all the materials at different T_d .

Worth noticing is that the $\varepsilon_a/\varepsilon_{macro}$ ratio increases with increasing T_d close to the value predicted by Eq. 4 (Fig.3), this effect being stronger at high X_c . This is an indication of a gradual evolution towards strain homogeneity, especially in the case of the more crystalline samples. This could be attributed to the enhancement of the molecular mobility in the crystalline phase that makes the lamellae more compliant as T_d increases. This indeed enables stress relaxation in the equatorial stacks that proved to be less compliant than the average.

Crist *et al.*³¹ have argued on the sensitivity to temperature and crystallinity of the elastic modulus of the amorphous phase in PE. These authors argued that the amorphous chains are able to relax stresses owing to the activation of the crystalline mechanical relaxation.¹⁹ Borrowing from this approach, previous dynamic mechanical data on the materials of the present study¹⁶ have been examined with special attention to the crystallinity and temperature effects. These data clearly show that the strength of the crystalline relaxation increases with X_c , at a given temperature. This suggests that the relaxation ability of the amorphous chains should increase

with X_c , that is actually observed. Besides, for a given sample, the crystalline relaxation strength increases with increasing T_d in the present T_d range, so that the amorphous chain relaxation should increase with T_d . This is also actually observed. Both these findings support the proposed mechanism for the heterogeneous-to-homogeneous deformation transition with increasing T_d , in relation to X_c .

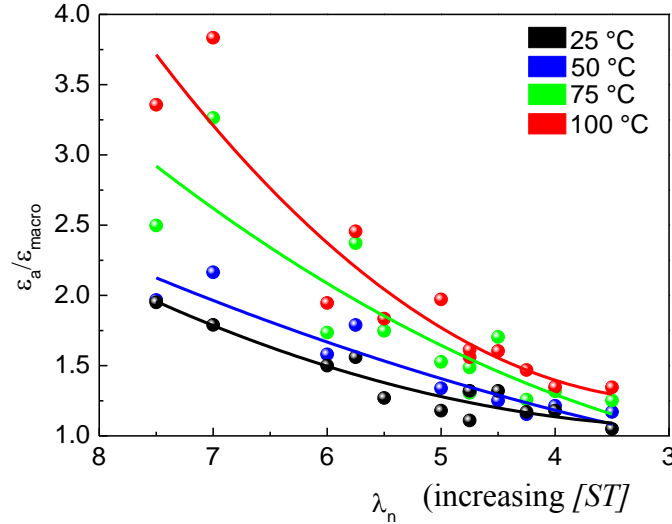


Figure 4 : Ratio $\varepsilon_a/\varepsilon_{macro}$ in equatorial region versus natural draw ratio λ_n for all the materials at different T_d .

The ratio $\varepsilon_a/\varepsilon_{macro}$ is plotted in **Figure 4** as a function of the natural draw ratio λ_n for different T_d . The corresponding $[ST]$ variation is indicated on the λ_n scale for the sake of the discussion. Irrespective of the T_d value, the $\varepsilon_a/\varepsilon_{macro}$ ratio decreases with decreasing λ_n , i.e. with increasing $[ST]$. The local deformation of the interlamellar amorphous phase in equatorial region appears to be strongly dependent on the content of stress transmitters : the higher $[ST]$ the stronger the amorphous phase resistance to deformation at equivalent ε_{macro} .

All the above data give evidence that the stiffness of the interlamellar amorphous phase in equatorial region is strongly temperature- and structure-dependent as judged from its strain relationship with the macroscopic strain. However, two major effects may contribute to these dependencies : the intrinsic amorphous modulus and the strain heterogeneity. A relevant way to alleviate the doubts on the actual contributions of the two factors is the experimental determination of the intrinsic elastic modulus of the amorphous phase.

Local stress in the amorphous phase

The methodology for determining the local stress in the amorphous layers of equatorial regions relies on using the crystal as a local stress gauge. The local stress at the scale of a single lamella can be estimated from the strain in the crystal as determined by *in situ* WAXS and from theoretical values of the crystal elastic constants. **Figure 5** shows a part of a twisted lamella stack in equatorial region and the corresponding SAXS and WAXS patterns used for computing the local strain and stress. Only two twisted lamellae are shown for clarity. The polar SAXS sector arising from the part of the twist normal to the tensile direction (\perp TD) that is under grazing incidence was previously used for determining the local strain in the amorphous layer, ε_a , parallel to the applied tensile stress. Regarding the local stress parallel to the tensile direction, the logical way would be to use the (002) crystal reflection in polar sector of the WAXS pattern arising from the same part of the twist. This reflection refers to the spacing of the crystallographic c -axis that is normal to the lamella surface and parallel to the tensile stress (see the \perp TD part in Fig.5). This reflection was used for computing the C_{33} elastic constant along the chain axis in the case of

oriented PE samples that obey an elastic behavior up to stress level as high as 1 GPa.⁴³⁻⁴⁵ The C_{33} constant is yet extremely high, i.e. several tens of GPa, so that the stress-induced shift of the (002) reflection turned out undetectable in the present study of the pre-yield strain domain for which the stress did not exceed 25 MPa.

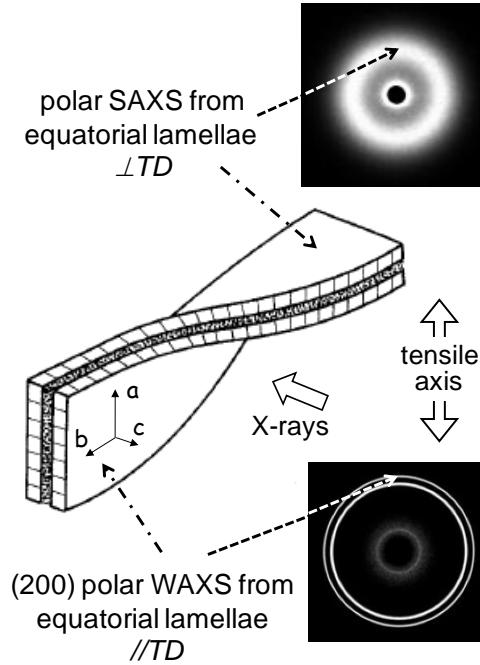


Figure 5 : Schematic of a twisted lamella stack in equatorial region of the spherulite and the corresponding SAXS and WAXS patterns prior to deformation ($\perp TD$ = normal to tensile direction; $//TD$ = parallel to tensile direction).

An alternative methodology is based on the analysis of the (200) reflection in the polar sector of the WAXS patterns arising from of the parts of the twisted lamellae parallel to the tensile direction ($//TD$) in equatorial region (Fig.5). This plane is normal to the crystallographic a -axis, i.e. normal to the tensile stress so that its spacing would change directly in relation to the local stress parallel to the tensile direction. This is actually an approximation due to the fact that the appearance of the (200) reflection implies that the (200) planes are inclined with an incident angle $\theta \approx 12^\circ$ to the X-ray beam so that they are not strictly normal to the tensile stress.

The proposed methodology assumes that, in the quasi-static conditions of the present experiments, the local stress parallel to the tensile direction is uniform in both the $//TD$ and the $\perp TD$ parts of the twisted equatorial lamellae. This is not a *strong* hypothesis considering that the twist length is a few microns compared to the several tens of microns for the lamella length. This structural characteristic makes the lamella stacks highly coherent on a mechanical standpoint. Indeed, if the local stress in equatorial region was not fairly uniform all along the lamellae, the stacking long period would rapidly vanish with increasing macroscopic strain in the viscoelastic domain. The long period from the equatorial region is actually well preserved up to $\varepsilon_{macro} = 0.2$, i.e. largely beyond the yield point (Fig.2).

Under such considerations, and taking advantage of the *series* coupling of the amorphous and crystalline phases in the $\perp TD$ lamella parts (Fig.5), it is quite reasonable to assume

$$\sigma_a \approx \sigma_c \quad (6)$$

This enable to focus on the local deformation of the crystal thanks to the evolution of (200) spacing, d_{200}^{eq} , in the tensile direction of the $//TD$ lamella parts (Fig.5). **Figure 6** shows an

example of the changes in intensity profile of the polar (200) reflection for isotherm PE-D drawn at $T_d = 50\text{ }^\circ\text{C}$. The (200) peak gradually moves to a smaller scattering angle indicating

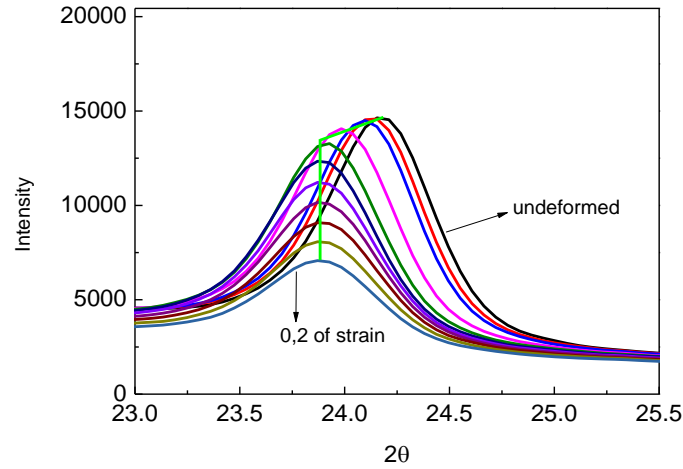


Figure 6 : Intensity profiles of the (200) polar reflection from the equatorial region of the spherulites as a function of macroscopic strain for isotherm PE-D at $T_d = 50\text{ }^\circ\text{C}$.

an increase of d_{200}^{eq} under strain. In parallel, the intensity of the (200) peak decreases with increasing strain. This is partly due to the thinning down of the sample and to the strain-induced texturing, i.e. the gradual tilting of the lamellae in preferred diagonal orientation.

The evolution of d_{200}^{eq} as a function of strain is reported in **Figure 7** for the various PE-D samples at different T_d . Prior to deformation, the d_{200}^{eq} value is the smallest one for isotherm PE-D whereas it is the greatest one for quenched PE-D. This is relevant to an increasing content of crystallographic defects with increasing crystallization rate due to an increasing occlusion of co-units in the crystals which should normally be excluded. The initial d_{200}^{eq} value prior to deformation also shows an increase with T_d due to the thermal expansion of the crystal. Both these observations apply to the four polymers.

Regarding the d_{200}^{eq} evolution with strain (Fig.7), it is to be noticed first a linear increase up to $\varepsilon_{macro} \approx 0.10$, indicating that the crystal obeys an elastic behavior before yield. Second, the slope of the linear domain is fairly the same for the various PE-D samples irrespective the draw temperature. This finding applies for the four polymers.

Computing the crystal strain along the tensile direction in the //TD parts of the equatorial lamellae, ε_c , via the following equation

$$\varepsilon_c = \Delta d_{200}^{eq} / d_{200}^{eq} \quad (7)$$

one gets a unique correlation $\varepsilon_c / \varepsilon_{macro} = 0.10 \pm 0.02$ for all T_d from Figure 7. This insensitivity on microstructure and temperature of ε_c in equatorial region as a function of ε_{macro} is rather surprising, especially in consideration that the corresponding ratio for the amorphous phase, $\varepsilon_a / \varepsilon_{macro}$, is highly variable (Figs. 3 and 4). This finding may result from compensation effects of several factors having inverse dependences on temperature or microstructure. This point will be argued in the *Concluding Discussion*, at the light of additional informations provided below.

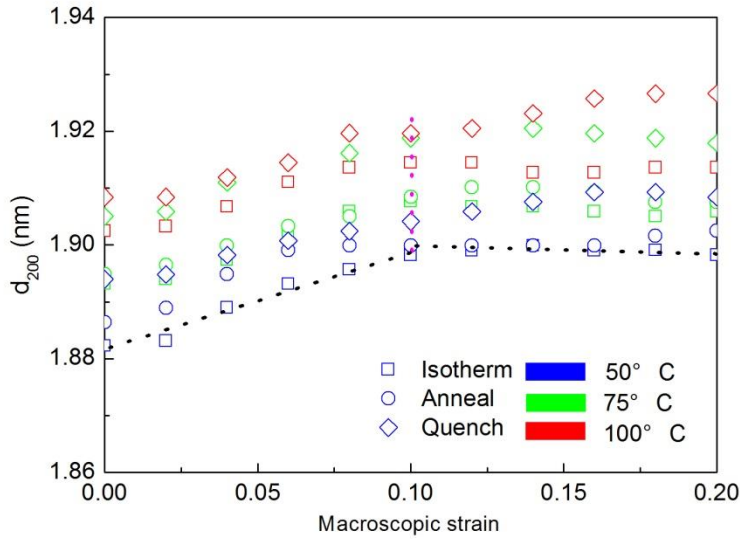


Figure 7 : Crystallographic spacing, d_{200}^{eq} , as function of nominal strain for the various PE-D samples for different T_d .

Beyond the macroscopic yield strain, d_{200}^{eq} levels off (Fig.7). This is a direct evidence of the activation of plastic deformation beyond the yield point via crystal shear with little change in crystallographic spacings due to the global stress levelling off. This finding however does not mean that the (200) planes are plastically active and does not provide information on the kind of crystal planes that do exhibit crystal shear.

The local stress in the crystal, σ_c , can be then computed from the general relation

$$\sigma_c = \varepsilon_c E_c \quad (8)$$

where E_c is the crystal elastic modulus in the direction under consideration, namely the C_{11} elastic constant along the crystallographic a -axis of the //TD crystals in equatorial regions (Fig.5). The E_c values used in the present study are taken from the C_{11} experimental data reported by Choy & Cheung⁴⁶ that are relevant to a real material having crystallographic defects. These E_c values are 7.0 GPa @ 25°C, 5.9 GPa @ 50°C, 5.6 GPa @ 75°C and 5.3 GPa @ 100°C. These data are somewhat lower than the theoretical ones from Goddard et al.⁴⁷ or Rutledge et al.⁴⁸ based on a perfectly crystalline material. It is yet to be noticed that the two kinds of C_{11} data display similar temperature-dependence.

Thanks to the *in-situ* tests, the local stress can be compared to the macroscopic stress and strain. **Figure 8** shows the local stress in equatorial region and the macroscopic stress of quenched PE-A as a function of the macroscopic strain at different T_d . The σ_c local stress is significantly higher than the macroscopic stress, σ_{macro} . However, σ_c linearly increases with

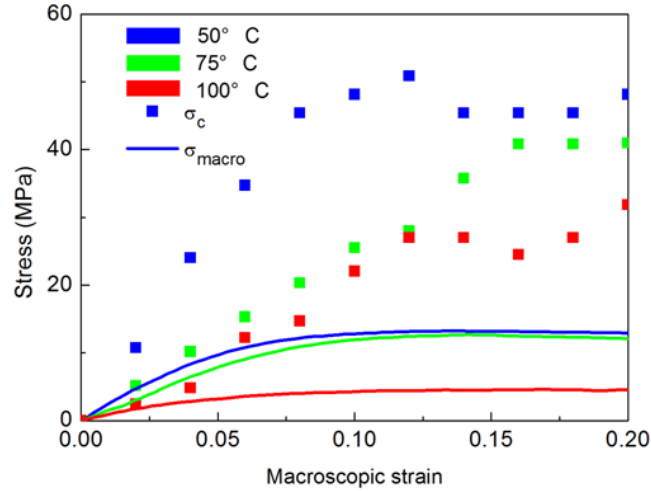


Figure 8 : Local stress, σ_c , in //TD parts of equatorial lamellae and macroscopic stress, σ_{macro} , as a function of macroscopic strain, ε_{macro} , for quenched PE-A at different T_d .

ε_{macro} before yield similar to σ_{macro} . Moreover, both σ_c and σ_{macro} reach a maximum value at nearly the same ε_{macro} value, i.e. that of the yield point. This latter observation provides additional support to the methodology presently chosen for determining σ_c .

The drop of σ_c with increasing T_d is related to the drop of the C_{11} values reported above. This is a direct consequence of the activation of the molecular mobility in the crystalline phase over a large temperature domain below the melting point.

Elastic modulus of the amorphous phase

It was assumed above that the \perp TD parts of the twisted crystalline lamellae and interlamellar amorphous layers in equatorial region are in *series* coupling. This implies a uniform stress distribution on the two components normal to the lamella surface, as expressed by Equation 6. This is the situation depicted in Figure 5. Considering the local strain measurement of the interlamellar amorphous phase by *in-situ* SAXS, the local tensile behavior of the amorphous phase could be readily determined.

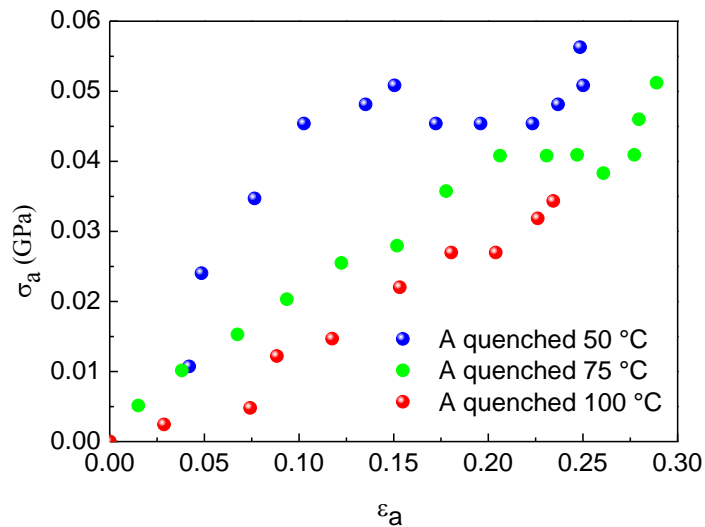


Figure 9 : Local stress – strain curves for quenched PE-A at different T_d .

Figure 9 shows the local stress - strain curves of the amorphous phase in equatorial region of quenched PE-A for various temperatures. The stress first exhibit a roughly linear increase with strain before to reach a pseudo-plateau corresponding to the plastic behavior due to activation of crystal shear. From the initial slope of these plots, an apparent tensile modulus of the amorphous phase, M_a , can be defined from the equation

$$\sigma_a = M_a \varepsilon_a \quad (12)$$

This elastic modulus of the amorphous phase in equatorial regions is said *apparent* tensile modulus since it is actually a combination of tensile and bulk moduli due to the stress triaxiality imposed on the amorphous layers by the structural confinement between the very large and stiff crystalline lamellae. It cannot be associated with the Young's modulus.

Figure 10a shows the M_a variations with X_c for all the materials of the study at different T_d . For every T_d , the apparent tensile modulus of the amorphous phase decreases with increasing X_c . This finding is quite surprising and even unexpected in consideration that the macroscopic modulus exhibits an inverse variation as can be seen in **Figure 11**. This latter figure is yet in perfect agreement with literature data essentially determined at RT.^{2,12,15,30,49,50}

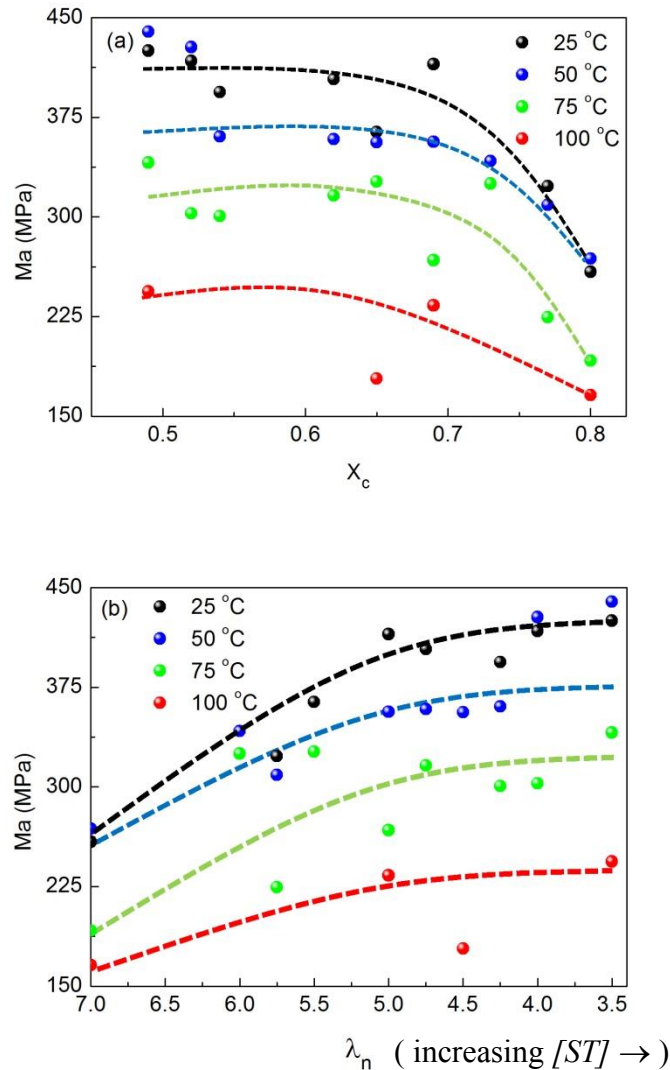


Figure 10: Apparent modulus of the amorphous phase as a function of a) the crystallinity and b) the natural draw ratio for all the PE samples at different T_d .

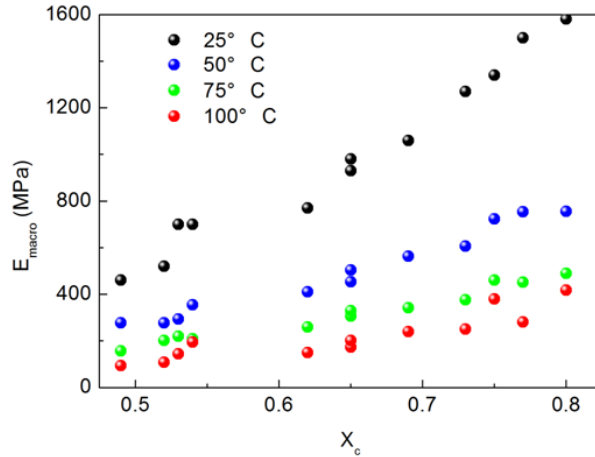


Figure 11: Macroscopic elastic modulus of all PE samples as a function of X_c for the various T_d .

Alternatively, M_a has been plotted in **Figure 10b** as a function of λ_n . Reminding that λ_n is an indirect indication of the concentration stress transmitters, $[ST]$, the monotonic increase of M_a with decreasing λ_n irrespective of T_d may be ascribed to the corresponding increase of $[ST]$ (see Table 2). The same explanation applies to the previous M_a drop with increasing X_c . It is

noteworthy that $250 < M_a < 420$ MPa at 25°C depending on the PE sample. These figures are much higher than those reported in the literature for the Young's modulus of bulk amorphous PE that is in the range 2-10 MPa.^{30,31} This point will be more precisely discussed in the next *Concluding Discussion* in the context of the controversial literature data.

Concluding discussion

Several points that have been addressed in this work deserve a critical discussion in regard to previous studies dealing with the mechanical properties of semi-crystalline polymers.

Point 1. The local stress-strain behaviour of interlamellar amorphous phase in equatorial regions of the spherulites was studied by in-situ SAXS and WAXS for PE samples covering a wide range of crystallinity and over the temperature range 25-100°C. For the lower crystallinity materials the local deformation in equatorial regions where the crystalline lamellae are perpendicular to the main stress fairly obeys a *series* coupling of the amorphous and crystal phases that is relevant of a homogeneous stress distribution. However, with the increase of crystallinity, it was shown that the mechanical coupling gradually changes from *series* to *parallel* giving an increasing role to the stiffer crystalline component. This is perfectly consistent with previous data¹⁶ showing that over a very large range $0.20 < X_c < 0.85$ the macroscopic modulus of PE-based polymers display an evolution from “close to *series* coupling” to “close to *parallel* coupling” that is assigned to the increasing shape factor of the stiff crystallites together with an increasing percolation of these crystallites. This makes the polar regions become gradually much stiffer than the equatorial regions due to the actual parallel arrangement in these regions in addition to the percolation effect that generates a strongly heterogeneous strain distribution.

Regarding the effect of the deformation temperature, the local strain in the amorphous phase of the equatorial regions became closer to the predicted value of the *series* coupling for any sample which is an indication of an increasing stress homogeneity. This can be intuitively attributed to the activation of chain mobility in the crystalline phase that enabled the relaxation of the more strained amorphous chains, the crystalline relaxation being all the more efficient as temperature increases. From a general standpoint, these findings and interpretation contribute to the understanding of the origins of the more or less homogeneous deformation of spherulites that has been clearly revealed by direct observation techniques for a number of semi-crystalline polymers, depending on experimental conditions.⁵¹⁻⁵⁹

Point 2. One may wonder about the opposite evolutions of the amorphous modulus M_a and the macroscopic modulus as a function of crystallinity (Figs.10 and 11). This is an indication that M_a does not contribute a predominant role to E_{macro} and that this contribution even recedes when X_c increases. It is suggested that a major contribution comes from the above-mentioned evolution with increasing X_c of the strain distribution throughout the spherulites, namely a gradual increase of *parallel* coupling giving an increasing role to the stiff crystal phase via a gradual percolation of the crystalline lamellae. This coupling effect largely counterbalances the M_a drop of the soft amorphous phase.

In support to this latter conclusion, it is worth looking at the evolution of the $\sigma_{local}/\sigma_{macro}$ ratio in equatorial region as a function of X_c . Considering a constant nominal strain $\epsilon_{macro} = 0.03$, one gets $\sigma_{local}/\sigma_{macro} \approx 2.5$ whatever T_d for quenched PE-A having the lower crystallinity (Fig.8). In contrast, for isotherm PE-D having the higher crystallinity, $\sigma_{local}/\sigma_{macro} \approx 1.7$. These data clearly show that the local loading in equatorial regions decreases with increasing X_c . This means that other regions of the spherulites are bearing an increasing part of the applied load. This is an indirect evidence that a percolating network of the crystalline lamellae gradually develops as X_c increases due to gradual build up of crystal interconnections, via the core region of the spherulites or via lamellae branching. This phenomenon gives the polar regions a predominant role at high X_c compared with the equatorial regions that may have a predominant role at low X_c .

Point 3. Regarding the high M_a values and the $M_a = f(X_c)$ relationship, the structural confinement effect due to the high shape factor of the crystalline lamellae^{38,60} has been suggested to restrict the lateral contraction of the soft interlamellar amorphous layers under tensile loading as in an oedometric test. The elastic modulus of the latter phase should be thus closer to the bulk modulus of rubbery PE, K , than to its Young's modulus, E . As a matter of fact, the so-called longitudinal modulus, M , of a material in the case of oedometric strain conditions is given by the relation⁶¹

$$M = \frac{3K(3K+E)}{9K-E} \quad (13)$$

It may be associated to the M_a modulus of the confined amorphous layers in the present study. Then considering the following values $K = 1-3$ GPa^{31,62-64} and $E = 3-10$ MPa^{65,66} for PE in the bulk rubbery state, Eq.13 predicts $M \approx K \approx 1-3$ GPa that is somewhat higher than the present experimental M_a values (Fig.10).

This M_a deviation from the prediction of Eq.13 suggests that the lamella stacks in equatorial regions are only under partial oedometric strain conditions. Moreover, the above computation does not account for the observed decrease of M_a with increasing X_c (Table2). Indeed, increasing X_c is likely to be accompanied by an increase of the lamella shape factor that would enhance the oedometric effect, i.e. an increase of M_a towards the M value predicted from Eq.13. This effect of the shape factor could be quantitatively taken into account by the so-called poker-chip model.⁶⁷⁻⁶⁹ In the present instance, the observed M_a decrease was attributed to the concomitant decrease of the density of stress-transmitters in the amorphous phase (see Table 2). The reason of the inverse evolution of $[ST]$ versus X_c lies in the capability of highly crystalline samples to undergo chain-reeling during crystallization that promotes chain-disentanglement and improves regular chain-folding.⁷⁰ Therefore one should suspect a contribution of the stress transmitter concentration in the amorphous phase stiffness, i.e. the E factor in Eq.13. Considering that $[ST]$ increases by a factor 8 over the whole X_c range (Table 2), one would expect a significant increase of E beyond the bulk isotropic value of 3-10 MPa. Moreover, this increase of the E modulus should be high enough to account for the M_a variation of 100-150 MPa that is observed over the whole X_c domain in opposition to the expected effect of the shape factor, for all the T_d values (Fig.10a).

In support to our claim, it is worth noticing Addiego et al.'s study⁷¹ of the volume strain under tensile testing of various PE materials in the crystallinity range $0.40 < X_c < 0.75$. The reduced ability for cavitation as well as increasing trend for homogeneous deformation with decreasing X_c was attributed to an increase of the stress transmitter density in the amorphous

phase as inferred from structural parameters. This is in perfect agreement with our observations and conclusion.

Point 4. The apparent modulus of the amorphous phase, M_a , was estimated by measuring both the local stress and the local strain in equatorial regions of the spherulites. The M_a values proved to be surprisingly high with regard to the bulk modulus of amorphous PE: indeed, $M_a \approx 250\text{--}450$ MPa at RT as compared with the values $E_a = 3\text{--}10$ MPa reported for the Young's modulus of bulk molten PE.^{31,65,66} As pointed out above, such high M_a values are suggested to result from two major factors : 1st the structural confinement of the amorphous phase between large and stiff crystalline lamellae; 2nd the density of stress transmitters that is much greater than in the molten material due to the presence of intercrystalline tie chains⁶⁹ and a higher concentration of crystallization-segregated chain entanglements.⁴ It is worth to discuss the present M_a experimental data in comparison to the ones quoted in the literature in the context of mechanical modelling. In recent years, several groups have tackled the problem of predicting the mechanical behavior of semicrystalline polymers by means of micromechanical modelling. Such approaches tried to take into account the microstructural aspects of the materials and the intrinsic properties of the components. The values of the elastic constants of the crystalline phase are rather consensual. These have generally been borrowed from theoretical computations or from WAXS experiments. In contrast, the amorphous phase modulus has often been postulated. Most authors dealing with the micromechanical modelling of PE have adopted very low values the Young's or shear moduli, i.e. $E_a = 3\text{--}10$ MPa or $G_a = 1\text{--}3$ MPa respectively, for the bulk rubbery state as pointed out above.^{14,15,72-76} These E_a or G_a values are extrapolated from macroscopic modulus data, either at $X_c = 0$ in the solid state, or at $T = 25^\circ\text{C}$ in the molten state. However, such methods only provide the rubbery modulus of bulk amorphous PE but not that of the confined amorphous phase in the semi-crystalline PE.

In contrast, several authors have been dealing with the identification of the E_a or G_a moduli of semi-crystalline polymers by means of inverse modeling, i.e. fitting macroscopic data with variable E_a or G_a values using a multi-phase or composite model. Most of these studies gave E_a or G_a values for PE about 2 orders of magnitude greater than the ones reported above,^{31,77,78} in agreement with the present study. Using a Halpin-Tsai model, Boyd⁷⁷ reported $G_a \approx 200$ MPa @ 0° decreasing to $G_a \approx 130$ MPa at RT, but insensitive to X_c . Also using a Halpin-Tsai modelling, Crist et al.³¹ reported $70 \text{ MPa} < E_a < 300 \text{ MPa}$ for $0.5 < X_c < 0.8$ at RT.

One should also mention an early experimental determination of the amorphous phase stiffness in medium density PE by in situ SAXS⁷⁹ giving 150 MPa @ RT, in agreement with the present M_a data.

Back to Crist et al.'s work,³¹ it is worth pointing out that E_a was reported to increase with X_c in strong contrast with Boyd's findings and the present ones as well. It was claimed that the crystalline relaxation becomes less active with increasing L_c (L_c increases in parallel with X_c) so that the amorphous chains gradually lose their relaxation ability. Our interpretation is quite different. Indeed, the opposite variations of M_a and X_c in the present study are assigned to the density of stress transmitters that increases with decreasing X_c . However, the role of the crystalline relaxation is also taken into account in our study via the M_a temperature sensitivity : indeed, the temperature-promoted chain relaxation in the crystal enables a relaxation of the amorphous chains that in turn involves a M_a drop with increasing T_d (Fig.10).

Point 5. The relation $\varepsilon_c/\varepsilon_{macro} = 0.10 \pm 0.02$ in equatorial regions for all samples, irrespective of X_c and T_d (Fig.7), is a quite surprising finding especially when considering that the corresponding ratio for the amorphous phase, $\varepsilon_d/\varepsilon_{macro}$, is highly variable (Figs.3 and 4). This observation may be ascribed to the combination of several factors involving compensation effects due to inverse dependences on temperature and/or microstructure. Here are two possible explanations. First, if considering an increase of T_d at constant values of ε_{macro} and X_c , the increase of $\varepsilon_d/\varepsilon_{macro}$ ratio (Fig.3) indicates an increase of the amorphous strain in equatorial regions due to

chain relaxation in the crystal. This involves a decrease of the local stress $\sigma_a = \sigma_c$, and of the C_{33} elastic constant as well so that the crystal strain is likely to change very little. Second, if considering a decrease of X_c at constant value of ε_{macro} and T_d , the drop of $\varepsilon_c/\varepsilon_{macro}$ ratio (Fig.4) results from an increase of $[ST]$. Concomitantly, the macroscopic stress drops with the decrease of X_c , involving a decrease of σ_c but this stress depression is compensated in the equatorial region by the reduction of crystal percolation that promotes a stress transfer from the polar to the equatorial regions. Both situations that correspond to an improvement of homogeneity of the macroscopic deformation do contribute to the $\varepsilon_c/\varepsilon_{macro}$ quasi-invariance, but they may not be the sole reasons.

Acknowledgments

The authors are indebted to the European Synchrotron Radiation Facility (ESRF, Grenoble, France) for time allocation on the BM02 beamline. The authors also acknowledge the Scholarship Council of China for the grant of a doctoral fellowship to B. Xiong.

References

- 1 (a) Schultz, J. M. *Polymer Materials Science*; Prentice-Hall, Englewood Cliffs, N.J. 1974.
(b) Hoffman, J. D.; Davis, G. T.; Lauritzen, J. I. The rate of crystallization of linear polymers with chain folding. In *Treatise on Solid State Chemistry, Vol. 3: Crystalline and Non-Crystalline Solids*; Hannay N. B. Ed.; Plenum Press New York; 1976: pp.497-614.
- 2 Peacock, A. *Handbook of Polyethylene: Structures, Properties and Applications* : CRC Press, New York; 2000.
- 3 Seguela, R. Critical review of the molecular topology of semicrystalline polymers: The origin and assessment of intercrystalline tie molecules and chain entanglements. *J. Polym. Sci., Polym. Phys.* **2005**, *43*, 1729–1748.
- 4 Lee, S.; Rutledge, G. C. Plastic deformation of semicrystalline polyethylene by molecular simulation. *Macromolecules* **2011**, *44*, 3096–3108.
- 5 Boyer, R. F. Apparent double glass transition in semi-crystalline polymers. *J. Macromol. Sci., Phys.* **1973**, *B8*, 503–537.
- 6 Kitamaru, R.; Horii, F. NMR approach to the phase structure of linear polyethylene. *Adv. Polym. Sci.* **1978**, *26*, 137–178.
- 7 Mandelkern, L.; Alamo, R. G.; Kennedy, M. A. The interphase thickness of linear polyethylene. *Macromolecules* **1990**, *23*, 4721–4723.
- 8 Cheng, J.; Fone, M.; Reddy, V. N.; Schwartz, K. B.; Fisher, H. P.; Wunderlich, B. Identification and quantitative analysis of the intermediate phase in a linear high-density polyethylene. *J. Polym. Sci., Polym. Phys.* **1994**, *32*, 2683–2693.
- 9 Singhal, A.; Fina, L. J. Dynamic two-dimensional infra-red spectroscopy of the crystal-amorphous interphase region in low-density polyethylene. *Polymer* **1996**, *37*, 2335–2343.
- 10 Baker, A.; Windle, A. Evidence for a partially ordered component in polyethylene from wide-angle X-ray diffraction. *Polymer* **2001**, *42*, 667–680.
- 11 Sajkiewicz, P.; Hashimoto, T.; Saijo, K.; Gradys, A. Intermediate phase in polyethylene as elucidated by WAXS. Analysis of crystallization kinetics. *Polymer* **2005**, *46*, 513–521.
- 12 Boyd, R. H. Relaxation processes in crystalline polymers : experimental behaviour - a review. *Polymer* **1985**, *26*, 323–347.
- 13 Popli, R.; Glotin, M.; Mandelkern, L. Dynamic mechanical studies of α and β relaxations of polyethylenes. *J. Polym. Sci., Polym. Phys.* **1984**, *22*, 407–448.
- 14 Sedighiamiri, A.; van Erp, T. B.; Peters, G. W. M.; Govaert, L. E.; van Dommelen, J. A. Micromechanical modelling of the elastic properties of semicrystalline polymers : a three-phase approach. *J. Polym. Sci., Polym. Phys.* **2010**, *48*, 2173–2184.

- 15 Ghazavizadeh, A.; Rutledge, G. C.; Atai, A. A.; Ahzi, S.; Remond, Y.; Soltani, N. Micromechanical characterization of the interphase layer in semi-crystalline polyethylene. *J. Polym. Sci., Polym. Phys.* **2013**, *51*, 1228–1243.
- 16 Humbert, S.; Lame, O.; Seguela, R.; Vigier, G. A re-examination of the elastic modulus dependence on crystallinity in semi-crystalline polymers. *Polymer* **2011**, *52*, 4899–4909.
- 17 Stachurski, Z. H.; Ward, I. M. (a) *Mechanical relaxations in polyethylene. J. Macromol. Sci., Phys.* **1969**, *B3*, 445–494. (b) *β -relaxations in polyethylenes and their anisotropy. J. Polym. Sci., Polym. Phys.* **1968**, *6*, 1817–1833.
- 18 Boyd, R. H. Strengths of the mechanical relaxation processes in linear polyethylene. *Macromolecules* **1984**, *17*, 903–911.
- 19 Boyd, R. H. Relaxation processes in crystalline polymers : Molecular interpretation - A review. *Polymer* **1985**, *26*, 1123–1133.
- 20 Khanna, Y. P.; Turi, E. A.; Taylor, T. J.; Vickroy, V. V.; Abbott, R. F. Dynamic mechanical relaxations in polyethylene. *Macromolecules* **1985**, *18*, 1302–1309.
- 21 Kolesov, I. S.; Androsch, R.; Radusch, H-J. Effect of crystal morphology and crystallinity on the mechanical α and β relaxation processes of short-chain branched polyethylene. *Macromolecules* **2005**, *38*, 445–453.
- 22 Boyd, R. H. Relaxation processes in crystalline polymers : Experimental behaviour - A review. *Polymer* **1985**, *26*, 323–347.
- 23 Galeski, A. Strength and toughness of crystalline polymer system. *Prog. Polym. Sci.* **2003**, *28*, 1643–1699.
- 24 Cheng, J. J.; Polak, M. A.; Penlidis, A. A tensile strain hardening test indicator of environmental stress cracking resistance. *J. Macromol. Sci., Pure & Appl. Chem.* **2008**, *A45*, 599–611
- 25 (a) Kurelec, L.; Teeuwen, M.; Schoffeleers, H.; Deblieck, R. Strain hardening modulus as a measure of environmental stress crack resistance of high density polyethylene. *Polymer* **2005**, *46*, 6369–6379. (b) Deblieck, R.; van Beek, D.; Remerie, K.; Ward, I. M. Failure mechanisms in polyolefins: The role of crazing, shear yielding and the entanglement network. *Polymer* **2011**, *52*, 2979–2990.
- 26 Lin, L.; Argon, A. S. Structure and plastic deformation of polyethylene. *J. Mater. Sci.* **1994**, *29*, 294–323.
- 27 Nitta, K.-H.; Takayanagi, M. Role of tie molecules in the yielding deformation of isotactic polypropylene. *J. Polym. Sci., Polym. Phys.* **1999**, *37*, 357–368.
- 28 Humbert, S.; Lame, O.; Chenal, J.-M.; Rochas, C.; Vigier, G. Small strain behavior of polyethylene: in situ SAXS study. *J. Polym. Sci., Polym. Phys.* **2010**, *48*, 1535–1542.
- 29 Pope, D. P.; Keller, A. Deformation of oriented polyethylene. *J. Polym. Sci., Polym. Phys.* **1975**, *13*, 533–566.
- 30 (a) Holliday, L.; White, J. W. The stiffness of polymers in relation to their structure. *Pure & Appl. Chem.* **1971**, *26*, 545–582. (b) Andrews, E. H. Morphology and mechanical properties of semi-crystalline polymers. *Pure & Appl. Chem.* **1974**, *39*, 179–194.
- 31 Crist, B.; Fisher, C. J.; Howard, P. R. Mechanical properties of model polyethylenes : Tensile elastic modulus and yield stress. *Macromolecules* **1989**, *22*, 1709–1718.
- 32 Wunderlich, B. *Macromolecular Physics, Vol. 3; Crystal melting*; Academic Press: New York 1980; chap. 8.
- 33 Hubert, L.; David, L.; Seguela, R.; Vigier, G.; Corfias-Zucalli, C.; Germain, Y. Physical and mechanical properties of polyethylene for pipes in relation to molecular architecture. *J. Appl. Polym. Sci.* **2002**, *84*, 2308–2317.
- 34 Cazenave, J.. Seguela, R.; Sixou, B.; Germain, Y. Short-term mechanical and structural approaches for the evaluation of polyethylene stress crack resistance. *Polymer* **2006**, *47*, 3904–3914.
- 35 Humbert, S.; Lame, O.; Vigier, G. Polyethylene yielding behaviour: What is behind the correlation between yield stress and crystallinity? *Polymer* **2009**, *50*, 3755–3761.

- 36 Huang, Y.-L.; Brown, N. The effect of molecular weight on slow crack growth in linear polyethylene homopolymers. *J. Mater. Sci.* **1988**, *23*, 3648–3655.
- 37 Huang, Y.-L.; Brown, N. Dependence of slow crack growth in polyethylene on butyl branch density: Morphology and theory. *J. Polym. Sci., Polym. Phys.* **1991**, *29*, 129–137.
- 38 Unpublished data from S.Humbert Thesis, INSA de Lyon, France, 2009.
- 39 Balta-Calleja, F. J.; Gonzalez Ortega, J. C.; Martinez Salazar, J. Distribution of chain defects and microstructure of melt crystallized PE. *Polymer* **1978**, *19*, 1094–1099.
- 40 (a) VanderHart, D. L.; Perez, E. A C-13 NMR method for determining the partitioning of end groups and side branches between the crystalline and non-crystalline regions in polyethylene. *Macromolecules* **1986**, *19*, 1902–1909. (b) Perez, E.; VanderHart, D. L.; Crist, B.; Howard, P. R. Morphological partitioning of ethyl branches in polyethylene by C-13 Nuclear magnetic resonance. *Macromolecules* **1987**, *20*, 78–87.
- 41 Seguela, R. On the natural draw ratio of semi-crystalline polymers: Review of the mechanical, physical and molecular aspects. *Macromol. Mater. Eng.* **2007**, *292*, 235–244.
- 42 Xiong, B.; Lame, O.; Chenal, J.-M.; Rochas, C.; Seguela, R.; Vigier, G. In-situ SAXS study of the mesoscale deformation of polyethylene in the pre-yield strain domain: Influence of microstructure and temperature. *Polymer* **2014**, *55*, 1223–1227.
- 43 Matsuo, M.; Sawatari, C. Elastic modulus of polyethylene in the crystal chain direction as measured by X-ray diffraction. *Macromolecules* **1986**, *19*, 2036–2040.
- 44 Prasad, K.; Grubb, D. T. X-ray modulus and strain distribution in single fibers of polyethylene. *J. Polym. Sci., Polym. Phys.* **1990**, *28*, 2199–2212.
- 45 Nakamae, K.; Nishino, T.; Ohkubo, H. Elastic modulus of crystalline regions of polyethylene with different microstructures. Experimental proof of homogeneous stress distribution. *J. Macromol. Sci., Phys.* **1991**, *B30*, 1-23
- 46 Choy, C. L.; Leung, W. P. Elastic moduli of ultra drawn polyethylene. *J. Polym. Sci., Polym. Phys.* **1985**, *23*, 1759–1780.
- 47 Karasawa, N.; Dasgupta, S.; Goddard III, W. A. Mechanical properties and force field parameters for polyethylene crystal. *J. Phys. Chem.* **1991**, *95*, 2260–2272.
- 48 Lacks, D. J.; Rutledge, G. C. Simulation of the temperature dependence of mechanical properties of polyethylene. *J. Phys. Chem.* **1994**, *98*, 1222–1231.
- 49 Bensason, S.; Minick, J.; Moet, A.; Chum, S.; Hiltner, A.; Baer, E. Classification of homogeneous ethylene-octene copolymers based on comonomer content. *J. Polym. Sci., Polym. Phys.* **1996**, *34*, 1301–1315.
- 50 (a) Kennedy, M.; Peacock, A. J.; Mandelkern, L. Tensile properties of crystalline polymers: Linear polyethylene. *Macromolecules* **1994**, *27*, 5297–5310. (b) Kennedy, M.; Peacock, A. J.; Failla, M. D.; Lucas, J. C.; Mandelkern, L. Tensile properties of crystalline polymers: Random copolymers of ethylene. *Macromolecules* **1995**, *28*, 1407–1421.
- 51 Hay, I.; Keller, A. Polymer deformation in terms of spherulites. *Colloid Polym. Sci.* **1965**, *204*, 43-74.
- 52 Weynant, E.; Haudin, J.-M.; G'Sell, C. In situ observation of the spherulite deformation in polybutene-1. *J. Mater. Sci.* **1980**, *15*, 2677–2692.
- 53 Aboulfaraj, M.; G'Sell, C.; Ulrich, B.; Dahoun, A. In situ observation of the plastic deformation of polypropylene spherulites under uniaxial tension and simple shear in the scanning electron microscope. *Polymer* **1995**, *36*, 731–742.
- 54 Drechsler, D.; Karbach, A.; Fuchs, H. Morphology and in situ deformation of polyamide films investigated by SFM. *Surf. Interface Anal.* **1997**, *25*, 537–542.
- 55 Ferreiro, V.; Penneec, Y.; Seguela, R.; Coulon, G. Shear banding in polyamide 6 films as revealed by atomic force microscopy. *Polymer* **2000**, *41*, 1561–1569.
- 56 Nitta, K.-H.; Takayanagi, M. Direct observation of the deformation of isolated huge spherulites in isotactic polypropylene. *J. Mater. Sci.* **2003**, *38*, 4889–4894.
- 57 Thomas, C.; Seguela, R.; Detrez, F.; Miri, V.; Vanmansart, C. Plastic deformation of spherulitic semi-crystalline polymers: An in situ AFM study of polybutene under tensile drawing. *Polymer* **2009**, *50*, 3714–3723.

- 58 Uchida, M.; Tokuda, T.; Tada, N. Finite element simulation of deformation of semi crystalline polymers with spherulitic mesostructure. *Int. J. Mech. Sci.* **2010**, *52*, 158–167.
- 59 Teixeira-Pinto, J. M.; Touchard, F.; Castagnet, S.; Nadot-Martin, C.; Mellier, D. DIC strain measurements at the micro-scale in a semi-crystalline polymer. *Exp. Mech.* **2013**, *53*, 1311–1321.
- 60 Xiong, B.; Lame, O.; Chenal, J.-M.; Rochas, C.; Seguela, R.; Vigier, G. In-situ SAXS study and modelling of the cavitation/crystal-shear competition in semi-crystalline polymers. *Polymer* **2013**, *54*, 5408–5418.
- 61 Mavko, G.; Mukerji, T.; Dvorkin, J. *The Rock Physics Handbook*. Cambridge University Press; Cambridge UK, 2003.
- 62 Heydeman, P. L.; Houck, J. C. Bulk modulus and density of polyethylene to 30 kbars. *J. Polym. Sci., Polym. Phys.* **1972**, *10*, 1631-1637.
- 63 Morikami, K.; Kuchiki, E.; Kawamura, T.; Fujita, Y.; Toki, S. Molecular dynamics simulation study on the bulk modulus above and below the glass transition temperature. *Kobunshi Ronbunshu* **1996**, *53*, 852-859.
- 64 Kubat, M. J.; Vernel, J.; Rychwalski, R. W.; Kubat, J. Bulk moduli from physical aging and stress relaxation data. *Polym. Eng. Sci* **1998**, *38*, 1261-1269.
- 65 Krigas, T.; Carella, J. M.; Struglinski, M. J.; Crist, B.; Graessley, W.; Schilling, F. C. Model copolymers of ethylene with butene made by hydrogenation of polybutadiene : Chemical composition and selected physical properties. *J. Polym. Sci., Polym. Phys.* **1985**, *23*, 509–520.
- 66 Liu, C.; He, J.; van Ruymbeke, E.; Keunings, R.; Bailly, C. Evaluation of different methods for the determination of the plateau modulus and the entanglement molecular weight. *Polymer* **2006**, *47*, 4461–4479.
- 67 Gent, A. N.; Lindley, P. B. Internal rupture of bonded rubber cylinders in tension. *Proc. R. Soc. London Ser. A, Math. Phys. Sci.* **1959**, *249*, 195–205.
- 68 Fond C. Cavitation criterion for rubber materials: A review of void-growth models. *J. Polym. Sci., Polym. Phys.* **2001**, *39*, 2081–2096.
- 69 Gent A.N. in *The Science and Technology of Rubber*. Mark E. J., Erman B., Roland C. M. Eds. Academic Press / Elsevier : Waltham MA USA, 2013; Chap. 1.
- 70 Hoffman, J. D.; Miller, R. Kinetics of crystallization from the melt and chain folding in polyethylene fractions revisited: theory and experiment. *Polymer* **1997**, *38*, 3151–3212.
- 71 Addiego, F.; Dahoun, A.; G'Sell, C.; Hiver, J.-M.; Godard, O. *Effect of microstructure on crazing onset in polyethylene under tension*. *Polym. Eng. Sci.* **2009**, *49*, 1198–1205.
- 72 Doyle, M. J. On the effect of crystallinity on the elastic properties of semicrystalline polyethylene. *Polym. Eng. Sci.* **2000**, *40*, 330–335.
- 73 (a) Ahzi, S.; Bahlouli, N.; Makradi, A.; Belouettar, S. Composite modeling for the effective elastic properties of semicrystalline polymers. *J. Mech. Mater. Struct.* **2007**, *2*, 1–21. (b) Gueguen, O.; Ahzi, S.; Belouettar, S.; Makradi, A. Comparison of micromechanical models for the prediction of the effective elastic properties of semi-crystalline polymers. *Polym. Sci. Ser.A* **2008**, *50*, 523–532.
- 74 (a) Nikolov, S.; Doghri, I. A micro/macro constitutive model for the small-deformation behavior of polyethylene. *Polymer* **2000**, *41*, 1883–1891. (b) Nikolov, S.; Doghri, I.; Pierard, O.; Zealouk, L.; Goldberg, A. Multi-scale constitutive modelling of the small deformations of semi-crystalline polymers. *J. Mech. Phys. Solids* **2002**, *50*, 2275–2302.-75
- (a) Bedoui, F. ; Diani, J.; Regnier, G. Micromechanical modelling of elastic properties in polyolefins. *Polymer* **2004**, *45*, 2433–2442. (b) Bedoui, F. ; Diani, J. ; Regnier, G. ; Seiler, W. Micromechanical modelling of isotropic elastic behavior of semicrystalline polymers. *Acta Mater.* **2006**, *54*, 1513–1523.
- 76 (a) van Dommelen, J. A.; Parks, D. M.; Boyce, M. C.; Brekelmans, W. A. M.; Baaijens, F. P. T. Micromechanical modelling of the elasto-viscoplastic behavior of semi-crystalline polymers. *J. Mech. Phys. Solids* **2003**, *51*, 519–54.(b) van Dommelen, J. A.; Parks, D. M.;

- Boyce, M. C.; Brekelmans, W. A. M.; Baaijens, F. P. T. Micromechanical modelling of intra-spherulitic deformation of semicrystalline polymers. *Polymer* **2003**, *44*, 6089–6101.
- 77 (a) Boyd, R. H. The modulus of the amorphous component in polyethylenes. *Polym. Eng. Sci.* **1979**, *19*, 1010–1016. (b) Boyd, R. H. The mechanical moduli of lamellar semicrystalline polymers. *J. Polym. Sci., Polym. Phys.* **1983**, *21*, 493–504. (c) Boyd, R. H.; Liao, W. B. Mechanical moduli of spherulitic lamellar semicrystalline polymers. *Macromolecules*, **1986**, *19*, 2246–2249.
- 78 Guan, X.; Pitchumani, R. Micromechanical model for elastic properties of semicrystalline thermoplastic polymers. *Polym. Eng. Sci.* **2004**, *44*, 433–451.
- 79 Sakurada, I.; Kaji, K.; Wadano, S. Elastic moduli and structure of low density polyethylene. *Colloid Polym. Sci.* **1981**, *259*, 1208–1213.

IV.3 Summary of the article

The deformation of the lamella stacks in a spherulite within a very small strain depends on the orientation relatively to the stretch direction. The lamella stacks in equatorial region are stretched and elongated in the direction of the stacking axis while the lamella stacks in polar region close to each other due to lateral contraction.

Thanks to in-situ SAXS, local strain (ϵ_{local}) can be related to the macroscopic strain (ϵ_{macro}). ϵ_{local} and ϵ_{macro} obey a linearly relationship at the beginning of the deformation. The ratio $\epsilon_{local}/\epsilon_{macro}$ is a constant for all the samples at a given temperature. The ratio $\epsilon_{local}^{eq}/\epsilon_{macro}$ (ϵ_{local}^{eq} local strain in equatorial region) equal to 0.5, suggesting that the equatorial region deforms less than the average strain while others regions should have larger deformations to accommodate the macroscopic strain.

$\epsilon_{local}^{eq}/\epsilon_{macro}$ shifts to higher value at higher T_d , indicating that elevated T_d promotes homogeneous deformation. This is attributed to the temperature-dependence of the crystal stiffness that enables softening of the stiffer regions.

The deformation at the very beginning is mainly attributed to the deformation of the amorphous phase because the crystal is much stiffer than the amorphous phase. The amorphous phase strain in equatorial region (ϵ_a^{eq}) exhibits a linearly increase with macroscopic strain. The ratio $\epsilon_a^{eq}/\epsilon_{macro}$ is influenced by the crystallinity X_c and the content of stress transmitters [ST].

The measured $\epsilon_a^{eq}/\epsilon_{macro}$ fairly obeys a linearly relation with $1/(1-X_c)$. Additionally, $\epsilon_a^{eq}/\epsilon_{macro}$ increases with decreasing [ST] at a given temperature. $\epsilon_a^{eq}/\epsilon_{macro}$ is sensitive to the temperature which presents a bigger value at higher temperature. This is ascribed to the temperature can relax the coupling between crystalline and amorphous phase which promotes the amorphous phase deformation.

Local stress σ_c in the crystal is calculated by WAXS via the deformation of crystal lattice. This stress is considered to also apply on the amorphous phase, assuming a series coupling of the two phases at the local scale of the equatorial lamellar stacks. Local stress is slightly influenced by microstructure but strongly depended on the temperature. The local crystal deformation behaviour is similar to the macroscopic deformation behaviour. Local stress σ_c increases at the very beginning of the deformation and then levels off at a critical strain associated to a local yield.

The apparent modulus of the interlamellar amorphous phase M_a is estimated by the measured local stress and strain in equatorial regions. M_a increases with increasing stress transmitter content [ST] at a given drawing temperature. This is in agreement with reinforcement effect of ST on the mechanical properties of amorphous phase. Furthermore, the amorphous modulus reaches very high value between 250 to 500MPa at 25°C which is much higher than M_a of bulk amorphous PE between 4 to 10MPa. On the other hand, M_a decreases with increasing drawing temperature which is ascribed to the amorphous chain relaxation due to the crystal softening.

IV.4 Small strain deformation behaviour of polypropylene

4.1. Local deformation in equatorial region

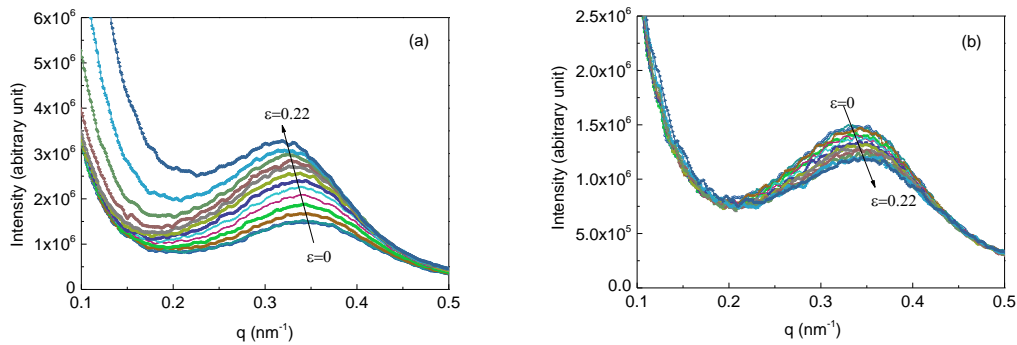


Figure 4.1. SAXS intensity profile of PPA annealed for different strains at draw temperature 23°C. (a) from equatorial regions; (b) from polar regions.

Like polyethylene, polypropylene forms a spherulite structure when crystallized from the melts. The crystal lamellae are oriented along the radius direction. The scattering patterns are similar to that of polyethylene owing to the similar lamellar structure. Figure 4.1 shows the intensity profile of PPA annealed in different strain for the draw temperature 23 °C. The meridian intensity from equatorial regions increases with the elongation and the peak shifts to small q value indicating the augmentation of the long period. In contrast, the intensity from the polar regions decreases with elongation and the peaks move to the larger q values indicating the reduction of the long period. This indicates the polyethylene and polypropylene have the similar deformation behavior in the elastic deformation regime at the scale of the lamella stacks, i.e. the lamella are separated in equatorial regions of the spherulites and move together in polar in polar regions.

The long period has been calculated from the Lorenz corrected intensity curves. Figure 4.2 shows the long period of PPA annealed in equator and polar respectively at draw temperatures 23°C, 70°C and 120 °C. In equatorial regions, it linearly increases with the elongation in the elastic strain domain, due to the separation of the lamella normal to the tensile force. And also L_p increases with the draw temperatures.

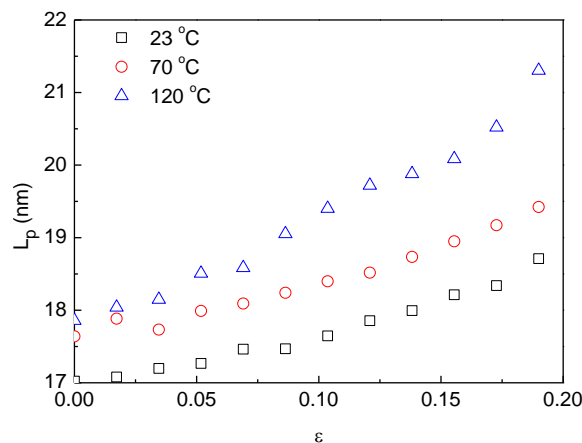


Figure 4.2 Long period of PPA annealed in equatorial region at draw temperatures 23°C, 70 °C and 120°C.

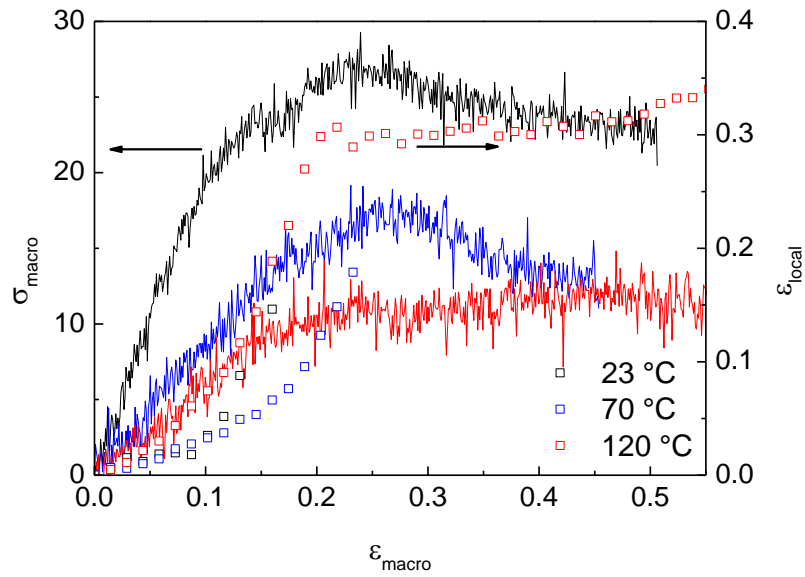


Figure 4.3. Macro stress and local strain in equatorial regions as a function of macroscopic strain for PP-C annealed at draw temperatures 23 °C, 70 °C and 120 °C.

As discussed in section 4.1, the local deformation of polypropylene in equatorial regions could be estimated by the variation of the long period during tensile deformation which is $\varepsilon_{local} = \Delta L_p / L_p$. Figure 4.3 shows that ε_{local} linearly increases with macroscopic strain ε_{macro} in elastic deformation. After yield, the linearly relation disappears. Similar to the polyethylene mentioned in section 4.1, the ratio $\varepsilon_{local} / \varepsilon_{macro}$ could be estimated from the slope of the ε_{local} versus ε_{macro} correlation for each sample. The results of $\varepsilon_{local} / \varepsilon_{macro}$ are plotted in Figure 4.4 in function of X_c . It shows that the ratio is a constant in the samples with different crystallinity. And this constant value is only a function of temperature. The ratio is smaller than unit, which means that in equatorial regions of polypropylene, the local deformation is smaller than the macroscopic deformation. This behaviour is similar to that of polyethylene which has been discussed in section 4.1.

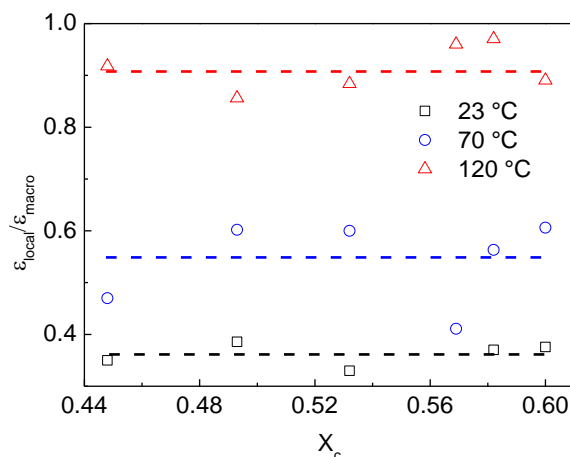


Figure 4.4. Ratio $\varepsilon_{local} / \varepsilon_{macro}$ in function of X_c at different temperature for polypropylene.

4.2. Comparison between deformation behavior of PE and PP

For both semicrystalline polymer PE and PP, there are several similarities deformation behavior during the elastic deformation.

The long period in equatorial regions of spherulites linearly increases with the increase of elongation in elastic deformation domain. The ratio $\varepsilon_{local}/\varepsilon_{macro}$ is a constant for various samples with different X_c and it is only in function of draw temperature for both PE and PP. This parameter is a useful one for correlating microscopic and macroscopic scale in view of micromechanical modelling which often requires a scale transition factor.

IV.5 Conclusion of the chapter

In this chapter, local deformation behaviors in elastic domain of polyethylene with various morphologies are investigated by the in-situ SAXS and WAXS. L_p in equator increases whereas it decreases in polar regions with the increase of elongation. In equatorial regions, ε_{local}^{eq} is proportional to the macroscopic strain ε_{macro} . The ratio $\varepsilon_{local}^{eq}/\varepsilon_{macro}$ proved to be prospective a constant for PE and PP samples with various X_c . This ratio increases with draw temperature. It is smaller than unit below 100 °C, indicating lower deformation of equatorial region than macroscopic deformation. By this value, the local deformation could be connected with macroscopic deformation. It plays a role of bridge between microscopic and macroscopic deformation which could be important to use in the model transformation between microscopic and macroscopic.

Local deformation of interlamellar amorphous phase has been estimated from the variation of the amorphous phase layer thickness measured by the in-situ SAXS with a hypothesis that the variation of long period is mainly contributed by the amorphous phase. In equator, local amorphous phase strain ε_a exhibits a linear dependence on ε_{macro} within the elastic domain. The ratio $\varepsilon_a / \varepsilon_{macro}$ is well agreed to a linear function with the crystallinity at a given temperature. The ratio $\varepsilon_a / \varepsilon_{macro}$ also increases with increasing λ_n value which is a indication parameters for stress transmitter content.

The apparent modulus of the local amorphous phase M_a was estimated by the measured local stress and strain. M_a increases with increasing of stress transmitter content (ST) at a given draw temperature due to reinforcement effect of taut tie molecules in the amorphous phase. The amorphous modulus presents very high value between 250 and 500MPa at 25°C which is much higher than bulk amorphous phase of PE. On the other hand, M_a decreases with increasing drawing temperature owing to the activation of chain mobility in crystalline phase that enable relaxation of amorphous phase.

Chapter V Plastic deformation

Table of content

Chapter V Plastic deformation	88
Context	89
V.1 Article III: “In-situ SAXS study and modeling of the cavitation crystal-shear competition in semi-crystalline polymers Influence of temperature and microstructure in polyethylene” .	90
V.2 Summary of the article	102
V.3 Martensitic transformation of polyethylene	103
3.1 Martensitic transformation onset	104
3.2 Evolution of scattering intensity of monoclinic crystal	106
3.3 Conclusion on martensitic transformation	108
V.4 Shearing at the scale of crystallite in PE	108
V.5 Competitions of plastic mechanisms onsets	111
V.6 Conclusion	114

Context

Plastic deformation of semicrystalline polymers has been a subject of many studies. It is a complex process because different microstructures participate in it.

Around yield point, various plastic phenomena have been observed such as cavitation, crystal shear etc. The initiation of these plastic mechanisms is proved to be dependent on the microstructures and temperatures. In Chapter 1, we mentioned a competition relation was observed for the cavity and crystal shear onset. This relation is correlated to the crystallite thickness. But at high temperature, the cavitation disappears. One could ask what the correlation between cavitation and the crystal shear is at high temperature.

Martensitic transformation also appears around yield which involves the transformation from orthorhombic to monoclinic crystal. Monoclinic phase is only stable under stress at low temperatures. In the previous studies, it was pointed out the martensitic transformation appears faster in HDPE than in LDPE. However, the precise correlation between martensitic transformation and microstructures still need more evidences. On the other hand, the relation of martensitic transformation onset and other plastic mechanisms such as cavitation and crystal shear onset is not clear.

In this work, the studies will be focused on these questions. To reach these aims, samples with wide range of microstructures (crystallinity ranges from 0.46-0.8, and crystallite thickness is between 8-28 nm) were used. The microstructure evolutions during the tensile test were probed by the in situ SAXS and WAXS. With these strategies, the onsets of the cavitation, crystal shear and martensitic transformation are compared in different temperatures and the influence parameters are studied.

This chapter is divided into following parts:

1. First, cavitation onset is studied by in-situ SAXS at different temperatures. It is correlated to the microstructures and temperatures. A competition between crystal shear and the cavitation formation was observed. A model had been proposed to estimate the stresses for the cavitation and crystal onset. The stress of cavitation and crystal shear onset is proved to be in relation to the crystallite thickness. Both onset stresses decrease with elevating temperatures however, stress of crystal shear onset is more sensitive to the temperatures. For this reason the crystal shear occurs faster than cavitation and the cavitation at higher temperatures.
2. Second, the martensitic transformation is detected by in situ WAXS at different temperatures. The martensitic transformation onset is evidenced to be associated to L_c and temperatures. The onset of martensitic transformation is compared with plastic mechanisms at different temperatures. A map concerned to the onset of plastic mechanisms is obtained in function of temperatures and crystallite thicknesses.

V.1 Article III: “In-situ SAXS study and modeling of the cavitation crystal-shear competition in semi-crystalline polymers Influence of temperature and microstructure in polyethylene”

B. Xiong, O. Lame, J.M. Chenal, C. Rochas, R. Seguela, G. Vigier. In-situ SAXS study and modeling of the cavitation crystal-shear competition in semi-crystalline polymers Influence of temperature and microstructure in polyethylene. Polymer, 2013, Vol. 54, p. 5408-5418

V.2 Summary of the article

The cavitation during the uniaxial tensile of polyethylene can be observed by SAXS. The cavitation behavior has been numerously studied due to the significantly influence on the plastic stress and the large deformation properties. However, the influence of microstructure and the molecule topologic structure are still being mysterious until recently. In this work, the attention has been paid to the microstructure parameters and the content of stress transmitters on the nucleation process of cavitation. Thanks to the in-situ SAXS, the evolution of cavities has been probed in different draw temperature. The evolution of volume and orientation of cavities has been obtained with this technique.

Three different behaviors were observed:

- Homogeneous cavities which formed before yield point.
- Cavities localized in the neck region beyond the yield point.
- No cavities appear during deformation process.

The nucleation of cavities strongly depends on the microstructure and draw temperature. Among the parameters of the microstructure, the crystal thickness L_c and the content of stress transmitters [ST] are the most important, where the stress for the crystal shear is mainly determined by L_c and the stress for cavities onset is controlled by [ST]. A competition between crystal shear and cavities onset is observed to be determined by a critical crystal thickness L_{cc} . Beyond L_{cc} , cavitation occurs first. This is associated to the homogeneous initiation of cavitation. Below L_{cc} , the shear of the crystal occurs before cavitation. The crystal shear also generates stress concentration which makes the happening of the localized cavitation. But in some cases, this stress concentration is too low to induce cavities.

A model has been proposed based on the competition of crystal shear and cavitation for case of homogeneous cavitation. The stresses for crystal shear (σ_{sh}) and cavitation onset (σ_{cav}) is related to the L_c and temperatures. σ_{sh} and σ_{cav} are compared to predict the cavitation onset in PE.

Draw temperature is another factor that determines the cavitation onset. The cavitation gradually disappears with elevating temperatures. The stress for crystal shear onset (σ_{sh}) and stress for cavitation onset (σ_{cav}) decrease with elevating temperatures. However, σ_{sh} is more sensitive to the temperatures than σ_{cav} promoting the crystal shear occurs faster in higher temperatures. When $\sigma_{cav} < \sigma_{sh}$ the homogeneous cavitation transforms to localized cavitation. Then, with elevating temperatures, local stress becomes smaller than σ_{cav} and the cavitation disappears in this condition.

Martensitic transformation also appears around yield which involves the transformation from orthorhombic to monoclinic crystal. It also participates to the plastic mechanisms likely in competition with the cavitation and crystal shear. This will be discussed in the next sections.

V.3 Martensitic transformation of polyethylene

Monoclinic phase is only stable under stress at low temperatures. In the previous studies, it was pointed out the martensitic transformation appears faster in HDPE than in LDPE [90,93,100]. However, the precise correlation between martensitic transformation and microstructures still need more evidences.

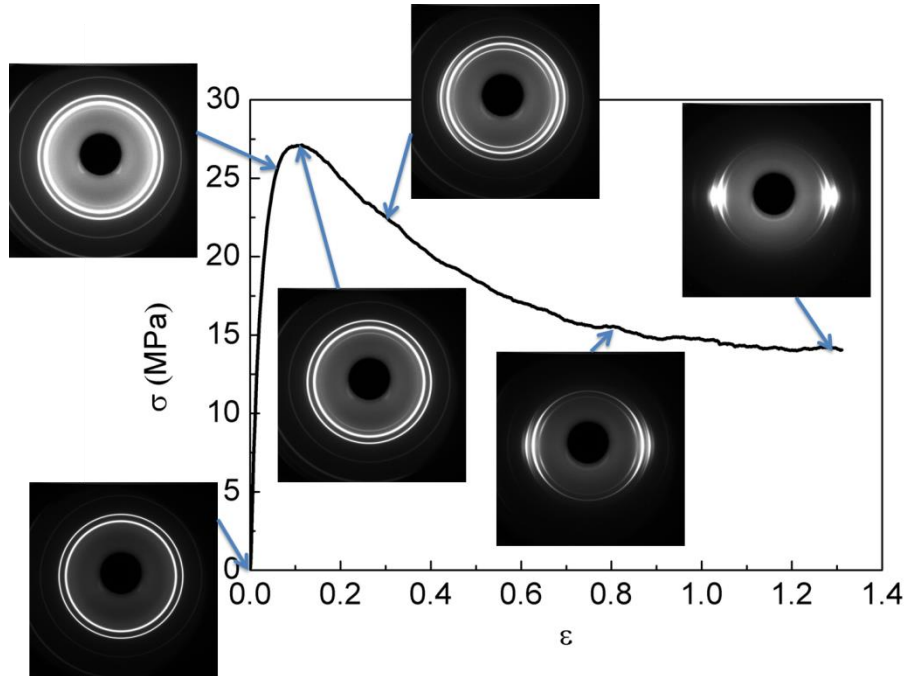


Figure 5.1. Evolution of the WAXS patterns along the tensile for the PE D isotherm in draw temperature 50 °C. Draw is in the vertical direction.

The technique in-situ WAXS can trace the scattering variation of crystal plane of semicrystalline polymers during tensile deformation. Figure 5.1 shows the evolution of the scattering patterns of PE D isotherm at draw temperature 50 °C. The initial sample is unoriented with two isotropic diffraction rings which could be indexed as (200) and (110) of orthorhombic crystal. With the increase of the tensile strain, the scattering rings gradually disappear [134,135]. Around yield point, new scatterings associating to the monoclinic phase appear.

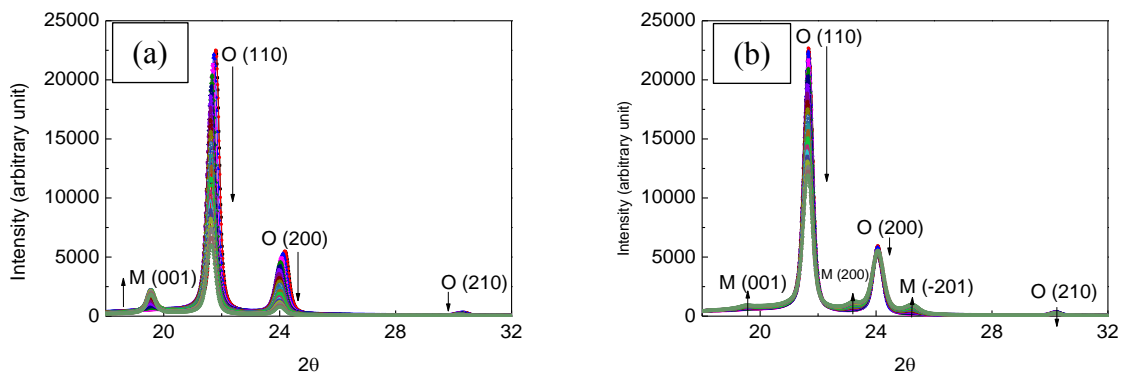


Figure 5.2. Intensity profile in function of scattering angle of PE D isotherm at 50°C; (a) meridional scattering, (b) equatorial scattering. The scattering curves are presented in every nominal strain 0.02 from 0 to 0.4. (O=Orthorhombic, M=Monoclinic)[136].

The one dimensional intensity profiles in radial and median versus diffraction angle 2θ were obtained from the scattering patterns (see Figure 5.2). For the sample without deformation, the crystal phase of polyethylene presents an orthorhombic phase with three scattering peaks (see

Figure 5.2a). The crystal planes which diffract in 21.6° and 24° are planes O(110) and O(200). With increasing of deformation, PE undergoes elastic and plastic deformations which show different scatterings. In the elastic domain, intensity of O(110) decreases in equator and meridian whereas O(200) decreases in meridian but remains in the equatorial regions with increasing deformation. This is ascribed to the different orientation of lamella in the polar and equator regions of spherulites. The crystal in equator region is under stretch and the crystal size changes with deformation which can be verified by the shift of peak O(200). Additionally, the scattering halo intensity of amorphous phase increases in meridian but decreases in radial with increasing deformation indicating the orientation of the amorphous, which has been discussed in chapter IV. Beyond elastic deformation, the materials undergo a plastic deformation. Intensity of O(200) and O(110) decrease in equatorial and meridian of scattering patterns with increasing deformation due to the orientation of crystals. Additionally, the orthorhombic lattice can turn into monoclinic lattice which is only stable under stress [90,93,100]. New diffraction planes associated to the monoclinic phase appear: M(001) plane at 19.8° , M(200) plane at 23.3° and M(-201) at 25.1° (see Figure 5.2 and Figure 5.3).

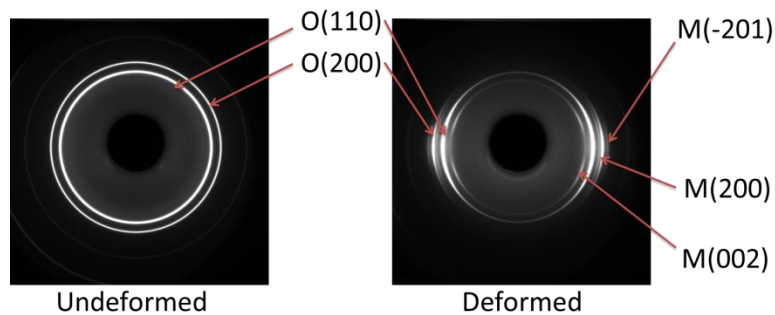


Figure 5.3. Schematic of WAXS patterns of undeformed and deformed polyethylene. (O=Orthorhombic, M=Monoclinic, tensile direction: vertical)

3.1 Martensitic transformation onset

The martensitic transformation onset is observed by WAXS with the appearance of new diffraction peaks corresponding to the monoclinic planes (001) at 19.8° , (200) at 23.3° , and (-201) at 25.1° (see Figure 5.2 and Figure 5.3). Figure 5.4 shows diffraction plane M(001) of the monoclinic unit cell in lamella located at the equator and polar regions of spherulites. The crystallographic c-axis in the monoclinic unit cell is the growth direction of lamellae [137]. The monoclinic plane (001) located in the equatorial region of spherulites diffracts in the horizontal areas of scattering pattern, whereas the plane (001) located in the polar region diffract vertically in the pattern. The horizontal and vertical diffraction pattern areas are respectively called zone H and zone V (see Figure 5.4).

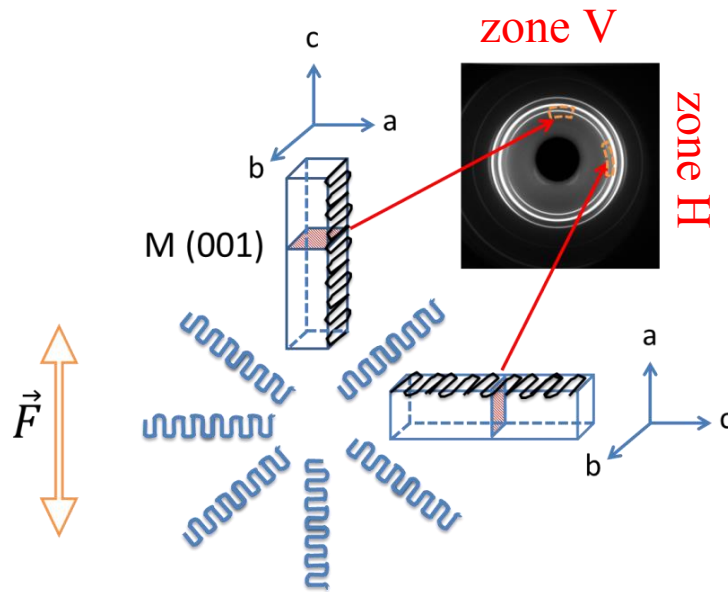


Figure 5.4. Diffraction plane (001) of the monoclinic unit cell in lamella located at the equatorial and polar region of spherulite.

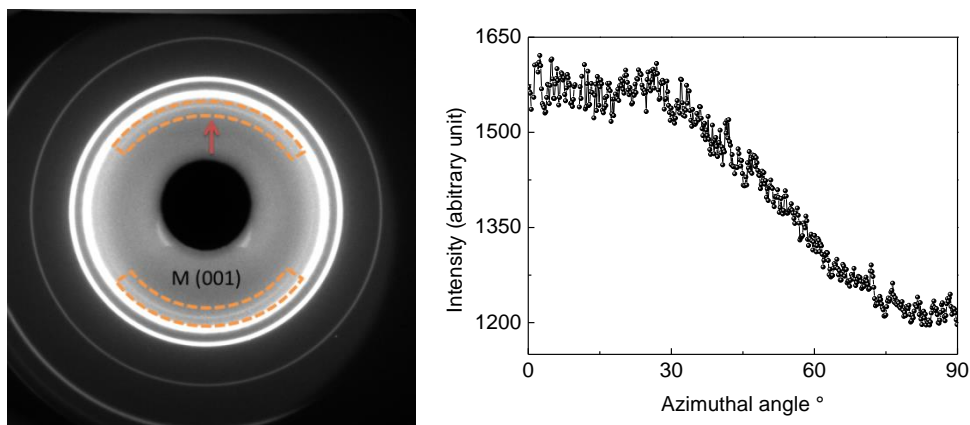


Figure 5.5. (a) Diffraction pattern of PE D isotherm: initiation of the monoclinic phase in the radial scattering. (b) Intensity of peak $I_{M(001)}$ in function of azimuthal angle. Draw is in the vertical direction at 50 °C. (M=Monoclinic)

Figure 5.5a shows the first WAXS patterns with monoclinic phase scattering. PE D isotherm is an example here. M(001) scattering appears only in zone V, suggesting that the martensitic transformation occurs initially in lamellae located in polar region.

The scattering of M(001) mainly located in the section areas marked in Figure 5.5a. From intensity of M(001) in azimuthal angle (see Figure 5.5b), it is observed that M(001) scattering appears in a $\pm 30^\circ$ section areas in zone V indicating that the lamellae within $\pm 30^\circ$ inclined respect to the tensile direction are subjected to the martensitic transformation (see Figure 5.5b).

The strain of martensitic transformation onset $\epsilon_{\text{martensitic}}$ is estimated by the appearance of M(001) scattering in zone V. Figure 5.6 shows $\epsilon_{\text{martensitic}}$ in function of the crystallinity X_c and crystal thickness L_c . $\epsilon_{\text{martensitic}}$ decreases with increasing X_c and L_c suggesting martensitic transformation is influenced by microstructures. With X_c below 0.7, $\epsilon_{\text{martensitic}}$ strongly decreases while above 0.7 $\epsilon_{\text{martensitic}}$ remains constant. This suggests $\epsilon_{\text{martensitic}}$ is not only dependent on the crystalline structure. It should be mentioned that few samples can observe the martensitic transformation at 100 °C owing the unstable of monoclinic phase in high temperature, thus the data of $\epsilon_{\text{martensitic}}$ does not appear in Figure 5.6.

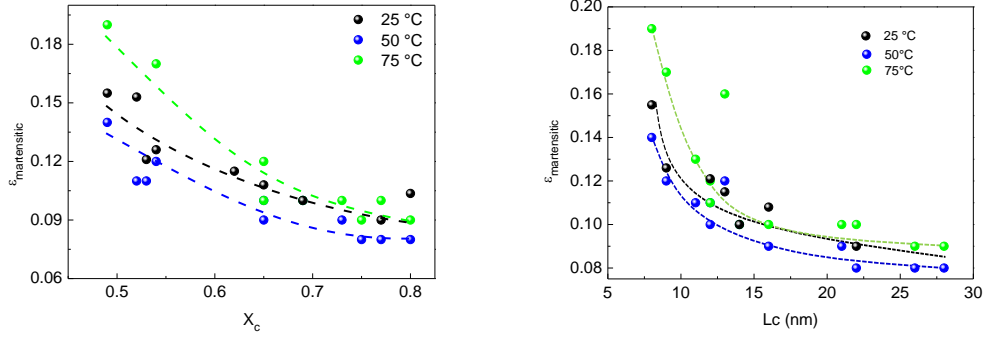


Figure 5.6. $\epsilon_{\text{martensitic}}$ of polyethylene samples in function of crystallinity X_c and crystalline thickness L_c at different draw temperatures.

The macroscopic stress of the martensitic transformation onset $\sigma_{\text{martensitic}}$ is also estimated. $\sigma_{\text{martensitic}}$ linearly increases with increasing X_c and L_c at different temperatures in Figure 5.7. $\sigma_{\text{martensitic}}$ is correlated to the local stress for the martensitic transformation onset. Indeed, some authors considered martensitic transformation as results of the crystal transverse slips or crystal twinning [70,96,99,138], which is correlated to the thickness of the crystallite.

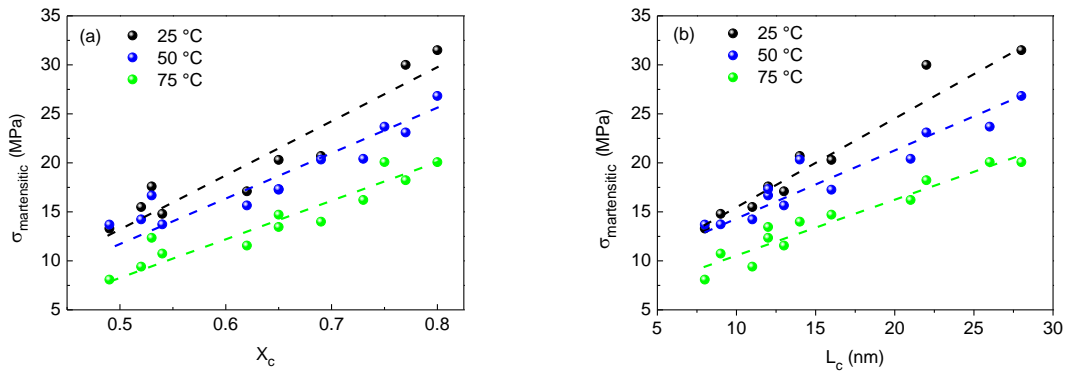


Figure 5.7. $\sigma_{\text{martensitic}}$ in function of (a) X_c and (b) L_c at draw temperature 50 °C and 75 °C.

In conclusion, the onset of martensitic transformation is strongly influenced by the microstructures and temperatures. The martensitic transformation occurs first in lamellae located at the polar region of the spherulites. $\epsilon_{\text{martensitic}}$ decreases and $\sigma_{\text{martensitic}}$ increases with increasing L_c and X_c . Regarding the influence of temperatures, martensitic transformation occurs later above T_α and $\sigma_{\text{martensitic}}$ decreases with elevating temperatures.

The monoclinic crystal is only stable under stress which depends on the local stress distribution and orientation of crystal. The orientation of crystal and local stress changes with deformations. Thus the scattering of monoclinic crystal also changes with deformation and this will be discussed in next subsection.

3.2 Evolution of scattering intensity of monoclinic crystal

The monoclinic phase in polyethylene is not stable and then returns to the orthorhombic phase during the relaxation of stress. The monoclinic phase content and orientation vary with deformations. Figure 5.9 shows the $M(001)$ intensity of PE D isotherm in zone H and zone V at different draw temperatures. It can be noted that the first $M(001)$ appears in zone H which confirms the initiation of martensitic transformation is in the polar region of spherulite. In zone V, $I_{M(001)}$ increases quickly to a maximum value and then monotonically reduces until disappearing. This could be due to the rotation of the crystal and orientation of the chains in tensile direction. Two possible rotations manner according to the direction of the chains (see Figure 5.8) could be proposed for the lamellae located in polar regions. With the orientation of the crystal lamella, the

scattering patterns of $M(001)$ varies from an isotropic ring to finally two arc in zone V (see Figure 5.3).

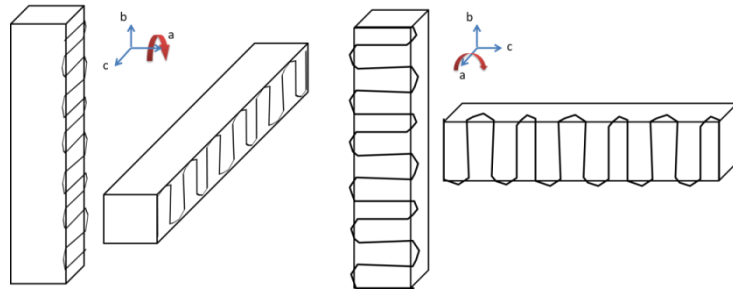


Figure 5.8. Schematic of the rotation of crystal lamellae in polar. Tensile is in the vertical direction.

In zone H, $I_{M(001)}$ monotonically increases indicating monoclinic crystal also appear in equatorial regions. $I_{M(001)}$ is more intense in zone V than that in zone H (see Figure 5.9) indicating the content of monoclinic phase is higher in polar region than that in equator region. On the other hand, the increase of $I_{M(001)}$ accompanied with the decreased of $I_{O(200)}$ scattered by crystal in equator region (see Figure 5.10) since the martensitic transformation involves the decreasing of orthorhombic crystal content. $I_{O(200)}$ decreases and $I_{M(001)}$ increases faster in higher temperatures. However, the $I_{M(001)}$ is lower in higher temperature. These results suggest the orthorhombic crystal can transform to monoclinic crystal fast but the content of monoclinic crystal is low in high temperatures.

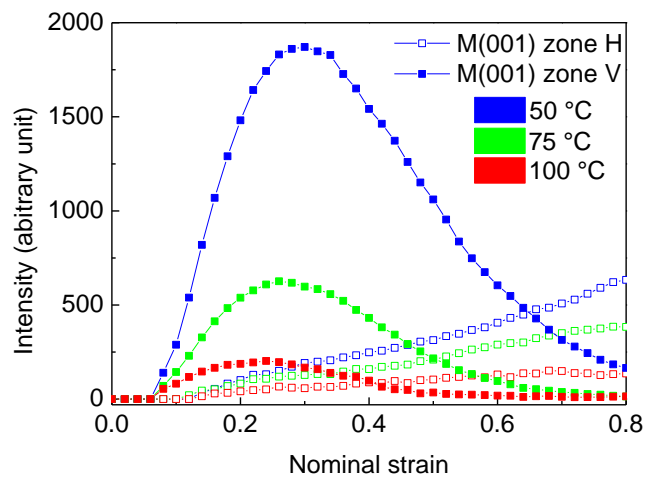


Figure 5.9. $M(001)$ intensity of PE D isotherm scattering in zone H and zone V at different draw temperature.

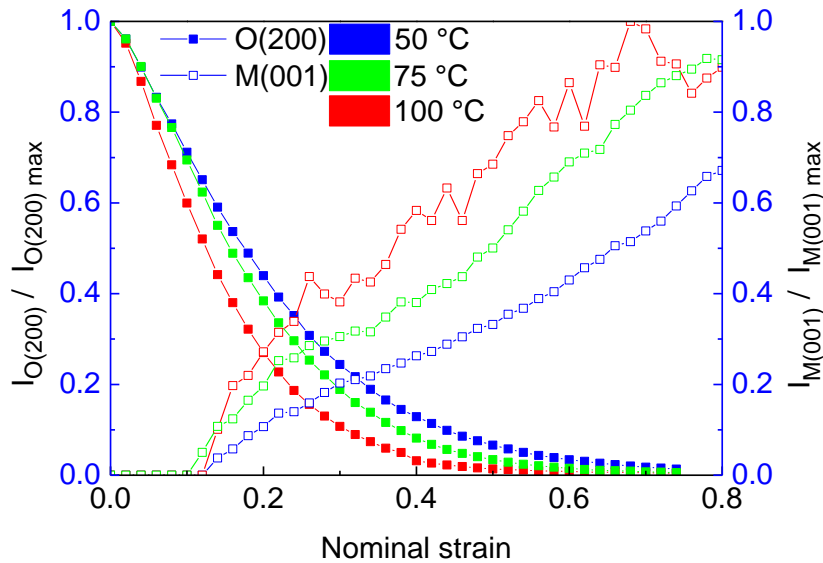


Figure 5.10. Nominated intensity of O(200) and M(001) scattered by the lamellae in equator of PE D isotherm in different temperature.

3.3 Conclusion on martensitic transformation

The onset of martensitic transformation is strongly influenced by the microstructures. The strain of martensitic transformation onset decreases whereas the stress of martensitic transformation onset increases with increasing L_c and X_c . The martensitic transformation occurs first in lamellae located at the polar region of the spherulites and the content of monoclinic phase is higher in polar region than that in equator region. In higher temperature the orthorhombic crystal can transform to monoclinic crystal fast but the content is low. Due to the rotation of the crystal and orientation of the chains in tensile direction, the scattering intensity of monoclinic crystal located in polar region decreases whereas increases in equator region.

Except martensitic transformation and cavitation, crystal shear is another plastic mechanism observed around yield. We have studied the influences of microstructures and temperatures on the cavitation and martensitic transformation. Currently, we are interested in what influences of these parameters on the crystal shear onset are. The crystal shear onset in equatorial regions is detected by the in situ WAXS via the evolution of the distance of plane O(200). The strain and stress onsets are estimated and the influences parameters will be discussed in next section.

V.4 Shearing at the scale of crystallite in PE

During tensile test, lamellae in equator region of spherulite undergo stretching and the plane O(200) scattering in meridian of the patterns (see sketch in Figure 5.11). The distance of these planes (d_{200}) linearly increase with increasing deformation in elastic domain (see Figure 5.11). At the end of the linear increase, d_{200} reach a maximum value. After that, d_{200} reaches to a plateau which retains almost a constant with very little variations. This is ascribed to the crystal shearing occurs at the end of line. Actually, the local stress does not change when crystal start to shearing. The constant stress added between the plane O(200) making the d_{200} as a constant. The end of linear increase of d_{200} is considered as the crystal shear onset. The corresponded macroscopic strain is called strain of crystal shear onset (ϵ_{cs}). Similar evolution of d_{200} can be observed in different temperatures. At higher temperature, d_{200} is higher due to thermal expansion and also processes bigger variation.

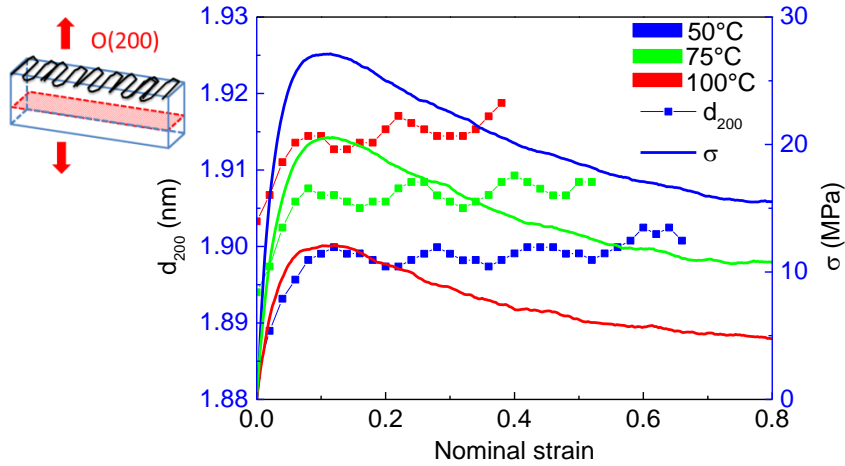


Figure 5.11. Evolution of distance of plane O(200) in equator of PE D isotherm at different draw temperature.

ϵ_{cs} is smaller than yield strain (see Figure 5.12), which means the crystal shear in equator region is before the yield. Yield is considered to be the crystal shears in whole of the spherulites. Thus the onset of crystal shear is before yield which is observed by the faster occurrence of crystal shear in equatorial regions. However, the first crystal shear may happen in other regions. So that the first onset strain of crystal shear is smaller than or equal to ϵ_{cs} . Furthermore, ϵ_{cs} decreases with increasing temperatures, which is due to the activation energy of crystal shear decreases with increasing temperatures, especially above the α transition temperature the activation energy strongly decreases with increasing temperatures.

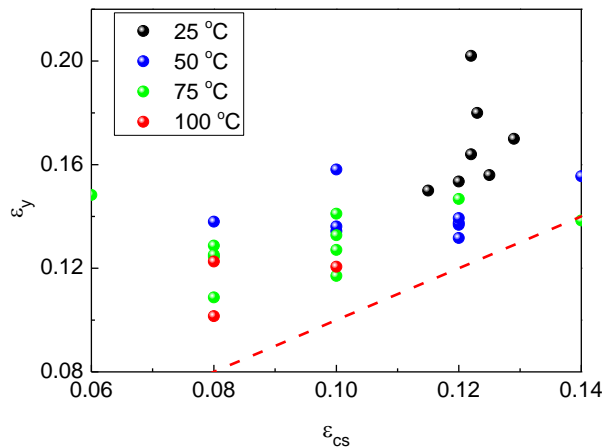


Figure 5.12. ϵ_{yield} in function of ϵ_{cs} at different temperatures.

The corresponded macroscopic stress σ_{cs} is estimated at ϵ_{cs} . Figure 5.13 shows the σ_{cs} and ϵ_{cs} in function of X_c at different temperatures. σ_{cs} increases with increasing X_c similarly to yield stress, owing to the increase of crystallite thickness and the activation energy of the dislocation nucleation [86]. Additionally, σ_{cs} decreases with increasing temperatures. Particularly, when temperature is above T_α , σ_{cs} strongly decreases where σ_{cs} decreases 50 % at 100 °C compared to the value at 75 °C.

On the other hand, at a given temperature, ϵ_{cs} almost remains in a constant with a deviation ± 0.01 , indicating the crystal shear onset strain is independent on the crystal structure. This can be explained by the balance between modulus (slope) and σ_{cs} increase with increasing X_c . High σ_{cs}

contributes to the higher ϵ_{cs} whereas the modulus increasing reduces ϵ_{cs} . These phenomena lead to the little variation of ϵ_{cs} . Furthermore, ϵ_{cs} presents temperature dependent which slightly decreases with increasing temperatures. This is attributed to the temperature dependence of the materials stiffness which decreases with temperatures.

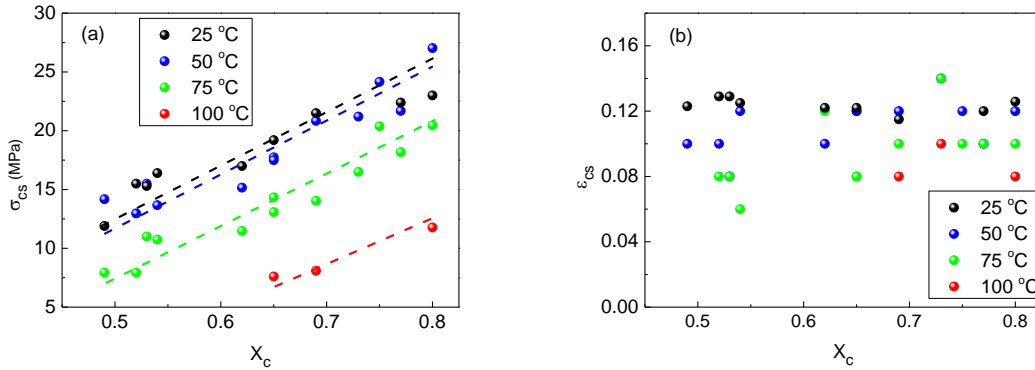


Figure 5.13. (a) σ_{cs} and (b) ϵ_{cs} in function of X_c at different temperatures

Martensitic transformation firstly occurs in polar region thus the $\epsilon_{martensitic}$ represent the plastic strain in polar region where ϵ_{cs} represent plastic strain in equator region. It is supposed that the lamellae in polar and equatorial regions are well oriented and the lamellae are under stretching. Comparison of $\epsilon_{martensitic}$ and ϵ_{cs} could give an indication to the local stress distribution in equator and polar regions.

It is supposed that the difference for the crystal shear in equator region and martensitic transformation in polar region is representative of the difference between local stresses in the equator and polar regions and also supposed that crystal shear and martensitic transformation have the same dependence on L_c . The ratio $\epsilon_{martensitic}/\epsilon_{cs}$ is in function of L_c (see Figure 5.14). If the ratio is higher than 1, more local stresses in the equator region is. On the contrary, the ratio is lower than 1, more local stresses present in the polar region.

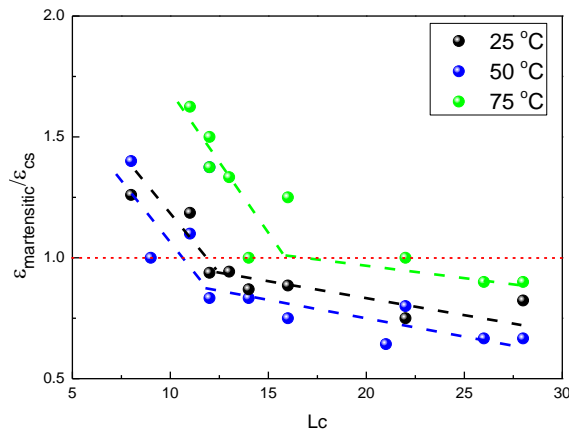


Figure 5.14. $\epsilon_{martensitic}/\epsilon_{cs}$ in function of L_c at different temperatures.

In conclusion, the strain (ϵ_{cs}) and stress (σ_{cs}) of crystal shear onset in equator region are estimated. ϵ_{cs} is independent on crystallinity whereas σ_{cs} increases with increasing crystallinity. But ϵ_{cs} and σ_{cs} both are deduced with elevating temperatures which is due to the activation energy of crystal shear decreases with increasing temperatures. ϵ_{cs} is smaller than yield strain, which means the crystal shear in equator region is before the yield.

Until now, we have studied the influences of microstructures and temperatures on cavitation onset, martensitic transformation onset and crystal shear onset and also the yield. Completion relation between crystal shear and cavitation has been observed in section V.2. But the relations between martensitic transformation and these two plastic mechanisms are not clear yet. The strains of these plastic mechanisms onsets will be compared to understand the relations these plastic mechanisms in next section.

V.5 Competitions of plastic mechanisms onsets

In above studies, the strains of cavitation onset, martensitic transformation onset and crystal shear onset and also yield strain have been estimated. Here we can compare these strains to real the relation of these plastic mechanisms and also to determine which one is the first plastic mechanism.

Figure 5.15 shows $\varepsilon_{\text{martensitic}}$ in function of yield strain $\varepsilon_{\text{yield}}$ of PE samples in different draw temperatures. At 50 °C and 25 °C, $\varepsilon_{\text{martensitic}}$ occurs before yield point. But at 75 °C, some samples present martensitic transformation after yield. This means at low temperature the plastic deformation has been activated before yield. Furthermore, $\varepsilon_{\text{martensitic}}$ increases with elevating draw temperature. This is ascribed to the monoclinic phase is unstable at higher temperature. The same comparison between the strain onset of cavitation ($\varepsilon_{\text{cavitation}}$) and yield strain has been presented in Figure 5 of subsection V.2. With increasing draw temperature, the number of samples exhibiting cavitation gradually decreases, and among the cavitating samples fewer and fewer exhibit homogeneous cavitation prior to yield.

It should be mentioned that the yield is regarded as macroscopic crystal flow which is a consequence of crystal shear. From Figure 5.12, we knew that the difference between yield strain and crystal shear strain of equator lamella is very small (about ± 0.02). On the other hand, yield involves crystal shear in different regions of spherulite, not only in the equatorial region. Yield strain is not far away from the strain of crystal shear onset.

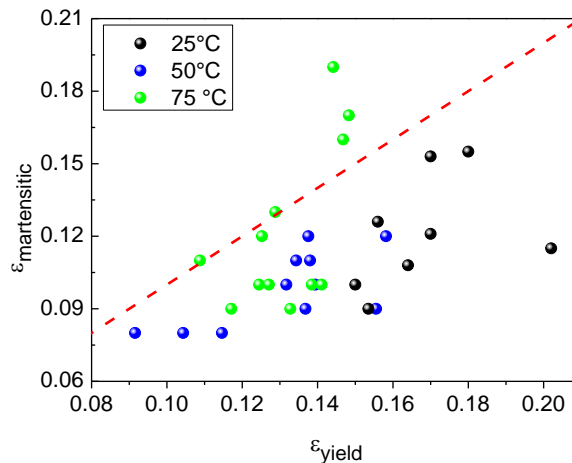


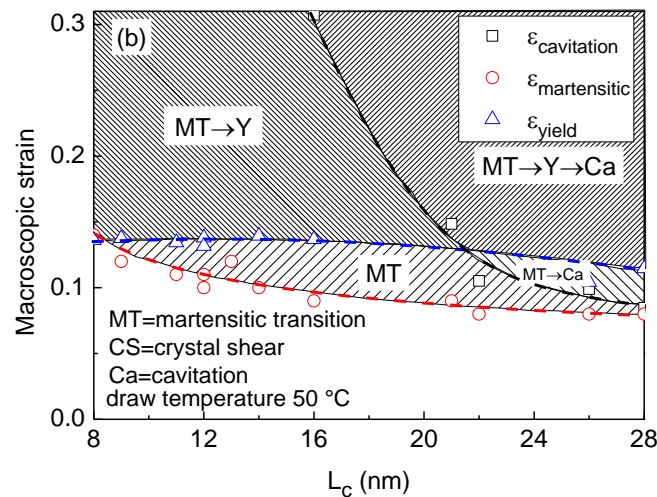
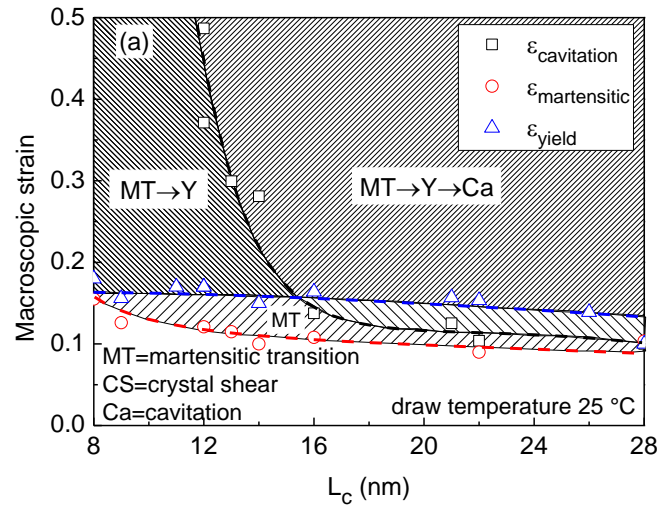
Figure 5.15. Onset strain of martensitic transformation ($\varepsilon_{\text{martensitic}}$) versus against yield strain for different temperature

As been observed, yield, cavitation and martensitic transformation are well related to the crystallite thickness (L_c) (Figure 5.6 and Figure 4 in article III). Indeed, the crystal shear, martensitic transformation are related to the dislocation or twinning of crystal which is proved to be correlated to L_c . The cavitation is mainly depended on the local stress which is controlled by the crystallinity and also L_c .

Figure 5.16 shows the strain onset of cavitation ($\epsilon_{\text{cavitation}}$), yield and martensitic transformation ($\epsilon_{\text{martensitic}}$) in function of L_c at different temperatures. $\epsilon_{\text{martensitic}}$ and $\epsilon_{\text{cavitation}}$ decrease while ϵ_{yield} almost remains a constant with increasing L_c . ϵ_{yield} , $\epsilon_{\text{martensitic}}$ and $\epsilon_{\text{cavitation}}$ curves divide the figure into different regions representing different plastic mechanisms. At 25 °C, 4 regions are observed. Martensitic transformation (MT) is the first plastic mechanism in L_c range 8 – 28 nm. When increase deformation, cavitations (Ca) present for L_c above 15.5 nm (MT +Ca). Then yield (Y) occurs in these samples accompanied with MT and Ca (MT+Y+Ca). Below 12 nm, no cavitation appears while crystal shear is observed after MT (MT+Y).

The intersection for the martensitic transformation and yield curves can be estimated. The corresponded L_c is called the critical crystallite thickness for the martensitic transformation and yield ($L_{\text{cc}}^{\text{MT-Y}}$). This value gives the frontier: the yield occurs first below $L_{\text{cc}}^{\text{MT-Y}}$ where martensitic transformation is in the first above $L_{\text{cc}}^{\text{MT-Y}}$. Similarly, critical crystallite thickness for cavitation and yield ($L_{\text{cc}}^{\text{Y-Ca}}$) can be estimated. Additionally, we had obtained that the critical thickness for the cavitation initiation $L_{\text{cc}}^{\text{Ca}}$ in different temperatures (see Figure 11 in article III). Then first plastic mechanism can be determined by these critical thicknesses. However, the intersection of MT and Ca can not be observed due to the limited range of L_c .

Regarding to the temperature effect, $L_{\text{cc}}^{\text{MT-CS}}$ and $L_{\text{cc}}^{\text{CS-Ca}}$ increase with increasing temperatures. This is ascribed to the increase of the onset strain of cavitation and martensitic transformation with elevating temperature.



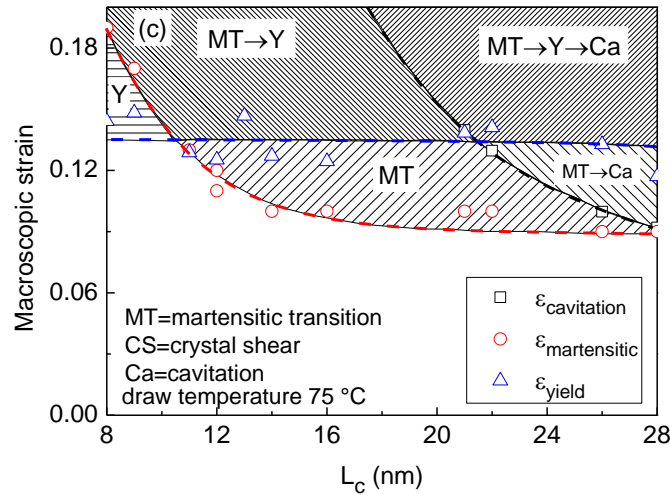


Figure 5.16. The strain onset of cavitation, yield and martensitic transformation in function of crystallite thickness. (a) 25 °C; (b) 50 °C; (c) 75 °C.

As we discussed in subsection V.4, the crystal shear in equatorial region is observed before yield, thus the first crystal shear occurs before the yield. The first crystal shear also may appear in other regions, thus it can conclude that the first crystal shear occur at or before crystal shear in equatorial regions. The strain of crystal shear onset in equatorial regions (ϵ_{cs}) is closer to the first crystal shear strain than yield strain. ϵ_{cs} also remains a constant with increasing L_c similarly to the yield strain. Similarly, by replacing yield strain with ϵ_{cs} , critical crystallite thickness for the martensitic transformation and crystal shear (L_{cc}^{MT-CS}) and critical crystallite thickness for cavitation and crystal shear (L_{cc}^{CS-Ca}) can be estimated.

A map involves the plastic mechanisms sequence (see Figure 5.17) can be obtained with these critical L_c . As shown in the Figure 5.17a, samples undergo different plastic mechanisms: In region (1), yield occurs before martensitic transformation and no cavitation appears in the samples; In region (2), martensitic transformation is before yield and also no cavitation appears in the samples; In region (3), Martensitic transformation is in the first place, then yield occurs and finally cavitation forms; In region (4) Martensitic transformation still is the first but yield occurs after cavitation. It should be mentioned that L_{cc}^{Y-Ca} value at 100 °C is obtained by the propagation of the curves of yield and cavitation due to the limit of samples. Similarly regions present in Figure 5.17b except the macroscopic yield replaced by microscopic crystal shear.

The plastic mechanisms can be clearly distinguished. The plastic mechanism strongly depends on temperatures. For example, for the sample process L_c 15 nm, the sample undergoes the third type of plastic mechanism located in region (3) (see Figure 5.17b) at low temperature. In this condition, the martensitic transformation occurs first and the cavitation appears in the sample. With elevating temperature, cavitation disappears in sample which undergoes the second type of plastic mechanism located in region (2). At high temperature, the sample undergoes the first type of plastic mechanism located in region (1) in Figure 5.17b. In this condition, crystal shear will occur before martensitic transformation. On the other hand, the plastic mechanism depends on the L_c . For example, at 50 °C, samples with increasing L_c will pass 4 types of plastic mechanism as shown in Figure 5.17b. Finally, one can conclude that the undergoing plastic mechanisms during tensile deformation are affected by the crystallite thickness and temperatures.

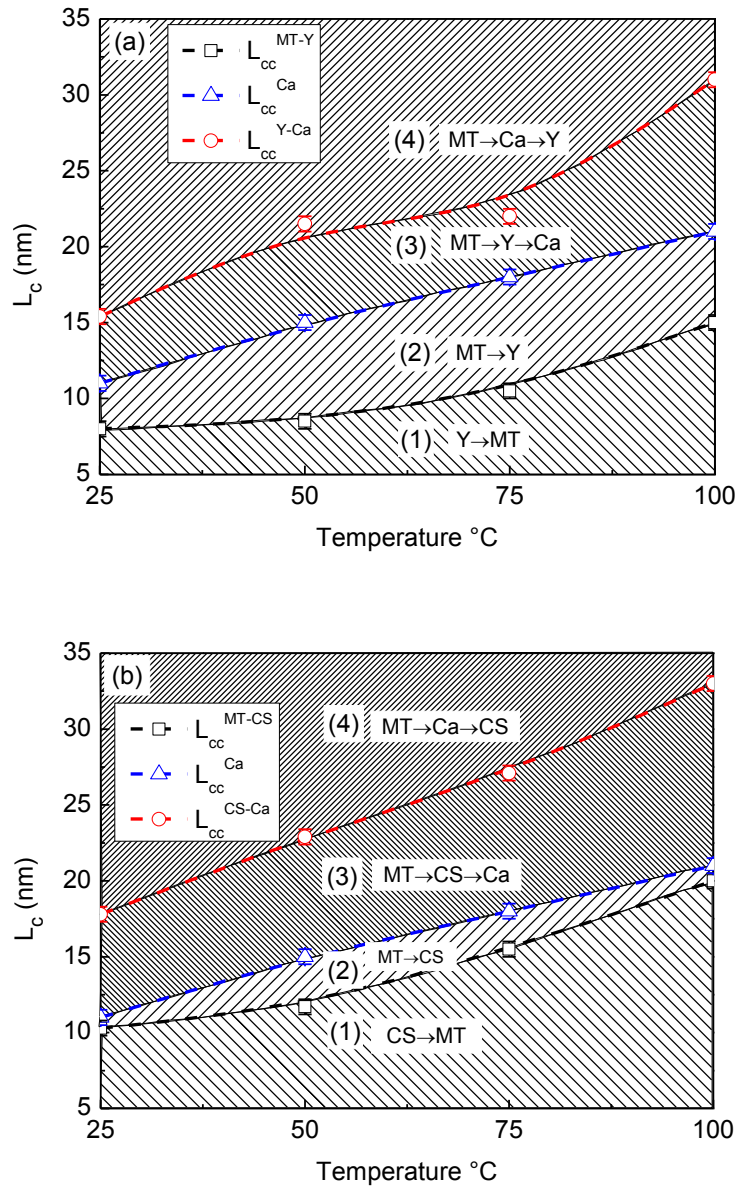


Figure 5.17. Plastic mechanisms in function of crystallite thickness and temperature. (a) cavitation, yield and martensitic transformation; (b) cavitation, crystal shear and martensitic transformation.

CS=crystal shear; Y=yield; MT= martensitic transformation; Ca=cavitation.

In conclusion, competition relations are observed between crystal shear, cavitation, and martensitic transformation. These plastic mechanisms strongly depend on temperatures and crystallite thickness. A map in function of temperatures and L_c is obtained. 4 types of plastic mechanisms are distinguished in this map.

V.6 Conclusion

The crystal shear in equatorial regions of spherulite was studied by in situ WAXS. The strain of crystal shear onset in equator region (ϵ_{cs}) was evaluated by the variation of the distance between plane O(200). ϵ_{cs} is smaller than yield strain (ϵ_{yield}) suggesting the crystal shear in equator region occur before the yield. ϵ_{cs} remains a constant with increasing crystallinity but decreases with elevating temperatures.

The strain of cavitation onset ($\epsilon_{\text{cavitation}}$) was estimated by in situ SAXS. Different behaviors were observed: (1) Homogeneous cavities, which cavities generate before yield. (2) Cavities are localized in the neck region after yield. (3) No cavities appear in the whole deformation process.

Cavitation onset strongly depends on the microstructure and draw temperature. Among the parameters of the microstructure, the crystal thickness L_c and the content of stress transmitters [ST] are the most important, where the stress for the crystal shear is mainly determined by L_c and the stress for cavities onset is controlled by [ST]. A critical crystallite thickness $L_{cc}^{\text{CS-Ca}}$ for the competition between crystal shear and cavitation onset is determined. Beyond $L_{cc}^{\text{CS-Ca}}$, the cavitation occurs first whereas below $L_{cc}^{\text{CS-Ca}}$, the shear of the crystal occurs before cavitation. With increasing temperature, $L_{cc}^{\text{CS-Ca}}$ increases. A model has been proposed based on the competition of crystal shear and cavitation. The stresses for crystal shear (σ_{sh}) and cavitation onset (σ_{cav}) is related to the L_c and temperatures. σ_{sh} and σ_{cav} are compared to predict the cavitation onset in PE. The cavitation gradually disappears with elevating temperatures. The crystal shear stress (σ_{sh}) and stress for cavitation onset (σ_{cav}) decreases with elevating temperatures. However, σ_{sh} is more sensitive to the temperatures than σ_{cav} .

The strain onset ($\epsilon_{\text{martensitic}}$) and stress onset ($\sigma_{\text{martensitic}}$) of martensitic transformation were estimated by in situ WAXS. The onset of martensitic transformation is strongly influenced by the microstructures. The martensitic transformation occurs first in lamellae located at the polar region of the spherulites. $\epsilon_{\text{martensitic}}$ decreases with increasing X_c and L_c . $\epsilon_{\text{martensitic}}$ is smaller than ϵ_{yield} suggesting the plastic deformation has been activated before yield.

$\epsilon_{\text{martensitic}}$, $\epsilon_{\text{cavitation}}$ and ϵ_{yield} were compared to reveal the first plastic mechanism onset during tensile deformation. A map involves the first plastic mechanisms were obtained. The plastic mechanism strongly depends on temperature and crystallite thickness. Samples with different microstructures undergo four different plastic mechanisms at different draw temperatures: (1) crystal shear occurs before martensitic transformation and no cavitation appears in the samples; (2) martensitic transformation is before crystal shear and also no cavitation appears in the samples; (3) martensitic transformation is in the first place, then crystal shear occurs and finally cavitation forms; (4) martensitic transformation still in the first but crystal shear occurs after cavitation.

With increasing of L_c , the martensitic transformation becomes the first plastic mechanism. This is ascribed to the lamellae are well connected in polar regions of high crystallinity samples (see Figure 5.18), permitting the stress transformation through polar lamellae in spherulites. The stress transform in polar lamellae could prevent the occurrence of the crystal shear. However, at high temperature, the connection of polar lamellae is weak due to the movement of chain in crystal, few stress transforming in polar lamellae of spherulites. This increases the local stress in other regions promoting the crystal shear.

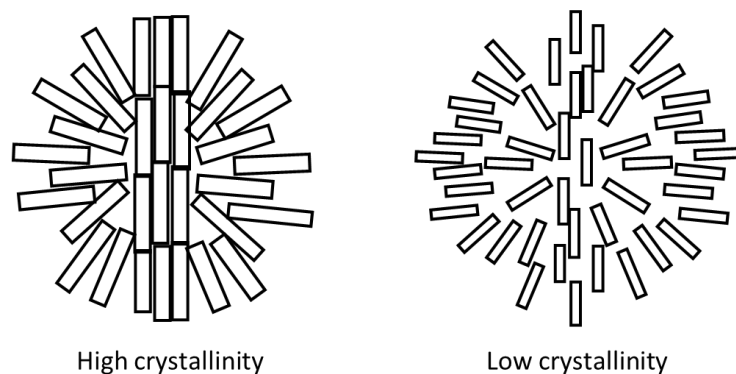


Figure 5.18. Schematic of spherulites of high crystallinity and low crystallinity

General conclusion and perspective

General conclusion

In this work, we investigated the impact of microstructure and temperature on the micro-mechanism of elastic and plastic deformation of PE and PP during tensile test. To achieve the goal, a series of samples with wide range of microstructure were prepared. Four PEs with similar molecular weight (M_w) but different comonomer concentration and 3 PPs with different isotactic index were used. Three thermal treatments were performed to get samples with various levels of crystallinity and crystal thickness.

The microstructures of the semicrystalline PE and PP were characterized by different techniques. In situ WAXS and SAXS in different temperatures were performed to investigating the variation of microstructures during the tensile test which permit to follow up the micro-mechanisms of deformation and also the influence of temperature.

With this strategy, we were able to answer a number of questions pointed out at the end of the Chapter 1.

✧ *Micro/macro strain correlations*

Local strain ε_{local} in elastic domain is estimated by the variation of the long period L_p in equator and polar regions of spherulites of PE and PP. ε_{local} linearly increases with increasing macroscopic strains in elastic domain. The ratio $\varepsilon_{local}/\varepsilon_{macro}$ is fairly constant which is only dependent on temperatures. This ratio was used in a mechanical modelling as a transition factor from mesoscopic to macroscopic scale.

In equator, local interlamellar amorphous phase strain ε_a also exhibits a linear dependence on ε_{macro} in elastic domain. The ratio $\varepsilon_a/\varepsilon_{macro}$ is in a linear function of crystallinity at a given temperature. Furthermore, $\varepsilon_a/\varepsilon_{macro}$ increases with decreasing density of stress transmitters.

✧ *Intrinsic properties of interlamellar amorphous phase*

The apparent modulus of the amorphous phase, M_a , was estimated by measuring both the local stress and the local strain in equatorial regions of the spherulites. The M_a values proved to be surprisingly high with regard to the bulk modulus of amorphous PE: indeed, $M_a \approx 250\text{--}500$ MPa at RT as compared with $E_a = 3\text{--}10$ MPa reported for the Young's modulus of bulk molten PE. Such high M_a values may be attributed to two major factors : Firstly, the structural confinement of the amorphous phase between large and stiff crystalline lamellae; Secondly, the density of stress transmitters that is much greater than in the molten material due to the presence of intercrystalline tie chains and a higher concentration of crystallization - segregated chain entanglements.

M_a strongly decreased with increasing crystallinity. This phenomenon was attributed to the concomitant decrease of the density of stress-transmitters in the amorphous phase due to the mechanism of crystallization. Furthermore, M_a decreased with increasing T_d due to the activation of chain mobility in the crystalline phase which promote the relaxation of the amorphous chains and reduce the amorphous phase stiffness.

✧ *Local stress distribution in spherulites*

The $\sigma_{local}/\sigma_{macro}$ ratio in equatorial region is a function of X_c . $\sigma_{local}/\sigma_{macro}$ ranges from 2.5 to 1.7 and decreases with increasing crystallinity. This means the local loading in equatorial regions decreases with increasing X_c suggesting that other regions of the spherulites are sharing an increasing part of the applied load.

Regarding the effect of the deformation temperature, the local strain in the amorphous phase of the equatorial regions became closer to the predicted value of the *series* coupling for any sample which is an indication of increasing stress homogeneity. With the increasing of temperature, $\sigma_{local}/\sigma_{macro}$ close to 1. This can be intuitively attributed to the activation of chain mobility in the crystalline phase that enabled the relaxation of the more strained amorphous chains, the crystalline relaxation being all the more efficient as temperature increases.

✧ *Plastic deformation mechanism*

In the plastic domain, cavitation, martensitic transformation and crystal shear were observed by in situ SAXS and WAXS. The strain onsets of these plastic mechanisms were shown to be strongly dependent on crystallite thickness and temperature. Compared with these strains, competition relations between these plastic mechanisms were observed and the first plastic mechanism was found.

Thanks to the in-situ SAXS, the occurrence of cavitation was studied at different draw temperatures. Different behaviors were observed: (1) Homogeneous cavities, which cavities generate everywhere at the same time before yield. (2) Cavities are localized in the neck region beyond the yield point. (3) No cavities appear in the whole deformation process. A comparison between the strain onset of cavitation and the yield strain clearly showed the competition between these two phenomena. The crystal thickness proved to be a major structural factor of the competition. Moreover, it was clearly shown that the occurrence of homogeneous cavitation prior to yielding promotes the occurrence of yield as evidenced by the yield stress depression. The nucleation of cavities strongly depends on the draw temperature. The main influence of an increase of T_d was to either promote localized cavitation after yielding for samples that displayed homogeneous cavitation at RT, or to inhibit cavitation in the case of localized cavitation at RT. With increasing temperature, cavitation gradually disappears.

The onset of martensitic transformation, cavitation and yield were compared in relation to microstructure and temperature in order to establish a mapping of the “plastic processes initiation”. This map enables describing the chronology of occurrence of the 3 different plastic processes.

✧ *Influences of temperatures*

Temperatures strongly influence the mechanical properties of semicrystalline polymers. The elastic modulus PE decreases with elevating temperatures, especially above α transition temperature the elastic modulus dramatically decreases which is ascribed to the activation of chain mobility in crystal below melting temperature. This also promotes the relaxation of amorphous phase relaxations which makes the deducing of apparent modulus of interlamellar amorphous phase at high temperatures. Temperature is a major factor determining the movement of crystal chains that strongly modifies the plastic processes.

✧ *Comparison of PE and PP*

Due to the difference of molecular natures, the mechanical properties are different at a given temperature such as the elastic modulus and yield stress. However, some mechanical behaviors are similar for PE and PP. Similar local deformation behavior is observed in elastic domain which the ratio between local strain and macro strain is a constant for both PE and PP. The plastic deformations of PE and PP are influenced by the crystalline structure and also the stress transmitter content.

Perspective

Firstly, we have successfully determined the local stress in equatorial regions, but we do this in polar regions. However, this could be possible via the variation of the O(020) reflexion in the meridian direction by further in-situ WAXS since it refers to the growth face of the crystalline lamellae. The (020) reflexion was unfortunately out of our recorded patterns, so that the new WAXS experiments are necessary in view of confirming our indirect conclusion regarding the stress distribution through the spherulites and its dependence on temperature and microstructure.

Secondly, we have got a large collection of data that allow us to analyse the yielding in the frame work of the dislocation model. The dependence on temperature of this model has never been checked. We could also check how this model applies in case of competition of cavitation and martensitic transformation with crystal shear.

Thirdly, we have shown that PE and PP has similar micro/macro correlation in the elastic strain range. But other mechanisms for example, crystal shear and local stress distribution in PP still retain unclear.

WAXS and SAXS at large strains have given us worthy information on the mechanism of fibrillar transformation. Work is still need to be done for analysing these data. We expect to be able to progress in the understanding of the so called melting-recrystallization process.

From a mechanical point of view, we could consider to model the mechanical behavior of PE using different microstructural and molecular parameters. Indeed, we demonstrated the influence of each parameter and temperature on the various micro-mechanisms of deformation. It would be possible to incorporate them into a mechanical model. However, this task is still very difficult because of the number of scales involved and the large number of parameters to be included.

Annex

Context	120
1 Yield behavior	121
1.1 Influence of morphology	121
1.2 Influence of temperature	123
1.3 Conclusion for yield behavior	124
2 Fibrillar transformation behavior of polyethylene	124
Article IV ‘Impact of molecular topology and initial microstructure on the fibrillar transformation of polyethylene during uniaxial stretch at elevating temperature: in situ SAXS experiment.’	124
2.2 Fibrillar transformation of polypropylene	135
2.3 Influence of temperature	136
2.4 Conclusion	137
3 Orientation of crystalline lamella	139
3.1 Orientation of PE lamellae	139
3.2 Deformation of PP lamellae	142
3.3 Comparison of lamella deformation between PP and PE	143

Context

A large number of papers concerning yield of semicrystalline polymers have been published. However, it is still not fully understood the mechanisms involved. Yield is considered as a collapse of the crystal lamellae structure, which is generally associated to the nucleation and motion of screw dislocation in the crystal lamella. Yield stress is in function of the crystallite thickness and draw temperatures. The analysis of the yielding in the frame work of the dislocation model has been studied but the dependence on temperature of this model has never been checked. In this work, yield stresses at high temperatures have been collected but checking the temperature dependence of this model needs more works and will be the part of future work.

The deformation in large strain of semicrystalline polymers proceeds via a necking. At a microscopic level, this phenomenon involves the orientation of lamellar microstructure known as fibrillar transformation.

This transformation process involves the fragmentation and rearrangement of the initial lamellae into blocks. The fragmentation of lamellae is influenced by the initial structures via the local stress distribution in the lamellae. However, the precise effects of initial structure on the micro-fibrils structure are not clear. On the other hand, long period of the micro-fibrils (L_{pf}) decreases compared to the initial period structure indicating the new lamellar structure formed. L_{pf} presents to be independent to the initial structure but only dependent on temperatures. This phenomenon can not be explained by the 'fragmentation-rearrangement' mechanism. Based on the evolution of long period, the mechanism of 'melt-recrystallization' was proposed in the previous studies, however, no direct evidence to support this mechanism.

In this work, the influence of molecular topology and microstructure on the fibrillar transformation induced by draw of semicrystalline polyethylene with various co-unit concentrations was studied by in situ SAXS at different draw temperatures. The diameter of micro-fibrils (D_f) shows a good correlation to the initial microstructures via a correlation to the interphase content, the stress transmitters density and crystallite thickness. This provides an evidence of fibrillar transformation mechanism 'fragmentation-rearrangement'. Furthermore, the crystallinity changes after fibrillar transformation. The long period decreases with increasing temperatures which provides an indirect evidence of 'melt-recrystallization' mechanism. A large of data have been collected, however, more works need to be done to understanding the deformation mechanisms at large strain.

The isotactic polypropylene also studied with the same method to compare the fibrillar transformation between semicrystalline polymers of different natures but with similar microstructures.

1 Yield behavior

Yield behavior of semicrystalline polymers has been widely studied during last forty years. Until recently, it is still not fully understood and improvements could be made to clarify the mechanisms involved [81,139,140,141]. According to the previous studies, the yield is generally associated to the nucleation and motion of screw dislocation in the crystal lamella and the yield stress is in function of the crystallite thickness and draw temperatures [136,141]. The tie molecules also play an important role on the yield stress [142]. Yield behavior should be affected by the crystal structure, temperatures and also stress transmitters, however, few models consider the parameters of temperatures and stress transmitters.

1.1 Influence of morphology

The yield stress is strongly affected by the morphology. The yield stress (σ_y) is in function of the crystallinity (X_c) according to the previous investigations [87,143], and this can be observed in our experiment results at different temperatures (see Figure 1.1). A good correlation is shown but no physical explanation is brought for this phenomenological approach. Regarding the influence of temperature, σ_y decreases with elevating temperatures. Particularly, little difference of σ_y is observed between 25 °C and 50 °C but σ_y decreases a lot above 75 °C. The slope of σ_y is smaller at 100 °C than at 50 °C. This could be due to the α transition above 50 °C which promotes the mobility of chains in crystal.

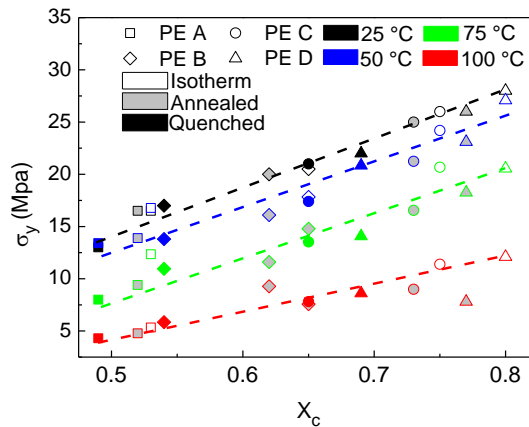


Figure 1.1. Yield stress of PE at different temperatures in function of crystallinity. Strain rate = $6.4 \times 10^{-4} \text{ s}^{-1}$.

In chapter 1 we mentioned that yielding in polymers is controlled by the nucleation of screw dislocations. Based on dislocation theory, σ_y is given by the expressions [87,140]:

$$\sigma_y = \frac{K}{2\pi} \alpha(T) \exp\left[-\left(\frac{2\pi\Delta G_a}{lKb^2} + 1\right)\right] \quad (1)$$

$$\text{with } \alpha(T) = \frac{b}{r_0} \exp\left(\frac{2\pi\Delta E_0}{lKb^2}\right)$$

where ΔG_a Gibbs free energy for nucleation of dislocation, b magnitude of the Burgers vector, K crystalline shear modulus, T temperature, l stem length, r_0 core radius of dislocation and E_0 is the core energy.

Equation (1) can be rewritten in the form:

$$\ln(\sigma_y) = \left[\ln\left(\frac{K}{2\pi}\right) \alpha(T) - 1 \right] - \left(\frac{2\pi\Delta G_a}{lb^2}\right) \quad (2)$$

It should be mentioned that this method assumed the yield stress can be determined from the energy required to nucleate screw dislocations within the crystalline lamellae, the direction of the

Burgers vector for this dislocation being parallel to the chain axis and the stem length l equals to the thickness of lamella L_c .

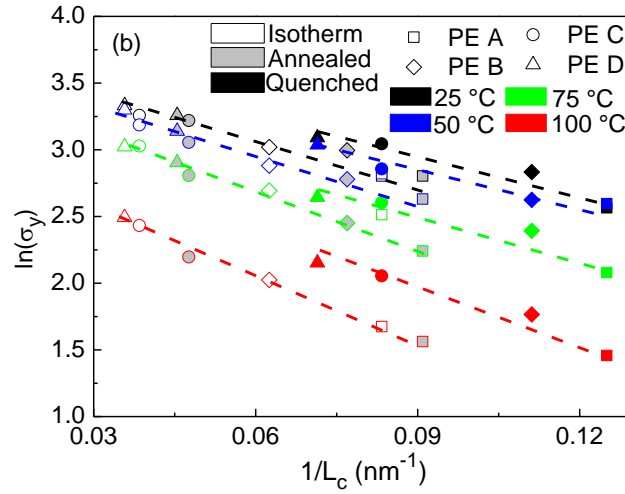


Figure 1.2. $\ln(\sigma_y)$ of PE in function of $1/L_c$ at different temperatures. Strain rate= $6.4 \times 10^{-4} \text{ s}^{-1}$.

$\ln(\sigma_y)$ and $1/L_c$ present a linear relation as expected in Equation 2 (see Figure 1.2). However, the quenched samples and the annealed samples are not in the same line indicating there should be other structure parameters affect the yield stress. Stress transmitters play an important role on the local shear of the crystal which promotes the yield of samples. Consequently the initiation of the crystallite shearing should be described by a function of L_c and $[ST]$. A model borrowed from Humbert [139] is employed to take into account of parameters $[ST]$. In this model, σ_y is written as:

$$\sigma_y = k \times \left(\frac{\sigma_c}{\sigma_{c0}}\right) \times \left(\frac{[ST]}{[ST]_0}\right)^{0,6} \quad (3)$$

$\frac{\sigma_c}{\sigma_{c0}}$ is obtained from Equation 1:

$$\frac{\sigma_c}{\sigma_{c0}} \propto \exp\left[-C_1 \left(\frac{1}{L_c} - \frac{1}{L_{c0}}\right)\right] \quad (4)$$

$$\text{with } C_1 = \frac{2\pi(\Delta G_a - E_0)}{Kb^2}$$

L_{c0} and $[ST]_0$ are the minimal values of L_c and $[ST]$ of the samples. σ_{c0} is calculated using Equation 1 and substituting L_c with L_{c0} . In this model, C_1 equals to 2.3×10^{-8} taking $K = 2630 \text{ MPa}$, $k = 1.38 \times 10^{-8} \text{ J/K}$, $\Delta G_a = 60 \text{ kT}$, $b = 1.27 \text{ \AA}$ and $E_0 = 0.93 \times 10^{-9}$ [139].

A good correlation can be observed between σ_y and $\left(\frac{\sigma_c}{\sigma_{c0}}\right) \times \left(\frac{[ST]}{[ST]_0}\right)^{0,6}$ in different drawing temperature (see Figure 1.3) indicating that yield stress is influenced by crystallite thickness and stress transmitters.

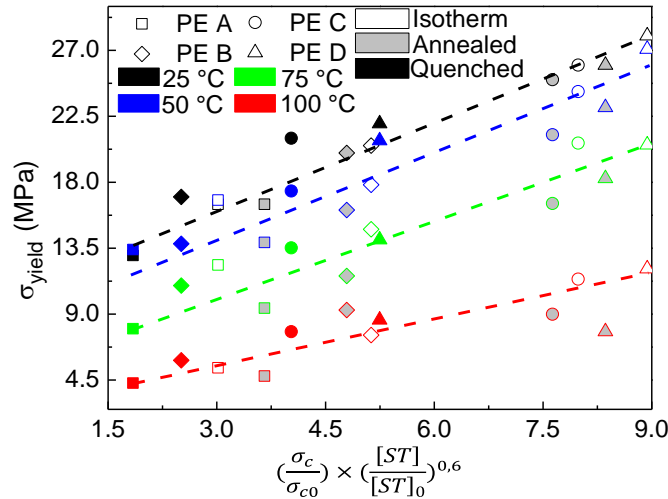


Figure 1.3. σ_y of PE in function of $(\frac{\sigma_c}{\sigma_{c0}}) \times (\frac{[ST]}{[ST]_0})^{0,6}$ at different temperatures.

1.2 Influence of temperature

Temperature is an important factor for the plastic deformation of semicrystalline polymers. For all the samples, irrespective the thermal treatments methods, σ_y decreases with elevating temperatures (see Figure 1.1, 1.2 and 1.3).

Figure 1.4 shows the stress/strain curves of quenched PE A and PP C in different draw temperatures. Here, just quenched PE A and PP C are studied for examples. With elevating drawing temperature, the yield stresses of polyethylene and polypropylene are decreased and also the yield strain moves to small values.

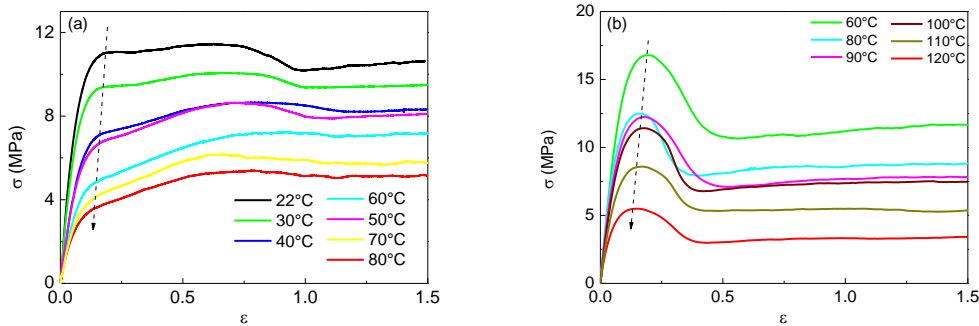


Figure 1.4. The stress-strain curves of (a) quenched PE A and (b) quenched PP C in different temperature. Strain rate= $1.4 \times 10^{-4} \text{ s}^{-1}$.

Yielding is generally considered to be an activated energy rate phenomenon. In the Eyring view of thermally activated processes, an energy barrier E must be overcome for the motion to proceed. According to Eyring model, the yield stress can be expressed as [88]:

$$\sigma_y = \frac{E}{V} + \frac{RT}{V} \ln\left(\frac{\dot{\epsilon}}{\dot{\epsilon}_0}\right) \quad (5)$$

where σ_y is the yield stress, E is the activation energy, V is the activation volume, and $\dot{\epsilon}$ is the strain rate.

Figure 1.5 shows σ_y of quenched PP C and PE A as a function of drawing temperature with a strain rate $1.4 \times 10^{-4} \text{ s}^{-1}$. At a given strain rate, σ_y is linearly correlated to the drawing temperature. Regarding the differences of polymers, yield stresses of PE and PP present different dependence

of temperatures. PP processes higher activation energy and lower activation volume than those of PE.

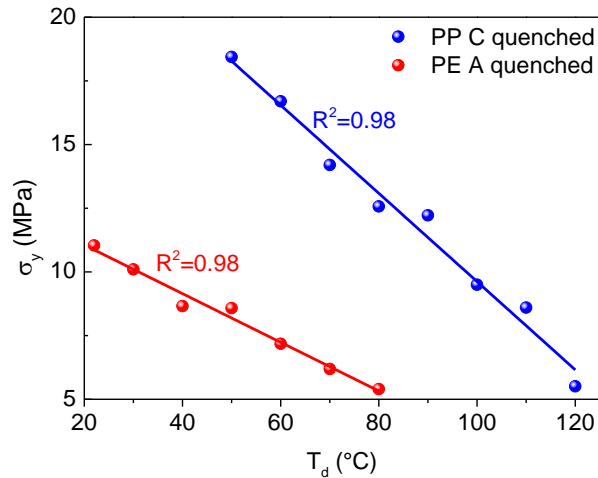


Figure 1.5. σ_y in function of drawing temperature for quenched PP C and PE A.

1.3 Conclusion for yield behavior

Yield behavior is proved to be affected by the crystallite thickness, stress transmitter density and also temperatures. A model borrowed from precious work which takes into account of stress transmitter density works well at different temperatures. However, the influence of temperature is not checked in this model and this will be one of the future works.

The yield stresses of PE and PP are strongly depending on temperatures which decrease with increasing temperatures but PP processes higher activation energy and lower activation volume than those of PE calculated from Eyring model.

2 Fibrillar transformation behavior of polyethylene

Article IV ‘Impact of molecular topology and initial microstructure on the fibrillar transformation of polyethylene during uniaxial stretch at elevating temperature: in situ SAXS experiment.’

Abstract

The influence of molecular topology and microstructure on the fibrillar transformation induced by draw of semicrystalline polyethylenes with various co-unit concentrations was studied by in situ SAXS at different draw temperatures. The long period of micro-fibrils (L_{pf}) proved to be dependent not only on the draw temperature but also slightly on the thermal treatment. L_{pf} was smaller than initial L_p which could be explained by melt and recrystallization mechanisms. Both L_{pf} and micro-fibrils diameter (D_f) decreased with increasing co-unit concentrations suggesting the micro-fibrils was affected by the molecular topology. D_f depended on the initial microstructure via a correlation to the interphase content, the stress transmitters density and crystallite thickness. This provides an evidence of fibrillar transformation mechanism ‘fragmentation-rearrangement’. On the other hand, D_f also presented temperature dependency which increases with increasing draw temperature. The long period decreases with increasing temperatures which provides an indirect evidence of ‘melt-recrystallization’ mechanism.

Introduction

The deformation at large strains of semicrystalline polymers often involves spherulite structure of polymers converts into an oriented fibrous structure known as fibrillar transformation [71,117,118,119,120,121]. The long period of the micro-fibrils L_{pf} is very different to the long period of original isotropic crystalline lamellae stacks L_p . The axial long period of the drawn micro-fibrils could be 30% larger or 50% smaller than the original long period when drawn the PE quenched film [144]. The long period after deformation seems to be independent in the starting material but in function of drawing temperature. The long period increases with the drawing temperature in a way similar to its dependence on crystallization from melt or from solution, i.e. the higher the drawing temperature the longer the long period [121,145]. The original long period of the materials should be destructed and then reconstructed after the fibrillar transformation. For this reason, many authors concluded that fibrillar transformation is accompanied with a strain-induced melting-recrystallization process [92,118]. This process may results from the plastic work which is eventually sufficient to partial or completely melt under negative pressure of the tensile stress.[71]

The crystal blocks within the micro-fibrils of the deformed PE mats were observed under TEM and SAXS that the dimension of the crystalline blocks in the stretching direction are close to the thickness of the initial crystals [117,120,122]. Based on these reports, the fibrillar transformation process were described as the fragmentation of the lamellar crystals into blocks that rearrange into the micro-fibrils via chain unfolding from the fracture surface of the crystal blocks. Several description models at the molecular scale had been proposed for the mechanism of lamella fragmentation. The mosaic block structure of the crystalline lamellae of PE plays a role in the initiation of lamellae fragmentation due to the presence of defects that may promote localized slip [146,147]. The chain defects at the crystal surface also could accelerate the stress concentration in the lamella crystal surface [108,139]. The molecule structure, such as co-unit density and molecular weight distribution, and initial microstructure from the crystallization process are the two major impacts in the generation of crystalline defects[148].

Many researchers studied on the influence of the initially topological structures including entanglement and tie molecule on the plastic deformation of polyethylene [71,149,150,151,152,153,154]. These initial microstructures affect the local stress distribution which should have an impact on the fragmentation of crystalline lamella. However, this seems contradict to the L_{pf} dependence on the drawing conditions only. Humbert et al [148] reported that the diameter of micro-fibrils was determined by the defects in interphase and the initial microstructure influence the morphology of micro-fibrils at room temperature. However, they did not considering the influence of temperatures. Therefore, one may wonder what are effects of molecular topology, initial microstructure at elevated temperatures on the strain-induced fibrillar transformation?

To answer the above question, a series of polyethylene with wide distribution of topological microstructure were employed to the study. The microstructure of micro-fibrils were characterized and related to the initial microstructure for understanding the influence of the molecular topology and initial microstructure on the micro-fibrils transformation process at elevated temperatures.

Experiment

Materials

Four polyethylenes consisted of different hexane concentrations [C6] were synthesized by mean of Philips chromium-oxide catalysis and supplied by Total-Petrochemicals. The molecular and physic characteristics of the 4 materials are given in Table 1. They differ from their molecule topology.

Table 1. Molecular and physical characteristics of materials

Materials	[C6] (mol%)	M_n (kDa)	M_w (kDa)	T_c^a (°C)
PE A	1.8	14.3	231	114
PE B	0.8	15.8	187	114
PE C	0.1	15.4	216	124
PE D	0.1	15.0	229	124

^aT_c: crystallization temperature measured by DSC

Sample preparation

The pellets were compression-molded at 170 °C into 500 μm sheets between aluminum foils in a press and then quenched into water at room temperature. These samples were called ‘quenched’. To modify the microstructure, partial quenched samples were treated with anneal and isotherm. Samples labeled as ‘annealed’ are heated from quenched-state to the crystallization temperature T_c (see Table 1) and are held in this temperature for about 15 hours. The samples called ‘isotherm’ are melted at 170 °C and then cooled in a thermostatic oil bath at a temperature T_c and held at this temperature for 15 hours. Samples were well sealed between aluminum plates tightly jointed with a silicone rubber gasket to prevent the oil pollution.

Differential scanning calorimetry (DSC)

The thermal analysis was conducted by an indium-calibrated perkin-Elmer DSC7 apparatus, using samples 5 to 7 mg. The crystallization temperature, T_c, and the melting temperature, T_m, were measured at the peak of the crystallization exotherm and the melting endotherm, respectively. The melting and cooling thermograms were recorded at a rate 10 °C/min, under nitrogen flow 25 ml/min.

The crystal weight fraction was computed from the equation:

$$X_c = \frac{\Delta H_m}{\Delta H_m^0} \quad (1)$$

where ΔH_m is the heat of fusion and ΔH_m^0 is the heat fusion of a perfect crystal and equal to 290 J/g[155]. The standard deviation of the X_c data is about 1%.

Tensile measurements

The tensile test was performed at different temperature with a MTS machine. Dumbbell-shaped samples of 12 mm gauge length, 4 mm width and 0.5 mm thickness were tested with strain rate $5 \times 10^{-3} \text{ s}^{-1}$ and nominal stress/strain curves were obtained. The high reproducibility of the data promises a standard deviation about 2%.

SAXS measurement

Small angle X-ray scattering experiments were performed on the BM2-D2AM beamline of the European Synchrotron Radiation Facility (ESRF, Grenoble France) using a wavelength $\lambda=0.154$ nm. The 2D-SAXS patterns were recorded on a CCD camera (Ropper Scientific) which was set at 1580 mm sample-detector distance.

In-situ uniaxial tensile experiments were performed using a homemade mini tensile machine, which stretched the sample symmetrically. This ensured that the focused X-ray beam could illuminate the same sample position during deformation. Dumbbell-shaped samples with dimensions of 11 mm (gauge length), 4 mm (neck with), and 0.5 mm (thickness) were tested. The strain rate was chosen as $6.4 \times 10^{-4} \text{ s}^{-1}$ to make sure the strain < 0.1% during the 5s exposure time. The experiments were performed at 25 °C, 50°C, 75°C and 100 °C respectively for each sample.

The Lorentz-corrected intensity profiles of the isotropic samples Iq^2 were obtained by azimuthal integration of 2D patterns. The long period of the lamellar stacking, L_p , was determined from the relation:

$$L_p = 2\pi/q_{max} \quad (2)$$

Where q_{max} is the scattering vector at the maximum of the correlation peak. The standard deviation of the L_p data does not exceed 1 nm.

To calculate the long period of the fibrils, the intensity profiles along the meridian were obtained by projection of the 2D-patterns on the meridian according to Stribeck's method[156], before applying the Lorentz correction factor. Then the long period was estimated by Equation 1.

The crystal thickness, L_c , was computed from the following relation:

$$L_c = L_p X_c \rho / \rho_c \quad (3)$$

Where $\rho_c = 1.00 \text{ g/cm}^3$ is the density of the crystalline phase.

For the computation of diameter of micro-fibrils, the scattering objects were supposed as the individual micro-fibrils embedded in a medium of lower electron density consisting of amorphous chains and cavities. The corresponding models consist of either elongated cylinders or discs, respectively. In both instance, the equatorial contribution of the scattering factor can be performed via the Guinier's approximation leading to an estimation of the equatorial size of the scattering element [148,157,158]. In the case of a scattering cylinder, the Guinier's approximation function is [158]:

$$I(q) = I_0 \exp\left(-\frac{q^2 D_f^2}{4}\right) \quad (4)$$

Where D_f is the diameter of the scattering cylinder. This equation is only valid for $qD_f \ll 1$. Thus Guinier's approximation only fits at very low q values. The diameter of micro-fibrils D_f had a deviation 0.5 nm.

All the physical data regarding the thermally treated samples are reported in Table 2.

Table 2. structure and physical characteristic of the samples with various thermal treatments

Materials	X_c (%)	L_p (nm)	L_c (nm)	[ST]	X_i %	
PE A	quenched	49	17	8	0.24	13
	annealed	52	23	11	0.17	13
	isotherm	53	24	12	0.15	11
PE B	quenched	54	19	9	0.19	8
	annealed	62	22	13	0.14	8
	isotherm	65	26	16	0.09	4
PE C	quenched	65	20	12	0.19	5
	annealed	73	30	21	0.08	5
	isotherm	75	36	26	0.03	5
PE D	quenched	69	22	14	0.17	0
	annealed	77	30	22	0.08	5
	isotherm	80	37	29	0.03	3

X_i : interphase content, obtained from reference [148]. [ST]: stress transmitters density, calculated from Brown's model

Results

Figure 1 shows SAXS pattern recorded in drawing PE A quenched in the neck region at 50 °C. Structure parameters of the micro-fibrils, for instance, long period L_{pf} and diameter D_f , can be obtained from the equatorial and meridian scattering respectively. The scattering in the center of

the SAXS pattern is very intense which are originating from cavities in the boundary of two micro-fibrils. Cavity scattering is so intense that it could be emerged onto the meridian scattering, prohibiting the analysis of the micro-fibrils structure. However, elevating draw temperature (T_d) promotes decrease of cavities. For this reason, more samples were analyzed at 100 °C than that at 50 °C.

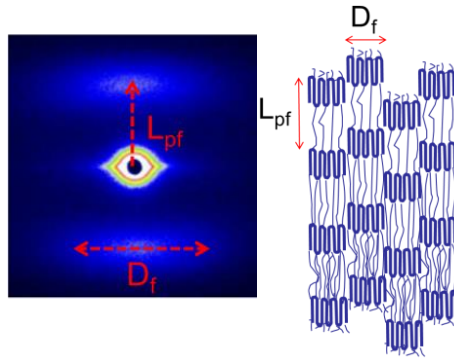


Figure1. In-situ SAXS pattern of micro-fibril and correlated structure information obtained from the SAXS patterns

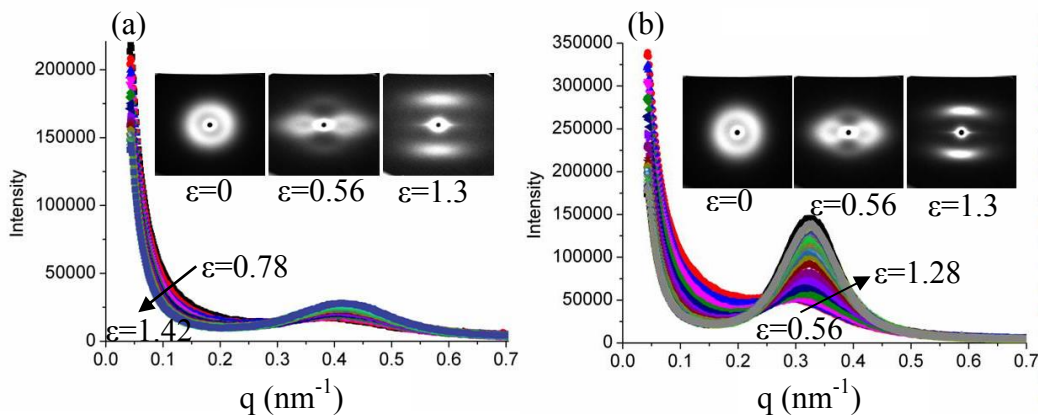


Figure 2. Meridian intensity profile of quenched PE A in various strains at (a) 50 °C and (b) 100 °C.

Figure 2 shows the meridian intensity profile of quenched PE A at different temperature. The SAXS patterns transfer from isotropic to highly anisotropic patterns with two streak-like scattering patterns during the elongation of samples (see insert illustration in Figure 2). The beginning of the two streak-like scattering is above the 0.56 of nominal strain for quenched PE A. This strain decreases with elevating drawing temperature, suggesting the fully orientated structure forms faster at higher drawing temperature. Indeed, formation of fibrils structure usually accompanies with fraction of crystal which could be strongly promoted by elevating drawing temperature due to the stiffness – temperature dependence in the relaxation domain. Additionally, at a given temperature, the streak-like scattering intense during the elongation. This is due to the enhancement of the orientation with the increase of deformation.

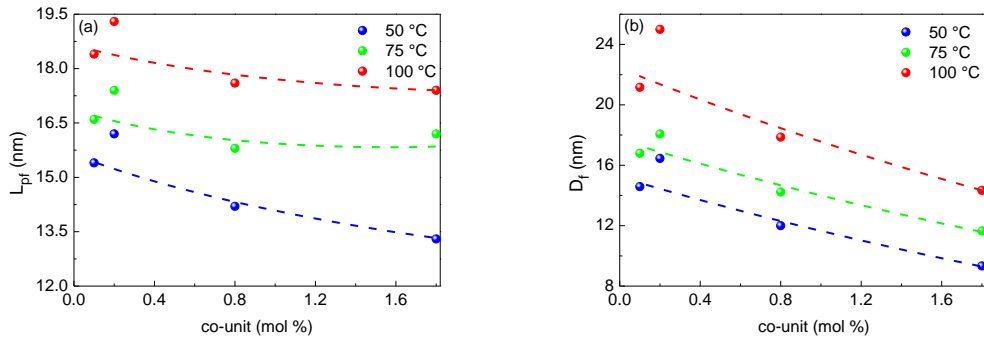


Figure 3. Micro-fibrils microstructure parameters of quenched samples in function of co-unit density at different T_d . (a) L_{pf} and (b) D_f which were measured at strain 1.3.

L_{pf} and D_f were estimated by Equations 2 and 4 from meridian and equatorial intensity profile. Figure 3 shows the influence of the co-unit concentration on L_{pf} and D_f of quenched samples measured at $\varepsilon=1.3$ in various T_d . L_{pf} and D_f decrease with increasing co-unit concentration indicating the molecule topology strongly affects the micro-fibrils structure.

Figure 4 shows L_{pf} in function of initial L_p in different T_d measure at deformation strain 1.3. In low T_d , annealed and isotherm samples were prevented to quantitatively analyze the meridian scattering due to intensify of the central scattering from numerous cavities. However, more L_{pf} data were obtained by elevating T_d since high temperature reduces cavities.

As shown in Figure 4, L_{pf} is smaller than L_p indicating that new lamella structure is reconstructed during the plastic deformation. In addition, L_{pf} increases with elevating T_d . Furthermore, at a given T_d , samples with different thermal treatments present different L_{pf} ; for example, at 100 °C, L_{pf} of quenched PE A equals 17.3 nm while annealed PE A is 18.3 nm. This indicates L_{pf} depends on the thermal treatment which induces the initial microstructure difference. This proves that the initial structure affects L_{pf} . However, this result seems contradict to the previously study that L_{pf} is only dependent on the drawing condition.

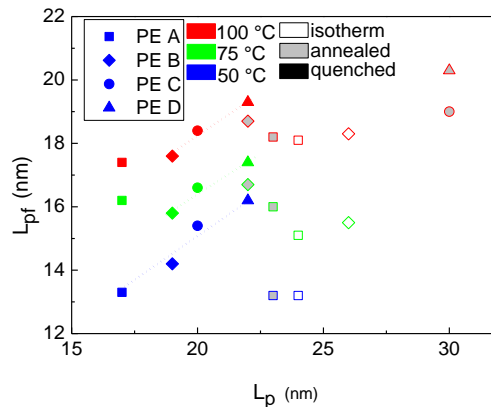


Figure 4. L_{pf} versus L_p initial at T_d 50 °C, 75 °C and 100 °C. L_{pf} measured at nominal strain 1.3.

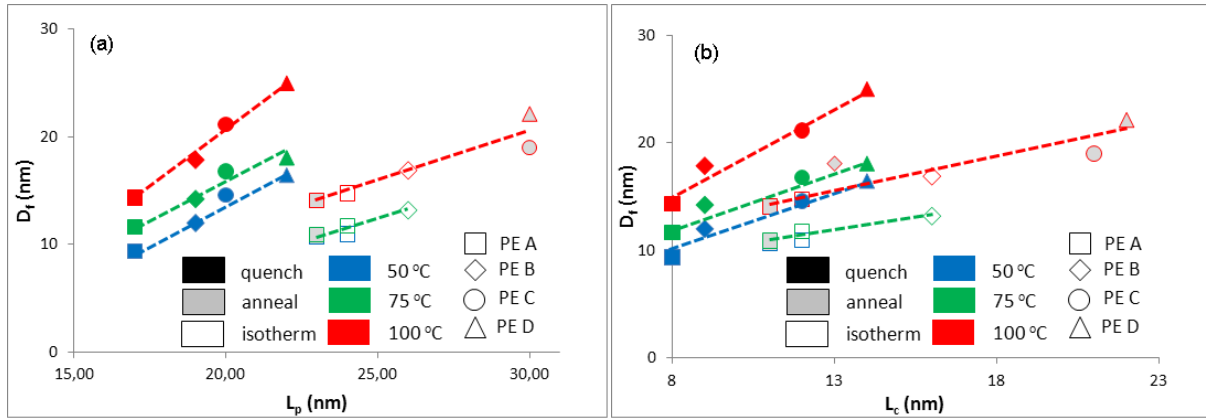


Figure 5. Micro-fibrils diameters (D_f) in function of (a) initial long period (L_p), (b) initial crystallite thickness (L_c) at different temperatures. D_f measured at strain 1.3.

Figure 5 shows the micro-fibrils diameters (D_f) in function of initial crystallite thickness (L_c) and long period (L_p) at different T_d . D_f was measured at strain 1.3. D_f linearly increases with increasing initial L_c and L_p at a given temperature. However, the quenched samples and annealed or isothermal samples are not in the same line suggesting that micro-fibrils structure of quenched and annealed samples process different dependent on the initial microstructure. At 100 °C, D_f of quenched PE A is 14.3 nm, annealed PE A is 14.1 nm and isothermal PE A is 14.7 nm. This suggests that thermal treatments do not affect D_f . Furthermore, D_f presents a strongly temperature sensitive which increases with elevating T_d .

Figure 6 shows D_f as a function of natural draw ratio λ_n . λ_n is a macroscopic representation of stress transmitters density [ST]. At a given temperature, D_f for samples with the same thermal treatments is linearly increases with increasing λ_n and decreasing [ST]. However, the quenched and annealed or isothermal samples present different dependents on λ_n . Quenched samples exhibit higher D_f than that of annealed or isothermal samples which is similar to the relation between L_c and D_f . Thus, one can conclude that ST influences D_f of the micro-fibrils but there should be other factors affect D_f . Furthermore, similarly, D_f increases with increasing T_d .

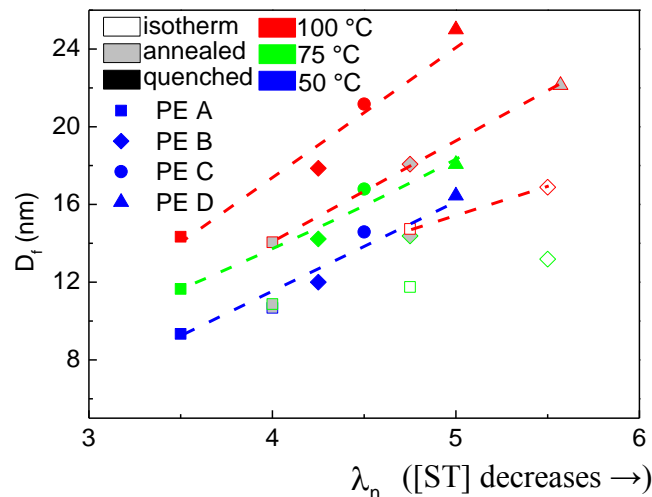


Figure 6. D_f versus natural draw ratio λ_n at different T_d .

Figure 7 shows D_f as a function of Nitta's topological factor, $L_c/[ST]^{0.5}$, where [ST] deduced from Brown's model [159]. The Nitta's factor is featuring the average distance between neighbor tie molecules. A clearly tendency appears for the quenched samples at different temperature. D_f linearly increases with increasing $L_c/[ST]^{0.5}$ for quenched samples which means D_f increases with

increasing the distance between neighbor tie molecules. Therefore, one can conclude that D_f is the consequence of the fragmentation of crystal lamellae in tie molecules. But this tendency disappears for the annealed and isothermal samples, indicating complex influences of microstructure on D_f . Additionally, D_f is smaller than $L_c/[ST]^{0.5}$ which could be due to chains unfolding after fragmentation. From above results, it can be concluded that the $[ST]$ is not the unique topological factor affecting the D_f and it should be correlated to the crystalline condition (thermal treatment), chain topology and ST .

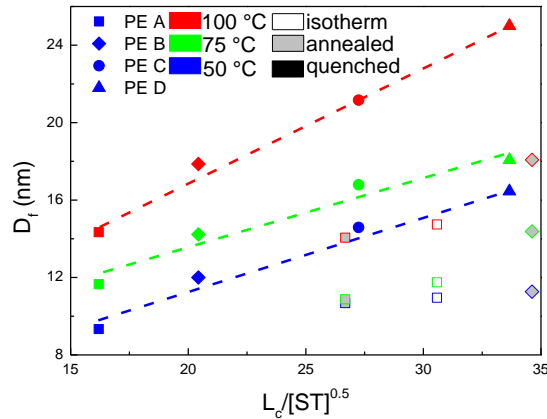


Figure 7. D_f versus Nitta's topological factor $L_c/[ST]^{0.5}$ at different draw temperature

On the other hand, the interphase (transition region at the crystal-amorphous boundary) content X_i , was shown to depend on both the chain architecture and the crystallization condition: high regularity chains as well as slow crystallization result in lower X_i values [148]. Figure 8 shows D_f as a function of X_i (see Table 2) at different temperatures. At a given T_d , a monotonous correlation between D_f and X_i is observed. This suggests that the topological defects in the interphase contribute to the fibrils transition of the crystals, not only the stress transmitters such as tie molecule and chain entanglement. The interphase is regarded as the gathering all topological defects derived from the chain-folding crystallization. Furthermore, D_f increases with increasing T_d , but no matter the T_d is, similar tendency appears indicating the interphase process the same impact to the micro-fibrils in different T_d .

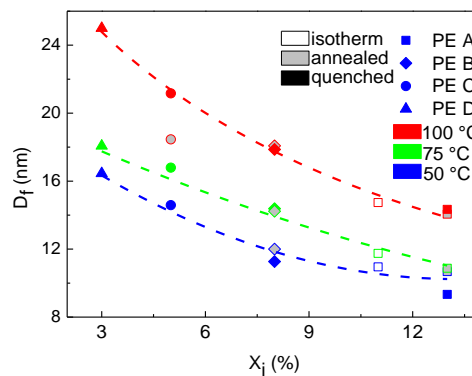


Figure 8. D_f as a function of interphase weight fraction, X_i , at different temperatures.

Discussion

Long period of micro-fibrils is quite different from the initially isotropic material L_p . In the results above, L_{pf} is smaller than the initial long period L_p (see Figure 4). The abrupt long period change indicates the transformation from the original micro-spherulite structure to the final fiber structure is a discontinuous process. This means the long period structure should undergo a destruction and

reconstruction process. Moreover, some authors reported that the L_{pf} is correlated to drawing temperature but independent to the crystalline structure of the original materials [121,144,160]. This means the original crystalline structure is not related to the reconstruction process. To explain, the authors believed that the fibrillar transformation is accompanied with a strain-induced melting-recrystallization process [92,118,126]. The breakage of lamellae into smaller blocks and the longitudinal displacement of some straight sections in the block require quite a large amount of energy. It is equivalent to a very specific partial melting [121]. The plastic work is sufficient for much chain mobilization and eventually for melting under the negative pressure of the tensile stress [71]. During subsequent cooling in the environment temperature, the highly mobilized chains in the blocks may get adjusted to this temperature[117]. With this assumption, the long period of the recrystallized material is mainly dependent on the actual temperature of melt, which strongly depends on the intensity of the self-heating effect, and the ability of recrystallization which depends on the molecular topology. However, until now, there is not direct observation to support the melt and recrystallization during the tensile deformation.

If the recrystallization happens during the fibrillar transformation process, the crystalline thickness L_{cf} should depend on the drawing temperature like the crystallization from the melt. According to the theory of Lauritzen-Hoffman, when polymers crystallized from a quiescent molten state, it could be described as the following [161,162]:

$$T_f^\infty - T = \frac{4\sigma}{\Delta H_f} \frac{T_f^\infty}{L_c} \quad (6)$$

where T_c^∞ is the fusion temperature of the perfect polyethylene crystal; ΔH_f is fusion entropy of perfect crystal; σ is the surface energy of crystal and T is the crystallization temperature of isotherm. Here, T equals to T_d . Figure 9 shows T_d in function of $1/L_c$ of quenched PE A. A linear relation between T_d and $1/L_c$ as expected can be observed. This result indirectly supports that the melt and recrystallization occurs in fibrillar transformation process of polyethylene.

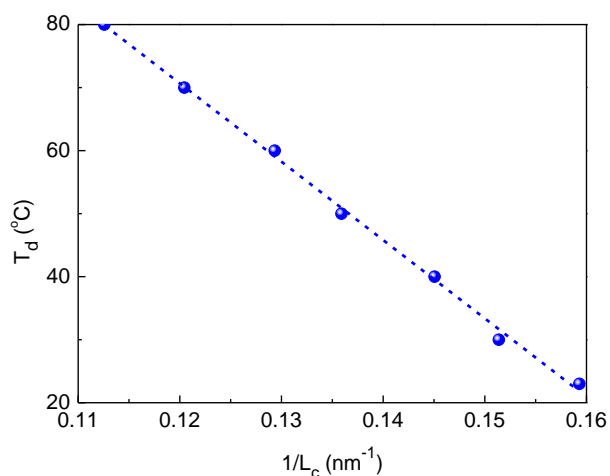


Figure 9. T_d in function of $1/L_c$ of quenched PE A. L_c is measured by DSC and SAXS at strain 1.3.

Stress transmitters should play a major role in the crystal shear and fragmentation due to the generation of local stress concentration on the crystalline lamella surface according to previous investigations [163][33]. Based on previous studies, the transformation process involves a fragmentation of every single lamella into folded chain blocks and rearrangement of these blocks into micro-fibrils, the basing element of the fiber structure via chain unfolding from the fracture surface of the crystal blocks[117,145,164]. This fragmentation process also accompanies with crystal shear and chain unfolded from the crystal[124]. The fracture of crystal could lead to the largely destruction of the original lamella structure. Indeed, each lamella should yield its own set

of micro-fibrils according to the model of Peterlin [160]. The tie molecule which originally joined two different lamellae now connects two different micro-fibrils. With the higher concentration of original tie molecule content, the smaller deformation of the micro-fibrils displacement caused by the shearing between two adjacent micro-fibrils. Hence, the macroscopic natural draw ratio is smaller for the higher [ST] sample. The higher concentration of stress transmitters the smaller the crystal block size, and consequently the smaller D_f is (see Figure 6). According to Nitta's investigation [159,165], the fragmentation of crystal lamella could be attributed to the content of the tie molecule and D_f is a function of tie molecule content with equation:

$$D_f = C \times \frac{L_c}{[ST]^{0.5}} \quad (7)$$

where C is a constant, L_c is thickness of crystalline lamella and $[ST]$ is the content of tie molecule. D_f is linear relation with Nitta's topological factor, $L_c/[ST]^{0.5}$, which can be observed in Figure 7.

Regarding the influence of drawing temperature, local stress distribution is more homogeneously with elevating temperature according to the temperature dependence of the crystal stiffness. Above α transition temperature, taut tie molecule could be relaxed due to mobilization of chains in crystal. This reduces the impact of tie molecule to the crystal fragmentation, thus inducing wider micro-fibrils in higher drawing temperature.

To understand the role of molecular topology on the fibrillar transformation, let's go back to the mechanism of transformation: fragmentation-rearrangement [117,120,122] and melt-recrystallization [92,118]. The mechanism fragmentation-rearrangement involves crystal lamella shear and fragmentation processes which strongly depends on the crystal structure and local stress distributions. In study of the fibrillar transformation of semi-crystalline polymers, Tarin and Thomas [164] suggested that all chain topology defects were likely to contribute in the initiation of crystal fragmentation. Furthermore, the higher co-unit density promotes the formation of inter or intra links in crystal lamella which serve to produce stress concentration in the crystal surface and lead the crack and fracture of crystal [159,166,167]. This could be indirectly proved by decreasing of D_f with increasing co-unit density (see Figure 3b). The higher co-unit density, the higher tie molecule content and smaller distance of neighbor tie molecule, thus the smaller diameter is. D_f provides an evidence that the interphase at the crystal-amorphous boundary has a direct incidence on the generation of the nascent micro-fibrils especially on the diameters (see Figure 8). This structure is more related to the initial lamellar structure than the experiment condition. On the other hand, the melt-recrystallization mechanism involves crystallization from melt. Many authors studied that the molecular defects prevent crystallites formations and the long period and crystallite thickness will be deduced with increasing molecular defects from co-unit [42,155,168]. The long period dependence on co-unit density can also be observed in our experiment (see Figure 3a).

Conclusion

The fibrillar transformation in semi-crystalline polymers involves the destruction-reconstruction and melting-recrystallization mechanisms. The long period L_{pf} of micro-fibrils is smaller than the initial long period suggesting the new lamellae structures formed in the fibrillar transformation process. L_{pf} depends on the drawing temperature and molecule topology. L_{pf} also slightly depends on the thermal treatment which seems contradict to the previous studies. These results provide an indirectly evidence to the melting-recrystallization mechanism of the fibrillar transformation.

Micro-fibrils diameters (D_f) provide evidence that the crystal-amorphous phase boundary directly correlates to the fibrils transformation, especially to the diameter of the nascent micro-fibrils. The interphase plays a major role on the fragmentation of crystal due to inducing stress concentration in the crystal lamella surface. D_f is proved to be more related to the initial microstructure than the drawing condition. D_f also presents drawing temperature dependency. The diameter increases with increasing drawing temperature. This is mainly ascribed to the relaxation of crystal and stress transmitters which lead to the homogeneously distribution of the local stress in crystal lamella.

The molecule topology directly influences the morphology of microfibrils. The higher co-unit concentration, the higher tie molecule content and the smaller distance of neighbor tie molecule and thus the smaller diameter. The long period of micro-fibrils is deduced with increasing molecular defects from co-unit via the melt-crystallization mechanism.

2.2 Fibrillar transformation of polypropylene

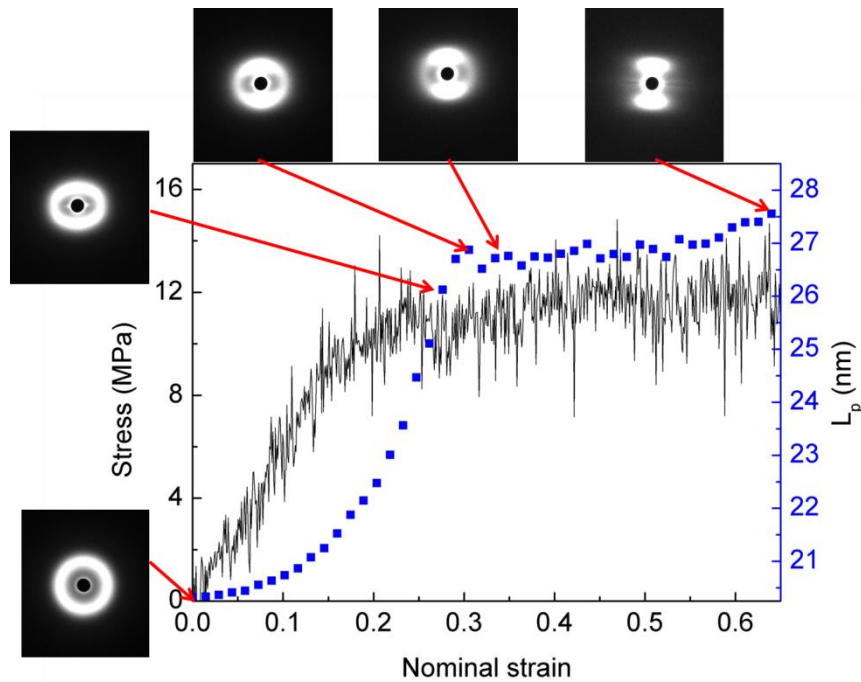


Figure 2.1. Stress-strain curve of PP C annealed sample in drawing temperature 120 °C.

Under stretch, similar to the polyethylene, the SAXS patterns of the polypropylene transfer from isotropic to highly anisotropic patterns with two streak-like scattering patterns along the elongation of samples (see Figure 2.1). At $\epsilon=0.3$, the SAXS pattern starts to present two streak-like scattering. The fibrils lamella does not completely oriented at this point as shown in the SAXS pattern with weak scattering in equator region.

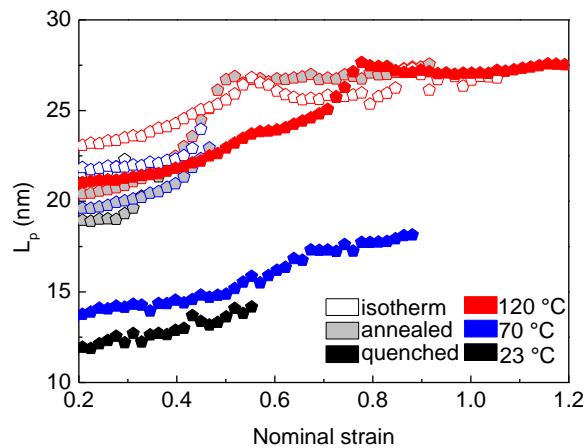


Figure 2.2. Long period variation of PP C measured with meridian scattering after yield in different drawing temperature during the deformation

The scattering of cavitation could cover the scattering of fibrils structure which prevents the analysis of the fibrils structure. The experiment has to be stopped when the cavitation appears owing the strong scattering intensity which exceeds the maximum value of detector. Finally, few samples could analysis the long period of micro-fibrils by in-situ SAXS.

Figure 2.2 shows the long period (L_p) of PP C measured with meridian scattering. L_p increases with increasing deformation. At 120 °C, the long period of fibrils structure is higher than the initial lamella stacks. This behavior is contrast with the results of polyethylene that the new

generated lamella stacks have smaller long period than initial materials. For polypropylene, no evidence to prove the lamella experiences melt and recrystallization mechanism. The increasing of the long period in polypropylene after fibrillar transformation may be owing to the stretch of the fragmented lamellae. It is worth to note that PP C in drawing temperature 120 °C present the same long period of micro-fibrils for samples with different thermal treatment. This means the long period of micro-fibrils only correlates to the drawing condition which is similar to the previous studies.

2.3 Influence of temperature

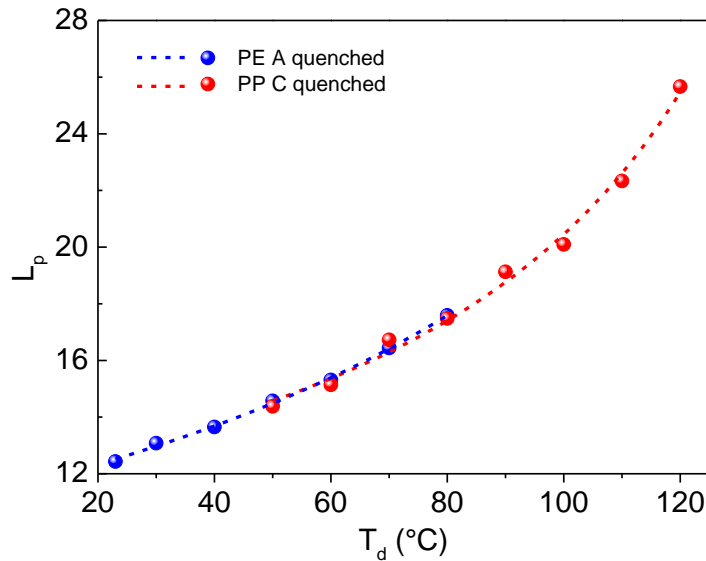


Figure 2.3. Long period of quenched PE A and PP C stretched at strain 1.3 at different drawing temperature.

To verify the influence of the drawing temperature, the quenched PE A quenched and PP C was drawn in different temperatures and the microstructure is measured by ex situ SAXS. The long period of the micro-fibrils L_{pf} was measured for the series samples with the same draw ratio (see Figure 2.3). According to the study of Peterlin, the relation between L_{pf} and drawing temperature could be described as [117]:

$$L_{pf} = A + \frac{B}{T_m - T_d}$$

where T_m is the melting temperature and T_d is the drawing temperature, A and B are constants.

The quenched sample could be well fitted with this formula (see Figure 2.3). This could be due to the recrystallization during the formation of the micro-fibrils structure. Similar to the crystallization process from the melt, L_{pf} strongly depends on the supercooling ($\Delta T = T_m - T_d$).

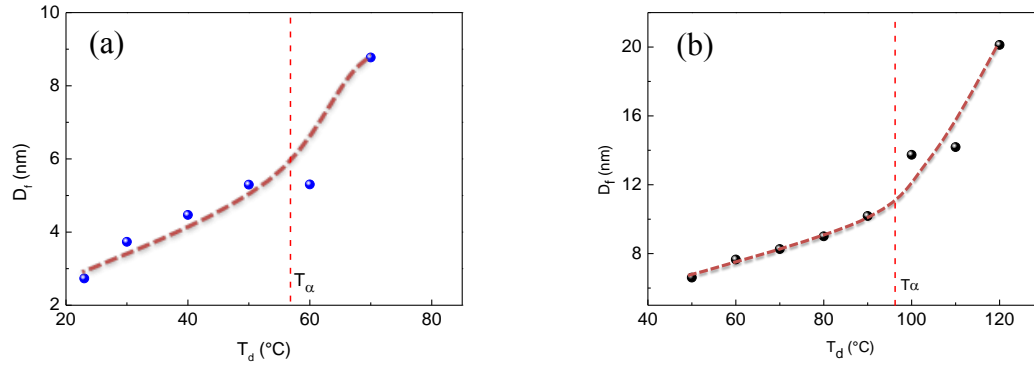


Figure 2.4. Diameter of micro-fibrils in function of temperature. Diameter measured at strain 0.3. (a) quenched PE A; (b) quenched PP C.

Regarding the influence of the drawing temperature on the diameters of the micro-fibrils D_f , both PE and PP show an augment of the D_f with elevating of the drawing temperature (see Figure 6.5). Below α transition temperature T_α , D_f linearly increases with elevating temperature. Above T_α , D_f presents higher increase rate with increasing drawing temperature. With the elevating of drawing temperature, taut tie molecule relaxed due to the activation of chain mobility in crystal and fragmentation is prevented which leads increasing of D_f .

If the recrystallization happens during the fibrillar transformation process, the crystalline thickness L_{cf} depends on the drawing temperature similar to the crystallization from the melt. T_d is plotted against $1/L_c$ of quenched PE A and PP C in Figure 2.5. Linear relation between T_d and $1/L_c$ is observed as expected. This result provide an indirectly evidence to support that the melt and recrystallization occurred in the fibrillar transformation process of PE and PP.

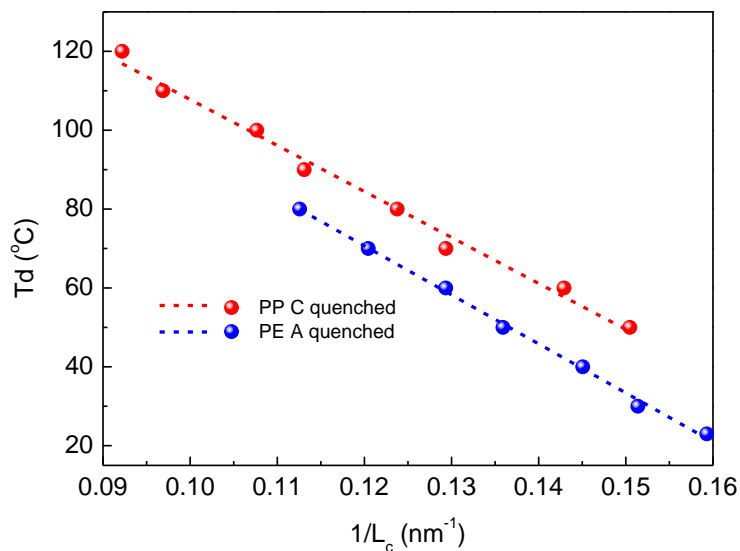


Figure 2.5. T_d in function of $1/L_c$ of quenched PE A and PP C. L_c was measured by DSC and SAXS at strain 1.3.

2.4 Conclusion

The deformation at large strains of PE and PP involve spherulite converts into an oriented fibrous structure known as fibrillar transformation. The fibrillar transformation in semi-crystalline polymers involves the fragmentation-rearrangement and melting-recrystallization mechanisms.

The long periods L_{pf} of both polyethylene and polypropylene depends on the drawing temperature. However, L_{pf} of PE is smaller while PP is higher than the initial long period L_p . Both L_{pf} of PE and PP present discontinuous variation which provides an indirectly evidence to melting-recrystallization mechanism of the fibrillar transformation.

Micro-fibrils diameters (D_f) provide evidence that the crystal-amorphous phase boundary directly correlates to the fibrils transformation, especially to the diameter of the nascent micro-fibrils. The interphase plays a major role on the fragmentation of crystal due to inducing stress concentration in the crystal lamella surface. D_f is proved to be more related to the initial microstructure than the draw condition. D_f also presents draw temperature dependency. Both PE and PP show an increase of the D_f with elevating of the drawing temperature. Above T_a , D_f presents faster increase rate with increasing draw temperature. At this temperature, the tie molecule is relaxed due to the movement of chain in crystal and prevented the fragmentation of crystal which could lead increasing of D_f .

3 Orientation of crystalline lamella

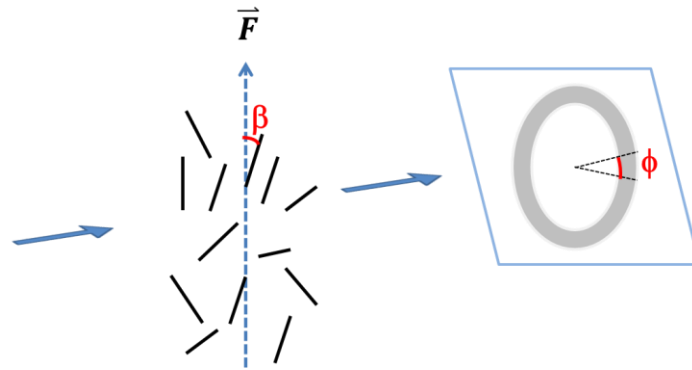


Figure 3.1. Schematization of X-ray scattered intensity for a system with a preferential orientation with respect to the direction of the stretch force \vec{F} . Lamellae are represented by the small rods.

The orientation of lamellae with respect to the stretch direction \vec{F} is described by the angle β (Figure 3.1). This angle β can be related to the azimuthal angle ϕ by the relation: $\beta = \frac{\pi}{2} - \phi$. The symmetry is uniaxial around \vec{F} . The average degree of orientation of chain segments is described by the orientation order parameter (second order Legendre polynomial)[169]:

$$\langle P_2 \cos(\beta) \rangle = \left\langle \frac{3 \cos^2 \beta - 1}{2} \right\rangle \quad (1)$$

The orientation order parameter is calculated as:[170]

$$\langle P_2 \cos(\beta) \rangle = \frac{\int_0^{\pi/2} P_2(\phi) I(\phi) \sin(\phi) d\phi}{\int_0^{\pi/2} I(\phi) \sin(\phi) d\phi} \quad (2)$$

3.1 Orientation of PE lamellae

The scattering of lamella structure can be detected by SAXS. Figure 3.1 shows the scattering intensity of quenched PE A in function of azimuth angle at different strains at draw temperature 75°C. The inset pictures are the corresponded 2D SAXS patterns at each draw ratio. The one dimensional intensity curve is integrated in a cycle within $0.1 < q < 0.5 \text{ nm}^{-1}$.

As shown in Figure 3.2, at azimuthal angle $\phi = 0^\circ$, the intensity decreases with elongation of samples indicating the lamellae gradually orient to the tensile direction. A transformation from two maxima to four maxima with increasing deformation appears which is due to the orientation of lamellae. The SAXS pattern obtained after the yield point (strain > 0.16) shows the beginning of splitting of each meridian reflection into two off-meridional reflections (four-point pattern, see scattering pattern at $\epsilon=0.16$) indicating the chevron-like structures formed after yield. As the tensile deformation proceeds, the off-meridional reflections rotate toward the equatorial axis (see scattering pattern at $\epsilon=0.56$).

The orientation parameter $\langle P_2 \cos(\beta) \rangle$ was calculated with Equation (1) from azimuthal intensity curves. Figure 3.3 plots $\langle P_2 \cos(\beta) \rangle$ as a function of nominal strain for quenched PEs. Only quenched samples are studied because the cavitation does not appear in these samples. At 50°C, $\langle P_2 \cos(\beta) \rangle$ slightly decreases with elongation of samples before yield ($\epsilon < 0.16$), suggesting the increase of β . This means the lamellae orient towards normal of the tensile direction before yield.

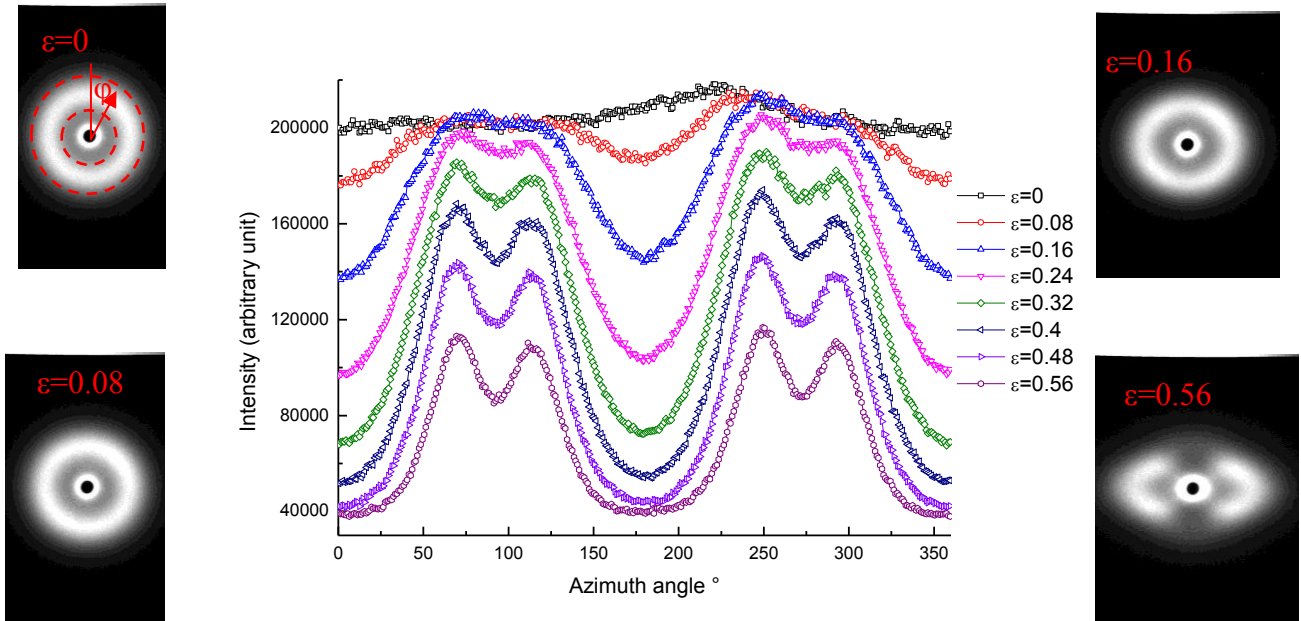


Figure 3.2. Scattering intensity of quenched PE A in function of azimuth angle with different strain at drawing temperature 75°C. Tensile direction is in vertical.

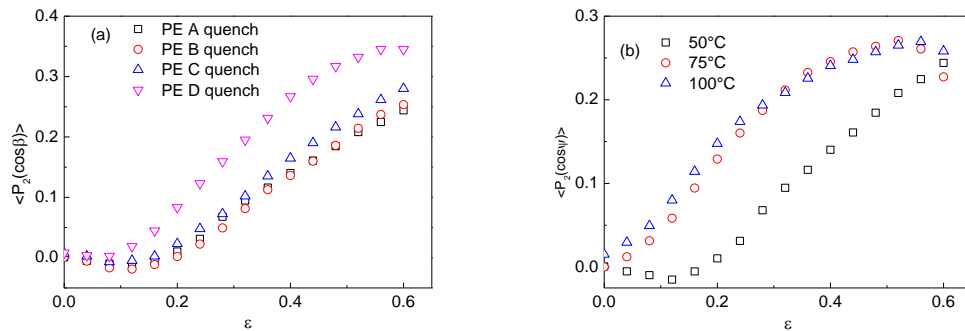


Figure 3.3. (a) $\langle P_2 \cos(\beta) \rangle$ of different quenched samples in function of the nominal strain at drawing temperature 50 °C; (b) $\langle P_2 \cos(\beta) \rangle$ of PE A quenched at different drawing temperatures in function of nominal strain.

After yield, the value of $\langle P_2 \cos(\beta) \rangle$ presents an increasing with the elongation suggesting the lamellae orient to the tensile direction. This could be due to the chevron-like structures formed after yield.

Regarding the influence of drawing temperature, $\langle P_2 \cos(\beta) \rangle$ value shows monotonic increase before yield above draw temperature 75 °C. This suggests the lamellae orient to the tensile direction starting at the beginning of the stretch. Indeed, the tensile temperature is above the α transformation temperature and the chains mobility in crystal is activated promoting the shear of crystal and formation of chevron-like structure.

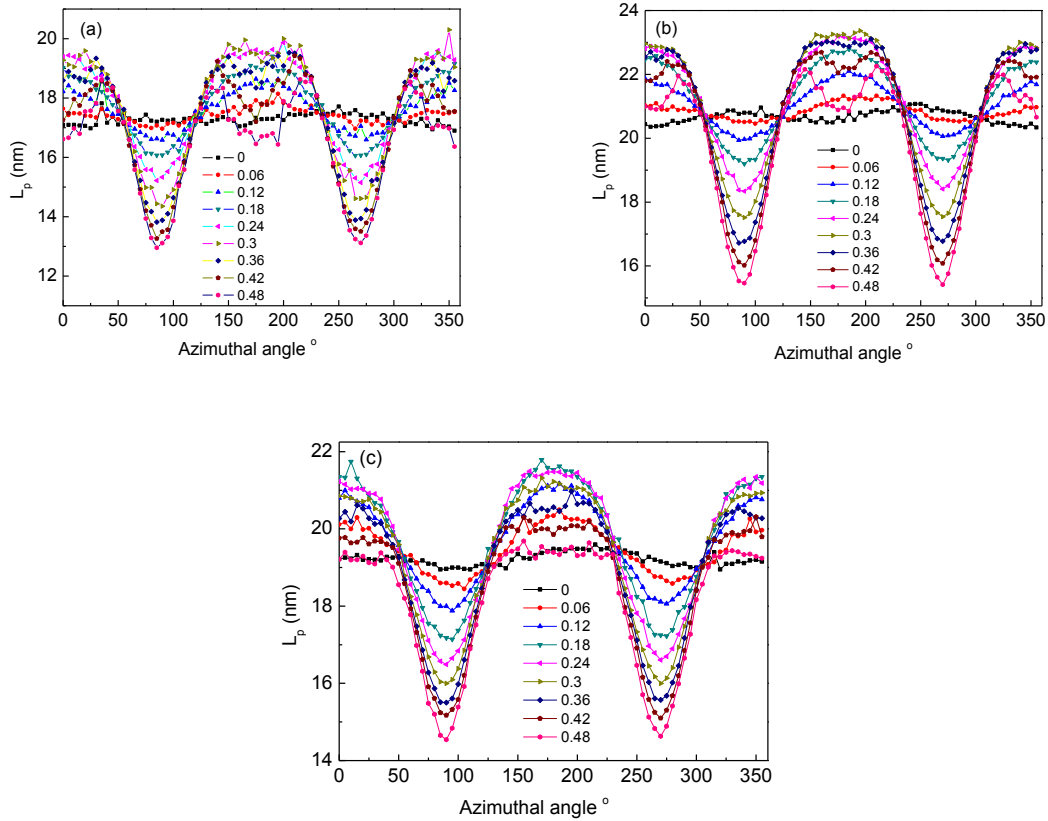


Figure 3.4. L_p of PE A quenched at various draw ratio in function of azimuth angle in different drawing temperature. (a) 50 °C; (b) 75 °C; (c) 100 °C. Tensile direction is in parallel.

For each azimuth angle, the long period L_p was estimated with the Lorenz correction method mentioned in Chapter 2. To get a curve with good resolution, each 5° of azimuth angle is chosen as integration area. Figure 3.4 shows L_p in function of azimuth angle for different nominal strain at draw temperature 50 °C, 75 °C and 100 °C respectively. At azimuth angle $\varphi=0^\circ$, L_p increases with the elongation of the samples until a maximum value. L_p decreases at $\varphi=90^\circ$ whereas remains a constant at $\varphi=55^\circ$ with elongation of the sample. This means that the crystal show different deformation behavior in the different regions of the spherulites. The scattering pattern is symmetry, so here we only discuss the scattering from 0° to 90°.

The scattering at $\varphi=90^\circ$ of the SAXS patterns comes from the lamellae in polar regions of the spherulite. During the tensile test, the crystal lamellae move close due to the lateral force. After yield the lamellae in polar are reconstructed due to the fragment of the lamellae.

The scattering at $\varphi=0^\circ$ is from the scattering of the lamellae in equatorial regions of spherulites. The lamellae are separated to each other due to the stretch. L_p increases with increasing deformation. After yield, lamellae fragment and L_p is reconstructed with smaller L_p .

L_p at $\varphi=55^\circ$ remains a constant suggesting that the lamella in region with 35° angle respect to tensile direction is purely shearing deformed.

To conclusion, three kinds of typically deformation types for the lamellae are observed: separation, compression (L_p decrease) and purely shearing. Before yield, the lamellae orient towards normal of the tensile direction below T_α whereas orient to tensile direction above T_α . After yield, chevron-like structure formed and lamellae orient to tensile direction.

3.2 Deformation of PP lamellae

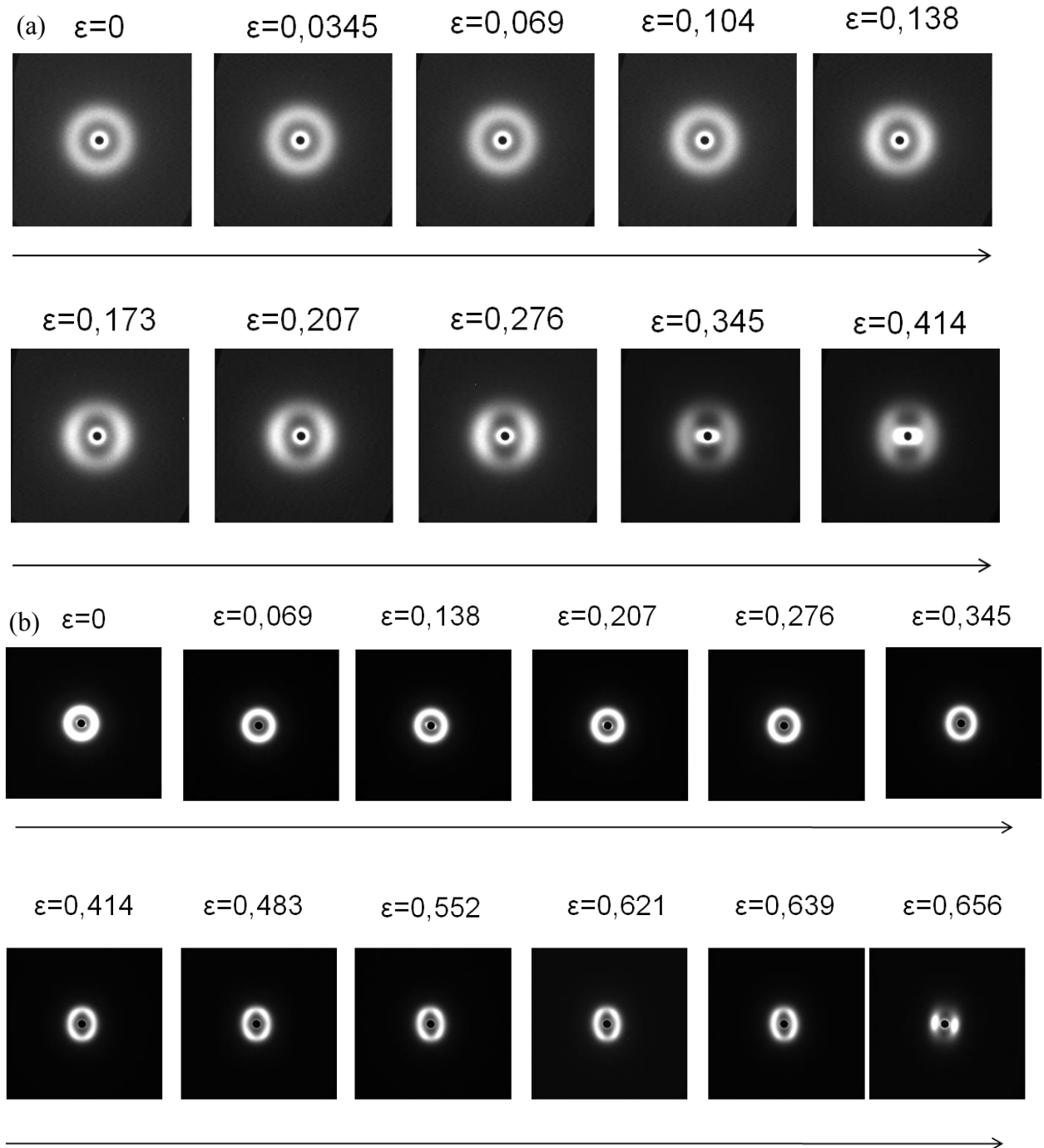


Figure 3.5. In situ SAXS patterns obtained simultaneously stress-strain trace of quenched PP C at drawing temperature (a) 23°C and (b) 120 °C. Tensile direction is in parallel.

In situ SAXS was used to study the evolution of lamellas structure during the uniaxial deformation of polypropylene (see Figure 3.5). The scattering patterns are isotropic without deformation, and then change to an ellipse form. After yield point, it presents two or four symmetric scattering dashes which depend on drawing temperature. As shown in Figure 3.5, before yield, the scattering patterns turn to ellipse form which presents higher meridional intensity at drawing temperatures 23°C and 120°C. After yield, different scattering evolutions appear. At 23 °C, the ellipse transforms to the pattern with symmetrically two dashes with highest intensity located in meridian (see Figure 3.4a $\epsilon=0.173$). At 120 °C, the ellipse form transforms to the patterns with symmetrically four dashes which the highest intensity located in region about 45 °

respect to the meridian (see Figure 3.5b $\epsilon=0.414$). And then, the four dashes merged to two dashes similar to the patterns in Figure 3.5a. Four dashes pattern indicates chevron-like structure formed at 120 °C. But at 23 °C, lamellae directly oriented in direction of tensile force after yield. This difference indicates that the crystal lamellae orientation manner is different at these two temperatures. This difference means more regular structures form at higher drawing temperature. This could be ascribed to the mobility of chain crystal above transition temperature which promote plastic deformation and orientation of lamellae. On the other hand, at 23 °C, the cavities appear beyond yield (strong scattering around the center, see Figure 3.5a $\epsilon=0.345$) whereas the scattering of cavities disappears at drawing temperature 120°C.

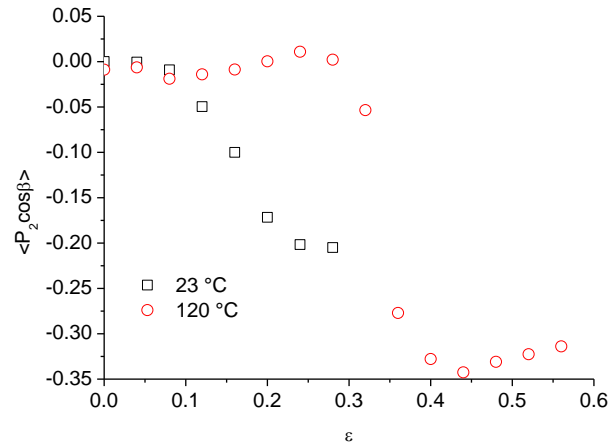


Figure 3.6. Orientation factor of quenched PP C in function of deformation at drawing temperature 23 °C and 120 °C. Tensile direction is in parallel.

The orientation factor was computed from the azimuth curves (see Figure 3.6). $\langle P_2 \cos(\beta) \rangle$ slightly decreases with increase of elongation before yield, indicating the orientation of the crystal lamellae in the normal of tensile direction. $\langle P_2 \cos(\beta) \rangle$ strongly decreases after yield at 23 °C indicating the orientation at normal of tensile direction. In contrast, $\langle P_2 \cos(\beta) \rangle$ firstly increases slightly and then strongly decreases after yield at 120 °C. The increase of $\langle P_2 \cos(\beta) \rangle$ is due to the formation of chevron-like structure which orients in the tensile direction. This could be attributed to the fragmentation and reconstruction of crystal lamellae are promoted above T_α owing to the activation of chain mobility in crystal.

3.3 Comparison of lamella deformation between PP and PE

For the lamella evolution of PE and PP, the SAXS pattern obtained both shows evolution from isotropic strike-like patterns indicating similar lamellae deformation behavior of PE and PP. However, for PP, this transformation of SAXS patterns only presents at high temperature.

Reference

- [1] G.H. Michler, Semicrystalline Polymers, Electron Microscopy of Polymers, Springer Berlin Heidelberg, 2008, pp. 295-327.
- [2] B.A.G. Schrauwen, R.P.M. Janssen, L.E. Govaert, H.E.H. Meijer, Intrinsic deformation behavior of semicrystalline polymers, *Macromolecules* 37 (2004) 6069-6078.
- [3] M. Okura, The Control of Structural Morphology of Polyethylene by Shear-induced Crystallization, University of Leeds, 2010.
- [4] C.W. Bunn, The crystal structure of long-chain normal paraffin hydrocarbons. The "shape" of the >CH₂ group, *Transactions of the Faraday Society* 35 (1939) 482-491.
- [5] D. Meer, structure property relationships in isotactic polypropylene, University of Twente, 2003.
- [6] A. Peacock, Handbook of polyethylene: structures: properties, and applications, CRC Press, 2000.
- [7] H. Zhou, structure properties relationships model studies on melt extruded uniaxially oriented high density polyethylene films, Virginia Polytechnic Institute and State University, 1997.
- [8] S.J. Organ, J.K. Hobbs, M.J. Miles, Reorganization and melting of polyethylene single crystals: Complementary TEM, DSC, and real-time AFM studies, *Macromolecules* 37 (2004) 4562-4572.
- [9] A. Keller, S. Sawada, On the interior morphology of bulk polyethylene, *Die Makromolekulare Chemie* 74 (1964) 190-221.
- [10] C.Y. Li, D. Yan, S.Z.D. Cheng, F. Bai, T. He, L.-C. Chien, F.W. Harris, B. Lotz, Double-Twisted Helical Lamellar Crystals in a Synthetic Main-Chain Chiral Polyester Similar to Biological Polymers, *Macromolecules* 32 (1998) 524-527.
- [11] J. Xu, B.-H. Guo, Z.-M. Zhang, J.-J. Zhou, Y. Jiang, S. Yan, L. Li, Q. Wu, G.-Q. Chen, J.M. Schultz, Direct AFM Observation of Crystal Twisting and Organization in Banded Spherulites of Chiral Poly(3-hydroxybutyrate-co-3-hydroxyhexanoate), *Macromolecules* 37 (2004) 4118-4123.
- [12] Y. Fujiwara, The superstructure of melt-crystallized polyethylene. I. Screwlike orientation of unit cell in polyethylene spherulites with periodic extinction rings, *Journal of applied polymer science* 4 (1960) 10-15.
- [13] H.D. Keith, F.J. Padden Jr, Twisting orientation and the role of transient states in polymer crystallization, *Polymer* 25 (1984) 28-42.
- [14] K. Okano, Note on the Lamellar Twist in Polymer Spherulites, *Japanese Journal of Applied Physics* 3 (1964) 351.
- [15] J. Schultz, D. Kinloch, Transverse screw dislocations: A source of twist in crystalline polymer ribbons, *Polymer* 10 (1969) 271-278.
- [16] B. Lotz, S.Z. Cheng, A critical assessment of unbalanced surface stresses as the mechanical origin of twisting and scrolling of polymer crystals, *Polymer* 46 (2005) 577-610.
- [17] T. Ikehara, T. Kataoka, Relation between the helical twist and S-shaped cross section of the lamellar crystals of polyethylene, *Sci. Rep.* 3 (2013).
- [18] S. HUMBERT, Influence de la topologie moléculaire et de la microstructure sur les propriétés mécaniques des Polyéthylènes, Laboratoire de recherche: MATEIS, INSA de Lyon, 2009.
- [19] J.C. Halpin, J.L. Kardos, The Halpin-Tsai equations: a review, *Polymer Engineering & Science* 16 (1976) 344-352.
- [20] J.C. Halpin, J.L. Kardos, Moduli of crystalline polymers employing composite theory, *Journal of Applied Physics* 43 (1972) 2235-2241.

- [21] S. Hosoda, Y. Nozue, Y. Kawashima, K. Suita, S. Seno, T. Nagamatsu, K.B. Wagener, B. Inci, F. Zuluaga, G. Rojas, Effect of the Sequence Length Distribution on the Lamellar Crystal Thickness and Thickness Distribution of Polyethylene: Perfectly Equisquential ADMET Polyethylene vs Ethylene/ α -Olefin Copolymer, *Macromolecules* 44 (2010) 313-319.
- [22] R.K. Eby, A copolymer with lamellar morphology, *J. Res. Nat. Bur. Std.(US) A* 68 (1964) 269-272.
- [23] J. Rault, E. Robelin, Crystallization of quenched polyethylene. Part III: Mixtures of fractions, *Journal de Physique* 43 (1982) 1437-1452.
- [24] P. Calvert, Polymer crystallization from the melt at large undercoolings, *Journal of Polymer Science: Polymer Physics Edition* 17 (1979) 1341-1354.
- [25] J. Yang, B.J. McCoy, G. Madras, Temperature effects for isothermal polymer crystallization kinetics, *The Journal of chemical physics* 122 (2005) 244905.
- [26] J. Martinez-Salazar, P. Barham, A. Keller, The identification of the initial lamellar thickness of polyethylene crystals grown from the melt using synchrotron X-radiation, *Journal of materials science* 20 (1985) 1616-1624.
- [27] E. Fischer, Effect of annealing and temperature on the morphological structure of polymers, *Pure and applied chemistry* 31 (1972) 113-132.
- [28] G.S. Yeh, R. Hosemann, J. Loboda-Čačković, H. Čačković, Annealing effects of polymers and their underlying molecular mechanisms, *Polymer* 17 (1976) 309-318.
- [29] W. Statton, Coherence and deformation of lamellar crystals after annealing, *Journal of Applied Physics* 38 (1967) 4149-4151.
- [30] S. Rastogi, A. Spoelstra, J. Goossens, P. Lemstra, Chain mobility in polymer systems: on the borderline between solid and melt. 1. Lamellar doubling during annealing of polyethylene, *Macromolecules* 30 (1997) 7880-7889.
- [31] J.D. Hoffman, J.I. Lauritzen, Jr., E. Passaglia, G.S. Ross, L.J. Frolen, J.J. Weeks, Kinetics of polymer crystallization from solution and the melt, *Kolloid-Zeitschrift und Zeitschrift für Polymere* 231 (1969) 564-592.
- [32] H.-G. Kilian, Phänomenologische „Thermodynamik“ des Schmelzens von Polymeren, *Kolloid-Zeitschrift und Zeitschrift für Polymere* 231 (1969) 534-564.
- [33] J. Hoffman, G.T. Davis, J. Lauritzen, Jr., The Rate of Crystallization of Linear Polymers with Chain Folding, in: N.B. Hannay (Ed.), *Treatise on Solid State Chemistry*, Springer US, 1976, pp. 497-614.
- [34] A. Alizadeh, L. Richardson, J. Xu, S. McCartney, H. Marand, Y. Cheung, S. Chum, Influence of structural and topological constraints on the crystallization and melting behavior of polymers. 1. Ethylene/1-octene copolymers, *Macromolecules* 32 (1999) 6221-6235.
- [35] A.M. Jonas, T.P. Russell, D.Y. Yoon, Synchrotron X-ray scattering studies of crystallization of poly (ether-ether-ketone) from the glass and structural changes during subsequent heating-cooling processes, *Macromolecules* 28 (1995) 8491-8503.
- [36] M. McCready, J. Schultz, J. Lin, R. Hendricks, Effect of crystallization time on the properties of melt-crystallized linear polyethylene, *Journal of Polymer Science: Polymer Physics Edition* 17 (1979) 725-740.
- [37] J. Petermann, H. Gleiter, Elektronenmikroskopische Beobachtung des Dickenwachstums von Lamellen in teilkristallinen Polymeren (1), *Colloid and Polymer Science* 254 (1976) 247-248.
- [38] E.W. Fischer, G.F. Schmidt, Long Periods in Drawn Polyethylene, *Angewandte Chemie International Edition in English* 1 (1962) 488-499.
- [39] S. Kavesh, J. Schultz, Lamellar and interlamellar structure in melt-crystallized polyethylene. II. Lamellar spacing, interlamellar thickness, interlamellar density, and

- stacking disorder, *Journal of Polymer Science Part A-2: Polymer Physics* 9 (1971) 85-114.
- [40] L. Mandelkern, J. Fatou, R. Denison, J. Justin, A calorimetric study of the fusion of molecular weight fractions of linear polyethylene (1), *Journal of Polymer Science Part B: Polymer Letters* 3 (1965) 803-807.
- [41] R. Seguela, Critical review of the molecular topology of semicrystalline polymers: The origin and assessment of intercrystalline tie molecules and chain entanglements, *Journal of Polymer Science Part B: Polymer Physics* 43 (2005) 1729-1748.
- [42] R. Seguela, F. Rietsch, Tensile drawing behaviour of ethylene/ α -olefin copolymers: influence of the co-unit concentration, *Polymer* 27 (1986) 703-708.
- [43] R. Seguela, F. Rietsch, Molecular topology in ethylene copolymers studied by means of mechanical testing, *Journal of materials science* 23 (1988) 415-421.
- [44] Y.-L. Huang, N. Brown, The effect of molecular weight on slow crack growth in linear polyethylene homopolymers, *Journal of materials science* 23 (1988) 3648-3655.
- [45] Y.L. Huang, N. Brown, Dependence of slow crack growth in polyethylene on butyl branch density: morphology and theory, *Journal of Polymer Science Part B: Polymer Physics* 29 (1991) 129-137.
- [46] J. Yeh, J. Runt, Fatigue crack propagation in high-density polyethylene, *Journal of Polymer Science Part B: Polymer Physics* 29 (1991) 371-388.
- [47] R. Séguéla, On the Natural Draw Ratio of Semi-Crystalline Polymers: Review of the Mechanical, Physical and Molecular Aspects, *Macromolecular Materials and Engineering* 292 (2007) 235-244.
- [48] H. Keith, F. Padden, R. Vadimsky, Intercrystalline links in polyethylene crystallized from the melt, *Journal of Polymer Science Part A-2: Polymer Physics* 4 (1966) 267-281.
- [49] P.J. Flory, Molecular morphology in semicrystalline polymers, *Nature* 272 (1978) 226-229.
- [50] R.H. Boyd, Relaxation processes in crystalline polymers: molecular interpretation - a review, *Polymer* 26 (1985) 1123-1133.
- [51] P.J. Flory, D.Y. Yoon, K.A. Dill, The interphase in lamellar semicrystalline polymers, *Macromolecules* 17 (1984) 862-868.
- [52] L. Mandelkern, R. Alamo, M. Kennedy, The interphase thickness of linear polyethylene, *Macromolecules* 23 (1990) 4721-4723.
- [53] A. Singhal, L.J. Fina, Dynamic two-dimensional infra-red spectroscopy of the crystal—amorphous interphase region in low-density polyethylene, *Polymer* 37 (1996) 2335-2343.
- [54] S.K. Kumar, D.Y. Yoon, Lattice model for crystal-amorphous interphases in lamellar semicrystalline polymers: effects of tight-fold energy and chain incidence density, *Macromolecules* 22 (1989) 3458-3465.
- [55] S. Bensason, J. Minick, A. Moet, S. Chum, A. Hiltner, E. Baer, Classification of homogeneous ethylene-octene copolymers based on comonomer content, *Journal of Polymer Science Part B: Polymer Physics* 34 (1996) 1301-1315.
- [56] P. Barham, A. Keller, The problem of thermal expansion in polyethylene spherulites, *Journal of materials science* 12 (1977) 2141-2148.
- [57] D.C. Bassett, *Developments in crystalline polymers*, Springer, 1982.
- [58] P.J. Barham, *Crystallization and Morphology of Semicrystalline Polymers*, *Materials Science and Technology*, Wiley-VCH Verlag GmbH & Co. KGaA, 2006.
- [59] J. Schultz, Microstructural aspects of failure in semicrystalline polymers, *Polymer Engineering & Science* 24 (1984) 770-785.
- [60] M. Matsuo, C. Sawatari, Elastic modulus of polyethylene in the crystal chain direction as measured by x-ray diffraction, *Macromolecules* 19 (1986) 2036-2040.

- [61] D.J. Lacks, G.C. Rutledge, Simulation of the temperature dependence of mechanical properties of polyethylene, *The journal of physical chemistry* 98 (1994) 1222-1231.
- [62] P.J. Flory, *Principles of polymer chemistry*, Cornell University Press, 1953.
- [63] F. Bédoui, J. Diani, G. Régner, Micromechanical modeling of elastic properties in polyolefins, *Polymer* 45 (2004) 2433-2442.
- [64] R.H. Boyd, The modulus of the amorphous component in polyethylenes, *Polymer Engineering & Science* 19 (1979) 1010-1016.
- [65] K.H. Nitta, A. Tanaka, Dynamic mechanical properties of metallocene catalyzed linear polyethylenes, *Polymer* 42 (2001) 1219-1226.
- [66] K.M. Sinnott, Mechanical relaxations in single crystals of polyethylene, *Journal of Applied Physics* 37 (1966) 3385-3400.
- [67] Y.P. Khanna, E.A. Turi, T.J. Taylor, V.V. Vickroy, R.F. Abbott, Dynamic mechanical relaxations in polyethylene, *Macromolecules* 18 (1985) 1302-1309.
- [68] R. Popli, M. Glotin, L. Mandelkern, R.S. Benson, Dynamic mechanical studies of α and β relaxations of polyethylenes, *Journal of polymer science: polymer physics edition* 22 (1984) 407-448.
- [69] D.H. Reneker, Point dislocations in crystals of high polymer molecules, *Journal of Polymer Science* 59 (1962) S39-S42.
- [70] L. Lin, A. Argon, Structure and plastic deformation of polyethylene, *Journal of materials science* 29 (1994) 294-323.
- [71] A. Peterlin, Molecular model of drawing polyethylene and polypropylene, *Journal of Materials Science* 6 (1971) 490-508.
- [72] P. Bowden, R. Young, Deformation mechanisms in crystalline polymers, *Journal of materials science* 9 (1974) 2034-2051.
- [73] D.P. Pope, A. Keller, Deformation of oriented polyethylene, *Journal of Polymer Science: Polymer Physics Edition* 13 (1975) 533-566.
- [74] R. Young, P. Bowden, J. Ritchie, J. Rider, Deformation mechanisms in oriented high-density polyethylene, *Journal of materials science* 8 (1973) 23-36.
- [75] J. Petermann, J. Schultz, Lamellar separation during the deformation of high-density polyethylene, *Journal of materials science* 13 (1978) 50-54.
- [76] T. Tagawa, K. Ogura, Piled-lamellae structure in polyethylene film and its deformation, *Journal of Polymer Science: Polymer Physics Edition* 18 (1980) 971-979.
- [77] M. Kennedy, A. Peacock, L. Mandelkern, Tensile properties of crystalline polymers: linear polyethylene, *Macromolecules* 27 (1994) 5297-5310.
- [78] G. Capaccio, T.J. Chapman, I.M. Ward, Preparation of ultra-high modulus linear polyethylenes: effect of initial crystallization conditions, *Polymer* 16 (1975) 469.
- [79] K. Ushui, Y. Kondo, K. Hatada, S. Gima, Effect of tie molecules on the craze strength of polypropylene, *Polymer* 37 (1996) 5375-5379.
- [80] M. Takayanagi, K. Nitta, Application of a tie molecule model to the postyielding deformation of crystalline polymers, *Macromolecular theory and simulations* 6 (1997) 181-195.
- [81] B. Crist, C.J. Fisher, P.R. Howard, Mechanical properties of model polyethylenes: tensile elastic modulus and yield stress, *Macromolecules* 22 (1989) 1709-1718.
- [82] A. Peterlin, Plastic deformation of crystalline polymers, *Polymer Engineering & Science* 17 (1977) 183-193.
- [83] P.H. Geil, Polymer deformation. II. Drawing of polyethylene single crystals, *Journal of Polymer Science Part A: General Papers* 2 (1964) 3813-3833.
- [84] L.G. Shadrake, F. Guiu, Dislocations in polyethylene crystals: line energies and deformation modes, *Philosophical Magazine* 34 (1976) 565-581.

- [85] P.B. Bowden, S. Raha, A molecular model for yield and flow in amorphous glassy polymers making use of a dislocation analogue, *Philosophical magazine* 29 (1974) 149-166.
- [86] R.J. Young, A dislocation model for yield in polyethylene, *Philosophical magazine* 30 (1974) 85-94.
- [87] N.W. Brooks, M. Ghazali, R.A. Duckett, A.P. Unwin, I.M. Ward, Effects of morphology on the yield stress of polyethylene, *Polymer* 40 (1999) 821-825.
- [88] I.M. Ward, J. Sweeney, *Mechanical properties of solid polymers*, John Wiley & Sons, 2012.
- [89] A.N. Gent, S. Madan, Plastic yielding of partially crystalline polymers, *Journal of Polymer Science Part B: Polymer Physics* 27 (1989) 1529-1542.
- [90] M.F. Butler, A.M. Donald, W. Bras, G.R. Mant, G.E. Derbyshire, A.J. Ryan, A real-time simultaneous small-and wide-angle X-ray scattering study of in-situ deformation of isotropic polyethylene, *Macromolecules* 28 (1995) 6383-6393.
- [91] M.F. Butler, A.M. Donald, A.J. Ryan, Time resolved simultaneous small-and wide-angle X-ray scattering during polyethylene deformation 3. Compression of polyethylene, *Polymer* 39 (1998) 781-792.
- [92] M.F. Butler, A.M. Donald, A.J. Ryan, Time resolved simultaneous small-and wide-angle X-ray scattering during polyethylene deformation—II. Cold drawing of linear polyethylene, *Polymer* 39 (1998) 39-52.
- [93] M.F. Butler, A.M. Donald, A.J. Ryan, Time resolved simultaneous small-and wide-angle X-ray scattering during polyethylene deformation: 1. Cold drawing of ethylene- α -olefin copolymers, *Polymer* 38 (1997) 5521-5538.
- [94] H. Kiho, A. Peterlin, P. Geil, Polymer deformation. VIII. Stability of the monoclinic phase of polyethylene, *Journal of Polymer Science Part B: Polymer Letters* 3 (1965) 157-160.
- [95] Y. Kikuchi, S. Krimm, Infrared studies of the role of monoclinic structure in the deformation of polyethylene, *Journal of Macromolecular Science, Part B: Physics* 4 (1970) 461-472.
- [96] R. Young, P. Bowden, Twinning and martensitic transformations in oriented high-density polyethylene, *Philosophical Magazine* 29 (1974) 1061-1073.
- [97] P. Allan, M. Bevis, Deformation processes in thin melt-cast films of high-density polyethylene: I. Experimental methods and deformation processes in the equatorial regions of spherulites, *Philosophical Magazine* 35 (1977) 405-430.
- [98] P. Allan, M. Bevis, Deformation processes in thin melt-cast films of high-density polyethylene† II. Deformation processes in the non-equatorial regions of spherulites, *Philosophical Magazine A* 41 (1980) 555-572.
- [99] P. Allan, E. Crellin, M. Bevis, Stress-induced twinning and phase transformations in polyethylene single crystals, *Philosophical Magazine* 27 (1973) 127-145.
- [100] M.F. Butler, A.M. Donald, A real-time simultaneous small-and wide-angle X-ray scattering study of in situ polyethylene deformation at elevated temperatures, *Macromolecules* 31 (1998) 6234-6249.
- [101] A. Pawlak, A. Galeski, A. Rozanski, Cavitation during deformation of semicrystalline polymers, *Progress in Polymer Science* 39 (2014) 921-958.
- [102] N.E. Zafeiropoulos, R.J. Davies, S.V. Roth, M. Burghammer, K. Schneider, C. Riekel, M. Stamm, Microfocus X-Ray Scattering Scanning Microscopy for Polymer Applications, *Macromolecular rapid communications* 26 (2005) 1547-1551.
- [103] A. Lazzeri, Y. Thio, R. Cohen, Volume strain measurements on CaCO₃/polypropylene particulate composites: the effect of particle size, *Journal of applied polymer science* 91 (2004) 925-935.

- [104] A. Pawlak, Cavitation during tensile deformation of high-density polyethylene, *Polymer* 48 (2007) 1397-1409.
- [105] A. Pawlak, A. Galeski, Plastic deformation of crystalline polymers: the role of cavitation and crystal plasticity, *Macromolecules* 38 (2005) 9688-9697.
- [106] N. Stribeck, *X-ray scattering of soft matter*, Springer, 2007.
- [107] B. Chu, B.S. Hsiao, Small-angle X-ray scattering of polymers, *Chemical Reviews* 101 (2001) 1727-1762.
- [108] S. Humbert, O. Lame, J. Chenal, C. Rochas, G. Vigier, New insight on initiation of cavitation in semicrystalline polymers: in-situ SAXS measurements, *Macromolecules* 43 (2010) 7212-7221.
- [109] J.K. Lee, J.H. Kim, H.C. Chu, K.D. Pae, Macroscopic observation of healing process in stress-whitened polypropylene under hydrostatic pressure, *Polymer Engineering & Science* 42 (2002) 2351-2360.
- [110] M. Yamaguchi, K.-H. Nitta, Optical and acoustical investigation for plastic deformation of isotactic polypropylene/ethylene-1-hexene copolymer blends, *Polymer Engineering & Science* 39 (1999) 833-840.
- [111] A. Pawlak, A. Galeski, Cavitation and morphological changes in polypropylene deformed at elevated temperatures, *Journal of Polymer Science Part B: Polymer Physics* 48 (2010) 1271-1280.
- [112] S. Castagnet, S. Girault, J. Gacougnolle, P. Dang, Cavitation in strained polyvinylidene fluoride: mechanical and X-ray experimental studies, *Polymer* 41 (2000) 7523-7530.
- [113] K.-H. Nitta, M. Takayanagi, Direct observation of the deformation of isolated huge spherulites in isotactic polypropylene, *Journal of materials science* 38 (2003) 4889-4894.
- [114] S. Castagnet, Y. Deburck, Relative influence of microstructure and macroscopic triaxiality on cavitation damage in a semi-crystalline polymer, *Materials Science and Engineering: A* 448 (2007) 56-66.
- [115] A. Pawlak, A. Galeski, Cavitation during tensile deformation of polypropylene, *Macromolecules* 41 (2008) 2839-2851.
- [116] C. Thomas, R. Seguela, F. Detrez, V. Miri, C. Vanmansart, Plastic deformation of spherulitic semi-crystalline polymers: An *in situ* AFM study of polybutene under tensile drawing, *Polymer* 50 (2009) 3714-3723.
- [117] A. Peterlin, F. Balta-Calleja, Diffraction studies of plastically deformed polyethylene, *Kolloid-Zeitschrift und Zeitschrift für Polymere* 242 (1970) 1093-1102.
- [118] Z.Y. Jiang, Y.J. Tang, J. Rieger, H.F. Enderle, D. Lilge, S.V. Roth, R. Gehrke, W. Heckmann, Y.F. Men, Two Lamellar to Fibrillar Transitions in the Tensile Deformation of High-Density Polyethylene, *Macromolecules* 43 (2010) 4727-4732.
- [119] H.P. Wang, S.P. Chum, A. Hiltner, E. Baer, Deformation of Elastomeric Polyolefin Spherulites, *Journal of Polymer Science Part B-Polymer Physics* 47 (2009) 1313-1330.
- [120] A. Peterlin, R. Corneliussen, Small-angle x-ray diffraction studies of plastically deformed polyethylene. II. Influence of draw temperature, draw ratio, annealing temperature, and time, *Journal of Polymer Science Part A-2: Polymer Physics* 6 (1968) 1273-1282.
- [121] A. Peterlin, Drawing and extrusion of semi-crystalline polymers, *Colloid and Polymer Science* 265 (1987) 357-382.
- [122] K. Sakaoku, A. Peterlin, Electron microscopy of drawn polypropylene, *Journal of Polymer Science Part A-2: Polymer Physics* 9 (1971) 895-915.
- [123] R. Popli, L. Mandelkern, Influence of structural and morphological factors on the mechanical properties of the polyethylenes, *Journal of Polymer Science Part B: Polymer Physics* 25 (1987) 441-483.

- [124] W.W. Adams, D. Yang, E.L. Thomas, Direct visualization of microstructural deformation processes in polyethylene, *Journal of materials science* 21 (1986) 2239-2253.
- [125] T. Juska, I. Harrison, A criterion for craze formation, *Polymer Engineering & Science* 22 (1982) 766-776.
- [126] R. Séguéla, Plasticity of semi-crystalline polymers: crystal slip versus melting-recrystallization, *e-Polymers* 7 (2007) 382-401.
- [127] G. Höhne, W. Hemminger, H.-J. Flammersheim, *Differential scanning calorimetry*, Springer, 2003.
- [128] J.J. Janimak, G.C. Stevens, Comparative crystallisation and exploratory microstructure studies of novel polyethylenes with tailored molecular characteristics, *Polymer* 41 (2000) 4233-4248.
- [129] T. Parenteau, G. Ausias, Y. Grohens, P. Pilvin, Structure, mechanical properties and modelling of polypropylene for different degrees of crystallinity, *Polymer* 53 (2012) 5873-5884.
- [130] P. Wanakamol, Deformation behavior of cylindrical block copolymer bicrystals: pathway to understanding block copolymer grain boundaries, Massachusetts Institute of Technology, 2006.
- [131] A. Prudom, Performance of multi-component polymers at high strain rates, © Andrew John Prudom, 2012.
- [132] J. QIAO, Propriétés mécaniques des verres métalliques massifs: Influence de la microstructure, Laboratoire MATEIS, INSA de Lyon, Villeurbanne, 2013.
- [133] S. Humbert, Influence de la topologie moléculaire et de la microstructure sur les propriétés mécaniques des Polyéthylènes, INSA de Lyon, villeurbanne, 2009.
- [134] H. Guo, Y. Zhang, F. Xue, Z. Cai, Y. Shang, J. Li, Y. Chen, Z. Wu, S. Jiang, In-situ synchrotron SAXS and WAXS investigations on deformation and α - β transformation of uniaxial stretched poly (vinylidene fluoride), *CrystEngComm* 15 (2013) 1597-1606.
- [135] K. Nakamura, D. Sawai, Y. Watanabe, D. Taguchi, Y. Takahashi, T. Furukawa, T. Kanamoto, Effect of annealing on the structure and properties of poly(vinylidene fluoride) β -form films, *Journal of Polymer Science Part B: Polymer Physics* 41 (2003) 1701-1712.
- [136] Z. Bartczak, A. Argon, R. Cohen, Deformation mechanisms and plastic resistance in single-crystal-textured high-density polyethylene, *Macromolecules* 25 (1992) 5036-5053.
- [137] T. Seto, T. Hara, K. Tanaka, Phase transformation and deformation processes in oriented polyethylene, *Japanese Journal of Applied Physics* 7 (1968) 31.
- [138] I. Hay, A. Keller, Mechanically induced twinning and phase transformations, *Journal of Polymer Science Part C: Polymer Symposia*, Wiley Online Library, 1970, pp. 289-295.
- [139] S. Humbert, O. Lame, G. Vigier, Polyethylene yielding behaviour: What is behind the correlation between yield stress and crystallinity?, *Polymer* 50 (2009) 3755-3761.
- [140] R. Young, A dislocation model for yield in polyethylene, *Philosophical magazine* 30 (1974) 85-94.
- [141] R. Séguéla, Dislocation approach to the plastic deformation of semicrystalline polymers: Kinetic aspects for polyethylene and polypropylene*, *Journal of Polymer Science Part B: Polymer Physics* 40 (2002) 593-601.
- [142] K. Nitta, M. Takayanagi, Tensile yield of isotactic polypropylene in terms of a lamellar-cluster model, *Journal of Polymer Science Part B: Polymer Physics* 38 (2000) 1037-1044.
- [143] K.-h. Nitta, N. Yamaguchi, Influence of morphological factors on tensile properties in the pre-yield region of isotactic polypropylenes, *Polymer journal* 38 (2006) 122-131.

- [144] A. Peterlin, Plastic deformation of polyethylene by rolling and drawing, *Kolloid-Zeitschrift und Zeitschrift für Polymere* 233 (1969) 857-862.
- [145] A. Peterlin, Folded chain model of highly drawn polyethylene, *Polymer Engineering & Science* 9 (1969) 172-181.
- [146] T. Kajiyama, T. Okada, M. Takayanagi, The role of mosaic block structure on onset of deformation and fatigue of bulk crystallized polyethylene, *Journal of Macromolecular Science, Part B* 9 (1974) 35-69.
- [147] K. Suehiro, T. Terashima, M. Takayanagi, Change of mosaic block size of bulk polyethylene in drawing processes, *Journal of Materials Science* 9 (1974) 1563-1568.
- [148] S. Humbert, O. Lame, J.M. Chenal, R. Seguela, G. Vigier, Memory effect of the molecular topology of lamellar polyethylene on the strain-induced fibrillar structure, *European Polymer Journal* 48 (2012) 1093-1100.
- [149] A. Pawlak, A. Galeski, Plastic Deformation of Crystalline Polymers: The Role of Cavitation and Crystal Plasticity, *Macromolecules* 38 (2005) 9688-9697.
- [150] L. Hubert, L. David, R. Séguéla, G. Vigier, C. Corfias-Zuccalli, Y. Germain, Physical and mechanical properties of polyethylene for pipes in relation to molecular architecture. II. Short-term creep of isotropic and drawn materials, *Journal of applied polymer science* 84 (2002) 2308-2317.
- [151] Z. Bartczak, Effect of Chain Entanglements on Plastic Deformation Behavior of Linear Polyethylene, *Macromolecules* 38 (2005) 7702-7713.
- [152] R. Séguéla, On the Natural Draw Ratio of Semi-Crystalline Polymers: Review of the Mechanical, Physical and Molecular Aspects, *Macromolecular Materials and Engineering* 292 (2007) 235-244.
- [153] S. Humbert, O. Lame, J.M. Chenal, C. Rochas, G. Vigier, Small strain behavior of polyethylene: in situ SAXS measurements, *Journal of Polymer Science Part B: Polymer Physics* 48 (2010) 1535-1542.
- [154] G. Meinel, A. Peterlin, Plastic deformation of polyethylene II. Change of mechanical properties during drawing, *Journal of Polymer Science Part A-2: Polymer Physics* 9 (1971) 67-83.
- [155] B. Wunderlich, *Macromolecular physics*, Elsevier, 2012.
- [156] N. Striebeck, Analysis of SAXS fiber patterns by means of projections, ACS symposium series, ACS Publications, 2000, pp. 41-56.
- [157] H. Hasegawa, T. Hashimoto, H. Kawai, T.P. Lodge, E.J. Amis, C.J. Glinka, C.C. Han, SANS and SAXS studies on molecular conformation of a block polymer in microdomain space, *Macromolecules* 18 (1985) 67-78.
- [158] A. Guinier, G. Fournet, C.B. Walker, K.L. Yudowitch, *Small-angle scattering of X-rays*, (1955).
- [159] K.H. Nitta, M. Takayanagi, Tensile yield of isotactic polypropylene in terms of a lamellar-cluster model, *Journal of Polymer Science Part B: Polymer Physics* 38 (2000) 1037-1044.
- [160] A. Peterlin, Plastic deformation of polymers with fibrous structure, *Colloid and Polymer Science* 253 (1975) 809-823.
- [161] Y. Wang, Z. Jiang, L. Fu, Y. Lu, Y. Men, Stretching Temperature Dependency of Lamellar Thickness in Stress-Induced Localized Melting and Recrystallized Polybutene-1, *Macromolecules* 46 (2013) 7874-7879.
- [162] J.D. Hoffman, R.L. Miller, Kinetic of crystallization from the melt and chain folding in polyethylene fractions revisited: theory and experiment, *Polymer* 38 (1997) 3151-3212.
- [163] B. Xiong, O. Lame, J. Chenal, C. Rochas, R. Seguela, G. Vigier, In-situ SAXS study and modeling of the cavitation/crystal-shear competition in semi-crystalline polymers:

- Influence of temperature and microstructure in polyethylene, *Polymer* 54 (2013) 5408-5418.
- [164] P.M. Tarin, E.L. Thomas, The role of inter- and intra-links in the transformation of folded chain lamellae into microfibrils, *Polymer Engineering & Science* 19 (1979) 1017-1022.
- [165] K.-h. Nitta, A molecular theory of stress-strain relationship of spherulitic materials, *Computational and Theoretical Polymer Science* 9 (1999) 19-26.
- [166] L.L. Bohm, H.F. Enderle, M. Fleißner, High-density polyethylene pipe resins, *Advanced Materials* 4 (1992) 234-238.
- [167] A. Peterlin, Chain scission and plastic deformation in the strained crystalline polymer, *Journal of Polymer Science Part C: Polymer Symposia* 32 (1971) 297-317.
- [168] T.Y. Cho, B. Heck, G. Strobl, Equations describing lamellar structure parameters and melting points of polyethylene-co-(butene/octene)s, *Colloid and Polymer Science* 282 (2004) 825-832.
- [169] G. Mitchell, A wide-angle X-ray study of the development of molecular orientation in crosslinked natural rubber, *Polymer* 25 (1984) 1562-1572.
- [170] E.R. Zubarev, M.U. Pralle, E.D. Sone, S.I. Stupp, Scaffolding of Polymers by Supramolecular Nanoribbons, *Advanced Materials* 14 (2002) 198-203.

Acknowledgements

Firstly, I would like to thank laboratory MATEIS and group PVMH for offering an opportunity to accomplish my thesis and also many thanks for the financial supporting of my study from China Scholarship Council.

I am very grateful to my supervisor, Prof. Olivier LAME, for the coaching, the thorough discussions, excellent scientific guidance and suggestions throughout this period. I have learned a great deal of research activity from him. I'd like to thank Dr. Roland Séguela to be my second supervisor and providing me a lot helps during the whole period of my PhD. I would like to thank the members of Jury, Dr. Sylvie CASTAGNET, Prof. Lucien LAIARINANDRASANA, Prof. Jean-Marc LEFEBVRE and Prof Gilles REGNIER. Their comments and discussions are very important to my thesis.

I would like to say thank you to Jean-Marc Chenal and Prof. Gerard Vigier. Thanks for your kind and patient helps to my experiments and also many thanks to the other members of group: Prof. Laurent chazeau, Prof. Jean-Yves Cavallé, Rinaldi Renaud...

I also gratefully acknowledge European Synchrotron Radiation Facility (ESRF, Grenoble, France) for granting the beamtimes for making this research successful and also I would like thank Mr Cyrille Rochas for support during the beamtimes for experimental works.

I would also like to appreciate all the people from my research group. In particular: Tiana, Nicolas, Coralline, Chloé... I do really enjoy the time working with you.

I appreciate rest of the staff from Laboratory MATEIS, for their assistance during 3 years of my PhD research. Finally, I express my deepest appreciate to my family for their boundless moral support during my studies.

FOLIO ADMINISTRATIF

THESE SOUTENUE DEVANT L'INSTITUT NATIONAL DES SCIENCES APPLIQUEES DE LYON

NOM : XIONG

DATE de SOUTENANCE : 09/12/2014

Prénoms : Bijin

TITRE : Contribution to the study of elastic and plastic deformation mechanisms of polyethylene and polypropylene as a function of microstructure and temperature

NATURE : Doctorat

Numéro d'ordre : 2014ISAL0120

Ecole doctorale : Ecole doctorale matériaux de Lyon

Spécialité : Génie des matériaux , microstructure, propriétés mécaniques

RESUME :

Les propriétés mécaniques des polymères semi-cristallins en relation avec leur microstructure ont fait l'objet d'un grand nombre d'études. Cependant, il reste encore des questions non résolues, concernant les mécanismes de la déformation plastique à température élevée, les propriétés intrinsèques de la phase amorphe interlamellaire ou encore la distribution des contraintes locales dans les sphérolites... L'objectif de cette thèse est d'adresser ces questions dans les cas du PE et du PP en fonction de la température. Pour atteindre cet objectif, une série d'échantillons de PE et PP des différents microstructures ont été préparés et caractérisés par DSC, SAXS, WAXS et spectroscopie Raman. Dans le domaine élastique, la déformation locale (ϵ_{local}) dans les régions équatoriales et polaires des sphérolites ont été mesurés par SAXS in situ. Le ratio $\epsilon_{local} / \epsilon_{macro}$ a été utilisé dans un modèle mécanique permettant le changement d'échelle de mésoscopique macroscopique. En outre, le module apparent de la phase amorphe interlamellaire M_a a été estimé par la contrainte et la déformation locale. Les M_a valeurs du PE sont dans la gamme 250 - 500 MPa, ce qui est très élevé par rapport au module du PE amorphe caoutchoutique. Dans le domaine plastique, la cavitation, la transformation martensitique et le cisaillement du cristal ont été observées par SAXS et WAXS in situ. Une concurrence entre ces mécanismes plastiques a été mise en évidence. L'augmentation de la température entraîne une disparition progressive de la cavitation et un retard de la transformation martensitique vers de plus haute déformation. La structure fibrillaire, induite par étirage à différentes températures a été étudiée par SAXS in-situ. Il a été observé que la longue période et le diamètre des micro-fibrilles dépendent de la température d'étirage de la structure initiale, via les mécanismes de « fusion-recristallisation » et « fragmentation-réarrangement ». Une étude similaire a été effectuée pour le PP.

MOTS-CLES :

propriétés mécaniques ; polyéthylène; microstructure; polypropylène; temperature

Laboratoire (s) de recherche :MATEIS

Directeur de thèse: Olivier LAME

Président de jury : Lucien LAIARINANDRASANA

Composition du jury : Sylvie CASTAGNET, Lucien LAIARINANDRASANA, Jean-Marc LEFEBVRE, Gilles REGNIER, Olivier LAME, Roland SEGUELA